Multistability and switching dynamics in vascular networks

George William Atkinson

Linacre College

University of Oxford

A thesis submitted for the degree of

Doctor of Philosophy

Hilary 2023

Acknowledgements

I would like to thank my supervisors Helen Byrne, Ester Hammond, Philip Maini and Joe Pitt-Francis who have all gone above and beyond to ensure that this thesis is possible. It has been a privilege to work with you all and I greatly appreciate the freedom you have given me to explore my research question whilst giving me valuable advice and guidance these past three years.

I would also like to thank CRUK and the EPSRC for funding my research during my graduate studies.

Additionally, I would like to thank Yaron Ben-Ami, I have always found discussions with Yaron about microcirculation to be incredibly stimulating and I benefited from his presence towards the end of my time at Oxford. It was also a pleasure to collaborate with him on a publication and the organisation of a mini-symposium at ECMTB 2022. The latter I consider to be one of the highlights of my graduate studies.

I would like to thank the members of OCIAM that encouraged me to join them at 2021 APS Division of Fluid Dynamics annual meeting and for the adventure to Sedona we shared after the conference. Among these, I would like to single out Edwina Yeo who was the main driving force behind this undertaking.

I would like to thank Anna Saroldi for helping me manage the stressful situation of completing my thesis.

Lastly, I would like to thank my family, without whom my success in life would not be possible. I would like to thank my sister Josie Atkinson for helping me with my application to Oxford, my Grandmother Diana Atkinson for so fervently believing in me and my father Mark Atkinson for funding my education. I would also like to give special thanks to my mother Penny Atkinson. As a child a suffered greatly with dyslexia and my mother put in great effort to ensure I received the support I required. Without her I may not have been able to read or write, and this thesis would not have been possible.

Abstract

The formation of regions of low oxygen concentration, or hypoxia, within tumours is a hallmark of many types of cancer. Oxygen starvation of cancerous cells within tumours creates an environment that causes tumours to become more aggressive and more resistant to treatment. Hypoxia within tumours is described as chronic or cycling. Chronic-hypoxia describes permanently hypoxic regions of tissue, and cycling-hypoxia describes short term fluctuations of hypoxia. Counterintuitively, the short term application of oxygen to hypoxic regions does not reverse the negative impact of hypoxia and in many cases exacerbates the negative health impacts associated with hypoxia. A recent hypothesis for the formation of chronic-hypoxia based on the equilibria of steady-state models of blood flow in vasculature networks has been computationally verified. Blood flow within the vasculature dictates the distribution of RBCs (Red Blood Cells) within a tumour, and if the distribution of RBCs for a blood flow equilibrium is asymmetric and uneven, then the tissue surrounding vessels with fewer RBCs suffers hypoxia.

Our goal for this thesis is to expand upon blood flow models to propose a possible mechanistic explanation for the formation of cycling-hypoxia. We propose a model of blood flow switching between multiple stable equilibria of vascular networks. In this thesis we link the existence of multiple equilibria with the change in the flow direction in network motifs. After demonstrating the importance of flow direction for the existence of multiple equilibria, we show that stochastic fluctuations of RBC partitioning at vessel junctions can force the blood flow in vasculature to change direction, resulting in the blood flow switching between stable equilibria. We hypothesise that this switching of the blood flow between at least two equilibria may result in part of a tumour being exposed to cycles of normoxic and hypoxic conditions.

Statement of Originality

The creation of the bifurcation diagrams in Chapters 3, 4 and 5 was made possible by the use of AUTO 07p software (Doedel et al., 1999). However, the equations for each bifurcation diagram have been implemented by myself.

The code to solve the time-dependent equations in Chapter 3 was originally written by Dr. Ben-Ami but was modified for the purpose of the research carried out in this thesis.

The code for solving the stochastic differential equations in Chapter 5 is also a modified code that was first implemented by Dr. Ben-Ami. However, the addition of stochastic noise was not present in the original code base and was implemented solely by myself.

Contents

Chapter 1

Introduction

Hypoxia (lower than normal oxygen concentration) is a common phenomenon in tumours with implications for the prognosis and treatment of patients. Hypoxic regions within tumours have been shown to be less susceptible to chemo, immuno and radiotherapies, to increase tumour cell migration, and to increase the number of tumour cells with aggressive cell phenotypes (Gilkes et al., 2014; Muz et al., 2015; Shannon et al., 2003; Tan et al., 2009; Ward et al., 2013). These problems present significant obstacles for clinicians seeking to treat cancer patients. Hypoxia promotes angiogenesis (the formation of new blood vessels) to alleviate oxygen deficiency in the tumour microenvironment. As tumour cells proliferate rapidly, the formation of new blood vessels does little to alleviate hypoxia; the persistence of hypoxia promotes more angiogenesis, causing the tumour microenvironment to become hypoxic but vascularised (Carmeliet and Jain, 2011). Hypoxia can be broadly defined as chronic or cycling. Chronic-hypoxic regions are regions in the tumour microenvironment that are permanently starved of oxygen, and cycling-hypoxic regions are regions that experience short term fluctuations between hypoxia and normoxia (normal concentration of oxygen). Instead of reducing the growth of more aggressive and treatment resistant cell phenotypes, cycling-hypoxia often leads to increased growth of these phenotypes (Muz et al., 2015).

Therefore, it is important to understand the physical mechanisms that result in hypoxia and how such factors can be managed to reduce the detrimental effects. Anti-angiogenic factors have been shown to improve the prognosis of patients with certain cancers (Browder et al., 2000; Carmeliet and Jain, 2000; Ferrara et al., 2004; Jain, 2001). Anti-angiogenic drugs prevent the binding of Vascualar Endothelial Growth Factor (VEGF) to VEGF receptors on cell surfaces. VEGF are signalling molecules that promote the formation of additional

blood vessels; therefore, the presence of anti-angiogenic drugs reduces the growth of new vasculature (Faivre et al., 2007; McCormack and Keam, 2008). In a series of articles, Jain (2001, 2005) suggested these treatments are effective against tumours because they reduce hypoxia by allowing for capillary pruning in the tumour vasculature, reducing overall tortuosity, allowing blood to flow more easily. Anti-angiogenic drugs have also proven to be effective at treating instances of cycling-hypoxia. Matsumoto et al. (2011) treated mice experiencing cycling-hypoxia with Sunitinib, an anti-angiogenic drug. They found that mice treated with the drug no longer experienced cycling-hypoxia. The mechanism of action of these anti-angiogenic drugs and their impact on chronic- and cycling-hypoxia strongly indicates that the structure of the vasculature is a leading cause of hypoxia within tumours.

By reducing cycling-hypoxia in tumours, the emergence of these problematic phenotypes can be controlled. The effectiveness of anti-angiogenic drugs at reducing instances of cycling-hypoxia indicates that the blood flow in tumours is partially responsible for the emergence of cycling-hypoxia (Matsumoto et al., 2011). However, it is not clear why preventing the formation of new blood vessels provides a therapeutic benefit. One possible hypothesis as to why anti-angiogenic drugs are effective at treating cancers is due to the concept of normalisation of the tumour vasculature. Jain (2005) suggested that abnormal vasculature causes oxygen and nutrients to be unevenly distributed within the tumour microenvironment, and preventing the formation of new blood vessels allows for blood vessels to be removed. This leads to more effective distribution of oxygen and nutrients. Although Jain (2005) did not explicitly reference cylcing hypoxia, changes to the vascular geometry could also provide an explanation of why anti-angiogenic drugs are effective at reducing instances of cycling-hypoxia.

Mathematical models of blood flow could prove useful to understanding why these drugs are so effective. Ben-Ami et al. (2022) showed how a blood flow model admitted self-sustained oscillations in a simple vascular network. They suggested that similar oscillations could result in cycling-hypoxia in tumours. In this thesis I will suggest a different mechanistic explanation for the emergence of cycling-hypoxia by demonstrating that a blood flow model predicts the blood flow switching between multiple stable states in simple vascular networks. By demonstrating that network geometry can leading to switching behaviour in small network motifs, it is possible to hyothesies that the geometry of larger vascular networks can also result in blood flow switching. This would support the hypothesis that cycling-hypoxia emerges from abnormal vasculature and that anti-angiogentic drugs allow for normalization of the vasculature and prevent switching from occuring.

The remainder of this chapter is dedicated to discussing the current literature of vascular geometry in tumours and blood flow models in microcirculation: Section 1.1 discusses the geometric features of tumour vasculature, Section 1.2 details the main assumptions and principles of blood flow in microcirculation, in Section 1.3 we discuss how the vasculature within tumours is abstracted with the use of vasculature networks, in Section 1.4 we discuss the mathematical model for the time-dependent blood flow in a single vessel, Section 1.5 describes the full list of the variables and constants in vascular networks, Section 1.6 describes the common geometric features described in this thesis, in Section 1.7 we detail the construction of the steady-state network equations from the boundary conditions and network geometry, Section 1.8 describes the time-dependent network equations for a vascular network, Section 1.9 describes some key properties of the steady-state and time-dependent equations that are critical for understanding the results in this thesis, Section 1.10 contains a discussion of the modelling of blood flow in microcirculation and how we will apply these models to understand blood flow in tumour vasculature, and Section 1.11 contains an outline of remainder of the thesis.

1.1 Microvessels in tumours

Tumour vasculature is often described as highly heterogeneous with leaky vessels and irregular diameters (Jain, 2005). To study blood flow in tumour vasculature using mathematical models of blood flow, it is important to try and quantify the differences between healthy vasculature and tumour vasculature. A common metric used to quantify the vasculature is the percentage of small vessels. Vogel (1965) showed that 97% of the capillaries within healthy vasculature have diameters of less than 12μm; by contrast, only 11% of vessels within tumour vasculature have diameters less than 12μm. Yamaura and Sato (1974) showed that between days 3 and 5 of tumour growth, the number of vessels with diameters smaller than 10μm increased from 40% to 70%. They then observed that after day 10 of tumour growth, smaller vessels began to dilate or disappear as the tumour grows. This suggests that vessel diameters in tumour vasculature depend on the stage of growth, that the vasculature may initially be immature and small, and that these smaller vessels will collapse or dilate over time. Deane and Lantos (1981) measured the diameters of the vessels of tumours that grew in mice. They found that when the diameter of a tumour was less than 4mm, the tumour contained an avascular core containing few vessels surrounded by a periphery of well vascularised tissue consisting of mostly small vessels with diameters less than 5μm. As the tumours grew beyond 4mm, the tumour was divided into three regions: the avascular

core, the tumour boundary where most vessels have diameters of less than 5μm, and an intermediate region where most vessels have diameters in the range of 3 to 40μm. These results could explain the discrepancy between Yamaura and Sato (1974) and Vogel (1965): the vasculature is initially small but eventually dilates or collapses, creating regions with larger vessels. Therefore, as the tumour grows, the periphery contains vessels with smaller diameters, but vessels closer to the core have had more time to dilate, resulting in regions with different vessel diameters observed by Deane and Lantos (1981).

More recently, microvascular density (MVD) has been used to evaluate the vasculature. MVD is a measurement of the mean number of microvessels within an area of tissue. Although there is no consensus on the expected MVD for normal tissue, most of the results appear to indicate that tumours have a higher vascular density: Shieh et al. (2009) found that normal tissue had a MVD of $18.7 \pm 5.23(\text{mm}^{-2})$ and the intratumour region of a tumour had a MVD of $63.9 \pm 23.2(\text{mm}^{-2})$; Sharma et al. (2010) found that normal tissue had a MVD of $64.4 \pm 13.53(\text{mm}^{-2})$ and the tumour had a MVD of $240.53 \pm 92.3(\text{mm}^{-2})$; and Mohtasham et al. (2010) found that normal tissue had a MVD of $27.5 \pm 12.5(\text{mm}^{-2})$ and cancerous tumours had an MVD of $57.8 \pm 10.8(\text{mm}^{-2})$. Although the results are inconsistent for the MVD of normal or cancerous tissue, they imply that the MVD of cancerous tissue is greater than the MVD of healthy vasculature.

In addition to vessel diameter measurements and MVD, the structure of the vasculature in tumours is another potentially important abnormality. Tumour vasculature has been observed to contain looped structures (Less et al., 1991). Until recently, quantifying loops has been difficult due to the difficulties of classifying loops in images of tumour vasculature. Topological data analysis (TDA) has been used to quantify vasculature structures by measuring the number of loops and voids per vessel segment in tumour vasculature. Stolz et al. (2022) used TDA to measure these two quantities in tumours and observed that they changed over time for different cancer treatments. They argue that TDA gives an unprecedented quantification of the structural features of tumour vasculature. Although they did not use TDA to compare tumour vasculature with healthy vasculature, instead they compared tumour vasculature of a control tumour group against the vasculature in tumours treated with Bevacizumab, an anti-angiogenic drug. They found fewer loops and more voids in treated tumours. Voids can be interpreted at avascular regions, and so these measurements imply that as tumours are treated, loops become less frequent, and avascular spaces within the vasculature emerge. Jain (2001, 2005) have suggested that anti-angiogenic drugs normalise vasculature within tumours, therefore, one interpretation of these results is

that the number of loops and voids provides a quantitative measure of vasculature normality.

The presence of looped structures would be consistent with the observation of greater vascular density because it is reasonable to assume that the vasculature is more connected if the vasculature is packed into tighter spaces in tumour vasculature. Secomb et al. (2012) suggested that the vasculature in tumours contains short wide vessels known as functional shunts that potentially redirect blood flow. The presence of looped structures could be the result of the formation of many functional shunts.

1.2 Flow in microcirculation

Although the vascular geometry in tumours is abnormal, blood flow in micro-vessels (capillaries, venules) within the tumour microenvironment are governed by the same equations and principles as blood flow in healthy vasculature. Most resistance to blood flow occurs in the microvessels, due to the blood flow changing direction regularly (Katanov et al., 2015). As a result, blood flow through microvessels is often slower than in larger vessels. Therefore, blood flow through microvessels is characterised by laminar flow or flow with a Reynolds number less than one (Secomb, 2017). Thus, blood in a single microvessel can be modelled with a constant viscosity of μ(g/(μm s) in a solid cylinder with no-slip boundary conditions, flowing according to Poiseuille's law (Hagenbach, 1860; Poiseuille, 1846):

$$Q = \frac{\pi \Delta P D^4}{128 L \mu}, \tag{1.1}$$

where $L(\mu m)$, is the length of the vessel, $D(\mu m)$, is the diameter of the vessel, $\Delta P(Pa)$ is the pressure drop across the vessel and Q $(m^3 s^{-1})$ is the volumetric flow rate. We can use this equation to determine the resistance to flow R:

$$R = \frac{\Delta P}{Q} = \frac{128 L \mu}{\pi D^4}. \tag{1.2}$$

It has been suggested that this inverse relationship between the resistance and the fourth power of the diameter is the primary factor influencing the distribution of flow through the vasculature.

Although this simple model describes the relationship between the viscosity of any fluid and volumetric flow for small Reynolds numbers, it assumes that the blood acts as a Newtonian fluid. This assumption does not reflect the complicated behaviour of suspended

particles in blood. Blood consists of cells and proteins suspended in plasma, and, as a result, its viscosity depends on the density of the suspended material. The percentage of white blood cells is negligible in most studies of blood flow in microcirculation (Gaehtgens, 1991; Pries et al., 1994), therefore, we will ignore their effects in this thesis. Most studies of blood flow in microcirculation do not consider the impact of other constituents of blood (such as platelets and fibrinogen) on its viscosity. Therefore, we will assume that the effects of cells, other than Red Blood Cells (RBCs), and suspended proteins are negligible.

RBCs tend to move away from the walls of blood vessels with diameters smaller than $0.3mm$ (Goldsmith et al., 1989). The tendency of RBCs to travel in the centre of blood vessels has a significant effect on the viscosity of the blood. Fåhraeus and Lindqvist passed human blood through narrow glass tubes of varying diameters and showed that viscosity decreased significantly in tubes with diameters smaller than $300\mu m$; this is commonly referred to as the Fåhraeus-Lindqvist effect (Fåhraeus and Lindqvist, 1931; Pries et al., 1992; Secomb and Pries, 2013). The tendency of RBCs to move away from the vessel wall results in the formation of a cell free layer (CFL) in the vicinity of the vessel walls, which subsequently reduces the resistance to flow (Goldsmith et al., 1989). The CFL is simply the space between the vessel wall and the central channel through which the RBCs travel. This trend continues until the diameter of the blood vessel decreases to $6\mu m$, at which point the RBCs begin to travel in single file through the blood vessel and the CFL decreases in size. Pries et al. (1992) collected and analysed multiple experimental results on the flow of RBC suspensions in glass tubes to construct an empirical relationship between the density of RBCs and the viscosity of the blood. Their formulas depend on the haematocrit. There are two definitions of haematocrit that we need to consider. The first is the tube haematocrit or the ratio of the volume of red blood cells to the volume of blood. The second is discharge haemocrit, the ratio of the volumetric flow of red blood cells to the volumetric flow of the blood. The tube and discharge haematocrits are often denoted by H_T and H_D respectively. Discrepancies between the two definitions of haematocrit arise due to the movement of RBCs away from the vessel walls. Regardless of the two definitions, the only biologically realistic values of H_T and H_D are within the unit interval. The viscosity is a function of the discharge haematocrit because the initial experiments measuring the viscosity in glass tubes assumed that haematocrit entering the tubes must be equal to the haematocrit out. This assumption makes it easier to formulate the equations in terms of blood leaving the experimental apparatus rather than to measure the blood within the apparatus. Pries et al. (1994) later used in vivo experiments to obtain a more accurate expression for the viscosity

relative to plasma viscosity:

$$\mu^{(\mathrm{rel})}(H_D) = \left[1 + (\mu_{45} - 1)\frac{(1 - H_d)^C - 1}{0.55^C - 1}\left(\frac{D}{D - 1.1}\right)^2\right]\left(\frac{D}{D - 1.1}\right)^2. \tag{1.3}$$

μ_{45}, defined as,

$$\mu_{45} = 6\exp(-0.085D) + 3.2 - 2.44\exp(-0.06D^{0.645}), \tag{1.4}$$

is the relative apparent blood viscosity when $H = 0.45$. The coefficient C can be defined by

$$C = (0.8 + \exp(-0.075D))\left(-1 + \frac{1}{1 + 10^{-11}D^{12}}\right) + \frac{1}{1 + 10^{-11}D^{12}}. \tag{1.5}$$

To obtain the actual viscosity $\mu(H)$, we multiply the relative viscosity with the plasma viscosity μ_p:

$$\mu(H) = \mu_p\mu^{(\mathrm{rel})}(H). \tag{1.6}$$

The resistance in a vessel is then defined by the following equation:

$$R(H) = \frac{128L\mu(H)}{\pi D^4}. \tag{1.7}$$

Unless otherwise specified, we will refer to the discharge haematocrit with H instead of H_D because the viscosity of the blood within a vessel depends on the discharge haematocrit (Equation (1.3)). Fåhraeus and Lindqvist (1931) were the first to notice the discrepancy between the two definitions of haematocrit and now this phenomenon, known as the Fåhraeus effect. Pries et al. (1992) quantified this difference with the following ratio:

$$\frac{H_T}{H_D} = H_D + (1 - H_D)(1 + 1.7\exp((-0.35D)) - 0.6\exp(-0.01D)). \tag{1.8}$$

1.2.1 Conservation laws

Mathematical models of flow in microcirculation are underpinned by the key assumption of conservation. The main assumption underlying most studies of blood flow in microcirculation is conservation of mass at vessel junctions. This applies to RBCs and blood as a whole. For example, at a flow bifurcation such as that in Figure 1.1, a feeding vessel indexed with F flows into two daughter vessels labelled with α and β. At this vessel junction, conservation

of mass is described by the following equation:

$$Q_F = Q_\alpha + Q_\beta. \tag{1.9}$$

If the flows are reversed and vessels α and β flow into F, then this is known as a flow

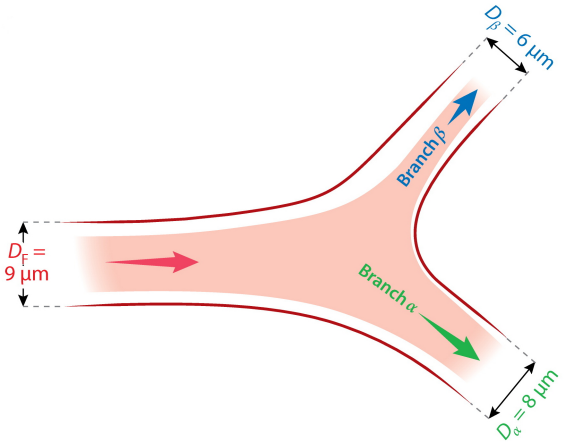

Figure 1.1: Example of a bifurcation unit, the blood flow direction is indicated by arrows and D_F, D_α and D_β are the diameters of the respective vessels. The area shaded red indicates the region of RBCs and the remaining white space indicates the CFL. This diagram has been copied from (Secomb, 2017).

convergence, and the same relation holds. Conservation of flow can be intuitively described as "flow in equals flow out."

The number of RBCs is also conserved at vessel junctions. If the numbers of RBCs that pass through each vessel in Figure 1.1 are defined by the following expressions $Q_F H_F, Q_\alpha H_\alpha$ and $Q_\beta H_\beta$, then mass conservation law for RBCs dictates that:

$$Q_F H_F = Q_\alpha H_\alpha + Q_\beta H_\beta. \tag{1.10}$$

As before, if the flows are reversed, this equality still holds. Even when the flows at a vessel junction are known, the haematocrit may not be uniquely defined. If flows, Q_F, Q_α and Q_β are known at a flow convergence, then as long as the inlet haematocrit values H_α and H_β are also known, then Equation (1.10) uniquely defines the one unknown, H_F. If, however, the inlet haematocrit H_F, and the flows are known for a flow bifurcation, then from Equation (1.10) we deduce that H_α and H_β can take values that obey the following linear relationship:

$$H_\alpha = \frac{Q_F}{Q_\alpha} H_F - \frac{Q_\beta}{Q_\alpha} H_\beta. \tag{1.11}$$

To uniquely define the haematocrit values of the daughter vessels, an additional equation is needed, this equation is called a splitting rule.

1.2.2 Splitting rules

Splitting rules relate the RBC flow in a daughter vessel to the RBC flow in its parent. They enable the haematocrits in two daughter vessels of a flow bifurcation to be uniquely defined. Let:

$$\psi_\alpha = \frac{Q_\alpha H_\alpha}{Q_F H_F},$$

be the ratio that we need to specify. There is no consensus on how this ratios should be defined, but most functions depend on the flow ratio and the haematocrit of the preceding vessel (Bernabeu et al., 2020; Kiani et al., 1994; Pries et al., 1989, 1990; Pries and Secomb, 2005). For example, Pries et al. (1989) proposed the following relationship between the ratio ψ_α and the blood flow ratio, $r_\alpha = Q_\alpha/Q_F$:

$$\text{logit}(\psi_\alpha) = A + P \cdot \text{logit}\left(\frac{r_\alpha - X_0}{1 - 2X_0}\right), \tag{1.12}$$

for $X_0 \leq r_\alpha \leq 1 - X_0$. $\text{logit}(x) = \ln(x/(1-x))$, P serves as a fitting coefficient and A, introduces nonlinearity. X_0 is introduced to prevent the formation of a singularity. The splitting rule can be reformulated as a function of r_α:

$$\psi_\alpha(r_\alpha) = \begin{cases} 0 & \text{if } r_\alpha < X_0 \\ 1 & \text{if } r_\alpha > 1 - X_0 \\ \frac{e^A (r_\alpha - X_0)^P}{e^A (r_\alpha - X_0)^P + (1 - r_\alpha - X_0)^P} & \text{if } X_0 \leq r_\alpha \leq 1 - X_0 \end{cases} \tag{1.13}$$

To the best of our knowledge, all splitting rules follow this basic format. There have been several attempts to find a general expression for the coefficients. For example, Pries and Secomb (2005) used experimental data to obtain the following formulae for A, P and X_0:

$$A = -13.29[(D_\alpha^2/D_\beta^2 - 1)/(D_\alpha^2/D_\beta^2 + 1)](1 - H_F)/D_F, \tag{1.14}$$

$$P = 1 + 6.98(1 - H_F)/D_F, \tag{1.15}$$

$$X_0 = 0.964(1 - H_F)/D_F, \tag{1.16}$$

where D_α, D_β are the diameters of the daughter vessels, D_F is the diameter of the parent vessel, and H_F is the haematocrit value at the end of the parent vessel.

Although these coefficients allow the splitting of the RBCs to be uniquely defined, they also have physical interpretations. The coefficient X_0 can be viewed as the minimum flow ratio required for the RBCs to enter a daughter vessel; we will refer to A as the phase separation coefficient due to the effect this coefficient has on the phase separation of the RBCs (Pries and Secomb, 2005; Pries et al., 1990) and P will be referred to as the plasma skimming coefficient. Larger values of P dictate that the vessel with the larger flow ratio receives a disproportionate fraction of RBCs. When $P = 1$, the splitting rule does not incorporate the plasma skimming effect, and at a bifurcation where the daughter vessels have equal diameter, the fraction of RBCs each vessel receives is proportional to the flow ratio. If $P < 1$, then the vessel with the smaller volumetric flow would receive a smaller fraction of the RBCs. Antagonistic to this plasma skimming effect is the phase separation effect observed by Barber et al. (2008) and Doyeux et al. (2011). The phase separation effect implies that the RBCs will favour the daughter vessel with a lower flow rate. Barber et al. (2008) came to this conclusion after simulating red blood cells as solid spheres and deformable membranes and found that the sphere was more likely to be biased towards the branch with a smaller volumetric flow, but Doyeux et al. (2011) simulated this effect with solid spheres and used microfluidic devices with vesicles to support their claims. Although this may seem to contradict the plasma skimming effect, both Barber et al. (2008) and Doyeux et al. (2011) observed that the vessel with the higher flow rate obtained a larger fraction of RBCs, but once the RBCs were sufficiently close to the entrance of the bifurcation, the migration of RBCs towards the vessel with a low flow rate became stronger[1]. Incorporating the effect of both plasma skimming and phase separation is difficult because they act antagonistically on the partition of RBCs. The phase separation coefficient in Equation (1.14) devised by Pries and Secomb (2005) biases the fraction toward the vessel with a smaller diameter. Defining A with this principle allows both effects to be incorporated; if one daughter vessel is wider than the other, the volumetric flow in that vessel is likely to be larger due to the fourth power relationship between the flow and the diameter. Therefore, based on the relationship between volumetric flow and the fraction of RBCs, this vessel would obtain a larger fraction of the RBCs. This is known as the plasma skimming effect, because the vessel with less flow receives more plasma relative to the number of RBCs. The formula for A in Equation (1.14) helps counterbalance this effect by biasing the RBC fraction towards the opposite

[1]It should be noted that in the absence of plasma skimming. It would still be expected that a disproportionate fraction of the RBCs would migrate towards the vessel with the highest flow due to the linear relationship between RBC fraction and the volumetric flow fraction.

vessel. The coefficients of Pries et al.'s (Pries and Secomb, 2005) splitting rule have been verified by the simulations performed by Barber et al. (2008) for single RBCs travelling through a flow bifurcation. Based on these observations, we can summarise the following principles for splitting rules that we will consider:

1. $0 \leq X_0 \ll 0.5$
2. $P > 1$.
3. A biases the flow toward the smaller vessel.

Equation (1.12) is just one example of a splitting rule from the literature. From a mathematical perspective, the only constraint on admissible splitting rules is that $\psi_\alpha \in [0, 1]$ and the ratio chosen for the other daughter vessel:

$$\psi_\beta = \frac{Q_\beta H_\beta}{Q_F H_F},$$

is equal to $1 - \psi_\alpha$, to satisfy the conservation of RBCs described by Equation (1.10).

1.3 Vascular Networks

Oxygen concentration within the tumour microenvironment is assumed to diffuse evenly, therefore, oxygen concentration is modelled with a parabolic PDE containing a diffusion term, an oxygen consumption term and an oxygen source term (Bernabeu et al., 2020; Pogue et al., 2001; Schiavo et al., 2022; Secomb et al., 1993; Welter et al., 2016). The source term represents the influx of oxygen into the tumour microenvironment from the vasculature. This vasculature is often represented with a vascular network. Networks are objects that contain two sets: the set of nodes, N, and the set of edges, E. An edge, $e \in E$, is a pair of nodes belonging to N, edges act as the abstract interpretation of vessels. For example, if $v, w \in N$ for which an edge exists between these two, then $(v, w) \in E$. The vasculature networks are incorporated into the diffusion model by acting as source terms for the differential equations for every point along an edge of the network. Most of these models predict that hypoxic regions form in regions which are not well vascularised (Pogue et al., 2001; Schiavo et al., 2022; Secomb et al., 1993). Therefore, these model predicts that regions of hypoxia are dependent on the tissue's proximity to the vasculature. Although this is a good model for chronic-hypoxia, this model is unlikely to be capable of predicting the existence of cycling-hypoxia because tissue at the centre of the tumour will always be subjected to hypoxic conditions.

Bernabeu et al. (2020) and Welter et al. (2016) both used a different approach to incorporate the effect of vasculature within the tumour. They modelled the source terms as a function of the number of RBCs flowing in the network by coupling the diffusion model of oxygen with blood flow equations for the RBCs within the vessels. The results by Welter et al. (2016) demonstrate that the proximity of the vasculature is not the only factor influencing the formation of hypoxia. They observed that acute[2]-hypoxia formed around the periphery of the tumour. This result is interesting because this region of the tumour had a higher than normal MVD and that the vessels often had smaller than normal diameters. Welter et al. (2016) concluded that this region formed because the narrow blood vessels prevented the RBCs reaching the vasculature resulting in fewer RBCs within these vessels.

Bernabeu et al. (2020) also demonstrated the impact of irregular vasculature on the surrounding tissue but unlike the results by Welter et al. (2016), they predicted the formation of chronic-hypoxia in well vascularised tissue. Bernabeu et al. (2020) investigated the impact of different length to diameter ratios for the blood vessels in a synthetic network. They discovered that for smaller ratios, the RBCs would tend towards one side of the network resulting in the formation of chronic-hypoxia in the side of the network with fewer RBCs. This region of hypoxia was not present for larger length to diameter ratios. This result implies that the formation of chronic-hypoxia in tumours can also result from asymmetric blood flow instead of just the tissue proximity to blood vessels.

Although Bernabeu et al. (2020) results only predict the formation of chronic-hypoxia, the fact that the oxygen distribution is coupled to the blood flow through vascular networks implies that changes to the blood flow could result in fluctuations of the oxygen concentration in the surrounding tissue. So far the blood flow models used to predict the distribution of RBCs in the vasculature have been assumed to have a unique stable equilibrium. However, Ben-Ami et al. (2022) showed that oscillations in blood flow in simple networks can result from abnormal vessel geometry. They proposed that self-sustained oscillations of blood in tumour vasculature could potentially cause fluctuations of the oxygen concentrations leading to the formation of cycling-hypoxia. Although they did not use an oxygen diffusion model to verify this claim, the results by Bernabeu et al. (2020) and Welter et al. (2016) would imply that so long as the number of RBCs in a vessel is predicted to be low, the surrounding tissue is likely to be hypoxic.

[2]Acute in this context referres to a region in the tumour micro-environment experiencing chronic-hypoxia, however, the level of oxygen in this acute-hypoxic region was only slightly less than the normoxic regions.

Given the success of vascular networks at predicting the emergence of hypoxia within tumours, this thesis will focus on demonstrating a possible mechanism of cycling-hypoxia arising from models of blood flow through vascular networks. Instead of demonstrating oscillations of the blood flow, we will instead focus on the possible formation of cycling-hypoxia resulting from mutli-stability of the equilibria of blood flow in vascular networks. Therefore, we dedicate the remainder of this chapter to describing the construction of the blood flow equations. This includes a discussion of the steady-state equations that have been used to predict the formation of chronic-hypoxia (Bernabeu et al., 2020; Welter et al., 2016), and the time-dependent equations neccesary to show how the blood flow changes with time. The equations for blood flow in any network that we present in this thesis can be derived from the steps we outline in this chapter and the network geometry. Instead of describing the network equations for specific networks in the main text, we describe the geometry of the network from which the network equations are constructed and refer the reader to Appendix A for a list of all network equations covered in this thesis.

1.4 Time-dependent haematocrit equations for a single vessel

Blood flow through a single vessel is modelled by imposing a fixed pressure drop across the vessel. For simplicity, we will also assume that all vessels have uniform radii, the blood flows according to Poiseuille's law, and haematocrit is transported at the same speed as the blood plasma. Let $\theta(x, y, z, t)$ be the concentration of RBCs within a vessel at the coordinate (x, y, z) at time t and let $u(x, y, z, t)$ be the velocity in the x direction. The evolution of θ can be modelled by the transport equation:

$$\frac{\partial \theta}{\partial t} + \frac{\partial}{\partial x}(u\theta) = 0. \tag{1.17}$$

The flow in the x direction does not vary throughtout the vessel due to the fact that the flow regime of the blood is laminar flow. Therefore, u is a function of y, z and t. The tube haematocrit, discharge haematocrit and average velocity can be defined in terms of θ and u as follows:

$$H_T(x,t) = \frac{\int_\Omega \theta \mathrm{d}y\mathrm{d}z}{\int_\Omega \mathrm{d}y\mathrm{d}z},\ H_D(x,t) = \frac{\int_\Omega u\theta \mathrm{d}y\mathrm{d}z}{\int_\Omega u\mathrm{d}y\mathrm{d}z},\ \overline{u}(t) = \frac{\int_\Omega u\mathrm{d}y\mathrm{d}z}{\int_\Omega \mathrm{d}y\mathrm{d}z}, \tag{1.18}$$

where Ω is the cross sectional domain of the vessel. Using these definitions, we can reformulate Equation (1.17) as a one-dimensional PDE for the haematocrit in a vessel:

$$\frac{\partial H_T}{\partial t} + \overline{u}(t)\frac{\partial H_D}{\partial x} = 0. \tag{1.19}$$

This derivation was proposed by Pop et al. (2007) and the resulting PDE has been used in other studies on the stability of blood flow in small networks (Ben-Ami et al., 2022; Carr and Lacoin, 2000; Carr et al., 2005; Davis and Pozrikidis, 2011; Geddes et al., 2007). Although the PDE governing the change in the haematocrit is the same for all these models, the authors use different modelling approximations to solve the governing equations. Two main approximations are considered in the literature; the first considers the difference between the tube haematocrit and discharge haematocrit, and the second focusses on the volumetric flow of non-uniform haematocrit distributions within a vessel.

We have already discussed the difference between the tube haematocrit and the discharge haematocrit in section 1.2. The difference between the two definitions has not been relevant so far because the equation for the relative viscosity (Equation (1.3)), RBC conservation law (Equation (1.10)), and splitting rule (Equation (1.13)) are posed in terms of discharge haematocrit. When solving the time-dependent equations, we consider two approaches. First we assume that the difference between the two quantities is sufficiently small and consider $H_D = H_T$. This approximation is common in the literature (Ben-Ami et al., 2022; Carr et al., 2005; Geddes et al., 2007).

The other option is to convert the partial derivative for H_T into a partial derivative for H_D. By rearranging Equation (1.8), the following expression for the tube haematocrit can be derived:

$$H_T = \lambda_D H_D + (1 - \lambda_D)H_D^2. \tag{1.20}$$

Differentiating Equation (1.20) with respect to time yields the following relationship between the derivatives for the tube and discharge haematocrit:

$$\frac{\partial H_T}{\partial t} = \frac{\partial H_D}{\partial t}(\lambda_D + 2(1 - \lambda_D)H_D), \tag{1.21}$$

were $\lambda_D = 1 + 1.7\exp(-0.415D) - 0.6\exp(-0.011D)$. Equation (1.21) can be subsituted into Equation (1.19) to obtain the following PDE for the discharge haematocrit:

$$\frac{\partial H_D}{\partial t} + \frac{\overline{u}(t)}{\lambda_D + 2(1-\lambda_D)H_D}\frac{\partial H_D}{\partial x} = 0. \tag{1.22}$$

This approach was used by Pop et al. (2007) and others (Carr and Lacoin, 2000; Davis and Pozrikidis, 2011).The approximation of $H_T = H_D = H$ is used throughout this thesis because modelling the haematocrit in a network using Equation (1.22) increases the complexity of simulating blood flow in large networks. Therefore, the following PDE is used to describe the transport of haematocrit in a single vessel:

$$\frac{\partial H}{\partial t} + \overline{u}(t)\frac{\partial H}{\partial x} = 0. \tag{1.23}$$

We note that the steady-state haematocrit distribution within a vessel is that of a uniform distribution for both forms of the haematocrit PDEs in Equations (1.22) and (1.23). The PDEs in Equations (1.22) and (1.23) are first-order in time and space, which means that only one spatial and time boundary condition are required for the system to be well posed. This means that the haematocrit PDEs only attain their equilibrium when the spatial boundary condition is that of a constant haematocrit:

$$H(0,t) = H_0. \tag{1.24}$$

Throughout this thesis, we set $H(x,0)$ as a smooth function to ensure regularity of the time boundary condition for the haematocrit PDEs.

If we use Poiseuille's law to approximate the volumetric flow in a vessel, then the volumetric flow at time t is given by:

$$Q(t) = \frac{\Delta P}{R(t)}, \tag{1.25}$$

where we assume that the pressure difference ΔP remains constant and $R(t)$ denotes the resistance to flow in the vessel at time t. As the resistance is proportional to the viscosity, we must define a function for the viscosity of the blood at time t. As the haematocrit is not constant for the time-dependent equation, Equation (1.3) does not define the viscosity of the blood for all possible haematocrit distributions within the vessel. Carr and Lacoin (2000) and Carr et al. (2005) viewed the viscosity as a time-dependent function of the average

haematocrit, $\overline{H}(t)$, where:

$$\overline{H}(t) = \frac{1}{L}\int_0^L H(x,t)\mathrm{d}x, \tag{1.26}$$

and used the following expression to approximate the resistance to blood flow in a vessel:

$$R(t) = \frac{128L\mu(\overline{H}(t))}{\pi D^4}. \tag{1.27}$$

An alternative approach is to average the resistance itself using the following equation:

$$R(t) = \frac{1}{L}\int_0^L \frac{128L\mu(H(x,t))}{\pi D^4}\mathrm{d}x = \frac{128L}{\pi D^4}\frac{1}{L}\int_0^L \mu(H(x,t))\mathrm{d}x = \frac{128L}{\pi D^4}\overline{\mu}(t), \tag{1.28}$$

were $\overline{\mu}(t)$ is the average viscosity at time t. This approach is more widely used throughout the literature (Ben-Ami et al., 2022; Davis and Pozrikidis, 2011; Geddes et al., 2007; Pop et al., 2007). Averaging the resistance is a more natural approach because it better takes into account the nonlinearity of the relative viscosity in Equation (1.3).

Substituting Equation (1.28) in Equation (1.25) yields an expression for $Q(t)$. Which can be used to define the average velocity of the haematocrit within a vessel. As blood always flows in one direction:

$$\overline{u}(t)A = Q(t), \tag{1.29}$$

where A is the cross-sectional area. Given that all blood vessels are viewed as cylinders, A is the area of a circle with radius D and we can define $\overline{u}(t)$ as follows:

$$\overline{u}(t) = \frac{4Q(t)}{\pi D^2}. \tag{1.30}$$

From Equation (1.25) we deduced that the haematocrit velocity can also be written in the form:

$$\overline{u}(t) = \frac{D^2\Delta P}{32L\overline{\mu}(t)}. \tag{1.31}$$

1.5 Variables and constants

Before we introduce the equations defining blood flow in a vascular network, the variables and constants of the networks must be defined. Henceforth, unless otherwise stated, we indicate whether a variable or parameter belongs to a node, v, or an edge, (v,w), by indexing them with subscripts v or (v,w) respectively.

The dependent variables that we use to model steady blood flow in a vascular network are:

- P_v: Pressure at node v,
- $Q_{(v,w)}$: Volumetric flow in vessel (v, w),
- $H_{(v,w)}$: Haematocrit in vessel (v, w).

The dependent variables for the time-dependent flow equations are as follows:

- $P_v(t)$: Pressure variable of node v,
- $Q_{(v,w)}(t)$: Volumetric flow in vessel (v, w),
- $\overline{H}_{(v,w)}(t)$: Average haematocrit of the blood in vessel (v, w),
- $\overline{\mu}_{(v,w)}(t)$: Average viscosity of the blood in vessel (v, w),
- $\overline{u}_{(v,w)}(t)$: Average velocity of haematocrit in vessel (v, w),
- $H_{(v,w)}(x, t)$: Haematocrit variable of vessel (v, w).

For both the steady-state equations and time-dependent equations, some of the variables can be reduced to functions of the other variables, but the variables stated in this section are often used and so it is convenient to include all variables in a comprehensive list.

The geometry of the network determines the set of edges E and the diameters and lengths of the vessels. Vessel diameters and lengths are assumed to remain constant. We denote the diameter and length of vessel (v, w), as $D_{(v,w)}$ and $L_{(v,w)}$ respectively.

As vascular networks are not self contained systems, they require inputs for the network equations to be well posed. All networks have a number of inlet vessels at which the pressure and haematocrit must be prescribed. Inlet haematocrits are marked in black to distinguish them from haematocrit variables ($H_{(v,w)}$ is the haematocrit of an inlet vessel, $H_{(v,w)}$ is the haematocrit variable associated with a non-inlet vessel[3]). A similar boundary condition is required for the time-dependent equations, but the prescribed inlet haematocrit may vary with time.

[3]Although we distinguish between variables and constants using colour in the main text, variables in Figure labels are always in black.

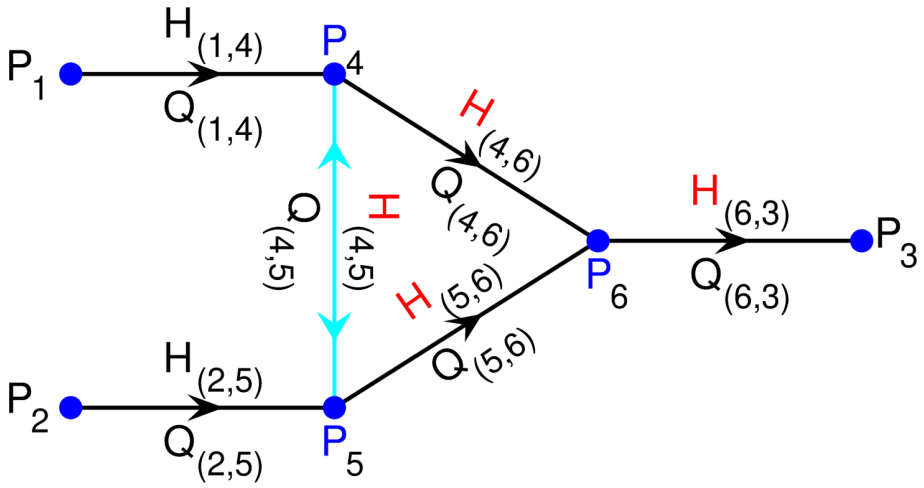

Figure 1.2: Diagram of the triangle network.

In addition to the haematocrit; pressure or flow boundary conditions must be defined. Pressure boundary conditions are used throughout this thesis because the resulting network equations in Section 1.7 are more general and simpler than those associated with flow boundary conditions. We explain how the equations are constructed when pressure boundary conditions are imposed. While we do not consider flow boundary conditions an example with flow boundary conditions can be found in (Gardner et al., 2010). All networks have boundary nodes at which the pressures must be specified. Boundary pressures are denoted in black to distinguish them from the unknown pressures at interior nodes (P_v is the pressure of a boundary node, P_v is the pressure variable associated with an interior node). As for the haematocrit, the boundary pressures for the time-dependent equations may be prescribed functions of time.

Figure 1.2 is a diagram of a triangle network motif with the associated variables of the network. The black lines denote the fixed vessels and the turquoise line denotes the redundant vessel. This network will is used throughout this thesis but has been placed here as an example.

1.6 Network design

All networks studied in this thesis share some common topological properties which are summarised in this section. All vascular networks have undirected edges as a convention; however, the direction of flow in a vessel is dictated by the pressure difference across the vessel's end nodes and so the flow in the network is directed.

Most variables and parameters of a vessel can be indexed using either order of the nodes v and w with the exception of the volumetric flow, $Q_{(x,y)}$, and the average velocity of the haematocrit, $\overline{u}_{(x,y)}$. Furthermore, $Q_{(x,y)} = -Q_{(y,x)}$; this is a consequence of Poiseuille's law in Equation (1.1). Rewriting Poiseuille's law in terms of the network variables yields the following equation:

$$Q_{(x,y)} = \frac{\pi D_{(x,y)}^4 (P_x - P_y)}{128 L_{(x,y)} \mu_{(x,y)}(H_{(x,y)})}, \tag{1.32}$$

where the viscosity, $\mu_{(x,y)}$, is defined in Equation (1.6). We note that, as $H_{(x,y)} \to 1$, $1/\mu_{(x,y)}(H_{(x,y)}) \to 0$. Therefore, we use the convention that $Q_{(x,y)} = 0$ when $H_{(x,y)} = 1$.

Blood flows in the direction of the pressure gradient. For this reason, the set of boundary nodes, $B_{\mathcal{N}}$, consists of a set of source nodes, $I_{\mathcal{N}}$, and a set of sink nodes, $S_{\mathcal{N}}$. The biological interpretation of these is that sources/sinks represent the blood flow into/out of larger vessels that are beyond the scope of our modelling. These sources and sinks have degree 1. The values for the pressure parameters at the source nodes must be greater than the values at the sink nodes to ensure that blood flows from the source nodes to the sink nodes. Boundary haematocrit values must also be introduced. These boundary values should be prescribed at inlet vessels. Inlet vessels have one node which is a source node.

In this thesis we consider a limited number of network topologies. The topology network is dicated by the connections between nodes and the degree of the nodes. The degree of a node in an undirected network is the number of edges which the node belongs to. Unless a node is a source or a sink, it must have degree 3[4]. The only possible configurations of flow at a degree 3 node can be seen in Figure 1.3: a bifurcation unit in Figure 1.3a, and a convergence unit in Figure 1.3b. Only these configurations are possible because if the direction of the volumetric flows are all towards the central node or away from the central node, the flow is not conserved.

1.7 Steady-state haematocrit equations

In this section, we will describe the construction for a network system of steady-state equations whose solutions are the equilibria of the time-dependent blood flow equations. As the steady-state of a single vessel is that of a constant haematocrit, the steady-state of a

[4]It is technically possible for a node to have a degree of 2 but two vessel connected by a single node is functionally the same as a single vessel as explained in Section 1.9.

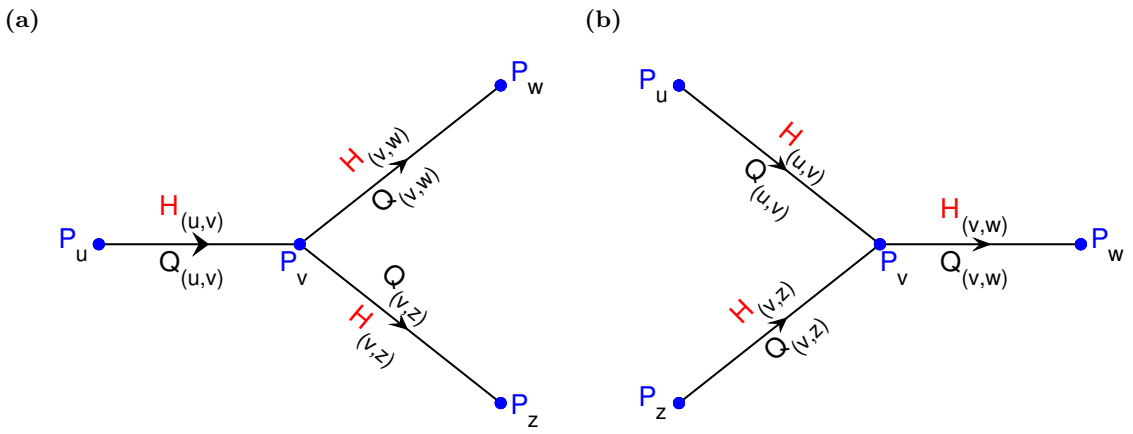

Figure 1.3: The two basic units which make up all flow networks that we will be studying. (a): Example of a bifurcation unit in a network, the arrows indicate the direction of flow. (b): Example of a convergence unit in a network, the arrows indicate the direction of flow.

vascular network must have a constant haematocrit in every vessel. Each vessel is viewed as a pipe, and the blood flow is modelled as a Newtonian fluid. The model of blood flow in a single microvessel can be extended to blood flow in a network representing the vasculature (Fenton and Zweifach, 1981). This description of blood flow in a network is similar to that of electricity in a circuit where volumetric flow, pressure difference, and hydraulic resistance are analogous to current, voltage, and electrical resistance, respectively (Pries and Secomb, 2008). The solution to the steady-state equations must satisfy the conservation laws and splitting rules defined by Equations (1.9), (1.10) and (1.13). While the details of the steady-state equations for blood flow depend on the choice of splitting rule and the geometry of the network, with few exceptions, their construction follows the same approach (Ben-Ami et al., 2022; Bernabeu et al., 2020; Davis and Pozrikidis, 2011; Gardner et al., 2010; Karst et al., 2017; Pries and Secomb, 2008; Tawfik and Owens, 2013).

The choice of boundary conditions is one variation of the network equations in the literature. For example, as stated in Section 1.5, it is possible to choose flow boundary conditions instead of pressure boundary conditions (Gardner et al., 2010). It is also possible to construct the network equations such that the network boundary nodes are not assigned pressure values and the blood flow equations do not obey a specific splitting rule (Fry et al., 2012; Sweeney et al., 2018). In these cases, the blood flow equations are in the form of a Lagrangian which ensures the conservation of flow and RBCs but instead of assigning boundary pressure values and a splitting ratio for RBCs at flow bifurcations, the equations minimise the sheer stress of the blood flow. Defining the network equations with

a Lagrangian is useful for solving the network flow equations for networks based on phenomenological networks for which the boundary conditions are unknown. However, since we only consider synthetic networks with known boundary conditions, Therefore, we will not describe the Lagrangian used in (Fry et al., 2012; Sweeney et al., 2018).

Given that the equations for networks are the same for most vascular networks, the remainder of this section will describe the common construction of the steady-state network equations when pressure boundary conditions are imposed. We define these equations with a function $F : [0,1]^m \times \mathbb{R}^n_{\geq 0} \to \mathbb{R}^{m+n}$, for a network with m non inlet vessels and n interior nodes such that the steady-state equations are defined by the following:

$$F(H, P) = 0. \tag{1.33}$$

We denote the splitting rules at bifurcation as:

$$\psi_{(v,w)} : [0,1]^2 \to [0,1]. \tag{1.34}$$

As described in Section 1.2.2, there are several different splitting rules, but most have the general form of Equation (1.13). Since one of the aims of this thesis is to understand the impact of the splitting rule on the number of equilibria, the equations will be presented using $\psi_{(v,w)}$ to represent the splitting rule (The specific forms of the three key coefficients: X_0, A and P in Equation (1.13) are defined for each network in subsequent chapters.). For the daughter haematocrit $H_{(v,w)}$, a function $F_{(v,w)}(H, P)$ is constructed such that solutions to $F_{(v,w)}(H, P) = 0$ ensure that the haematocrits and flows obey the splitting rule. Therefore, for the bifurcation unit in Figure 1.3a, the solution to $F_{(v,w)}(H, P) = 0$ must ensure the following relationship:

$$\psi_{(v,w)}(Q_{(v,w)}/Q_{(u,v)}, H_{(u,v)}) = \frac{Q_{(v,w)}H_{(v,w)}}{Q_{(u,v)}H_{(u,v)}}. \tag{1.35}$$

Rearranging Equation (1.35) yields the following equation:

$$0 = \psi_{(v,w)}(Q_{(v,w)}/Q_{(u,v)}, H_{(u,v)})Q_{(u,v)}H_{(u,v)} - Q_{(v,w)}H_{(v,w)}. \tag{1.36}$$

Therefore, if $F_{(v,w)}(H, P)$ takes the following form:

$$F_{(v,w)}(H, P) = \psi_{(v,w)}(Q_{(v,w)}/Q_{(u,v)}, H_{(u,v)})Q_{(u,v)}H_{(u,v)} - Q_{(v,w)}H_{(v,w)}, \tag{1.37}$$

the solution to $F_{(v,w)}(H, P) = 0$ satisfies the relationship between the variables of a bifurcation unit (Figure 1.3a) described by Equation (1.35). As described in Section 1.2, every flow bifurcation needs two equations to uniquely define the haematocrits of both daughter vessels. To recover the conservation of RBCs at a bifurcation, the following relation must hold:

$$\psi_{(v,w)}(Q_{(v,w)}/Q_{(u,v)}, H_{(u,v)}) + \psi_{(v,z)}(Q_{(v,z)}/Q_{(u,v)}, H_{(u,v)}) = 1,$$

The equation associated with the variables $H_{(v,z)}$ takes the same form as Equation (1.37) with the indices of (v, w) replaced by (v, z). The addition of $F_{(v,w)}(H, P) = 0$ and $F_{(v,z)}(H, P) = 0$ recovers the following expression for the conservation of RBCs at node v.

$$Q_{(u,v)}H_{(u,v)} - Q_{(v,z)}H_{(v,z)} - Q_{(w,v)}H_{(w,v)} = 0. \tag{1.38}$$

The function $F_{(v,w)}(H, P)$ corresponding to the haematocrit of the out flowing vessel in a convergence unit in Figure 1.3b must also ensure the conservation of RBCs. Therefore, the solutions to the equations $F_{(v,w)}(H, P) = 0$ must satisfy Equation (1.38). Therefore, the most obvious choice of $F_{(v,w)}(H, P)$ is:

$$F_{(v,w)}(H, P) = Q_{(u,v)}H_{(u,v)} + Q_{(z,v)}H_{(z,v)} + Q_{(w,v)}H_{(w,v)}. \tag{1.39}$$

Equations for each pressure variable P_v are obtained by appealing to conservation of flow, which supplies the following relation for the variables $(Q_{(u,v)}, Q_{(w,v)}, Q_{(v,z)})$:

$$0 = Q_{(u,v)} + Q_{(w,v)} + Q_{(z,v)}, \tag{1.40}$$

for both a convergence and bifurcation unit in Figures 1.3. Given that the volumetric flow in a vessel depends on the haematocrit in the vessel and the pressures of the end nodes, as described in Equation (1.32), the form of $F_v(H, P)$ is the following:

$$F_v(H, P) = Q_{(u,v)} + Q_{(w,v)} + Q_{(z,v)}. \tag{1.41}$$

Therefore, a system of equations $F(H, P) = 0$ for which each dependent variable of the network satisfies a function in the form of Equations (1.37), (1.39) or (1.41) can be defined for any network. The flow direction in certain vessels may change, corresponding to a change in the form of $F_{(v,w)}(H, P)$ between Equations (1.37) and (1.39) but the size of the system of equations remains the same.

Given a system of network equations, the magnitude value of the volumetric flow in a vessel scales with the size of the inlet pressures. This can be problematic when defining network equilibria. For example, if (H, P, Q) is a network equilibrium with pressure boundary conditions $\{P_{x_0}, P_{x_1}, ..., P_{x_k}\}$. Then $(H, \alpha P, \alpha Q)$ is also a network equilibrium of the network with the pressure boundary conditions $\{\alpha P_{x_0}, \alpha P_{x_1}, ..., \alpha P_{x_k}\}$. We circumvent this problem by introducing normalised volumetric flows:

Definition 1.1. (Normalised volumetric flow)
Let $\mathcal{N} = \{N, E\}$ be a network with the following set of inlet vessels:

$$\{(x_0, y_0), (x_1, y_1), ..., (x_m, y_m)\}. \tag{1.42}$$

For a vessel (v, w), the normalised flow in vessel (v, w) is defined as:

$$\hat{Q}_{(v,w)} = \frac{Q_{(v,w)}}{\sum_{i=0}^{m} Q_{(x_i,y_i)}}. \tag{1.43}$$

Defining the equilibria using normalised flows is useful because the values of the haematocrits and volumetric flows for an equilibrium, $(H, \alpha P, \hat{Q})$, are the same irrespective of the value of α.

1.8 Time-dependent haematocrit equations for a network

The PDE governing the evolution of the haematocrit in a particular vessel is the same as that governing the haematocrit in a single vessel described in Section 1.4 (Equation (1.23)). However, the time-dependent equations for a vascular network differ from those for a single vessel in two respects. The first are the equations for the volumetric flows. The volumetric flow in a vessel within a vascular network is governed by the following equation:

$$Q(t) = \frac{\Delta P(t)}{R(t)}. \tag{1.44}$$

The equation for the resistance is the same as Equation (1.28) but the pressure difference is now implicitly defined. As for the steady-state equations in Section 1.7, each node has an associate pressure variable. For vessel (v, w), $\Delta P_{(v,w)}(t) = P_v(t) - P_w(t)$. As for the steady-state equations, the pressures are defined implicitly via conservation of blood flow

at each internal node, v:

$$Q_{(u,v)}(t) + Q_{(w,v)}(t) + Q_{(z,v)}(t) = 0. \tag{1.45}$$

Given the resistance in each vessel, this linear system of equations implicitly defines the pressures of the interior nodes at time t.

The second difference between the time-dependent equations in a vasculature network and the equations for a single vessel are the boundary conditions. If a vessel is an inlet vessel, then the spatial boundary for the haematocrit can either be a constant value or a function of time. The boundary conditions for all other vessels are determined by conservation of RBCs and the splitting rules. For example, at the convergence unit in Figure 1.3b, the only spatial boundary condition for vessel (v, w) that conserves RBCs at the vessel junction is:

$$H_{(v,w)}(0,t) = \frac{H_{(u,v)}(L_{(u,v)},t)Q_{(u,v)}(t) + H_{(z,v)}(L_{(z,v)},t)Q_{(z,v)}(t)}{Q_{(v,w)}(t)}. \tag{1.46}$$

Depending on the flow direction in a vessel, a spatial boundary condition is prescribed at $x = 0$ or $x = L$. So long as the boundary condition is prescribed for the end of the vessel from which blood is flowing away from, the boundary condition is well defined. This flexibility in defining the boundary conditions of the network is convenient if the flow direction in certain vessels can change with time.

The boundary conditions a flow bifurcation must satisfy conservation of the RBCs and the splitting rules. The boundary conditions for vessels (v, w) and (v, z) in the bifurcation unit of Figure 1.3a are as follows:

$$H_{(v,w)}(0,t) = \psi_{(v,w)}(r_{(v,w)}(t), H_{(u,v)}(L_{(u,v)},t))\frac{H_{(u,v)}(L_{(u,v)},t)}{r_{(v,w)}(t)}, \tag{1.47}$$

$$H_{(v,z)}(0,t) = \psi_{(v,z)}(r_{(v,z)}(t), H_{(u,v)}(L_{(u,v)},t))\frac{H_{(u,v)}(L_{(u,v)},t)}{r_{(v,z)}(t)}, \tag{1.48}$$

where:

$$r_{(v,w)}(t) = Q_{(v,w)}(t)/Q_{(u,v)}(t), r_{(v,z)}(t) = Q_{(v,z)}(t)/Q_{(u,v)}(t).$$

The time-dependent network equations for any network can be derived from the network geometry and the steps in this section and Section 1.4. For example, consider the triangle network in Figure 1.2. This network has two inlet vessels and three boundary nodes, such

that $H_{(1,4)}(0,t), H_{(2,5)}(0,t), P_1(t), P_2(t)$ and $P_3(t)$ are either functions of time or constants for the time-dependent network equations for the triangle network. The conservation of flow equations are as follows:

$$0 = Q_{(1,4)}(t) + Q_{(6,4)}(t) + Q_{(5,4)}(t), \tag{1.49}$$

$$0 = Q_{(2,5)}(t) + Q_{(6,5)}(t) + Q_{(4,5)}(t), \tag{1.50}$$

$$0 = Q_{(3,6)}(t) + Q_{(4,6)}(t) + Q_{(5,6)}(t), \tag{1.51}$$

and the spatial boundary conditions for the haematocrit variables of the network are:

$$H_{(4,6)}(0,t) = \begin{cases} \frac{\psi_{(4,6)}(r_{(4,6)}(t), H_{(1,4)}(L_{(1,4)},t))H_{(1,4)}(L_{(1,4)},t)}{r_{(4,6)}(t)} & Q_{(4,5)}(t) > 0, \\ \frac{H_{(1,4)}(L_{(1,4)},t)Q_{(1,4)}(t) + H_{(4,5)}(0,t)Q_{(5,4)}(t)}{Q_{(4,6)}(t)} & Q_{(4,5)}(t) \leq 0, \end{cases} \tag{1.52}$$

$$H_{(5,6)}(0,t) = \begin{cases} \frac{\psi_{(5,6)}(r_{(5,6)}(t), H_{(2,5)}(L_{(2,5)},t))H_{(2,5)}(L_{(2,5)},t)}{r_{(5,6)}(t)} & Q_{(4,5)}(t) \leq 0, \\ \frac{H_{(2,5)}(L_{(2,5)},t)Q_{(2,5)}(t) + H_{(4,5)}(L_{(4,5)},t)Q_{(4,5)}(t)}{Q_{(5,6)}(t)} & Q_{(4,5)}(t) > 0, \end{cases} \tag{1.53}$$

$$H_{(4,5)}(0,t) = \frac{\psi_{(4,5)}(r_{(4,5)}, H_{(1,4)}(L_{(1,4)},t))H_{(1,4)}(L_{(1,4)},t)}{r_{(4,5)}(t)} \text{ if } Q_{(4,5)}(t) > 0, \tag{1.54}$$

$$H_{(4,5)}(L_{(4,5)},t) = \frac{\psi_{(5,4)}(r_{(5,4)}, H_{(2,5)}(L_{(2,5)},t))H_{(2,5)}(L_{(2,5)},t)}{r_{(5,4)}(t)} \text{ if } Q_{(4,5)}(t) \leq 0, \tag{1.55}$$

$$H_{(6,3)}(0,t) = \frac{H_{(4,6)}(L_{(4,6)},t)Q_{(4,6)}(t) + H_{(5,6)}(L_{(5,6)},t)Q_{(5,6)}(t))}{Q_{(6,3)}(t)}, \tag{1.56}$$

where:

$$r_{(4,6)}(t) = \frac{Q_{(4,6)}(t)}{Q_{(1,4)}(t)}, r_{(5,6)}(t) = \frac{Q_{(5,6)}(t)}{Q_{(2,5)}(t)}, r_{(4,5)}(t) = \frac{Q_{(4,5)}(t)}{Q_{(1,4)}(t)}, r_{(5,4)}(t) = \frac{Q_{(5,4)}(t)}{Q_{(2,5)}(t)}.$$

The evolution of the haematocrit in each vessel is governed by the PDE in Equation (1.23). We do not derive the full set of network equations for every network motifs we study in the main text of this thesis. However, the full set of the network equations for the remaining networks in this thesis can be found in Appendix A.

1.8.1 Non-dimensionalisation of the equations

Let $\mathcal{N} = \{N, E\}$ be a network with n nodes and m vessels. The time-dependent network equations have a common independent time variable but every haematocrit variable depends

on a different spatial variable. Let t denote the independent time variable and let x_i denote the independent spatial variable for the ith vessel. The goal is to find a non-dimensionalisation such that the resulting equations are defined in one independent time and spatial variable, $(\tilde{t}, x)$ such that $(t, x_1, x_2, ..., x_m) = (\beta\tilde{t}, \alpha_1 x, \alpha_2 x, ..., \alpha_m x)$. As $x_i \in [0, L_i]$, we fix $\alpha_i = L_i$. Under this coordinate transformation, the average viscosity of the blood is simplified:

$$\overline{\mu}_i(t) = \frac{1}{L_i}\int_0^{L_i} \mu(H(x_i, t))dx_i = \int_0^1 \mu(H(L_i x, t))dx. \tag{1.57}$$

Let $\tilde{H}(x, \tilde{t}) = H(L_i x, \beta\tilde{t}) = H(x_i, t)$,then:

$$\frac{\partial\tilde{H}}{\partial\tilde{t}} = \beta\frac{\partial H}{\partial t}, \frac{\partial\tilde{H}}{\partial x} = L_i\frac{\partial H}{\partial x_i}. \tag{1.58}$$

Then from Equation (1.23) with the the velocity of the blood defined by Equation (1.31), we obtain the following PDE for the haematocrit:

$$\frac{1}{\beta}\frac{\partial\tilde{H}}{\partial\tilde{t}} + \frac{(D_i/L_i)^2\Delta P_i(\tilde{t})}{32\overline{\mu}_i(\tilde{t})}\frac{\partial\tilde{H}}{\partial x} = 0, \tag{1.59}$$

such that Δ_{Pi} is the pressure difference across the ith vessel. Ideally, β is chosen to simplify the PDE. Each pressure is smaller than the largest input pressure, $P_{\max}$. The viscosity $\overline{\mu}_i(t) = \mu_p\overline{\mu}_i^{(\mathrm{rel})}(t)$ (Equations (1.3) and (1.6)). With:

$$\beta = \frac{32\mu_p}{P_{\max}}, \tag{1.60}$$

the non-dimensionalised PDEs[5] reduce to the following form:

$$\frac{\partial\tilde{H}}{\partial\tilde{t}} + \overline{\tilde{u}}(\tilde{t})\frac{\partial\tilde{H}}{\partial x} = 0, \tag{1.61}$$

were:

$$\overline{\tilde{u}}(t) = \frac{(D_i/L_i)^2(\Delta P_i(\tilde{t})/P_{\max})}{\overline{\mu}_i^{(\mathrm{rel})}(\tilde{t})}. \tag{1.62}$$

Henceforth, tildes will be dropped, t will refer to the dimensionless time variable and x will refer to the dimensionless spatial variable. Furthermore, only one spatial variable, $x \in [0, 1]$ will be needed to describe the system of PDEs.

[5]In this thesis, we use $\beta = 32/P_{\max}$ instead because we found that the time-dependent equations were easier to solve if we did not include the plasma viscosity in non-dimensionalisation.

1.9 Properties of the system

The volumetric flows influence the haematocrit values, and the volumetric flows in each vessel depend on the vessel haematocrit. Due to this nonlinear coupling between these variables, computing solutions to the steady-state network equations is difficult for large networks. However, the equations have important properties that facilitate solving these equations. In this section, we describe important properties that have not previously been described in the literature for vasculature networks.

1.9.1 Nodes with degree 2

Although all networks studied in this thesis comprise of boundary nodes with degree 1 and non-boundary nodes with degree 3, it is possible to divide vessels into vessel segments by introducing nodes with degree 2. Vessels in vascular networks often break vessels up into two or more vessel segments (Bernabeu et al., 2020; Karst et al., 2017). This modification does not make a significant difference to the equilibria. For example, consider a network $\mathcal{N} = \{N, E\}$ such that $(x, y) \in E$ and for a given equilibrium (P, H) such that $P_x > P_y$. Consider a new network $\hat{\mathcal{N}} = \{\hat{N}, \hat{E}\}$ such that $\hat{N} = N \cup \{z\}$ and $\hat{E} = (E \setminus \{(x, y)\}) \cup \{(x, z), (y, z)\}$; $L_{(x,z)} = \alpha L_{(x,y)}$ and $L_{(y,z)} = (1 - \alpha)L_{(x,y)}$ for some $\alpha \in (0, 1)$; and $D_{(x,y)} = D_{(x,z)} = D_{(z,y)}$. Then conservation of flow and haematocrit dictate that:

$$Q_{(x,z)} = Q_{(z,y)},$$

$$Q_{(x,z)}H_{(x,z)} = Q_{(z,y)}H_{(z,y)}.$$

The addition of the new variables $H_{(x,z)}, H_{(z,y)}$ and P_z and the removal of the variable $H_{(x,y)}$ requires adaptation of the steady-state equations. If $F(H, P) = 0$ are the steady-state equations for the network $\mathcal{N} = \{N, E\}$, then $\hat{F}(\hat{H}, \hat{P}) = 0$ denotes the steady-state system of $\hat{\mathcal{N}} = \{\hat{N}, \hat{E}\}$. Furthermore, the equation $F_{(x,y)}(H, P) = 0$ is replaced with a equation $\hat{F}_{(x,z)}(\hat{H}, \hat{P}) = 0$ and the system of equations $\hat{F}(\hat{H}, \hat{P}) = 0$ must now include the equations $\hat{F}_z(\hat{H}, \hat{P}) = 0$ and $\hat{F}_{(z,y)}(\hat{H}, \hat{P}) = 0$. To ensure the conservation of flow and RBCs, at node z, $\hat{F}_z(\hat{H}, \hat{P})$ and $\hat{F}_{(z,y)}(\hat{H}, \hat{P})$ take the following forms:

$$\hat{F}_z(\hat{H}, \hat{P}) = Q_{(x,z)} - Q_{(z,y)}, \tag{1.63}$$

$$\hat{F}_{(z,y)}(\hat{H}, \hat{P}) = Q_{(x,z)}H_{(x,z)} - Q_{(z,y)}H_{(y,z)}. \tag{1.64}$$

$\hat{F}(\hat{H}, \hat{P})$ shares all other equations with $F(H, P) = 0$. The only non-trivial solutions to $\hat{F}_z(\hat{H}, \hat{P}) = 0$ and $\hat{F}_{(z,y)}(\hat{H}, \hat{P}) = 0$ are those for which $H_{(y,z)} = H_{(x,z)}$ and $Q_{(z,y)} = Q_{(x,z)}$. Given this condition, P_z can be defined in terms of P_x, P_y and α. Using the fact that $\mu_{(z,y)}(H_{(z,y)}) = \mu_{(z,x)}(H_{(z,x)})$, $D_{(x,z)} = D_{(y,z)} = D_{(x,y)}$, and $Q_{(x,z)} = Q_{(z,y)}$; using Equation (1.32), the following relation holds:

$$\frac{P_x - P_z}{\alpha} = \frac{P_z - P_y}{1 - \alpha}. \tag{1.65}$$

As a result, we observe that:

$$P_z = (1 - \alpha)P_x + \alpha P_y. \tag{1.66}$$

By replacing the variable P_z in Equation (1.32) with the expression in Equation (1.66) we obtain the following equality:

$$Q_{(x,z)} = \frac{(P_x - P_z)\pi D_{(x,z)}^4}{128\alpha L_{(x,y)}\mu_{(x,z)}(H_{(x,z)})} = \frac{(P_x - (1-\alpha)P_x - \alpha P_y)\pi D_{(x,z)}^4}{128\alpha L_{(x,y)}\mu_{(x,z)}(H_{(x,z)})} \tag{1.67}$$

$$= \frac{(P_x - P_y)\pi D_{(x,y)}^4}{128 L_{(x,y)}\mu_{(x,y)}(H_{(x,z)})} = \frac{(P_x - P_y)\pi D_{(x,y)}^4}{128 L_{(x,y)}\mu_{(x,y)}(H_{(x,y)})} = Q_{(x,y)}. \tag{1.68}$$

As a result, $Q_{(x,z)}$ or $Q_{(z,y)}$ can be replaced by $Q_{(x,y)}$ in the system of steady-state equations. Therefore, any equilibrium for the vessel network $\mathcal{N} = \{N, E\}$, can be extended to an equilibrium of $\hat{\mathcal{N}} = \{\hat{N}, \hat{E}\}$ such that the values of the haematocrits of the new vessel segments are equal to the haematocrit of the original vessel. This process can be repeated to break up a vessel into an arbitrary number of segments.

1.9.2 Reduction to a linear set of equations

An important property of the system of steady-state network equations is the reduction of the equations to a set of linear equations. The only possible haematocrit distribution for a network with 0 inlet haematocrit in all inlet vessels is that of 0 haematocrit in all vessels. As a consequence, the viscosity of the blood in each vessel is a constant. Therefore, the conservation of flow equations (Equation (1.41)) form a linear set of equations for the pressure variables. This result implies that for multiple equilibria to exist, at least one inlet haematocrit must be positive.

A similar set of linear equations can also be formed by setting the haematocrit value of every vessels to any set of constant values so long as the haematocrit values are less than 1.

1.9.3 Properties of a convergence unit

Conservation of flow and RBCs at a convergence unit means that the haematocrit value in the outflowing vessel of a convergence unit in Figure 1.3b is lower than the haem in one of the inlet vessels. Rearranging the solutions to $F_{(v,w)} = 0$ for Equation (1.39) yields the following expression:

$$H_{(v,w)} = \frac{Q_{(u,v)}}{Q_{(v,w)}} H_{(u,v)} + \frac{Q_{(z,v)}}{Q_{(v,w)}} H_{(v,z)}. \tag{1.69}$$

This expression simplifies to the following form:

$$\underbrace{\frac{Q_{(u,v)}}{Q_{(v,w)}}}_{=r} H_{(u,v)} + \left(1 - \frac{Q_{(u,v)}}{Q_{(v,w)}}\right) H_{(v,z)} = H_{(v,w)}. \tag{1.70}$$

We obtain the following:

$$H_{(v,w)} = rH_{(u,v)} + (1-r)H_{(z,v)}. \tag{1.71}$$

As $0 \leq r \leq 1$, we have that:

$$\min(H_{(z,v)}, H_{(u,v)}) \leq H_{(v,w)} \leq \max(H_{(z,v)}, H_{(u,v)}). \tag{1.72}$$

1.9.4 Properties of a bifurcation unit

Similar results can be obtained at flow bifurcations. Consider the bifurcation unit in Figure 1.3a. With $F_{(v,w)}(H, P)$ defined by Equation (1.37), if $F_{(v,w)}(H, P) = 0$ then we have that:

$$H_{(v,w)} = \psi_{(v,w)}(\underbrace{Q_{(v,w)}/Q_{(u,v)}}_{=r}, H_{(u,v)}) \underbrace{\frac{Q_{(u,v)}}{Q_{(v,w)}}}_{=1/r} H_{(u,v)}, \tag{1.73}$$

for the haematocrit in the daughter vessel, $H_{(v,w)}$. is obtained by rearranging Equation (1.39). With $F_v(H, P)$ defined by Equation (1.41), if $F_v(H, P) = 0$ then Equation (1.73) simplifies to give:

$$H_{(v,w)} = \frac{1}{r}\psi_{(v,w)}(r, H_{(u,v)})H_{(u,v)}. \tag{1.74}$$

This equation is important because $H_{(v,w)}$ is greater than or less than $H_{(u,v)}$ depending on the properties of $\psi_{(v,w)}$ and the value of r.

Consider the general splitting rule of Equation (1.37) with:

$$A = -\frac{7}{D_{(u,v)}}\frac{(D_{(v,w)} - D_{(v,z)})}{(D_{(v,w)} + D_{(v,z)})}, P = 2.0, X_0 = 0.05.$$

In Figure 1.4, we sketch the ratio $\psi_{(v,w)}(r)$[6] for two sets of values of the diameters for the bifurcation unit in Figure 1.3a. In Figure 1.4a $D_{(v,w)} = D_{(v,z)}$, while in Figure 1.4b $D_{(v,w)} = 100\mu m, D_{(v,z)} = 5\mu m$ and $D_{(u,v)} = 10\mu m$. If $r = 0.6$ and the diameters of the daughter vessels are equal, Figure 1.4a indicates that $\psi_{(v,w)}(r)/r > 1$. In contrast, if $r = 0.6$ and the diameters of the vessels are the same as those used to generate Figure 1.4b, $\psi_{(v,w)}(r)/r < 1$. Therefore, the haematocrit in the daughter vessel depends on the splitting rule and the network parameters. However, if $A = 0$, $\psi_{(v,w)}(r) \geq r$ for $r \geq 0.5$ for all values of P and X_0. In this case, the daughter vessel with the larger flow also has a greater haematocrit value than the parent vessel.

A similar expression can be formulated for the haematocrit in the other daughter vessel, $H_{(v,z)}$. It is straightforward to show that:

$$H_{(v,z)} = \frac{(1 - \psi_{(v,w)}(r))}{1 - r} H_{(u,v)}. \tag{1.75}$$

If $\psi_{(v,w)}(r) > r$, then $1 - \psi_{(v,w)} < 1 - r$ and $H_{(v,z)} < H_{(u,v)}$. (and conversely when $\psi_{(v,w)}(r) < r$). We conclude that, the haematocrit value of one daughter vessel is always greater than the haematocrit value of the parent vessel and the haematocrit value of the other daughter vessel is always less.

Another important property of a splitting rules is the existence of maxima in Figures 1.4c and 1.4d. Both figures show the plot of:

$$f_{(v,w)}(r) = \frac{\psi_{(v,w)}(r)}{r}, \tag{1.76}$$

which is also the scaling factor for the daughter haematocrit in Equation (1.74). Equation (1.76) is once differentiable on $(0, 1)$ because $\phi_{(v,w)}(r)$ and $1/r$ are both once differentiable on $(0, 1)$. This maxima always exists in an interval between $(r_1, 1 - X_0)$, where r_1 is the value of $r \in (0, 1)$ for which $f_{(v,w)}(r_1) = 1$. Taking the derivative of $f_{(v,w)}(r)$ with respect

[6] As the values of A, P and X_0 do not depend on $H_{(u,v)}$, the splitting rule reduces to a function of r.

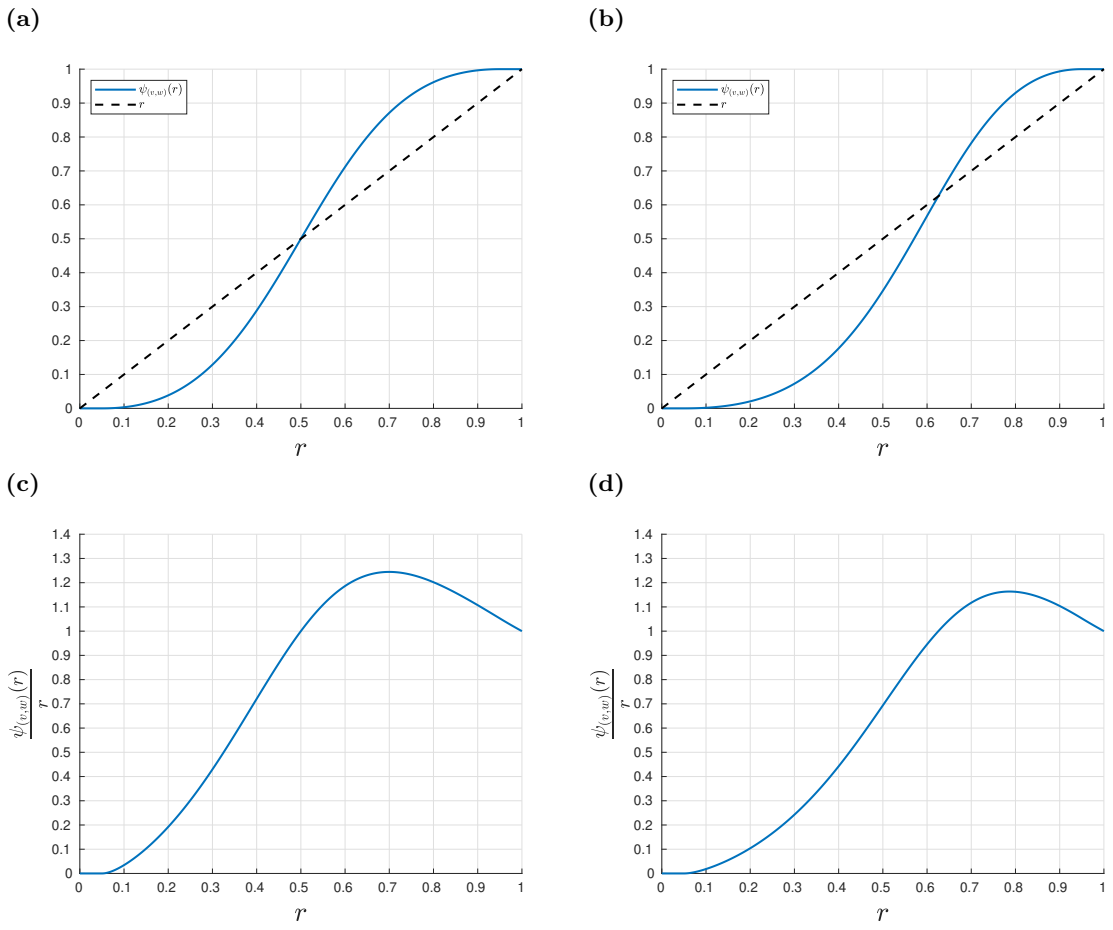

Figure 1.4: Comparison of $\psi_{(u,v)}$ with the two different parameter sets for the bifurcation unit in Figure 1.3a. (a): Plot of $\psi_{(u,v)}(r)$ for the vessel diameters $D_{(v,w)} = D_{(v,z)}$; (b): Plot of $\psi_{(u,v)}(r)$ when $D_{(v,w)} = 100\mu$m $, D_{(v,z)} = 5\mu$m and $D_{(u,v)} = 10\mu$m; (c): Plot of $\psi_{(u,v)}(r)/r$ when $D_{(v,w)} = D_{(v,z)}$; (d): Plot of $\psi_{(u,v)}(r)/r$ $D_{(v,w)} = 100\mu$m $, D_{(v,z)} = 5\mu$m and $D_{(u,v)} = 10\mu$m.

to r, it is straightforward to show that:

$$f'_{(v,w)}(r) = \frac{1}{r}(\psi'_{(v,w)}(r) - f_{(v,w)}(r)). \tag{1.77}$$

$\psi_{(v,w)}(r_1) > 1$, because $\psi_{(v,w)}(r)$ intersects r at $r = r_1$. We deduce that:

$$f'_{(v,w)}(r_1) = \frac{1}{r_1}(\underbrace{\psi'_{(v,w)}(r_1)}_{>1} - \underbrace{f_{(v,w)}(r_1)}_{=1}) > 0. \tag{1.78}$$

Since $\psi'_{(v,w)}(1 - X_0) = 0$ we have that:

$$f'_{(v,w)}(1 - X_0) = \frac{1}{1 - X_0}(\underbrace{\psi'_{(v,w)}(1 - X_0)}_{=0} - f_{(v,w)}(1 - X_0)) < 0. \tag{1.79}$$

Since $f'_{(v,w)}(r_1) > 0$ and $f'_{(v,w)}(1-X_0) < 0$, a maxima must exist in the interval $(r_1, 1-X_0)$. Another consequence of Equation (1.76) is that the value of the haematocrit in the daughter vessel with larger flow will eventually decrease as the flow ratio approaches 1.

1.9.5 Acyclic flow

As blood flow is driven by pressure gradients, the possible directions of blood flow in a network are restricted. Consider a vascular network network $\mathcal{N} = \{N, E\}$ with m vessels and n nodes. Let G be a directed network that has the same nodes and edges as $\mathcal{N}$ but the edges are directed. Let $\mathcal{G}_\mathcal{N}$ be the set of all directed networks based on network $\mathcal{N}$ for which: all inlet and outlet nodes have degree 1, all interior nodes have a minimum in degree of 1 and minimum out degree of 1, and the direction of flow can be induced by a distribution of nodal pressures. Another description of the criteria of $\mathcal{G}_\mathcal{N}$, is a set of directed networks that correspond to the possible directions of blood flow in $\mathcal{N}$. One consequence of these criteria is that all networks $G \in \mathcal{G}_\mathcal{N}$ must be acyclic because flow loops are not possible. A loop in a network is any path that starts and stops at the same node. Loops are not possible for the set of equations because the direction of flow in a vessel, (x, y), is dictated by values of P_x and P_y. For the flow in vessel (x, y) to flow from x to y, $P_x > P_y$. Now consider a sequence of k nodes, $\{u_i\}_{i=1}^k$, such that $u_1 = x, u_k = x, u_i \neq x$ for $1 < i < k$. For this loop to belong to a network $G \in \mathcal{G}_\mathcal{N}$, this would imply that:

$$P_x > P_{u_1} > .... > P_{u_{k-1}} > P_x. \tag{1.80}$$

This is clearly a contradiction. Therefore, loops of flow cannot exist. An important consequence of this property is that the number of possible flow directions in a network is limited by the topology of the network.

Definition 1.2. (Redundant vessels)
Consider a network $\mathcal{N} = \{N, E\}$. Let $\mathcal{G}_{\mathcal{N}}$ denote the set of all acyclic directed networks of $\mathcal{N}$. If $G_1 = \{N, E_1\} \in \mathcal{G}_{\mathcal{N}}$ and $G_2 = \{N, E_2\} \in \mathcal{G}_{\mathcal{N}}$ such that a vessel $(x, y) \in E, (x, y) \in E_1$ and $(y, x) \in E_2$, then vessel (x, y) is known as a redundant vessel.

The term "redundant vessel" was first used by Ben-Ami et al. (2022) to describe a vessel for which a solution existed with a haematocrit value of 0 in that specific vessel. However, the key topological property of the network that led to multiple equilibria and instability of the blood flow was the fact that the flow direction was not fixed in this vessel. Therefore, the redundant vessel introduced by Ben-Ami et al. (2022) is consistent with Definition 1.2.

If a vessel is not a redundant vessel, then it is known as a fixed vessel. From now on, we use triangular bracket notation to denote redundant vessels. For example, if a vessel between node x and node y is a redundant vessel, then this vessel is denoted by $\langle x, y \rangle$. Round brackets will be used as the notation for fixed vessels.

1.9.6 Single inlet/outlet networks

As the equations of flow and haematocrit are posed in terms of ratios of flow, the haematocrit distribution of a network with a single inlet and outlet vessel is independent of the inlet and outlet pressure. For example, consider a network $\mathcal{N} = \{N, E\}$ with n nodes and m edges. If the network nodes are indexed with $i \in \{1, ..., n\}$, let 1 be the inlet node and n be the outlet node. For any solution to the network equations, (P, H), let:

$$\{P_1, P_2, P_3, ..., P_{N-1}, P_n\} \text{ and } \{Q_{(x_1,y_1)}, Q_{(x_2,y_2)}, ..., Q_{(x_M,y_M)}\},$$

be the corresponding pressures and flows of the network. If the following transform is applied to every pressure:

$$\{\alpha(P_1 - \beta), \alpha(P_2 - \beta), \alpha(P_3 - \beta), ..., \alpha(P_{n-1} - \beta), \alpha(P_n - \beta)\}, \tag{1.81}$$

such that $\alpha > 0$ and $\beta < P_n$. Using the formula for flow in a vessel in Equation (1.32), the ratio of flows for any two vessels can be shown to be independent of this pressure

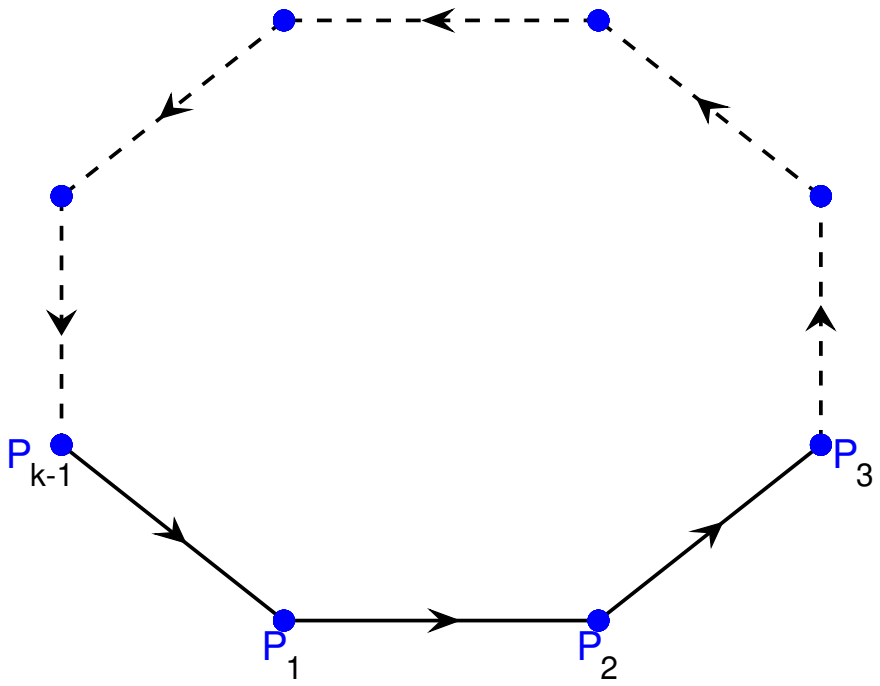

Figure 1.5: Diagram of a possible flow loop in a vasculature network.

transformation:

$$\frac{\frac{\pi D^4_{(x_i,y_i)}\left(\alpha\left(P_{x_i}-\beta\right)-\alpha\left(P_{y_j}-\beta\right)\right)}{128L_{(x_i,y_i)}\mu_{(x_i,y_i)}\left(H_{(x_i,y_i)}\right)}}{\frac{\pi D^4_{(x_j,y_j)}\left(\alpha\left(P_{x_j}-\beta\right)-\alpha\left(P_{y_j}-\beta\right)\right)}{128L_{(x_j,y_j)}\mu_{(x_j,y_j)}\left(H_{(x_j,y_j)}\right)}} = \frac{\frac{\pi D^4_{(x_i,y_i)}\left(P_{x_i}-P_{y_i}\right)}{128L_{(x_i,y_i)}\mu_{(x_i,y_i)}\left(H_{(x_i,y_i)}\right)}}{\frac{\pi D^4_{(x_j,y_j)}\left(P_{x_j}-P_{y_j}\right)}{128L_{(x_j,y_j)}\mu_{(x_j,y_j)}\left(H_{(x_j,y_j)}\right)}} = \frac{Q_{(x_i,y_i)}}{Q_{(x_j,y_j)}}. \tag{1.82}$$

Therefore, the flow ratios are independent of the choice of inlet and outlet pressures. As a consequence, the haematocrit distribution is the same regardless of the choice of pressure boundary conditions. Therefore, the inlet and outlet pressures can be adjusted to any pair of non-zero values without altering the haematocrit distribution using the transformation in Equation (1.81), so long as $P_1 > P_n$. A similar result is true for a network with a single outlet and multiple inlets by setting β to the value of the outlet pressure.

Conservation of flow and RBCs also dictates that the inlet haematocrit must be equal to the outlet haematocrit. For the example network, let $(1, 2)$ and $(n-1, n)$ correspond to

the inlet and outlet vessels. Then by conservation of flow and RBCs:

$$Q_{(1,2)} = Q_{(n-1,n)}, \tag{1.83}$$

$$Q_{(1,2)}H_{(1,2)} = Q_{(n-1,n)}H_{(n-1,n)}, \tag{1.84}$$

$$H_{(1,2)} = H_{(n-1,n)}. \tag{1.85}$$

1.10 Discussion

The construction of network equations are presented in this chapter are used througout this thesis because the equation construction allows for the derivation of the network equations for any size system using the same types of equations. The structure of the network equations not only allows for the derivation of equations from the network geometry and boundary conditions, but also facilitates some of the numerical techniques that we utilise to solve the system of steady-state network equations. These methods are described in Chapters 2 and 3.

Using the modelling framework described in this chapter, we will demonstrate a mechanism that may generate cycling-hypoxia within the tumour microenvironment. Bernabeu et al. (2020) showed that equilibria of blood flow within networks can result in the formation of chronic-hypoxia. We wish to demonstrate a similar mechanism for cycling-hypoxia. However, since cycling-hypoxia is a time-dependent process, we must include the time-dependent blood flow equations in our proposed mechanism. Ben-Ami et al. (2022) proposed that cycling-hypoxia could arise from the formation of self-sustained oscillations of blood flow. However, we propose that cycling-hypoxia results from the blood flow switching between multiple equilibria as an alternative hypothesis. We hypothesise that these switching events could either arise from stochastic fluctuations of RBC partitioning at flow bifurcations or from constantly changing network boundary conditions.

As we focus on deriving network properties that lead to multiple steady-state solutions, we restrict our attention to small motifs. Section 1.1 describes some of the key observations of the vasculature in tumours compared with healthy vasculature. Some of the key characteristics that are commonly described are the wide range of vessel diameters and the presence of loops. Therefore, the geometry of synthetic networks in this thesis should exhibit these characteristics. We also investigate the role of certain vessels, known as shunts, in redirecting blood flow in vascular networks. Section 1.9.5 introduced the concepts of

redundant and fixed vessels. The presence of redundant vessels in synthetic networks naturally introduces shunts to synthetic networks because multiple flow pathways must exist for a redundant vessel to exist.

In what follows, we will focus on investigating the impact of redundant vessels. Vascular networks with redundant vessels are important to study because the structural similarities to tumour vasculature. We discussed how tumour vasculature can often form looped structures in Section 1.1, the presence of redundant vessels in vascular networks can introduce looped structures in synthetic networks. Not only do these redundant vessels mimic the structure of tumour vasculature, networks that have been shown to admit multiple equilibria also had multiple different flow directions. Gardner et al. (2010) showed that the triangle network admitted three equilibria and identified one vessel in which the flow was not fixed. Karst et al. (2017) showed that hexagonal and Voronoi networks may admit multiple equilibria. Where multiple equilibria existed, most equilibria were associated with a unique set of flow directions. Furthermore, the flow directions were only different for a small proportion of the vessels. Therefore, although they did not explicitly identify the vessels for which the flow direction could change, they were aware that the flow did not change direction in all vessels.

1.11 Thesis outline

In this chapter, we have explained the significance of chronic- and cycling-hypoxia, described how vascular networks differ between tumour and normal tissues, and reviewed the mathematical models of blood flow in vascular networks. We considered steady-state and time-dependent models for the blood flow in the vasculature. We showed how the models are constructed by combining Stokes flow in pipes and phenomenological laws describing the blood viscosity and how RBCs partition have been derived from in vivo experiments. Finally, we introduced some properties of vascular networks that have implications for the existence of multiple equilibria. These properties were included in this chapter because we refer to them throughout the thesis. Importantly, we introduce the concept of redundant vessels. In the remaining chapters, we will show how the existence of multiple equilibria depends on the presence of redundant vessels and propose a mechanism by which blood flow in redundant vessels may change direction.

In Chapter 2 we review some of the techniques that we use to solve the network equations.

In Chapter 3 we investigate the impact of redundant vessels on the multiplicity of steady-state solutions for specific network motifs. Here, we are primarily interested in determining the relationship between the number of redundant vessels and the number of equilibria. More specifically, we show that the upper bound on the number of equilibria increases exponentially with the number of redundant vessels. By linking the number of equilibria to the number of redundant vessels, we aim to improve predictions about the number of possible equilibria a network may admit. We also show that for multiple equilibria to exist, the flow direction in at least one redundant vessel must be different for one of the equilibria. Furthermore, we show a consistent pattern of multiple equilibria, which applies to all network motifs that we study in the chapter for a range of vessel length ratios and network boundary conditions.

In Chapter 4 we show how the link between network redundancy and multiple equilibria applies to specific networks for a range of vessel diameters. Microcirculation contains vessels with diameters as large as 300μm, and blood behaves differently in vessels with smaller diameters. Due to the complication of investigating the link between redundancy and equilibria across a wide range of diameter scales and ratios.

In Chapter 5 we introduce mechanisms that may cause the direction of blood flow within redundant vessels to change. At the same time, we show how the time-dependent solutions switch between stable equilibria. As the distribution of RBCs within a network are different for each equilibrium, showing how these switches occur links the results in Chapters 3 and 4 with cycling-hypoxia. For this investigation, we introduce a deterministic mechanism based on hysteresis and a stochastic mechanism for switching between equilibria. The stochastic mechanism is especially important because unlike the deterministic mechanism, this mechanism does not require any additional inputs into the model. Therefore, it enables us to investigate how the time scales between switches depend on properties of the networks.

Finally, in Chapter 6 we discuss the implications of our results and how they provide insight into possible causes of cycling-hypoxia. We also outline possible directions for future investigation which have been made possible by our findings.

Chapter 2

Methods

2.1 Introduction

Given the complicated nonlinear coupled relationship between volumetric flow and discharge haematocrit of the steady-state network equations in Section 1.7, it is difficult to solve these equations for large networks. In this thesis, our aim is to determine if a mechanism exists that is able to push the time-dependent solution between multiple stable equilibria. Therefore, we require a numerical scheme that converges to the solution of the time-dependent equations described in Sections 1.4 and 1.8, and a numerical method capable of determining multiple solutions to the nonlinear steady-state network equations described in Section 1.7. The PDE for the motion of haematocrit in a vessel (Equation (1.23)) is in the form of the transport equation and there are many different schemes that can be applied to this problem. Furthermore, there is more literature on solving the time-dependent network equations (Ben-Ami et al., 2022; Carr and Lacoin, 2000; Carr et al., 2005; Davis and Pozrikidis, 2011; Geddes et al., 2007; Karst et al., 2017; Pop et al., 2007).

Solving the steady-state equations is more difficult than solving the time-dependent equations because the equations are coupled and nonlinear. Occasionally, it is possible to reduce the network equation to a single nonlinear equation (Gardner et al., 2010). When this is possible enumerating the solutions of this equation is feasible without the use of a complicated numerical method. However, this is rarely the case. Therefore, we require a more general method to reliably solve the system of network equations and find multiple solutions for a range of different network geometries. It has been shown in the literature that it is relatively easy to compute a single equilibrium for a network compared with computing multiple solutions. Furthermore, it is difficult, if not impossible, to determine if a set of

solutions is complete.

This chapter will contain a discussion of some of the methods used to solve both the steady-state and time-dependent network equations, as well as a full description of the techniques that we use throughout the thesis. This chapter contains the following sections: Section 2.2 details some of the methods that have been used to solve the network equations using pressure boundary conditions and describes in more detail the particular methods used in this thesis; Section 2.3 contains a discussion of the numerical methods for solving the system of network PDEs; and in Section 2.4 we discuss why the methods we use in this thesis have been selected.

2.2 Methods for solving the steady-state equations

The first method we discuss is the iterative approach to solving for the haematocrit distribution associated with the steady-state equilibrium. This method has been widely used to find the equilibria of vasculature networks (Bernabeu et al., 2020; Ganesan et al., 2010; Grogan et al., 2017; Kiani et al., 1994; Pries et al., 1990; Tawfik and Owens, 2013). Iterative methods are based on two properties of the network equations; the interior pressures are uniquely defined by the haematocrit distribution and the boundary conditions; and a unique haematocrit distribution can be defined by the flow and the previous haematocrit distribution. These two properties form a two step process to define a sequence which converges to the solution of steady-state network equations. A haematocrit distribution is used to uniquely define a set of pressures which, in turn, is used to define the flows for a network. Once the flow in every vessel is known, the haematocrit distribution and the flows are used to update the haematocrit distribution. The resulting sequence of haematocrit distributions, pressures, and flows will in theory converge to an equilibrium of the system for any initial starting haematocrit distribution.

Iterative methods are widely used to find a solution to the network equations for large networks. Pries et al. (1990) were some of the first to use this iterative approach to find the equilibria of networks based on rat mesentry. Using this method, they were able to evaluate networks with $436 - 913$ vessel segments. Bernabeu et al. (2020) used the same method to find the equilibria of a hierarchical network containing 46 vessels. Regardless of the network topology, this method does not restrict the choice of splitting rule, as long as it uses the same basic formula given in Equation (1.13), and in theory can be scaled to

any size network. However, the iterative approach relies on the assumption that the iteration will converge. Karst et al. (2017) demonstrated that the iterative approach displayed dynamic properties such as period-doubling and chaos for some choices of initial starting haematocrit distributions when computing the equilibria of a simple triangle network.

The other method we consider is that of numerical continuation. Continuation methods are a general set of methods that are used to find zeros of nonlinear systems of equations. Although they have rarely been used to find equilibria of vasculature networks, they have been successfully used to find multiple equilibria (Karst et al., 2017). Continuation methods are used primarily to solve systems comprising N nonlinear equations in N variables in the form:

$$F : \mathbb{R}^N \to \mathbb{R}^N,$$

where the Jacobian J_F, of F is of full rank. The idea underpinning continuation is that if a solution of $F = 0$ is known for a parameter value of the system and the solution of the system depends continuously on a parameter, it is possible to find solutions in the neighbourhood of the initial solution. For instance, let $F(x, \xi) = 0$ be a system of equations such that x is the set of variables and ξ is a parameter of the system. If the solution to $F(x, \xi) = 0$ is known for some $\xi = \xi_0$. This solution can be used to find a continuous set of solutions $x(\xi)$ which is implicitly defined by:

$$F(x(\xi), \xi) = 0. \tag{2.1}$$

We will now use the term zero of the system F when describing the solutions to Equation (2.1).

If a zero of F is not known for any value of ξ, it is possible to use numerical continuation to find a zero of F by construction of a homotopy function. Consider a different system of equations:

$$G : \mathbb{R}^N \to \mathbb{R}^N,$$

for which the zeros of G are trivial to find. A homotopy or deformation function deforms the zeros of G into the zeros of F[1]:

$$h : \mathbb{R}^{N+1} \to \mathbb{R}^N,$$

[1]In most of the literature, this function is denoted by $H : \mathbb{R}^{N+1} \to \mathbb{R}^N$. It has been changed here to address any possible confusion with the haematocrit variables H.

with the following proprieties; $h(x,1) = G(x)$ and $h(x,0) = F(x)$. G is known as the starting system and F is known as the target system. To find the zeros of F, one can track the paths from the known zeros of G such that $h(x,\xi) = 0, \forall \xi \in [0,1]$. However, the homotopy function must have certain properties for this method to be applicable. If we denote a zero of G by $\overline{x}$ and the corresponding zero of F by $\underline{x}$, then h must have the following properties:

1. A smooth curve $c(s) \in h^{-1}(0)$ must exist such that $(\overline{x}, 1)$ belongs to the range of $c(s)$.
2. $c : J \to \mathbb{R}^{N+1}$ such that J is an open interval.
3. The curve must intersect $F^{-1}(0)$ when $\xi = 0$.

The implicit function theorem guarantees the first and second properties so long as the Jacobian of $h(x,\xi)$ has full rank at the point $(\overline{x}, 1)$ (Any point that satisfies this condition is known as a regular point if h satisfies this condition), and a curve $c(s) \in h^{-1}(0)$ will belong to an open set containing $(\overline{x}, 1)$.

The second property is not true in all circumstances. However, so long as h satisfies some assumptions, it is possible to deduce two possible behaviours of the curve $c(s)$. For a function $f : \mathbb{R}^q \to \mathbb{R}^p$, if $y \in \mathbb{R}^p$ such that all $x \in f^{-1}(y)$ are regular points of f then y is known as a regular value. If 0 is a regular value of h then there are only two possibilities for the curve $c(s)$; (i) $c(s)$ is diffeomorphic to a circle, more precisely, $c(s_1) = c(s_2)$ if and only if $s_1 - s_2$ is an integer multiple of some T; (ii) $c(s)$ is diffeomorphic to the real line or c is injective and has no accumulation point for $s \to \pm\infty$. Details of the proof of these properties can be found in Allgower and Georg (2003). By carefully choosing G, we can ensure that $(\overline{x}, 1)$ is a regular point of h. It is possible that $c(s)$ never intersects $F^{-1}(0)$ if our curve is diffeomorphic to a circle. It is also possible that the curve $c(s)$ does not intersect $F^{-1}(0)$ because 0 is not a regular value of h. One strategy to overcome of these problems when finding zeros of F is to choose a different starting system, G, if h is unsuccessful at finding a zero of F.

Consider a homotopy function of the form of $h(x(\xi), \xi)$ and let $x(\xi)$ be the curve implicitly defined by $h(x(\xi), \xi) = 0$ starting at $(\overline{x}, 1)$. If we take the derivative of $h(x(\xi), \xi) = 0$ with respect to ξ, then we obtain the resulting system of differential equations, known as a Davidenko differential equation:

$$\frac{\mathrm{d}}{\mathrm{d}\xi} h(x(\xi), \xi) = J_h(x(\xi), \xi) \frac{\mathrm{d}x}{\mathrm{d}\xi} + \frac{\partial h}{\partial \xi}(x(\xi), \xi) = 0. \tag{2.2}$$

$J_h(x, \xi)$ is the Jacobian of $h(x, \xi)$ with respect to the variables $\{x_1, x_2, ..., x_n\}$. Therefore, to track the zeros of $G(x)$ to the zeros of $F(x)$, we simply need to numerically solve the differential equation from the initial value $(\overline{x}, 1)$, so that $G(\overline{x}) = 0$. In practice, finding the curve $x(\xi)$ will not solely be done by solving the system of differential equations because this method is inefficient. The most commonly accepted approaches to finding the curve is the predictor-corrector method or the piecewise linear method (Allgower and Georg, 2003). These methods allow for the curve to be traced more accurately by making corrections to the numerical solution of the ODE in Equation (2.2). Let (x_n, ξ_n) be a point on $(x(\xi), \xi)$, the predictor-corrector method uses Euler's method and the point (x_n, ξ_n) to find the point (y_0, ξ_{n+1}) that approximates the next point on the curve (x_{n+1}, ξ_{n+1}). Newton-Raphson's method is then used with this initial approximation y_0 to generate a sequence of points $\{y_i\}_{i=0}$. Once $|h(y_k, \xi_{n+1})| < \epsilon$ for some chosen tolerance, x_{n+1} is set to value of y_k. Another more complex method used to trace the curve is that of the piecewise-linear approximation method. We do not summarise this method in this thesis for the sake of brevity, but the details of this method can be found in Chapter 12 in Introduction to Numerical Continuation (Allgower and Georg, 2003).

Numerical continuation is not only useful for finding an initial zero of a system of equations. Once this zero is known, numerical continuation can be used to create a bifurcation diagram of the zeros as some key parameter varies. Instead of considering a homotopy function h, if we consider the following system of equations:

$$F : \mathbb{R}^{N+1} \to \mathbb{R}^N, \tag{2.3}$$

such that $x(\xi)$ is a zero of the system for the parameter value of ξ. Numerical continuation for finding the zeros of F as some parameter, ξ, changes is similar to finding an initial zero of F. If one zero of F is known for $\xi = \xi_0$ such that $(x(\xi_0), \xi_0)$ is a regular point, then numerical continuation can be used to find a curve $c(s)$ such that $c(0) = (x(\xi_0), \xi_0)$.

Unlike the system of equations h, 0 may not be a regular value for F. Therefore, the curve $c(s)$ may contain bifurcation points. For simplicity we focus on fold bifurcations because the existence of fold bifurcations for a system coincides with multiple equilibria. A fold bifurcation is a point, $c(s_1) = (x(\xi_1), \xi_1)$, at which one of the eigenvalues of $J_F(x(\xi_1), \xi_1)$ is equal to zero (Kuznetsov et al., 1998). The geometric implication of these fold points is that the curve $c(s)$ will contain a second branch that also tends towards the fold bifurcation. Test functions can detect bifurcation points by detecting a change in sign for a key

parameter. For example, a test function that detects the existence of a fold bifurcation for the system of equations $F(x, \xi) = 0$:

$$T(x, \xi) = \Pi_{i=1}^{n} \lambda_i(x, \xi), \tag{2.4}$$

where $\lambda_i(x, \xi)$ is the eigenvalue of $J_F(x, \xi)$. If the value of $T(x, \xi)$ changes sign between two points on the curve $c(s)$ then a fold bifurcation has occured. Test functions are also capable of detecting more complicated bifurcations points such as pitchfork and Hopf bifurcation but we restrict our attention to fold bifurcations in this thesis for simplicity. We will also not specify the types of test functions used for numerical continuation as we utilise standard software capable of detecting the fold bifurcations (Doedel et al., 1999).

2.3 Numerical methods for the time-dependent equations

The simplest method to solve the time-dependent network equations is to assume that the haematocrit in each vessel is well mixed by converting Equations (1.37) and (1.39) into the following:

$$\frac{\mathrm{d}\overline{H}_{(v,w)}}{\mathrm{d}t} = \psi_{(v,w)}(Q_{(v,w)}/Q_{(u,v)}, \overline{H}_{(u,v)})Q_{(u,v)}\overline{H}_{(u,v)} - Q_{(v,w)}\overline{H}_{(v,w)}, \tag{2.5}$$

$$\frac{\mathrm{d}\overline{H}_{(v,w)}}{\mathrm{d}t} = Q_{(u,v)}\overline{H}_{(u,v)} + Q_{(z,v)}\overline{H}_{(z,v)} + Q_{(w,v)}\overline{H}_{(w,v)}. \tag{2.6}$$

The subscript (v, w) in Equation (2.5) refers to the daughter vessel in the bifurcation unit in Figure 1.3a and the same subscript in Equation (2.6) refers to the outflow vessel in the convergence unit in Figure 1.3b. This method is known as the mixed method. Carr and Lacoin (2000) used the mixed method to evaluate the stability of a network and found that it predicted steady-states for networks for which other numerical methods resulted in oscillations. Therefore, this method is unreliable at accurately solving the time-dependent equations.

Various standard numerical schemes have been applied to the network PDEs in the literature. The Lax-Wernoff and Upwind schemes have been used by Geddes et al. (2007) to verify the instabilities of a simple two node network. The Upwind scheme has also been used by Davis and Pozrikidis (2011) to solve PDEs for branching networks. One problem with these schemes is that the numerical solution could lead to dispersive or diffusive behaviour (LeVeque, 2007). This is less of an issue for the networks studied by Geddes et al. (2007)

and Davis and Pozrikidis (2011) because they worked on networks with only one possible flow direction and the initial conditions chosen for the networks were smooth. However, this dispersive behaviour could prove to be more of an issue for networks with redundant vessels because the blood flow in the redundant vessels can change direction. When blood flow changes direction, there is no guarantee that haematocrit is uniformly 0 throughout the whole vessel, resulting in the formation of a discontinuity in the solution.

Pop et al. (2007) used the method of characteristics to evaluate the numerical solution to the PDEs with shocks and Carr and Lacoin (2000) used this method to solve PDEs for a network with redundant vessels. However, this method can be computationally expensive because it requires tracking the haematocrit distributions for every vessel. As our goal for solving time-dependent network equations is to understand when the solutions switches between stable equilibria, it is not necessary to understand how the haematocrit distribution evolves in each vessel.

The most common approach in the literature is to convert the system of PDEs described in Sections 1.4 and 1.8 into a system of Delay Differential Equations (DDEs). If we take the spatial average in the x direction for equations in the form of Equation (1.62).

$$\int_0^1 \frac{\partial H}{\partial t} \mathrm{d}x = -\int_0^1 \overline{u}(t) \frac{\partial H}{\partial x} \mathrm{d}x \tag{2.7}$$

$$\frac{\mathrm{d}\overline{H}}{\mathrm{d}t} = \overline{u}(t)(H(0,t) - H(1,t)). \tag{2.8}$$

Geddes et al. (2007), Carr et al. (2005) and Ben-Ami et al. (2022) used this method to study the dynamics of simple networks, but we will specifically focus on the method used by Ben-Ami et al. (2022). We converted this system of PDEs into a system of DDEs. The key step employed here is to use the fact that it takes a finite amount of time for haematocrit to propagate through a vessel. The haematocrit leaving the vessel at time t is equal to the haematocrit entering the vessel at some time $t - \tau(t)$ such that:

$$H(1,t) = H(0, t - \tau(t)). \tag{2.9}$$

As vessels have a fixed length, taking the integral of the propagation speed $\overline{u}$ between the limits of $(t - \tau(t), t)$, we know that:

$$1 = \int_{t-\tau(t)}^{t} \overline{u}(s) ds. \tag{2.10}$$

Therefore, $\tau(t)$ is the time needed to satisfy this equality. To find the average haematocrit, we need to solve the DDEs numerically, which is simpler than solving the PDEs. The difficulty of this method is determining the resistance of the vessel at time t. Carr et al. (2005) and Geddes et al. (2007) considered the resistance to be a function of the average haematocrit. This approximation does allow for the equations to be solved, but is an unnecessary simplification. Therefore, we will use the same method that we used in (Ben-Ami et al., 2022). If the partial derivative with respect to t is taken on both sides of the equation for the average viscosity, then the following differential can be derived:

$$\frac{\partial}{\partial t}\overline{\mu}(t) = \frac{\partial}{\partial t}\int_0^1 \mu(H(x,t))dx, \tag{2.11}$$

$$\frac{\mathrm{d}\overline{\mu}}{\mathrm{d}t}(t) = \int_0^1 \frac{\partial H}{\partial t}\frac{\mathrm{d}\mu}{\mathrm{d}H}dx, \tag{2.12}$$

$$\frac{\mathrm{d}\overline{\mu}}{\mathrm{d}t}(t) = -\overline{u}(t)\int_0^1 \frac{\partial H}{\partial x}\frac{\mathrm{d}\mu}{\mathrm{d}H}dx, \tag{2.13}$$

$$\frac{\mathrm{d}\overline{\mu}}{\mathrm{d}t}(t) = \overline{u}(t)[\mu(H(0,t)) - \mu(H(0,t-\tau(t)))]. \tag{2.14}$$

This differential equation can be calculated simultaneously with the equation for the average haematocrit, allowing the resistance and flow to also be known at time t. It is important to note that the differential equations for the average haematocrit are decoupled from the equations for the average viscosity. Both sets of differential equations depend on the haematocrit values at the beginning and end of each vessel, but these are both determined by the flow which are functions of the average viscosity.

The difficulty of this method is how to deal with vessels for which the flow can change direction. This method presents a different challenge from that presented by the mixed method. The system of equations for the mixed method could automatically take into account the direction of flow. The same does not apply to the DDEs, because the form of the equations depends on the haematocrit at either end of the vessel. When the direction of flow changes, the orientation of the two ends also changes, and this needs to be reflected by Equations (2.8) and (2.14). Furthermore, this complicates computing $H(1,t)$ because it is no longer possible to find a $\tau(t)$ such that Equation (2.10) holds if a sufficient amount of time has passed for the haematocrit to propagate from one end of the vessel to the other. This is also an issue for a small initial time interval, but this can be more easily circumvented by setting an initial haematocrit distribution and setting:

$$H(1,t) = H\Big(1 - \int_0^t \overline{u}(s)ds, 0\Big), \tag{2.15}$$

until:

$$1 = \int_0^t \overline{u}(s)ds. \tag{2.16}$$

Fortunately, it is still possible to use DDEs for networks with redundant vessels. Ben-Ami et al. (2022) devised a scheme by which the change in the direction of blood flow in a redundant vessel could be tracked and used to reconstruct the haematocrit values at the ends of the redundant vessels with changes in the direction of the flow. If we let τ_1 be the time at which $\overline{u} = 0$, the flow direction starts to reverse. We will adopt the convention that $H(1, t)$ is now the inlet haematocrit of the vessel at $t > \tau_1$ and $H(0, t)$ is now the outlet haematocrit for the vessel at $t > \tau_1$. Then the blood at time $t > \tau_1$ can only have travelled a length of L_1 along the vessel, which is defined as:

$$L_1 = \int_{\tau_1}^t \overline{u}(s)ds. \tag{2.17}$$

Assuming that $L_1 < 1$, this means that the blood has travelled L_1 back along the vessel displacing the haematocrit up to the length of L_1 from the vessel, and so:

$$H(0, t) = H(L_1, \tau_1). \tag{2.18}$$

A visual representation of the haematocrit from one end of the vessel displacing the haematocrit from the other end can be seen in Figure 2.1a. Therefore, to find the haematocrit for the outlet of the vessel, we need to find $H(L_1, \tau_1)$ but this can be done in a similar way to before, where the delayed time $\tau(\tau_1)$ can be found by solving for:

$$L_1 = \int_{\tau_1 - \tau(\tau_1)}^{\tau_1} \overline{u}(s)ds. \tag{2.19}$$

This means that:

$$H(0, t) = H(L_1, \tau_1) = H(0, \tau_1 - \tau(\tau_1)). \tag{2.20}$$

As soon as $L_1 = 1$, the equation reverts back to the original case, but with the flow in the opposite direction. It is possible that the flow changes direction again before $L_1 = 1$. If this occurs, we can use the same trick again with some alterations. If we now let τ_2 be the

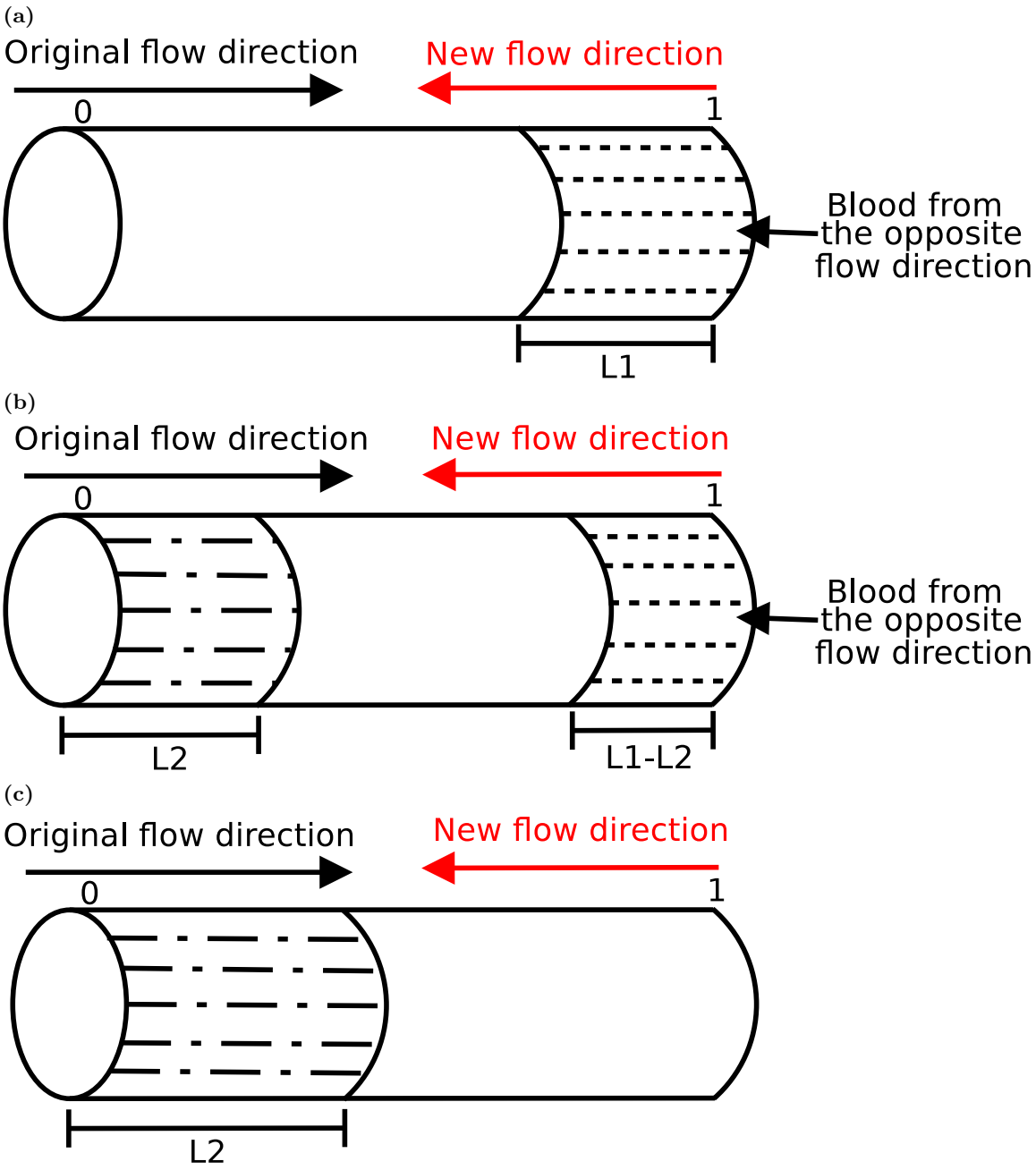

Figure 2.1: Vessel diagrams of the sequential cases for two changes of flow direction with a redundant vessel in a vascular network. (a): Vessel diagram showing the progress of the red blood cells along a non-dimensionalised vessel at time t for which the flow direction has changed once. (b): Vessel diagram showing the progress of the red blood cells along a non-dimensionalised vessel at time t for which the flow direction has changed twice and $L_2 < L_1$. (c): Vessel diagram showing the progress of the red blood cells along a non-dimensionalised vessel at time t for which the flow direction has changed twice and $L_2 \geq L_1$.

time for the second change in flow direction, then we define the following.

$$L_1 = \int_{\tau_1}^{\tau_2} \overline{u}(s)ds, \tag{2.21}$$

$$L_2 = \int_{\tau_2}^{t} \overline{u}(s)ds. \tag{2.22}$$

Assume that $L_2 < L_1$, then a similar situation to L_1 occurs, but in reverse. Blood travels a distance of L_2 along the vessel and blood up to the point of $L_1 - L_2$ is displaced from the vessel at the opposite end. A similar calculation can be performed to find the average haematocrit at the boundary:

$$H(1,t) = H(1 - L_2, \tau_2) = H(1, \tau_2 - \tau_2(\tau_2)), \tag{2.23}$$

where $\tau(\tau_2)$ is implicitly defined by:

$$L_2 = \int_{\tau_2 - \tau(\tau_2)}^{\tau_2} \overline{u}(s)ds. \tag{2.24}$$

A visual representation of the haematocrit from one end of the vessel displacing the haematocrit from the other end can be seen in Figure 2.1b. If $1 > L_2 > L_1$ then:

$$H(1,t) = H(1 - L_2 + L_1, \tau_1) = H(0, \tau_1 - \tau(\tau_1)), \tag{2.25}$$

where $\tau(\tau_1)$ is implicitly defined by:

$$1 - L_2 + L_1 = \int_{\tau_1 - \tau(\tau_1)}^{\tau_1} \overline{u}(s)ds. \tag{2.26}$$

This last case is visually represented by Figure 2.1c. When $L_2 > 1$ the equation reverts back to the original case before the flow changed direction at τ_1. It is possible for further cases of flow reversal to occur, in which case it is possible to define a sequence of lengths $\{L_i\}_{i=1}^{n}$ with the following formula:

$$L_i = \begin{cases} \left| \int_{\tau_i}^{\tau_{i+1}} \overline{u}(s)ds \right| & i < n, \\ \int_{\tau_i}^{t} \overline{u}(s)ds & i = n, \end{cases} \tag{2.27}$$

where τ_i defines the times at which the flow direction is reversed. As long as $1 > L_1 > L_2 > ... > L_n$, the sequence can be used to construct the haematocrit at the ends of the vessel. As soon as $L_n \geq L_{n-1}$, the sequence of lengths is replaced by $\{L_i\}_{i=1,i\neq n-1}^{n}$. As the interval $(0, 1)$ can be continuously divided, these rules can be applied recursively to the vessel because the sum of the lengths will always be less than 1 by construction.

This method has had some encouraging results. It has been shown in the literature that this method has correctly identified stable steady-states and oscillatory limit cycles for networks (Carr et al., 2005). Therefore, it is suitable for the purpose of correctly identifying stability of the equilibria. This method does have the drawback of not saving the distribution of haemaocrit over time changes, but this can be recreated from the speed of propagation function. However, this may be difficult to do at every time point especially if multiple changes in the flow direction in redundant vessel has occurred.

2.4 Discussion

For the remainder of this thesis, numerical continuation is used to find zeros of the system of network equations and DDEs are used to find time-dependent solutions. As discussed in Section 2.2, so far, only numerical continuation has proven successful at finding multiple equilibria in vasculature networks with more than six vessels. Numerical continuation is also useful because it allows for the generation of bifurcation diagrams. However, numerical continuation does have limitations. It is not clear which starting system, if any, would result in a path to the solution of the target system. For the specific purpose of solving the system of steady-state network equations, we consider more than one option for the starting system in Chapter 3 but this does not provide a theoretical guarantee of finding an equilibrium of the network. We did explore the possibility of using Homotopy continuation to solve the network equations because this has a theoretical guarantee of finding the zeros of an algebraic system of equations. It is possible to convert the system of steady-state network equations into an algebraic approximation that can be solved using homotopy continuation, but this method scales too poorly with network size to be practical, and so we do not provide details of this algebraic approximation in this thesis.

Converting the system of PDEs into a system of DDEs is advantageous for two reasons. The haematocrit distribution for every vessel does not need to be explicitly found which improves the computational expense for solving the system of equations for a whole network. Furthermore, the haematocrit distribution for any vessel is recoverable by using the history

of the haematocrit at the ends of the vessels and the volumetric flow. Secondly, converting the system into DDEs is also useful because we will modify the system of DDEs with the addition of stochastic noise in Chapter 5.

Chapter 3

Implications of network redundancy on multiple equilibria

3.1 Introduction

Vascular networks come in a wide range of geometries and topologies. Due to the complicated nonlinearity of the network equations, it is unclear whether the properties of a specific network leading to the existence of multiple equilibria generalise to other networks. Two networks that share common parameters, such as inlet haematocrits, can admit different numbers of equilibria even if the two network topologies are similar. Predicting the existence of multiple equilibria in a network based on equilibria of subnetworks may not be possible because even the addition of a single new vessel to a network may completely change the number of equilibria. One of the fundamental issues with finding network equilibria is the lack of understanding behind the causes of multiplicity of solutions. This chapter addresses this issue by linking the existence of multiple equilibria with the direction of blood flow in the network. Furthermore, the relationship between the stability of the equilibria and the flow direction in a network is also explored.

We remind the reader of the concept of redundant and fixed vessels first discussed in Section 1.9.5; the topology of the network allows the flow direction of certain vessels to change, these are known as redundant vessels (Definition 1.2), and vessels for which the flow direction cannot change are known as fixed vessels. As described in Section 1.9.5, all vessels that are specified with triangular brackets ($\langle, \rangle$) are redundant vessels and all fixed vessels are denoted by circular brackets. Karst et al. (2017) observed that the number of equilibria admitted by

honeycomb and Voroni networks correlated with the number of viable flow directions in the two networks. Almost all equilibria have a corresponding unique flow direction through the two networks. Distinguishing between different equilibria using the flow direction is more useful than comparing the haematocrit or volumetric flows of individual vessels because comparing flow directions allows for a natural categorisation of the equilibria into discrete sets. Comparing two equilibria via continuous values, such as haematocrits or volumetric flows, does not allow for the same categorisation. For example, if more than two equilibria were compared using the haematocrit of a specific vessel, it would be possible to group sets based on some specified ordering. For instance, each set could be defined by some interval of values and equilibria with a haematocrit value in that interval belong to that set. The danger of categorising the equilibria using some imposed order is that this order is arbitrary without some prior knowledge of the significance of categorising the equilibria using a chosen set of intervals. By contrast, comparing equilibria via flow directions allows for the number of equilibria to be predicted based upon the number of equilibria that share a flow direction.

Although (Karst et al., 2017) did not define vessels as redundant or fixed, they made the important observation that the flow direction in some vessels did not change. Furthermore, almost all equilibria had a unique corresponding flow direction in key vessels. Based on this observation, it is possible to conclude that networks with more vessels for which the flow direction can change have more equilibria. However, their description of the equilibria has a potential drawback, in that two of equilibria they found shared the same flow direction in the network vessels for a specific set of parameter values. Therefore, although the flow direction gives a more precise description of the equilibria, this description is not necessarily unique. A similar scenario has been observed in a simple triangle network; Gardner et al. (2010) identified three equilibria for the triangle network, but two of the three equilibria would always share the same flow direction in the redundant vessel.

In this chapter, a more selective categorisation of the equilibria, based on flow direction, is introduced. Instead of describing the flow in a redundant vessel as having a positive or negative flow direction, the blood flow is described as negative, positive, or intermediate. Intermediate flow is mostly easily understood for a network with a single redundant vessel.

Definition 3.1. (*Intermediate flow* for networks with a single redundant vessel)
Let $\mathcal{N} = \{N, E\}$ be a network with a single redundant vessel, $\langle x, y\rangle$. An equilibrium has *intermediate flow* in the redundant vessel if the equilibrium satisfies one of the two cases:

Case 1. $Q_{\langle x,y\rangle} = 0$.

Case 2. Consider a set of three equilibria, labelled as equilibria a,b and c. Let $Q^{(a)}_{\langle x,y\rangle}, Q^{(b)}_{\langle x,y\rangle}$ and $Q^{(c)}_{\langle x,y\rangle}$ denote the volumetric flows for the three equilibria. Suppose:

$$Q^{(a)}_{\langle x,y\rangle} < 0, Q^{(b)}_{\langle x,y\rangle} \leq 0 \text{ and } Q^{(c)}_{\langle x,y\rangle} > 0 \text{ or}$$
$$Q^{(a)}_{\langle x,y\rangle} < 0, Q^{(b)}_{\langle x,y\rangle} \geq 0 \text{ and } Q^{(c)}_{\langle x,y\rangle} > 0.$$

Equilibrium b is said to have *intermediate flow* in vessel $\langle x, y\rangle$ if:

$$\left|Q^{(b)}_{\langle x,y\rangle}\right| < \left|Q^{(a)}_{\langle x,y\rangle}\right| \text{ and } \left|Q^{(b)}_{\langle x,y\rangle}\right| < \left|Q^{(c)}_{\langle x,y\rangle}\right|.$$

An equilibrium has *negative flow* in a redundant vessel if the flow direction in the redundant vessel is negative, but does not meet the requirements of intermediate flow. *Positive flow* is analogously defined for an equilibrium with a positive flow direction in the redundant vessel.

Remark 3.1. Instead of describing an equilibrium as having negative, intermediate, or positive flow, it will sometimes be convenient to describe the equilibrium as having a negative, intermediate, or positive flow state.

Figure 3.1 shows an example of the three flow states in a simple triangle for which vessel $\langle 4, 5\rangle$ is a redundant vessel. Figure 3.1d shows the equilibria of the triangle network as $Q_{(1,4)}$ varies. Positive equilibria are represented in blue, negative equilibria are represented in red, and intermediate equilibria are represented in green. Figures 3.1a, 3.1b and 3.1c show negative, intermediate and positive equilibria, respectively, when $Q_{(1,4)} = 0.505$ as indicated on Figure 3.1d. As $Q^{(\mathrm{a})}_{\langle 4,5\rangle} < 0, Q^{(\mathrm{b})}_{\langle 4,5\rangle} < 0$ and $Q^{(\mathrm{c})}_{\langle 4,5\rangle} > 0$, the first part of the definition is satisfied. Moreover:

$$\left|Q^{(\mathrm{b})}_{\langle 4,5\rangle}\right| < \left|Q^{(\mathrm{a})}_{\langle 4,5\rangle}\right| \text{ and } \left|Q^{(\mathrm{b})}_{\langle 4,5\rangle}\right| < \left|Q^{(\mathrm{c})}_{\langle 4,5\rangle}\right|. \tag{3.1}$$

Therefore, the second criterion is satisfied, which implies that the equilibrium in Figure 3.1b has intermediate flow in vessel $\langle 4, 5\rangle$. Although the direction of flow is important for the definition of intermediate flow, the flow direction can be positive or negative as shown in Figure 3.1d. The definition of intermediate flow in a network with a single redundant vessel is extended to networks with multiple redundant vessels in Section 3.4.

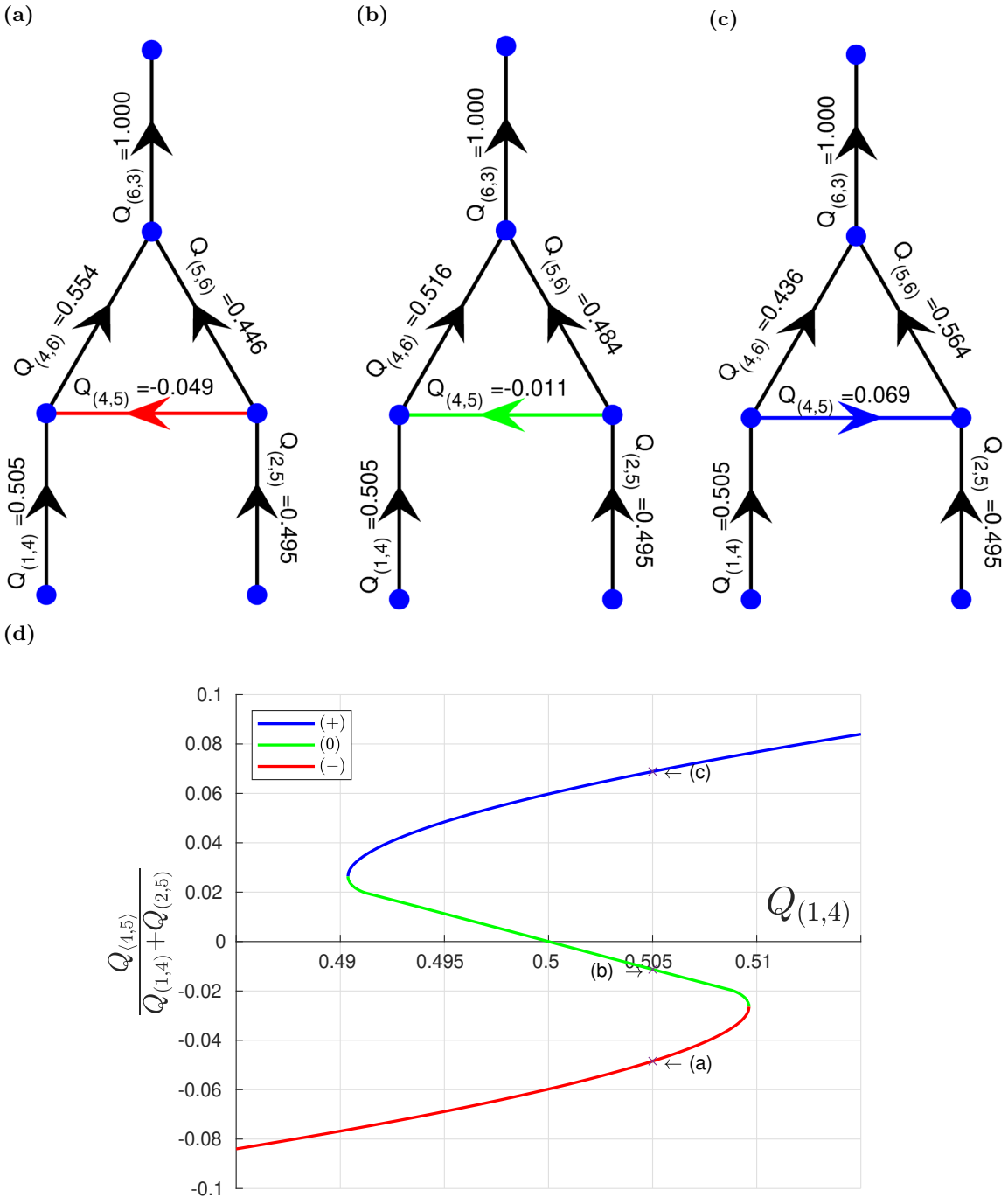

Figure 3.1: Schematic of three equilibria in the triangle network corresponding to negative, positive and intermediate flow in the redundant vessel $\langle 4,5\rangle$. The solid black lines indicate fixed vessels and the coloured vessels represent the redundant vessels. Arrows indicate flow direction for the vessels. (a): equilibrium with a negative flow state, $(-)$; (b): equilibrium with an intermediate flow state, (0); (c): equilibrium with a positive flow state, $(+)$; (d): bifurcation diagram showing how $Q_{\langle 4,5\rangle}$ changes as $Q_{(1,4)}$ varies.

To make use of this concept, new notation is introduced to describe the equilibria using combinations of flow states in the redundant vessels. For a specified order of redundant vessels, the equilibria can be described with a sequence of $-, +$ or 0 symbols to represent negative, positive, or intermediate flow in a redundant vessel, respectively. For instance, if a network has one redundant vessel, the three descriptions of the equilibria are as follows:

$$(-), (+) \text{ or } (0).$$

The equilibria in Figure 3.1d are labelled using this notation. For a network with two redundant vessels, the possible descriptions of the equilibria are as follows:

$$(-,-), (-,0), (-,+), (0,-), (0,0), (0,+), (+,-), (+,0) \text{ or } (+,+),$$

for some specified order of the two redundant vessels. From now on, these descriptions of the equilibria will be known as flow configurations. Some more informative examples of the different flow states and this notation will be explored in Section 3.4.

This chapter will show that equilibria often have unique flow configurations. To ensure that the uniqueness of the flow configurations is a common phenomenon in networks, this chapter contains a number of different example networks and choices of parameters for those networks. Given that the microvasculature contains many different scales of vessels, it is important to show that the key network properties leading to multiple equilibria in network motifs also lead to multiple equilibria in larger networks. The size of a network depends on three key factors; vessel length, number of vessels, and vessel diameters. If a network admits multiple equilibria for one set of vessel lengths, so long as the length ratios remain constant, scaling the vessel lengths of a network by the same factor does not change the flow ratios because the volumetric flow in a vessel is proportional to the reciprocal of the vessel length. Therefore, since the equations of flow and haematocrit are equations of the flow ratio, the haematocrit distribution remains the same. Each haematocrit distribution has a unique pressure distribution which implies that because the haematocrit distributions are unaffected by a change in the length scales, the number of equilibria remains the same.

Showing that multiple equilibria exist as the number of vessels grows is more difficult. Instead of trying to show that equilibria exist for a range of networks with different numbers of vessels, we will show how the number of equilibria changes with the number of redundant vessels. Showing that networks admit multiple equilibria for a range of diameter values is

more difficult than for a range of vessel lengths. As the viscosity of a vessel is a nonlinear function of the diameter and haematocrit, the flow ratios change with the diameters even if the diameter ratios remain constant. Furthermore, the splitting rules often depend on the diameters of the vessels. Due to the difficulty in investigating how the equilibria of a network change as the diameters vary, a full investigation of the impact of different diameters and diameter ratios can be found in Chapter 4.

This chapter will be broken up into the following sections: Section 3.2 describes how numerical continuation can be adapted to solve the network equations, Section 3.3 contains descriptions of the networks studied in this chapter, in Section 3.4 we compare the equilibria of the square plus triangle networks with different splitting rules, in Section 3.5 we show the relationship between the redundancy of the triangle and square plus triangle network with the number of equilibria the two networks admit, Section 3.6 shows how the number of equilibria scale with the number of redundant vessels, Section 3.7 explores the stability of the different flow configurations, and Section 3.8 contains a discussion of the implications of our results and directions for future work.

3.2 Numerical continuation for network equations

Karst et al. (2017) were the first to use numerical continuation to investigate the multiplicity of equilibria. As described in Section 1.9.2, a network for which the haematocrit of every inlet vessel is set to zero, only admits one equilibrium for which the haematocrit in every vessel is also zero. Karst et al. (2015) performed continuation by using inlet haematocrits as the continuation variable in hexagonal and Voronoi networks. Because they started with zero haematocrit in each of the inlet vessels, the initial equilibrium was unique and easy to compute. This approach of numerical continuation was sufficient to show the existence of multiple equilibria and show the relationship between flow direction and the number of equilibria.

Since we are interested in understanding how different network parameters and haematocrit splitting rules affect the solutions to the network equations we consider a different approach to numerical continuation. Given the difficulty of finding a single equilibrium of the network equations, numerical continuation is used to find an initial equilibrium and to determine the pattern of bifurcations as parameters of the network vary. This section describes how numerical continuation is adapted for both uses.

3.2.1 Finding an initial equilibrium

To find an initial equilibrium of the system, a homotopy function[1] known as a convex homotopy is used to first obtain a solution to the network equations. A description of the theory underpinning the technique can be found in Section 2.2 but some details of this method are summarised before the specifics for the network equations are described. The homotopy function of a convex homotopy tracks the solutions to an initial starting system of equations, G, to a target system equations, F. A convex homotopy function takes the form:

$$h(x, \xi) = F(x)(1 - \xi) + G(x)\xi. \tag{3.2}$$

It is easy to infer from Equation (3.2) that $h(x, 0) = F(x)$ and $h(x, 1) = G(x)$. In theory, a solution to F can be found by tracking a solution to G to a solution to F by varying the continuation variable, ξ, from 1 to 0.

In this case, the target system of equations is the full network equations. Therefore, the homotopy function for finding an initial equilibrium of the system of network equations takes the following form:

$$h(H, P, \xi) = F(H, P)(1 - \xi) + G(H, P)\xi, \tag{3.3}$$

where F is the system of network equations and G is a starting system of equations for which $G = 0$ is easy to solve. As there is no specific starting system; we considered two options for our starting system. The first choice of G is that of the network flow equations with a constant haematocrit distribution. In this case, fixing the haematocrit distribution uniquely defines the pressures of the network because the conservation of flow equations are linear for a fixed haematocrit distribution. For a network $\mathcal{N} = \{N, E\}$, the functions associated with the pressure and haematocrit variables for the starting system G are in the following forms:

$$G_v(H, P) = Q_{(u,v)} + Q_{(w,v)} + Q_{(z,v)}. \tag{3.4}$$

$$G_{(v,w)}(H, P) = H_{(v,w)} - H^*_{(v,w)}. \tag{3.5}$$

[1] This function is known as a homotopy function by convention. However, numerical continuation is exclusively used in this chapter despite the function sharing the same name as the homotopy functions used to perform homotopy continuation.

where G_v is the functions associated with the variable P_v, $G_{(v,w)}$ is the function associated with the haematocrit variable $H_{(v,w)}$, and $H^*_{(v,w)}$ is a constant haematocrit that has been set. This means that the solution to $G = 0$ is specified by the chosen haematocrit distribution H^*.

As the equations associated with the pressure variables in the network equations are the same as the starting system:

$$G_v(H, P) = F_v(H, P) = h_v(H, P, \xi). \tag{3.6}$$

Given that $F_{(v,w)}$ can take the form of Equations (1.37) or (1.39) the associate homotopy function $h_{(v,w)}$ can also take two different forms. Therefore, for the flow bifurcation in Figure 1.3a, the homotopy function associated with the haematocrit variable $H_{(v,w)}$:

$$h_{(v,w)}(H, P, \xi) = (\phi_{(v,w)} Q_{(u,v)} H_{(u,v)} - Q_{(v,w)} H_{(v,w)})(1 - \xi) + (H_{(v,w)} - H^*_{(v,w)})\xi, \tag{3.7}$$

where ξ is a continuation parameter. For the flow convergence in Figure 1.3b, the homotopy functions associated with the haematocrit variables $H_{(v,w)}$ takes the following form:

$$h_{(v,w)}(H, P, \xi) = (Q_{(u,v)} H_{(u,v)} + Q_{(w,v)} H_{(v,w)} + Q_{(z,v)} H_{(v,z)})(1 - \xi) + (H_{(v,w)} - H^*_{(v,w)})\xi. \tag{3.8}$$

It is possible that the homotopy function switches between the two forms in Equations (3.7-3.8) as ξ varies. Let $h^{(\text{bif})}_{(v,w)}$ and $h^{(\text{conv})}_{(v,w)}$ denote the homotopy functions in Equations (3.7-3.8). Therefore, the homotopy function associated with the variables $H_{(v,w)}$ takes the following form:

$$h_{(v,w)}(P, H, \xi) = \begin{cases} h^{(\text{bif})}_{(v,w)}(H, P, \xi) & P_u > P_v, P_v > P_w, P_z > P_v, \\ h^{(\text{conv})}_{(v,w)}(H, P, \xi) & P_u > P_v, P_w \leq P_v, P_v \geq P_z, \end{cases} \tag{3.9}$$

for a vessel junction present in either flow configuration in Figure 1.3. It is possible that the flow in a junction has more possible configurations depending on the position in the network. However, the only difference between the two flow configurations present in Figure 1.3 and other possible flow configurations are which vessels are the parent and daughter vessels. Therefore, the form of Equation (3.9) remains the same regardless of the flow configuration. The homotopy function is easily adaptable if a continuation is unsuccessful in obtaining an equilibrium of the network. A new haematocrit distribution, H^*, is chosen

until an equilibrium is obtained. Although in most cases this is sufficient to perform a successful continuation, in general, it is not possible to determine if a path between the solutions of the starting system and target systems exists.

The second starting system we consider is that of the network equations with a different splitting rule. If the solutions to the network equations for the splitting rule ϕ are known, then the network equations with ϕ as the splitting rule can be used as the starting system. The only difference with the homotopy functions described by Equations (3.6-3.9) and homotopy function based on a starting system of network equations is that Equations (3.7-3.8) are replaced with equations:

$$h^{(\text{bif})}_{(v,w)}(H, P, \xi) = (\phi_{(v,w)}\xi + \psi_{(v,w)}(1-\xi))Q_{(u,v)}H_{(u,v)} - Q_{(v,w)}H_{(v,w)}, \tag{3.10}$$

$$h^{(\text{conv})}_{(v,w)}(H, P, \xi) = Q_{(u,v)}H_{(u,v)} + Q_{(w,v)}H_{(v,w)} + Q_{(z,v)}H_{(v,z)}. \tag{3.11}$$

One strategy for finding solutions to the network equations for different splitting rules may be to start with a constant haematocrit distribution to find the solutions to the network equations for one splitting rule, then use these equilibria to find the equilibria to the network equations for other splitting rules.

3.2.2 Tracking equilibria in parameter space

Once at least one equilibrium of a network is known, numerical continuation can be used to investigate how the equilibria change as certain parameters vary. If $F : [0,1]^m \times \mathbb{R}^n_+ \to \mathbb{R}^{n+m}$ is the system of network equations for a network with m haematocrit variables and n pressure variables, then the homotopy function used to investigate how the equilibria change as the parameter varies is:

$$h(H, P, \xi) = F(H, P, \xi), \tag{3.12}$$

where ξ is the parameter of interest. For instance, ξ could be one of the inlet pressures or an inlet haematocrits. Once the solution to $h = 0$ is known for a starting value of $\xi = \xi_0$, this solution is used as the starting solution for numerical continuation as ξ varies. If the path of $h = 0$ encounters a bifurcation point, then one equilibrium can be used to find the other equilibria by tracking the equilibria emerging from the bifurcation point. This is the main method that will be used to find multiple equilibria of the network equations throughout this thesis.

The homotopy functions of Equations (3.9-3.12) are used to generate bifurcation diagrams or sets of equilibria of the network throughout this thesis. The process of generating a bifurcation diagram or a single equilibrium is summarised by the flow chart in Figure 3.2. The diamond boxes represent decisions on which direction to traverse the flow chart or a choice of which parameters to vary, the rectangles represent processes, the parallelograms with sharp corners represent inputs and the parallelograms with round corners represent outputs or results. All numerical continuation is performed by bifurcation analysis software AUTO 07p (Doedel et al., 1999).

3.3 Network construction for the test cases

To investigate the effect of different network configurations on the number of equilibria, we investigate three network topologies. First, we consider the triangle network, which is formed of six nodes: three interior nodes labelled $4, 5$ and 6; two input nodes labelled 1 and 2; and one outlet node labelled 3 (see Figure 3.3a). As there is one outlet node, the pressure of the outlet node can be set to 0 without changing the values of the haematocrit or flow variables of the equilibria (see Section 1.9.6 for details). Inlet pressures P_1 and P_2 can be rescaled to values between 0 and 1 without changing the haematocrit distribution. For instance, if:

$$(P_1, P_2, P_3 = 0, P_4, P_5, P_6), \tag{3.13}$$

are the pressures for a given haematocrit distribution, and if the pressures are scaled uniformly, then the flows will scale by the same factor since the governing equations depend on flow ratios; scaling the flows uniformly does not affect these ratios. If all pressures are scaled by $1/(P_1 + P_2)$, this results in the following pressures:

$$\left(\frac{P_1}{P_1+P_2}, \frac{P_2}{P_1+P_2}, \frac{P_3=0}{P_1+P_2}, \frac{P_4}{P_1+P_2}, \frac{P_5}{P_1+P_2}, \frac{P_6}{P_1+P_2}\right). \tag{3.14}$$

The flow ratios for the translated pressures are the same as the original pressures, which implies that the haematocrit distribution remains the same. The benefit of choosing these boundary conditions is that all possible choices for boundary pressures can be described by this simplification. As the triangle network only contains one redundant vessel, $\langle 4, 5\rangle$, only the following flow configurations are possible:

$$(-), (0), (+). \tag{3.15}$$

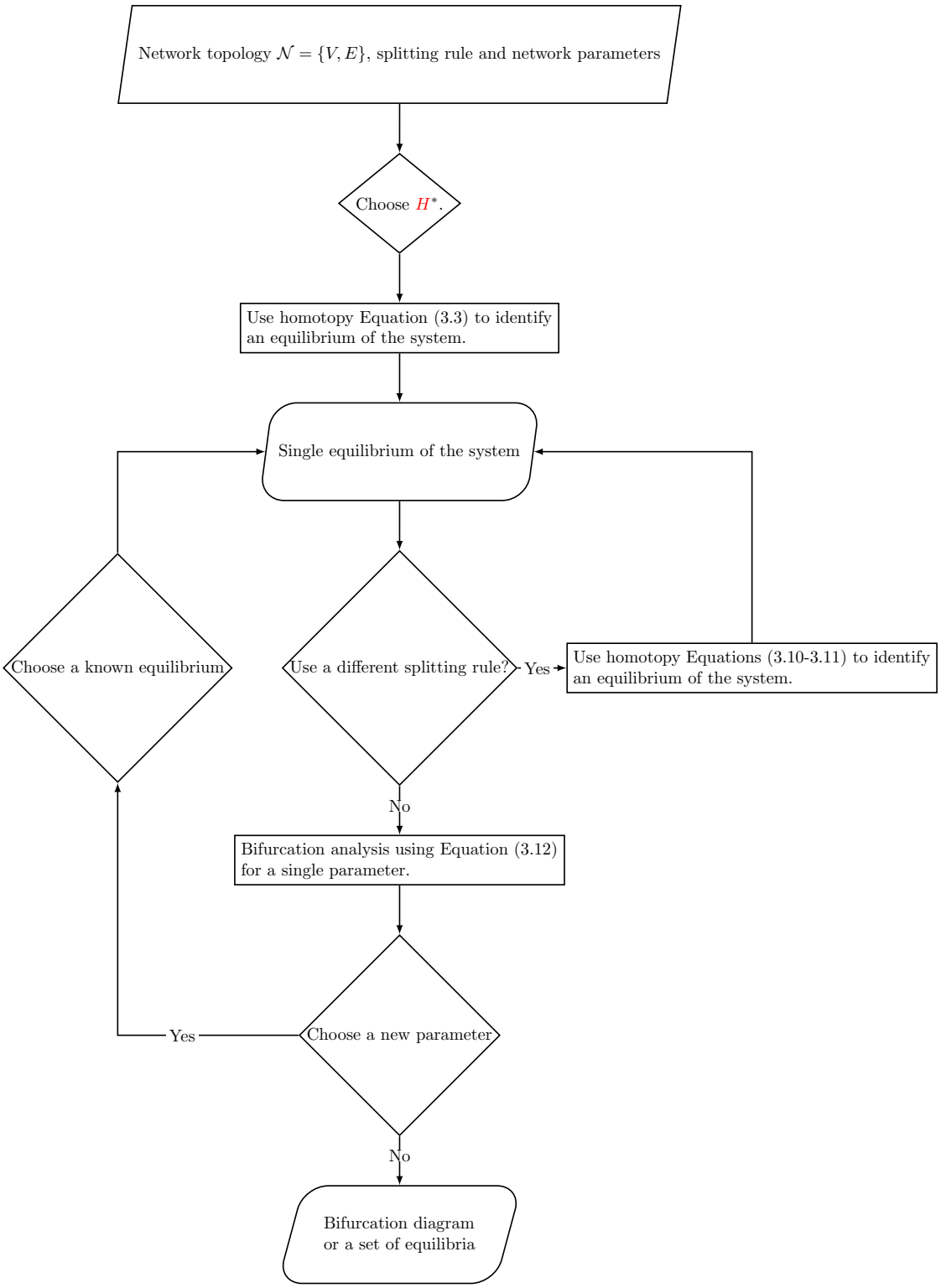

Figure 3.2: Flow diagram of a process to generate bifurcation diagrams for the system of network equations.

The square plus triangle network is similar to the triangle network, but with two extra interior nodes to form a quadrilateral. The boundary nodes have the same indices as those of the triangle network, with node 3 being the only outlet node. The interior nodes are labelled $4, 5, 6, 7, 8$: nodes $4, 5, 6, 7$ form a quadrilateral and nodes $6, 7, 8$ form a triangle (see Figure 3.3b). As the number of inlets and outlets is the same as that of the triangle network, it is possible to make the same simplification for the boundary pressures. Unlike the triangle network, the square plus triangle network contains two redundant vessels instead of one, $\langle 4, 5\rangle$ and $\langle 6, 7\rangle$. As the network contains two redundant vessels, the list of possible flow configurations are as follows:

$$(-,-),(-,0),(-,+),(0,-),(0,0),(0,+),(+,-),(+,0),(+,+), \tag{3.16}$$

for any order of the two redundant vessels. However, when describing the equilibria of a given network, the order of the redundant vessels must be specified to ensure that our descriptions of the equilibria are consistent. For example, if we choose the order $O_1 = (\langle 4, 5\rangle, \langle 6, 7\rangle)$ for the square plus triangle network, then the flow configuration $(-,+)$ corresponds to an equilibrium for which the flow in vessel $\langle 4, 5\rangle$ is negative and the flow in vessel $\langle 6, 7\rangle$ is positive. However, for the order $O_2 = (\langle 6, 7\rangle, \langle 4, 5\rangle)$, the flow configuration $(-,+)$ corresponds to an equilibrium for which the flow in vessel $\langle 4, 5\rangle$ is positive and the flow in vessel $\langle 6, 7\rangle$ is negative. All equilibria of the square plus triangle network will be described using order O_1 in this thesis. The square plus triangle network makes for a useful comparison with the triangle network because the network can be formed by adding a redundant vessel (vessel $\langle 6, 7\rangle$) to the triangle network bisecting vessels $(4, 6)$ and $(5, 6)$.

After identifying some of the necessary conditions for the existence of multiple equilibria in the triangle and square plus triangle networks, it is important to verify our findings in a larger unstudied network with similar properties. The triple triangle network is constructed by concatenating two diamond networks onto the triangle network (Figure 3.3c). The flow configurations for the triple triangle network will be defined by the order $(\langle 6, 7\rangle, \langle 8, 9\rangle, \langle 12, 13\rangle)$. An important difference between the triple triangle and the diamond subnetworks is the orientation of the redundant vessels. The two redundant vessels in the square plus triangle network are not upstream or downstream of the other redundant vessels.

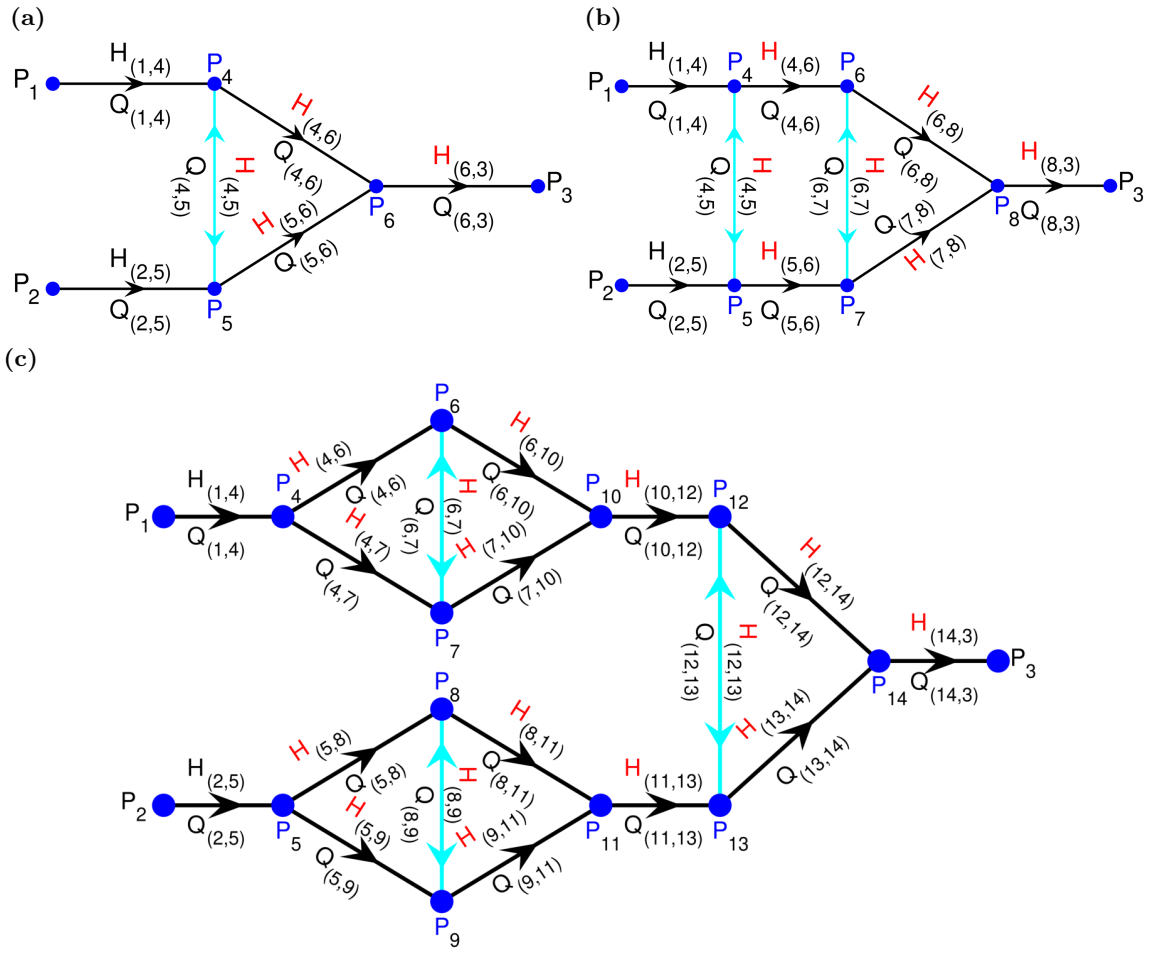

Figure 3.3: (a): Diagram of the triangle network; (b): diagram of the square plus triangle network; (c): diagram of the triple triangle network. The redundant vessels are coloured turquoise and the fixed vessels are coloured black for all three networks.

3.4 Effect of different splitting rules

So far, most results in the literature have used only one splitting rule per publication to investigate different networks. Although these splitting rules often share the same basic structure, it is not clear if the existence of multiple equilibria is dependent on the choice of splitting rule. This section considers the impact of splitting rules of the same form as Equation (1.13):

$$\psi_{(v,w)}(r_{(v,w)}) = \begin{cases} 0 & \text{if } r_{(v,w)} < X_0, \\ 1 & \text{if } r_{(v,w)} > 1 - X_0, \\ \frac{e^A(r_{(v,w)}-X_0)^P}{e^A(r_{(v,w)}-X_0)^P+(1-r_{(v,w)}-X_0)^P} & \text{if } X_0 \leq, r_{(v,w)} \leq 1 - X_0 \end{cases} \tag{1.13}$$

where the indices of the vessels can be seen in Figure 1.3a. This splitting rule dictates the ratio of red blood cells entering the daughter vessel (v, w). $r_{(v,w)} = Q_{(v,w)}/Q_{(u,v)}$ is the ratio of the volumetric flow of the blood entering vessel (v, w) and the coefficients of the splitting rule, X_0, A and P are specified for different splitting rules in Table 3.1.

For this section, we consider five different splitting rules, two from the literature, and three that have been created in this chapter. The two splitting rules from the literature are the Gardner[2] (Gardner et al., 2010; Pries et al., 1990) and Pries (Pries and Secomb, 2005) rules. The advantage of testing the Pries and Gardner splitting rules is that they share the same functional form of P (see Table 3.1 for details). The functional forms for A are also equivalent for this Chapter because $A = 0$ for both splitting rules when the diameters of all vessels are the same value. Therefore, the Gardner and Pries splitting rules only differ in terms of X_0. For the Gardner rule, X_0 depends on the diameter of the parent vessel, while for the Pries rule, X_0 also depends on the parent haematocrit (see Table 3.1 for details).

The three new simplified splitting rules that we introduce have properties similar to those of the Gardner and Pries rules, but were developed to understand the importance of the functional forms of X_0, P and A on the existence of multiple equilibria. The functional forms of A and X_0 of the Gardner and Pries rules share some common properties; A introduces a bias towards the narrowest vessel and X_0 is always small relative to 0.5 (see Table

[2]The Gardner splitting rule was first described by Pries et al. (1990). We call this the Gardner splitting rule to distinguish this rule from the other splitting rule described by Pries and Secomb (2005) and because the Gardner splitting rule was used by Gardner et al. (2010) to obtain important results for the triangle network.

Splitting rule	P	A	X_0
Gardner	$1+6.98^{\frac{1-H_{(u,v)}}{D_{(u,v)}}}$	$-\frac{6.96}{D_{(u,v)}}\log\left(\frac{D_{(v,w)}}{D_{(v,z)}}\right)$	$\frac{0.4}{D_{(u,v)}}$
Pries	$1+6.98^{\frac{1-H_{(u,v)}}{D_{(u,v)}}}$	$-13.29\left[\frac{D^2_{(v,w)}-D^2_{(v,z)}}{D^2_{(v,w)}+D^2_{(v,z)}}\right]^{\frac{1-H_{(u,v)}}{D_{(u,v)}}}$	$0.964^{\frac{1-H_{(u,v)}}{D_{(u,v)}}}$
Simple I, II & III	$1.1, 1.4, 2$	$-\frac{7}{D_{(u,v)}}\frac{(D_{(v,w)}-D_{(v,z)})}{(D_{(v,w)}+D_{(v,z)})}$	0.05

Table 3.1: Summary of the different functional forms that are used in Equation (1.13) to generate the different haematocrit splitting rules. The indices of the vessels correspond to the bifurcation unit in Figure 1.3a and the functions of P, A and X_0 determine the ratio of RBCs $Q_{(v,w)}H_{(v,w)}/Q_{(u,v)}H_{(u,v)}$.

3.1 for details). The functional forms of X_0 and A for the simple splitting rules also share these properties. We consider fixed values of P for the simple splitting rules to investigate if P depending on the parent haematocrit and the diameters of a bifurcation is required for multiple equilibria to exist.

For this section, we focus only on the square plus triangle network. Our motivation to study the square plus triangle network instead of the triangle network is due to the fact that the plasma skimming coefficient P is often a function of the haematocrit of the parent vessel. For the triangle network, this P is always constant because the topology of the network only admits one flow bifurcation immediately after one of the two inlet vessels. By contrast, the square plus triangle network admits two bifurcations; one at node 4 or 5 and a second at node 6 or 7. As a result, this network is better at determining whether P must be a function of the parent haematocrit or diameter for multiple equilibria to exist. To determine the impact of different splitting rules, the following parameters for the square plus triangle network have been chosen:

$$L_{(6,8)} = 110\mu m, L_{\langle 4,5\rangle} = L_{\langle 6,7\rangle} = 50\mu m, L = 100\mu m,$$
$$D = 10\mu m, H_{(1,4)} = H_{(2,5)} = 0.45,$$

where L and D denote the lengths and diameters of the vessels that have not been explicitly specified.

To generate the equilibria of the square plus triangle network with the Gardner, Pries and simple (II) splitting rules, the inlet pressure P_1 is used as the continuation parameter, and the second inlet pressure is set to $P_2 = 1 - P_1$. The splitting rules have been studied in sets of three to better distinguish the difference between the equilibria generated using

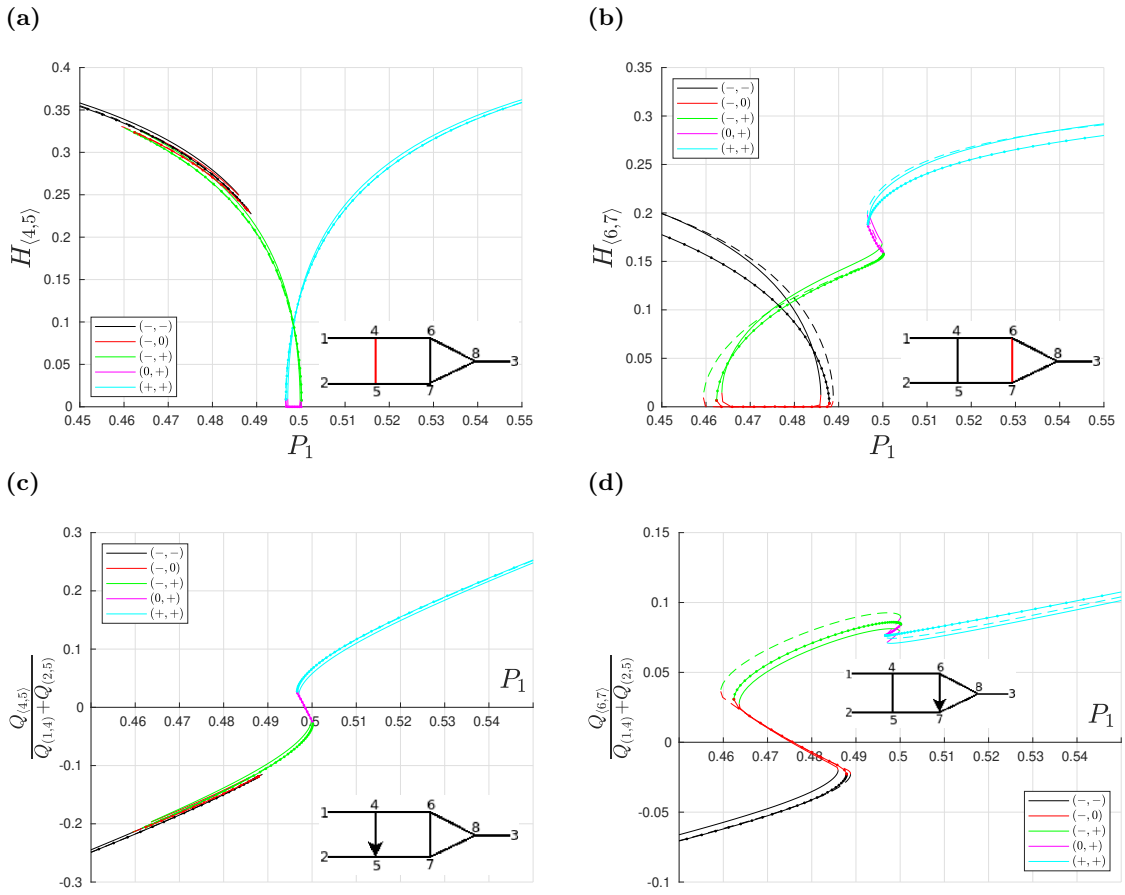

Figure 3.4: Series of plots showing how the haematocrit and volumetric flows in the redundant vessels of the square plus triangle network change as the inlet pressure P_1 varies. The different line styles represent the equilibria for different splitting rules: the solid lines represent the Gardner splitting rule; the dashed lines represent the Pries splitting rule; the solid lines with dots represent the simple splitting rule II (see Table 3.1).

different splitting rules. The first set of splitting rules considered are the Pries rule, Gardner rule and the simple splitting rule for which $P = 1.4$ because this is close to the value of P in the Gardner and Pries rules when $D = 10\mu$m and the value of the parent haematocrit is 0.45. This haematocrit value is important because this is the same value of the haematocrit for the two inlet vessels. Therefore, $P \approx 1.4$ for both the Pries and Gardner splitting rules for the first flow bifurcation.

Figure 3.4 shows that the equilibria for the first set of splitting rules are all qualitatively and quantitatively similar. Figures 3.4b and 3.4d indicate that differences in the haematocrit values for the different splitting rules are more pronounced for vessels that are further from the inlets. Regardless of the larger difference of the values of $H_{\langle 6,7\rangle}$, the three splitting rules

generally agree with each other.

The second observation to make is the consistent pattern of fold bifurcations for the three splitting rules. The continuation curve contains two intervals of P_1 created by two fold bifurcations. This first interval is approximately $0.45 \lesssim P_1 \lesssim 0.49$ and the second interval is approximately $0.495 \lesssim P_1 \lesssim 0.5$. The first interval can be more clearly identified in Figures 3.4b and 3.4d and the second interval can be more clearly identified in Figures 3.4a and 3.4c. Not only does this pattern of fold bifurcations make for a useful comparison, the position of the fold bifurcations also reveals a possible mechanism behind the formation of multiple equilibria. The section of the continuation curve between the two fold bifurcations of the second interval, labelled in pink, contains a point at which $Q_{\langle 4,5\rangle} = 0$. Therefore, the existence of three equilibria coincides with the change in the direction of flow in vessel $\langle 4, 5\rangle$. This would suggest that the existence of multiple equilibria is linked to the change in the direction of flow in one of the redundant vessels. Furthermore, the first interval contains a point at which $Q_{\langle 6,7\rangle} = 0$, implying a change in the direction of blood flow in vessel $\langle 6, 7\rangle$.

Figure 3.4 clearly reveals a link between the direction of flow in redundant vessels and the multiplicity of solutions for the network equations. However, if the equilibria are characterised solely on flow directions in the redundant vessels, the equilibria cannot be uniquely defined using the different flow directions. However, the existence of this pattern of fold bifurcations clearly indicates that the flow for one of the equilibria belongs to a transition phase for which the flow direction can be positive or negative. For this reason, we introduced the concept of intermediate flow to characterise this transition phase.

To determine whether the equilibria of the square plus triangle network can also be labelled by flow configuration, the definition of intermediate flow must be extended to networks with more than one redundant vessel. The definition of intermediate flow can be extended to networks with any number of redundant vessels by adding the criterion that all other vessels must have the same flow state.

Definition 3.2. (*Intermediate flow* for networks with multiple redundant vessels)
For a network, $\mathcal{N} = \{N, E\}$, with $n + 1$ redundant vessels, $\{\langle x_0, y_0\rangle, \langle x_1, y_1\rangle, ..., \langle x_n, y_n\rangle\}$. Let $s_{\langle x_i, y_i\rangle} = -, 0, +$ denote the flow state of redundant vessel $\langle x_i, y_i\rangle$. An equilibrium has *intermediate flow* in vessel $\langle x_0, y_0\rangle$ if the equilibrium satisfies one of the following cases:

Case 1. $Q_{\langle x_0, y_0\rangle} = 0$.

Case 2. For a set of three equilibria, equilibria *a*,*b* and *c*, let $Q^{(a)}_{\langle x_0,y_0\rangle}, Q^{(b)}_{\langle x_0,y_0\rangle}$ and $Q^{(c)}_{\langle x_0,y_0\rangle}$ denote the volumetric flows in vessel $\langle x_0, y_0\rangle$ for the three equilibria. If:

$$Q^{(\mathrm{a})}_{\langle x_0,y_0\rangle} < 0, Q^{(\mathrm{b})}_{\langle x_0,y_0\rangle} \leq 0 \text{ and } Q^{(\mathrm{c})}_{\langle x_0,y_0\rangle} > 0, \tag{3.17}$$

or:

$$Q^{(\mathrm{a})}_{\langle x_0,y_0\rangle} < 0, Q^{(\mathrm{b})}_{\langle x_0,y_0\rangle} \geq 0 \text{ and } Q^{(\mathrm{c})}_{\langle x_0,y_0\rangle} > 0, \tag{3.18}$$

and:

$$\left(s^{(\mathrm{a})}_{\langle x_1,y_1\rangle}, ..., s^{(\mathrm{a})}_{\langle x_n,y_n\rangle}\right) = \left(s^{(\mathrm{b})}_{\langle x_1,y_1\rangle}, ..., s^{(\mathrm{b})}_{\langle x_n,y_n\rangle}\right) = \left(s^{(\mathrm{c})}_{\langle x_1,y_1\rangle}, ..., s^{(\mathrm{c})}_{\langle x_n,y_n\rangle}\right). \tag{3.19}$$

Equilibrium b is said to have *intermediate flow* in the redundant vessel $\langle x_0, y_0\rangle$ if:

$$\left|Q^{(\mathrm{b})}_{\langle x_0,y_0\rangle}\right| < \left|Q^{(\mathrm{a})}_{\langle x_0,y_0\rangle}\right| \text{ and } \left|Q^{(\mathrm{b})}_{\langle x_0,y_0\rangle}\right| < \left|Q^{(\mathrm{c})}_{\langle x_0,y_0\rangle}\right|. \tag{3.20}$$

As with networks with a single redundant vessel, a redundant vessel is said to have *negative flow* if the direction of flow in the vessel is negative, but the definition of intermediate flow does not apply. Analogously, an equilibrium for which the flow in a redundant vessel is positive but the equilibrium does not satisfy the definition of intermediate flow is said to have *positive flow*.

Using this definition of intermediate flow allows the classification of these equilibria between fold bifurcations with unique flow configurations. For instance, $Q_{\langle 4,5\rangle} < 0$ for all three equilibria of the first intervals in Figure 3.4c, therefore, the flow state for $\langle 4, 5\rangle$ is negative for all three equilibria. Furthermore, $Q^{\text{black}}_{\langle 6,7\rangle} < 0$ and $Q^{\text{green}}_{\langle 6,7\rangle} > 0$ and $|Q^{\text{red}}_{\langle 6,7\rangle}| < |Q^{\text{green}}_{\langle 6,7\rangle}|, |Q^{\text{black}}_{\langle 6,7\rangle}|$. Hence, the equilibria of the red curve satisfy the definition of intermediate flow. This means that the equilibria belonging to the black, red and green curves in Figures 3.4d and 3.4b have the respective flow configurations:

$$\{(-,-),(-,0),(-,+)\}.$$

Therefore, every equilibria have a unique flow configuration for each value of P_1. When applying the definition of intermediate flow to the second interval of multiple equilibria, the network equilibria have unique flow configurations and these configurations are consistent for all splitting rules (see Figures 3.4d and 3.4b). Figures 3.4c and 3.4d reveal that the

pink curve satisfies the definition of intermediate flow in vessel $\langle 4, 5\rangle$. Therefore, the flow configuration for the equilibria belonging to the pink curve is $(0, +)$. This means that the equilibria belonging to the green, pink, and turquoise curves in Figures 3.4c and 3.4a have the respective flow configurations:

$$\{(-, +), (0, +), (+, +)\}.$$

Therefore, the set of possible flow configurations for the range of P_1 are as follows:

$$\{(-, -), (-, 0), (-, +), (0, +), (+, +)\}.$$

It is important to note that not all possible flow configurations correspond to an equilibrium of the square plus triangle network but every equilibrium has a unique flow configuration. Furthermore, these results show that there are multiple intervals of multiple equilibria, distinguished by a change in the flow state of a single redundant vessel in the first and second intervals in Figure 3.4.

Figure 3.5 shows a similar comparison to that of Figure 3.4 for the three simple splitting rules. As with the comparison in Figure 3.4, the equilibria for the different splitting rules are all qualitatively and quantitatively similar. However, the three sets of equilibria are more distinct than for the previous comparison of the splitting rules. For instance, the maximum difference in $H_{\langle 6,7\rangle}$ between the equilibria generated for the different splitting rules in Figure 3.5b is approximately 0.14 compared to 0.025 in Figure 3.4b.

Apart from differences in the haematocrit, the other characteristics of Figure 3.5 are very similar to those of Figure 3.4. The curves contain two intervals formed by two fold bifurcations for which the flow in one of the redundant vessels changes direction. Therefore, the equilibria for the two intervals are characterised by the same flow configurations present in Figure 3.4. However, the difference in the size of the intervals created by fold bifurcations are more pronounced for the three simple splitting rules. The simple splitting rule with $P = 1.1$ forms the smallest intervals and $P = 2.0$ forms the largest intervals. Furthermore, the intervals for $P = 2.0$, overlap, forming a small interval of five equilibria with the flow configurations:

$$\{(-, -), (-, 0), (-, +), (0, +), (+, +)\}.$$

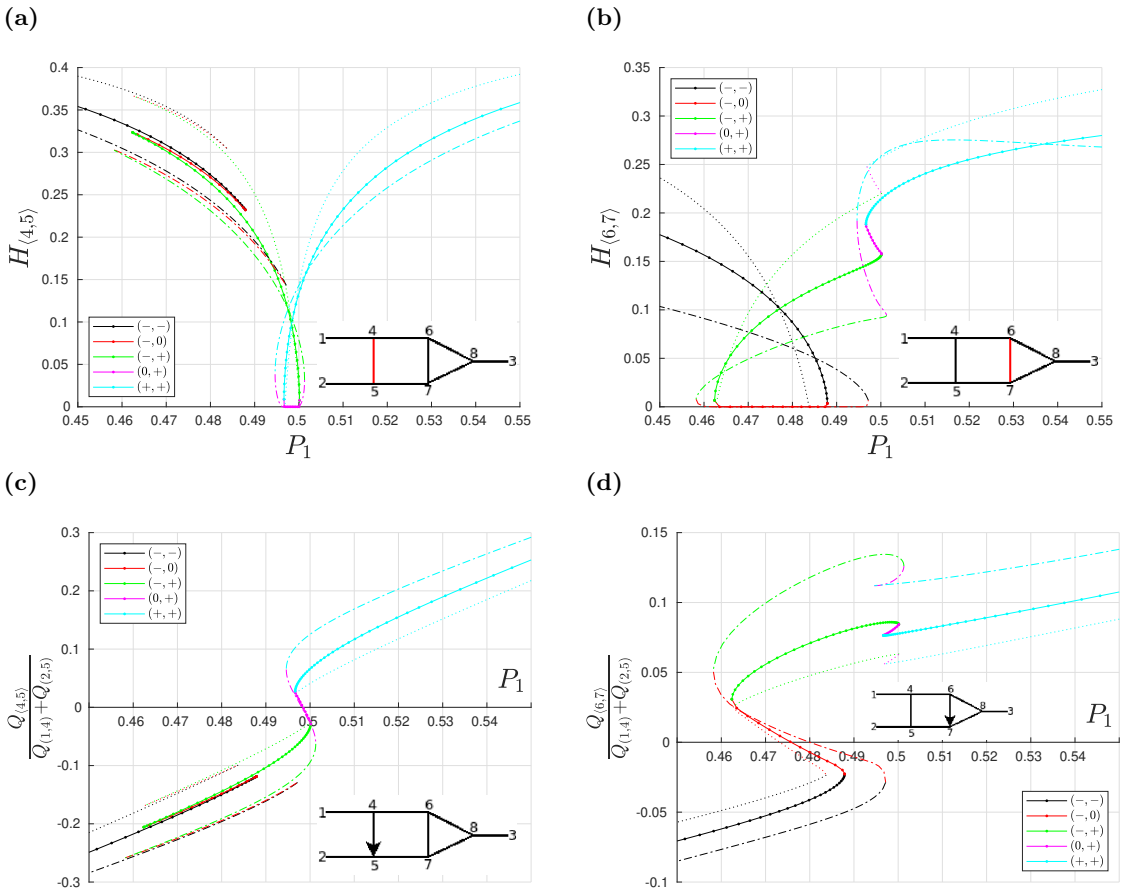

Figure 3.5: Series of plots showing how the haematocrit and volumetric flows in the redundant vessels of the square plus triangle network changes as the inlet pressure P_1 varies for the simple splitting rule with different values of P(see Table 3.1). The different line styles represent the different values of P: the solid lines with dots represent the simple splitting rule with $P = 1.4$; the dotted line represents the simple splitting rule with $P = 1.1$; and, the dotted dashed lines represents the simple splitting rule with $P = 2.0$.

These results present two important characteristics of the equilibria; the equilibria can be categorised by unique flow configurations of redundant vessels for each value of P_1 and the existence of multiple equilibria is not significantly affected by the choice of splitting rule. The one exception to this was the simple splitting rule when $P = 2.0$, but it should be noted that the continuation curves for the equilibria still contained two intervals created by the change in the flow directions in the two redundant vessels, which is consistent with the equilibria for the other splitting rules. From now on, unless otherwise specified, all results are generated using the Gardner splitting rule.

3.5 Comparing the triangle and square plus triangle networks

Now that it has been shown that the choice of splitting rules is not the key reason for the emergence of multiple equilibria in Section 3.4, it is possible to further investigate the link between redundancy and multiple equilibria. Thus far, our results indicate that the key property of networks leading to multiple equilibria is the existence of redundant vessels. Furthermore, the multiplicity to solutions to the network equations have been intrinsically linked with the flow states in the redundant vessels. The equilibria for the networks studied thus far, are found in intervals of parameter space for which the flow state in a single redundant can be negative, positive or intermediate. This means that for each set of parameters within these intervals, the network equations admit three solutions, each with a unique flow state for one of the redundant vessels. Therefore, finding parameters for which the network equations admit multiple solutions is equivalent to finding parameters for which the networks support multiple viable flow states in one or more redundant vessels. When these intervals of multiple viable flow states for different redundant vessels overlap, more combinations of flow configurations become viable coinciding with an increase in the number of equilibria. The implication of these results is that each network has a natural bound on the number of potential equilibria dictated by the number of possible flow configurations. This link between network redundancy and multiple equilibria provides insight into why multiple equilibria are present in certain networks and for which parameters multiple equilibria may be observed.

To justify our hypothesis that all equilibria have a unique flow configuration of flow states in the redundant vessels and that multiple equilibria are only possible when multiple flow configurations are viable, we must show this principle holds for a variety of parameters. Thus far, in Section 3.4, we have shown how this principle holds for some ratio of the inlet pressures. Ideally, this principle would be tested for all possible parameter combinations, but given the complexity of the network equations and size of parameter space, this is not possible. The focus of this Section is to investigate if multiple flow configurations remain viable for different vessel length ratios in the triangle and square plus triangle networks. The resistance to flow in a single vessel is proportional to the length as long as the haematocrit remains constant. Therefore, understanding which flow configurations remain viable as the length ratios provides insight into how changes to the resistance to blood flow influence the viability of flow configurations. By altering the length ratios, we can observe how asymmetry of a network's geometry determines which flow configurations remain viable.

3.5.1 Comparison of the length scales for the triangle and square plus triangle network

To compare the two networks as the geometry of the networks changes, common parameters that have a similar influence on the geometry must first be identified to perform a meaningful comparison. As the main focus of this section is to study the impact of network redundancy, an obvious candidate for a common parameter would be the length of the redundant vessels. As the network equations are based on the flow ratios, the common parameter is characterised as the length ratio of the redundant vessels to some reference length. The second length ratio parameter should introduce some bias to the resistance to the blood flow along the sides of the network. By introducing some bias to the network, the influence of the asymmetry of a network on the viability of the different flow states can be assessed. The length ratios used by Gardner et al. (2010) introduced bias to the flow in the network by increasing the length of one side of the network. Therefore, the same length ratios have been chosen for this section, and the resulting parameters for the triangle network are as follows:

$$D = 10\mu m, L = 100\mu m, P_1 = P_2 = 0.5,$$

$$H_{(1,4)} = H_{(2,5)} = 0.45, L_{\langle 4,5\rangle} = \alpha L, L_{(4,6)} = \beta L.$$

The diameters and lengths of the vessels that have not been specified take the values of D and L, respectively. As our goal is to compare the triangle network with the square plus triangle network, the same set of length ratios, (α, β), are used for the parameters of the square plus triangle network. As α dictates the length of the redundant vessel in the triangle network, α also dictates the length of both redundant vessels in the square plus triangle network, to be consistent with the geometry of the triangle network. There are two possible choices for the length ratio β. The length ratio β could be used in one of two ways; $L_{(4,6)} = \beta L$ and $L_{(6,8)} = \beta L$, or $L_{(4,6)} = L$ and $L_{(6,8)} = \beta L$. In this section, the second choice of network geometry has been used because the subnetwork created by the vessels $\{(4,6),(5,7),\langle 6,7\rangle,(6,8),(7,8),(8,3)\}$ has the same length as the triangle network for this choice of network parameters. The disadvantage of choosing this network geometry is that the side of the network no longer scales with the parameter β. Therefore, the parameters

of the square plus triangle network are as follows:

$$D = 10\mu m, L = 100\mu m, P_1 = P_2 = 0.5,$$

$$H_{(1,4)} = H_{(2,5)} = 0.45, L_{\langle 6,7\rangle} = L_{\langle 4,5\rangle} = \alpha L, L_{(6,8)} = \beta L.$$

Using the same length ratios for both networks, it is possible to determine whether there are any common trends between the length ratios and the number of equilibria for the two networks. To compare the two networks, we found the regions of multiple equilibria in the (α, β) plane for both networks. By finding the region in parameter space for which the two networks admit multiple equilibria, it is possible to compare how the number of equilibria are influenced by additional redundancy.

Gardner et al. (2010) identified a region of multiple equilibria in the (α, β) plane for the triangle network with flow boundary conditions. Flow boundary conditions allow the equations to be manipulated into an expression for the boundaries of the region of multiple equilibria. As pressure boundary conditions have been imposed instead of flow boundary conditions, it is not possible to generate the same results for the length ratios $\alpha = L_{\langle 4,5\rangle}/L$ and $\beta = L_{(4,6)}/L$ because the same manipulation of the equations is not possible. However, it is possible to generate a heatmap showing similar information for the triangle and square plus triangle networks. Figure 3.6 shows the regions of multiple equilibria for the two networks in the parameter space of the plane defined by (α, β). The plots were generated by finding a pair (α_0, β_0) for which only one equilibrium exists, then using continuation with single equilibrium as the initial solution to the homotopy function in Equation (3.12), the full set of equilibria for different values of β are found. Given the equilibria for all $(\alpha, \beta) \in \{\alpha_0\} \times [0.25, 2.50]$, the number of equilibria are counted for a fixed number of points in $\{\alpha_0\} \times [0.25, 2.50]$. A new value of α is chosen, and the process is repeated until the full range of α has been resolved.

The results in Figure 3.6 support our claim that for each value of α, the interval of β for which the two networks admit multiple equilibria is much larger for the square plus triangle network. Furthermore, the value of α for which the networks can only admit one equilibrium when $\beta = 1$ is also much larger for the square plus triangle network. Therefore, the size of the region in the (α, β) plane for which the two networks admit multiple equilibria is much larger for the square plus triangle network.

The region of multiple equilibria in the (α, β) plane for the triangle network contains only

three equilibria. Unlike the triangle network, the region of multiple equilibria for the square plus triangle network is further divided into regions for which the square plus triangle network admits different numbers of equilibria. For instance, for small α and $\beta \approx 1$, there are nine equilibria, but once β is sufficiently large or small, the network only admits three equilibria. This is indicated by the green region in Figure 3.6b.

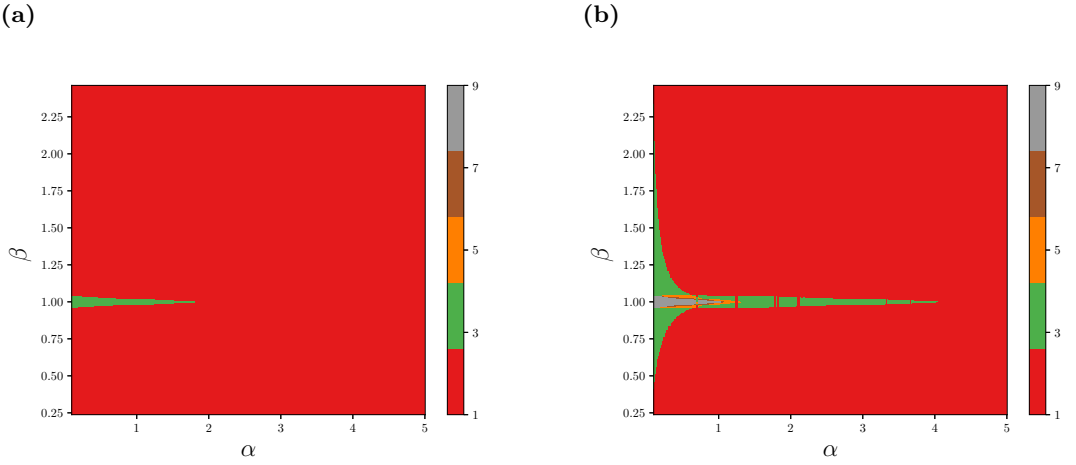

Figure 3.6: Two heatmaps displaying the number of equilibria present for the triangle and square plus triangle network in the (α, β) plane[a]. (a): the number of equilibria of the triangle network; (b): the number of equilibria of the square plus triangle network.

[a]Some bands in the plots appear to indicated that there is a jump in the number of equilibria present but this is because AUTO was not able to perform a full continuation for these particular parameter values.

Figure 3.5 shows that the square plus triangle network (with the Simple splitting rule (III)) admitted five equilibria for a small interval of inlet pressures. The interval of five equilibria was created by two overlapping intervals of three equilibria. These two intervals of three equilibria were created by a change in the flow state of one of the redundant vessels; therefore, the interval of five equilibria contained flow configurations from the two intervals of three equilibria. The same principle can be applied to the equilibria of the square plus triangle for the different length ratios. When $\alpha = 0.1$, Figure 3.7a shows that the flow in the redundant vessel of the triangle network is in two possible flow directions within the interval $0.96 \lesssim \beta \lesssim 1.04$. By contrast, for the same value of α and a similar interval of β, Figures 3.7b, 3.7c and 3.7d show four possible combinations of flow direction in the redundant vessels of the square plus triangle network. Furthermore, the change in the flow direction coincides with the fold bifurcations of the equilibria. In Figure 3.7a, the point at which $Q_{\langle 4,5\rangle} = 0$ lies between two fold bifurcations. The square plus triangle network admits a similar, but more complicated, pattern of fold bifurcations. As with the triangle network, the fold bifurcations indicate the intervals for which the flow in one of the redundant vessels

changes direction; Figure 3.7d shows that the six fold bifurcations in a neighbourhood of $\beta = 1$ dictate the interval of β for which $Q_{\langle 6,7\rangle}$ changes sign. Therefore, the other two fold bifurcations dictate the interval of β for which $Q_{\langle 4,5\rangle}$ changes sign. Given that the number of equilibria exceeds the number of flow directions, the equilibria do not have unique flow directions. However, the pattern of fold bifurcations and changing flow direction clearly shows that, although the two equilibria may share the same flow direction, the flow clearly undergoes the same transition in flow direction between the two fold bifurcations.

As in Section 3.4, when the definitions of the different flow states are applied to the equilibria in Figure 3.7a, the equilibria between the two fold bifurcations have intermediate flow in the redundant vessel. The other two equilibria have negative and positive flows. Therefore, each equilibria of the triangle network have a unique flow configuration:

$$(-), (0), (+).$$

It is difficult to apply the definition of flow states to the nine equilibria of the square plus triangle network in Figures 3.7b, 3.7c and 3.7d. The definition of intermediate flow (Definition 3.2) requires the identification of three equilibria for which the flow direction in one of the redundant vessels, in one of the equilibria, is opposite to the flow direction of the other two equilibria. If only three equilibria exist, Definition 3.2 can be applied directly. If more than three equilibria exist, it can be difficult to determine which three should be selected. However, for this example, all equilibria can be identified with a unique flow configuration in the intervals for which only three equilibria are admitted by the network. $Q_{\langle 6,7\rangle} > 0$ for all three equilibria when $1.04 \lesssim \beta \lesssim 2.3$ which implies that $s_{\langle 6,7\rangle} = +$ for all three equilibria in the interval. Therefore, applying the definitions of the different flow states to $Q_{\langle 4,5\rangle}$ for the same interval, we find that the flow configurations of the three equilibria are as follows.

$$(-,+), (0,+), (+,+). \tag{3.21}$$

$Q_{\langle 6,7\rangle} < 0$ for all three equilibria when $0.4 \lesssim \beta \lesssim 0.96$, which implies, by a similar process of elimination that the three equilibria are characterised by flow configurations:

$$(-,-), (0,-), (+,-). \tag{3.22}$$

The equilibria in the interval $0.96 \lesssim \beta \lesssim 1.04$ are harder to define because, unlike the other two intervals, the equilibria of the network have different flow directions in the redundant

vessels. However, the equilibria for the other two intervals also belong to the interval $(0.96, 1.04)$. If we use the convention that an equilibrium has the same flow configuration for all values of β until the equilibrium meets with a fold bifurcation, then it is possible to uniquely classify the equilibria. With this convention, the equilibria that belong to the interval $(0.96, 1.04)$ and one of the other intervals retain the same flow configurations. To determine the flow configurations of the other equilibria, the flows in the redundant vessels for the equilibria with the flow configuration $(s_{\langle 4,5\rangle}, s_{\langle 6,7\rangle})$ are denoted by:

$$Q_{\langle 4,5\rangle}^{(s_{\langle 4,5\rangle}, s_{\langle 6,7\rangle})}, Q_{\langle 6,7\rangle}^{(s_{\langle 4,5\rangle}, s_{\langle 6,7\rangle})}. \tag{3.23}$$

The flows in the redundant vessels for the equilibria represented by the equilibria that belong to the solid red, green and blue curves in Figures 3.7b, 3.7c and 3.7d:

$$Q_{\langle 4,5\rangle}^{(r,g,b)}, Q_{\langle 6,7\rangle}^{(r,g,b)}, \tag{3.24}$$

Figures 3.7b and 3.7d show that:

$$Q_{\langle 4,5\rangle}^{(+,-)} > 0, Q_{\langle 4,5\rangle}^{(+,+)} > 0, Q_{\langle 4,5\rangle}^{(b)} > 0, \tag{3.25}$$

$$Q_{\langle 6,7\rangle}^{(+,-)} < 0, Q_{\langle 6,7\rangle}^{(+,+)} > 0, Q_{\langle 6,7\rangle}^{(b)} \leq 0 \text{ or } Q_{\langle 6,7\rangle}^{(+,-)} < 0, Q_{\langle 6,7\rangle}^{(+,+)} > 0, Q_{\langle 6,7\rangle}^{(b)} \geq 0, \tag{3.26}$$

$$|Q_{\langle 6,7\rangle}^{(+,-)}| > |Q_{\langle 6,7\rangle}^{(b)}|, |Q_{\langle 6,7\rangle}^{(+,+)}| > |Q_{\langle 6,7\rangle}^{(b)}|. \tag{3.27}$$

This implies that the equilibria belonging to the solid blue curve have the flow configuration $(+, 0)$. By the same logic, the equilibria belonging to the solid red curve have the flow configuration $(-, 0)$. Lastly, the equilibria belonging to the green curve must have the flow configuration $(0, 0)$ because:

$$|Q_{\langle 4,5\rangle}^{(0,-)}| > |Q_{\langle 4,5\rangle}^{(g)}|, |Q_{\langle 4,5\rangle}^{(0,+)}| > |Q_{\langle 4,5\rangle}^{(g)}|, \tag{3.28}$$

$$|Q_{\langle 6,7\rangle}^{(-,0)}| > |Q_{\langle 6,7\rangle}^{(g)}|, |Q_{\langle 6,7\rangle}^{(+,0)}| > |Q_{\langle 6,7\rangle}^{(g)}|. \tag{3.29}$$

The example in Figure 3.7 also reveals how it can sometimes be difficult to directly apply the definition of intermediate flow. If the definition of intermediate flow is applied directly to the interval of $\beta \in (0.96, 1.04)$, then the flow configurations would not be uniquely defined. However, because six of the nine equilibria also belong to the other intervals of

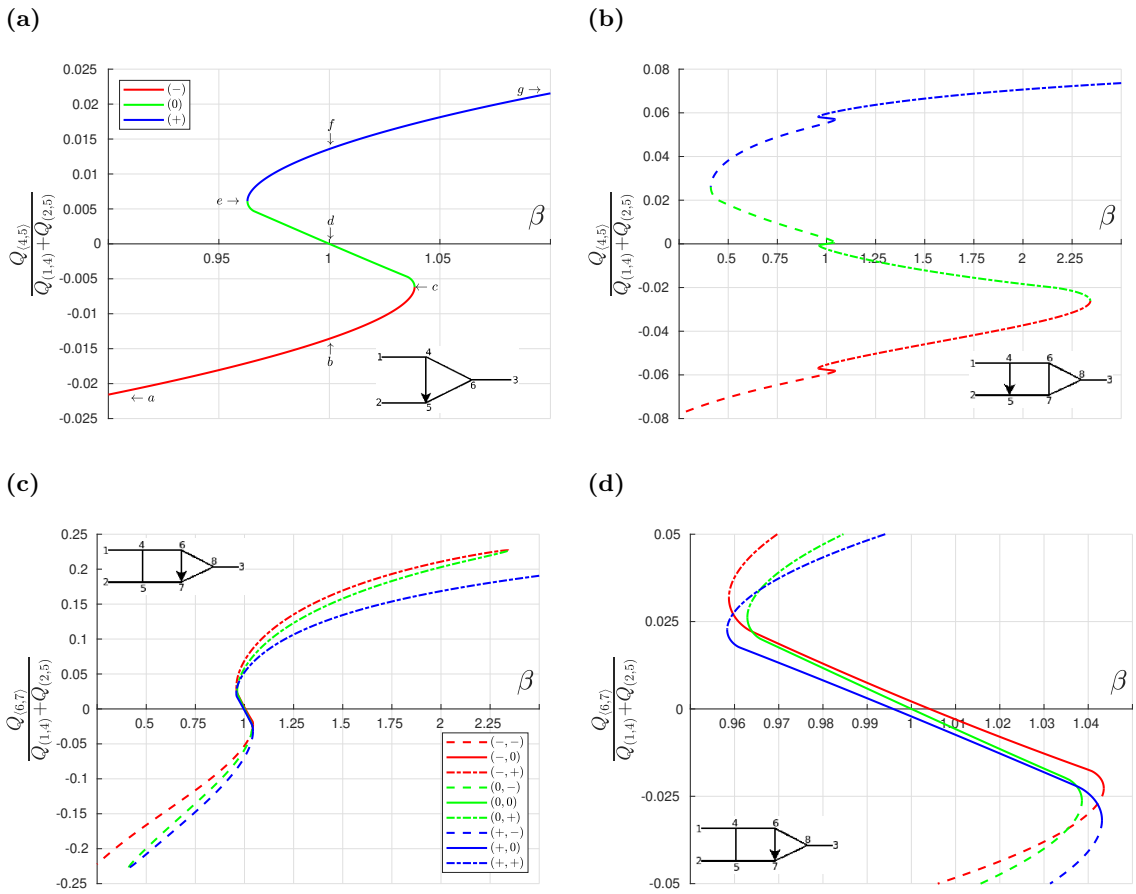

Figure 3.7: Series of plots of the flow in the redundant vessels in the triangle and square plus triangle network as the length ratio β changes for the length ratio $\alpha = 0.1$. (a): Flow of $Q_{\langle 4,5\rangle}$ as β changes in the triangle network. (b) Flow of $Q_{\langle 4,5\rangle}$ as β changes in the square plus triangle network. (c): Flow of $Q_{\langle 6,7\rangle}$ as β changes in the square plus triangle network. (d): close up of (c).

multiple equilibria. The implication of this approach to classifying equilibria is that it may be necessary to study how the flow configurations change as the parameters vary.

Just like the results in Section 3.4, the key defining characteristic of an equilibrium is the flow state of the redundant vessels. The implication of these results is that multiple equilibria are limited by the number of possible flow configurations in the redundant vessels, but not all flow configurations correspond to an equilibrium. Therefore, the only requirement for the existence of multiple equilibria is the existence of multiple viable flow states in a single redundant vessel. Furthermore, Figures 3.7b, 3.7c and 3.7d show that the interval of multiple viable flow states $s_{\langle 6,7\rangle}$ is embedded within the interval of multiple viable flow states $s_{\langle 4,5\rangle}$. As a result, the interval created by the overlap of these two intervals contains every possible combination of the two flow states. Therefore, the results from this section support the hypothesis that intervals of more than three equilibria are created by overlaps of intervals of changing flow direction in the redundant vessels.

Lastly, for completion, the flow configuration and pattern of equilibria for a larger value of α must also be considered. Figure 3.8 displays plots of the flows $Q_{\langle 4,5\rangle}$ and $Q_{\langle 6,7\rangle}$ for different values of the length ratio β, with $\alpha = 2.5$. The continuation curves for $Q_{\langle 4,5\rangle}$ and $Q_{\langle 6,7\rangle}$ both closely resemble the curve for the triangle network in Figure 3.7a. Both have a region of multiple equilibria created by two fold bifurcations and the section of the curve between the two bifurcations, represented in green, contains the equilibrium with the following parameter and variable values, $\beta = 1, Q_{\langle 4,5\rangle} = 0, Q_{\langle 6,7\rangle} = 0$. This equilibrium has intermediate flow in the two redundant vessels. All other equilibria that belong to the green curve have a flow configuration of $(-,-)$ or $(+,+)$. Given that the red curve contains equilibria with a flow configuration of $(-,-)$ and the blue curve contains equilibria with a flow configuration of $(+,+)$, the flow configurations for this example are not unique. However, it should be noted that this set of equilibria only occurs for realistic length ratios for the redundant vessels and symmetric boundary conditions. Therefore, cases of multiple flow configurations with the same flow states in the same redundant vessels are probably rare in more realistic networks. Given the similarity between Figures 3.7a and 3.8a, the two redundant vessels in the square plus triangle network can be considered to act as a single vessel. For this reason, the equilibria between the two-fold bifurcations have been labelled with the $(0,0)$ flow configuration.

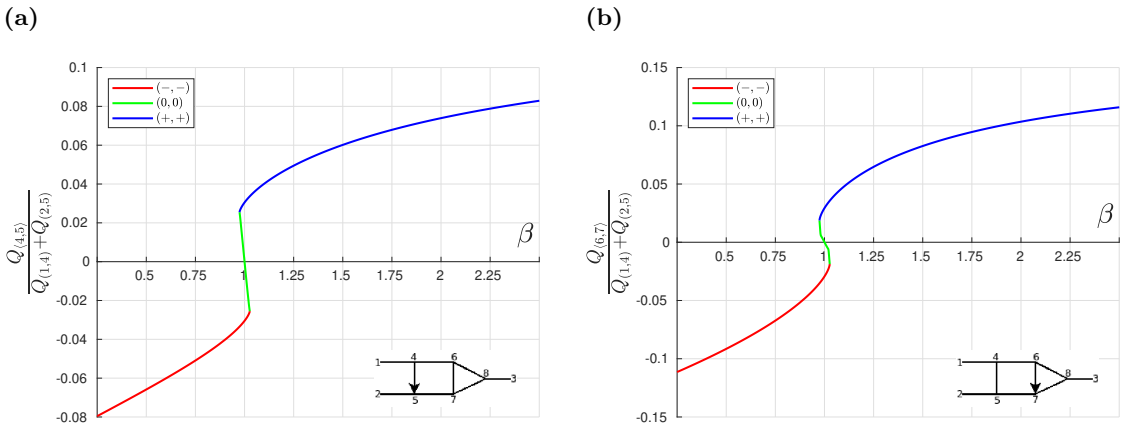

Figure 3.8: Plots of the flow in the redundant vessels as $\beta = L_{(4,6)}/L$ changes for the length ratio $\alpha = 2.5$.

3.5.2 Asymmetry of the haematocrit distribution in the triangle network

The link between possible flow configurations and the number of equilibria could be useful to determine an upper bound on the number of equilibria. Furthermore, the difference in the flow state of a single redundant vessel could prove critical when analysing larger networks. The results in Figure 3.6 indicate that the addition of a redundant vessel creates a larger region of multiple equilibria in the parameter space. Furthermore, the flow in only one of the redundant vessels needs to change for this region to exist. Therefore, despite the existence of redundant vessels that facilitate the emergence of multiple flow configurations, the geometry and boundary conditions of the network dictate which of these flow configurations are viable.

To better understand which network geometries and boundary conditions may give rise to the existence of multiple equilibria, it is important to understand why certain flow configurations are not viable for certain parameters. Due to the nonlinearity of the equations, it is not possible to give a rigorous explanation behind the formation of multiple equilibria. However, the example of the triangle network in Figure 3.7a provides an intuitive explanation behind this process.

Before providing an explanation as to why certain parameters prohibit the formation of multiple equilibria, it is important to understand why the existence of multiple equilibria can be inferred from network symmetry. As discussed in Section 1.9, multiple equilibria can exist only for non-zero inlet haematocrit because nonlinearity is key to the existence of multiple equilibria and the triangle network admits multiple equilibria provided the inlet

haematocrit is sufficiently large (Gardner et al., 2010). Therefore, for the symmetric triangle network, with equal inlet pressures and equal inlet haematocrits, H_{in}, if the following is an equilibrium for the network:

$$(P_4 = P_4^*, P_5 = P_5^*, P_6 = P_6^*, H_{\langle 4,5\rangle} = H_{\langle 4,5\rangle}^*, H_{(4,6)} = H_{(4,6)}^*, H_{(5,6)} = H_{(5,6)}^*), \tag{3.30}$$

such that the starred values represent constants, $Q_{\langle 4,5\rangle} > 0$ and $H_{(4,6)}^* > H_{(5,6)}^*$, then by symmetry

$$(P_4 = P_5^*, P_5 = P_4^*, P_6 = P_6^*, H_{\langle 4,5\rangle} = H_{\langle 4,5\rangle}^*, H_{(4,6)} = H_{(5,6)}^*, H_{(5,6)} = H_{(4,6)}^*), \tag{3.31}$$

with $Q_{\langle 4,5\rangle} < 0$, is also an equilibrium. This explains why the $(-)$ and $(+)$ equilibria exist in pairs for the symmetric triangle network. Additionally, the following equilibrium:

$$(P_4 = 0.375, P_5 = 0.375, P_6 = 0.25, H_{\langle 4,5\rangle} = 0, H_{(4,6)} = H_{\text{in}}, H_{(5,6)} = H_{\text{in}}), \tag{3.32}$$

always exists because the triangle network with $Q_{\langle 4,5\rangle} = 0$ is equivalent to a convergence unit in Figure 3.9. As $H_{(1,4)} = H_{(2,5)} = H_{in}$ and $P_1 = P_2 = 0.5$, the conservation of flow and RBCs in Equations (1.39) and (1.41) implies that $H_{(6,3)} = H_{in}$. Therefore, the viscosity of the blood is equal for every vessel and the network equations for the pressure variables can be reduced to linear equations of flow ratios. Given that the lengths of the two inlet vessels are twice the length of the outlet vessel, for this example, $P_6 = 0.25$, $P_4 = P_5 = 0.375$, due to the properties of the network when including additional nodes to break up the vessels into segments described in Section 1.9.

Therefore, the equilibria of the symmetric triangle network always occur as triples because the (0) equilibrium always exists and as soon as the inlet haematocrit is sufficiently large to support equilibria with nonzero flow in the redundant vessel, the $(-)$ and $(+)$ equilibria are mirror images of each other. As the network equations are continuous, multiple equilibria persist for small perturbations of the network parameters.

Figure 3.10 contains plots of the haematocrits, resistances and flow ratios for the equilibria in Figure 3.7a. Recall that the resistance is a function of the haematocrit in the vessel:

$$R_{(x,y)} = \frac{\mu(H_{(x,y)})L_{(x,y)}}{D_{(x,y)}^4}. \tag{3.33}$$

The first important observation to make is that of the pattern of $H_{\langle 4,5\rangle}$ in Figure 3.10g for the equilibria with intermediate flow. For most of the green curve, the haematocrit is 0, and is only non-zero close to the fold bifurcations. As this section of the curve also corresponds to the change in the flow direction in vessel $\langle 4,5\rangle$, a haematocrit of 0 would be expected because the splitting rules dictate that no RBCs can enter a vessel for small flow ratios. It should also be observed that fold bifurcations occur close to the points at which $H_{\langle 4,5\rangle} > 0$ for equilibria with intermediate flow. The corresponding plot for the resistance to flow in Figure 3.10h follows a similar pattern. Given that the resistance is a function of the haematocrit and the length ratio β does not influence the length of $L_{\langle 4,5\rangle}$, this result is intuitive to understand.

Predictions on the value of $H_{(4,6)}$ and $H_{(5,6)}$ can be made based on the flows $Q_{(4,6)}$ and $Q_{(5,6)}$, and the properties of the network. Notice that $H_{(4,6)} > H_{(1,4)} = 0.45$ and $H_{(5,6)} < H_{(2,5)} = 0.45$ for the $(+)$ equilibrium and the opposite is true for the $(-)$ equilibrium (see Figures 3.10a and 3.10b). The properties of the bifurcation unit in Section 1.9 adequately explain this result. The daughter vessel, for which the flow ratio is greater, has a greater haematocrit value than the parent vessel haematocrit value so long as the diameters of the daughter vessels are of equal size. As the bifurcation is at node 4, for the $(+)$ equilibrium, $H_{(4,6)} > H_{(1,4)}$.

Our results in Figure 3.10 also reveal some interesting trends between the relationship between resistance and haematocrit variables for vessels $(4,6)$ and $(5,6)$. These results provide an intuitive explanation behind the formation of the two fold bifurcations. This explanation is in the form of six cases. Before describing these six cases, we first need to remind the reader of some of the properties first discussed in Section 1.9. The first is the

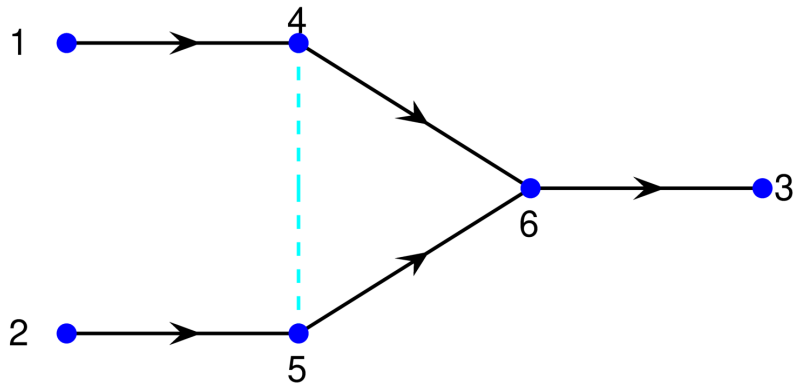

Figure 3.9: Diagram of the triangle network with the vessel $\langle 4,5\rangle$ removed, represented by the dashed line.

property of a convergence of flow. The value of the haematocrit in the daughter vessel of a flow convergence is always less than the maximum of the parent haematocrits. For instance, if $Q_{\langle 4,5\rangle} \geq 0$ then:

$$H_{(5,6)} = rH_{(2,5)} + (1-r)H_{\langle 4,5\rangle}, \tag{3.34}$$

where $r = Q_{(2,5)}/Q_{(5,6)}$. Therefore, $H_{(5,6)} \leq \max(\{H_{(2,5)}, H_{\langle 4,5\rangle}\})$. This also means that if $r = 1$, then $H_{(5,6)} = H_{(2,5)}$ and if $r = 0$, then $H_{(5,6)} = H_{\langle 4,5\rangle}$. The second important property is that $\psi_{(v,w)}(r)/r$ has a maxima, r_m, in the interval $(r_1, 1)$, where $\psi_{(v,w)}$ is a splitting rule and $r_1 \in (0,1)$ is the flow ratio for which $\psi_{(v,w)}(r_1)/r_1 = 1$. As a consequence, the derivative of $\psi(r)/r$ with respect to the flow ratio r is negative when $r > r_m$ and positive when $r < r_m$.

Seven points on the plots have been labelled to indicate which case corresponds to each section of the curve. These seven points include the three equilibria present when $\beta = 1$, the two fold bifurcations and the two equilibria present at $\beta = 0.9$ and 1.1.

Impact of increasing β on the (0) equilibrium

The first example describes the change in the values of the variables for the (0) equilibrium between points d and c in Figures 3.7a and 3.10. When $\beta = 1$: $Q_{\langle 4,5\rangle} = 0$, $H_{\langle 4,5\rangle} = 0$ and $H_{(4,6)} = H_{(5,6)} = H_{(1,4)} = H_{(2,5)}$ for the (0) equilibrium. As β increases, $R_{(4,6)}$ decreases. This may initially seem counter-intuitive because the resistance to the blood flow in a vessel is proportional to the length. However, as β increases, so does $Q_{\langle 5,4\rangle}$ (see Figure 3.7a). Due to the properties of a flow convergence, an increasing value of $Q_{\langle 5,4\rangle}$ for the $(-)$ equilibrium has the result of $H_{(4,6)}$ and $R_{(4,6)}$ decreasing (see Figures 3.10a and 3.10c). As $Q_{\langle 5,4\rangle}$ increases, this coincides with a decrease in the value of $Q_{(5,6)}/Q_{(2,5)}$ (see Figures 3.10d) and, due to the properties of the haematocrit values of the daughter vessels at a bifurcation, this results in an increase in $H_{(5,6)}$ and $R_{(5,6)}$ (see Figures 3.10b and 3.10d). As $R_{(4,6)}$ decreases and $R_{(5,6)}$ increases, $R_{\langle 4,5\rangle}$ remains constant because the flow in the redundant vessel is too small for additional RBCs to enter. Therefore, the resistance along the blood flow pathway $5 \to 4 \to 6$ decreases. This process continues until $Q_{\langle 5,4\rangle}$ is sufficiently large for the RBCs to enter the redundant vessel. At this point, the resistance $R_{\langle 4,5\rangle}$ sharply rises, coinciding with the existence of fold bifurcation. One interpretation of the emergence of this limit point is that the flow pathway $5 \to 4 \to 6$ is no longer viable due to the sharp increase in the value of $R_{\langle 4,5\rangle}$. At this point, the equilibrium must terminate at a limit point, which takes the form of a fold bifurcation in this case.

Impact of increasing β on the $(-)$ equilibrium

The process of how the values of the variables for the equilibrium $(-)$ change between points b and c in Figures 3.7a and 3.10, follows a different set of arguments, but can be explained using the same properties. The key to understanding this behaviour is understanding the process of the changing values of $H_{(5,6)}$ and $H_{\langle 4,5\rangle}$. The flow bifurcation for all $(-)$ equilibria is located at node 5. Due to the properties of a flow bifurcation $H_{(5,6)} > H_{(2,5)}$. When $\beta = 1$, $Q_{(5,6)}/Q_{(2,5)} > r_m$, therefore, if $Q_{(5,6)}/Q_{(2,5)}$ increases, then $H_{(5,6)}$ decreases, but if $Q_{(5,6)}/Q_{(2,5)}$ decreases, then $H_{(5,6)}$ increases. $H_{\langle 4,5\rangle} > 0$ for all the $(-)$ equilibria, as a result, $Q_{\langle 5,4\rangle}$ increasing leads to $H_{\langle 4,5\rangle}$ increasing, and $Q_{\langle 5,4\rangle}$ decreasing leads to $H_{\langle 4,5\rangle}$ decreasing. As β increases, so does $L_{(4,6)}$. Unlike the case for the (0) equilibrium, the value of $R_{(4,6)}$ increases (see Figure 3.10c). An increasing value of $R_{(4,6)}$ results in a decreasing value of $Q_{\langle 5,4\rangle}$ (see Figure 3.7a). As node 4 is a flow convergence, the decrease in $Q_{\langle 5,4\rangle}$ leads to an increase in $H_{(4,6)}$ and $R_{(4,6)}$ (see Figures 3.10a and 3.10c), further reducing the inflow from vessel $\langle 4,5\rangle$. The decrease in $Q_{\langle 5,4\rangle}$ corresponds to a decrease in $H_{\langle 4,5\rangle}$ and $R_{\langle 4,5\rangle}$ (see Figures 3.10g and 3.10h), and an increase in $Q_{(5,6)}/Q_{(2,5)}$ (see Figure 3.10f). Due to the property of bifurcations of flow, this simultaneously reduces the value of $H_{(5,6)}$ and $R_{(5,6)}$ (see Figures 3.10b and 3.10d). Therefore, the simultaneous increase of $R_{\langle 4,5\rangle}$ and $R_{(5,6)}$ results in an increase of the resistance along the blood flow pathway $5 \to 4 \to 6$. This reduction in flow $Q_{\langle 5,4\rangle}$ results in the flow ratio $Q_{(5,6)}/Q_{(2,5)}$ tending to 1, and eventually, the equilibrium is no longer viable close to this limit because for this process to continue, the blood flow would eventually need to change direction. As this equilibrium is defined by negative flow in the redundant vessel, this is not possible. Therefore, this equilibrium must cease to exist at a limit point. Although there is no fundamental reason why the (0) and $(-)$ equilibria would meet at the same fold bifurcation, since the difference between the two equilibria is decreasing, the presence of the fold bifurcation aligns with this explanation.

Impact of decreasing β on the $(-)$ equilibrium

The effect of a decreasing value of β is similar to that of an increasing β due to the symmetry of the network. As β decreases between points b and a, so does $R_{(4,6)}$ (see Figure 3.10c). As resistance to blood flowing into vessel $(4,6)$ decreases, the values of $Q_{\langle 5,4\rangle}$ and $H_{\langle 4,5\rangle}$ both increase (see Figures 3.7a and 3.10g). As node 4 is the central node of a flow convergence, the values of $H_{(4,6)}$ and $R_{(4,6)}$ decrease as $Q_{\langle 5,4\rangle}$ increases (see Figures 3.10a and 3.10c). This coincides with a decrease in $Q_{(5,6)}/Q_{(2,5)}$ (see Figure 3.10f) which results in an increase in $H_{(5,6)}$ and $R_{(5,6)}$ because $Q_{(5,6)}/Q_{(2,5)} > r_m$ when $\beta = 1$ (see Figures 3.10b and 3.10d). Therefore, despite the fact that $R_{\langle 4,5\rangle}$ is increasing, the change in β results in an overall

reduction of the resistance to the flow pathway $5 \to 4 \to 6$. As this reduces the resistance in the vessels along the current blood flow pathway, the equilibrium does not hit a limit point.

Impact of decreasing β on the (0) equilibrium

The effect of decreasing β on the (0) equilibrium is similar to the impact of increasing β due to the symmetry of the network. As β decreases between points d and e, the values of $H_{(4,6)}$ and $R_{(4,6)}$ increase (see Figure 3.10c). The reason for the increase of $H_{(4,6)}$ and $R_{(4,6)}$ is analogous to the increase of $H_{(5,6)}$ and $R_{(5,6)}$ between points d and c. The increase of $R_{(4,6)}$ coincides with an increase in $Q_{\langle 4,5\rangle}$ and a decrease in $Q_{(4,6)}/Q_{(1,4)}$ (see Figures 3.7b and 3.10e). Therefore, $H_{(4,6)}$ and $R_{(4,6)}$ both decrease (see Figures 3.10a and 3.10c) analogously to decreasing $H_{(5,6)}$ and $R_{(5,6)}$ between points d and c. As with the example of an increase in β in the (0) equilibrium, $H_{\langle 4,5\rangle}$ and $R_{\langle 4,5\rangle}$ are constant (see Figures 3.10g and 3.10h). As $R_{(5,6)}$ decreases, $R_{(4,6)}$ increases and $R_{\langle 4,5\rangle}$ remains constant, the resistance along the pathway $4 \to 5 \to 6$ decreases. As with the example of increasing β on the (0) equilibrium, once $Q_{\langle 4,5\rangle}$ is large enough, $R_{\langle 4,5\rangle}$ sharply increases, which coincides with the existence of a limit point.

Impact of decreasing β on the (+) equilibrium

The impact of decreasing β on the (+) equilibrium between points f and e is analogous to the impact of increasing β on the (−) equilibrium between points b and c. As β decreases, so does $R_{(4,6)}$ (see Figure 3.10c). This decrease in $R_{(4,6)}$ results in a decrease in the values of $Q_{\langle 4,5\rangle}$, $H_{\langle 4,5\rangle}$ and $R_{\langle 4,5\rangle}$ (see Figure 3.7a, 3.10g and 3.10h). The decrease in $Q_{\langle 4,5\rangle}$ leads to the decrease in the values of $H_{(4,6)}$ and $R_{(4,6)}$ (see Figures 3.10a and 3.10c). The reason for this is analogous to the decreasing values of $H_{(5,6)}$ and $R_{(5,6)}$ between points b and c. $H_{(5,6)}$ and $R_{(5,6)}$ increase (see Figures 3.10b and 3.10d). The reason for this increase is analogous to how $H_{(4,6)}$ and $R_{(4,6)}$ increase when β increases between points b and c. Therefore, the resistance to blood flow along the path $4 \to 5 \to 6$ also increases. As $Q_{\langle 4,5\rangle}$ is decreases, this means that the flow ratio $Q_{(4,6)}/Q_{(1,4)}$ tends toward 1, eventually the equilibrium is no longer viable.

Impact of increasing β on the (+) equilibrium

As β increases: $H_{(4,6)}$ and $R_{(4,6)}$, between points f and g, increase; $Q_{(4,6)}/Q_{(1,4)}$ decreases; and $H_{(5,6)}$ and $R_{(5,6)}$ decrease. The explanation is analogous to decreasing β for the (−) equilibrium between points b and a. Despite the increase in $R_{\langle 4,5\rangle}$, the resistance along the

path $4 \rightarrow 5 \rightarrow 6$ decreases. As this reduces the resistance in the vessels for the current flow direction, the equilibrium does not encounter a limit point.

To simplify the explanation for the formation of this pattern of two fold bifurcations, the processes have been described as a sequence of events. However, in reality, all processes occur simultaneously. Although the reason for each case is slightly different, the cases did share some common properties. In all cases, the resistance along the flow pathways would adjust to accommodate a change in the network parameters. For the cases that resulted in the existence of a limit point, the variables could no longer adapt to the change in geometry. For the cases that did not end at a limit point, the change in the resistances of the flow pathway was favourable to the current flow directions in the network.

The plots of the haematocrit and resistance variables for the square plus triangle network with the same geometry used to generate the continuation curve in Figures 3.7b and 3.7c share many of the same properties observed in Figure 3.10 (Results not shown). Given the complex nature of the square plus triangle network, an explanation for the existence of fold bifurcations similar to that of the triangle network is far more complex. Therefore, an explanation of the fold bifurcations for the square plus triangle network has not been attempted. However, given that the fold bifurcations are a common feature of equilibria, it is reasonable to suggest that the formation of the pattern of fold bifurcations in any network is similar to the description of the formation of fold bifurcations for the triangle network.

3.6 Equilibria for larger networks

Before considering the stability of different equilibria, we pause to investigate if the equilibria of the triple triangle network in Figure 3.3c have unique flow configurations. So far, the two networks we have studied demonstrate that each equilibrium corresponds to a unique flow configuration for the redundant vessels for most sets of network parameters. The implications of this being true limits the number of possible equilibria present in a network by the maximum number of flow configurations. The Triple triangle network has three redundant vessels: if the same principle applies to the triple triangle network, we can expect a limit of 27 equilibria.

Previously, the maximum number of equilibria was attained for symmetric networks with small diameters. Therefore, the following parameter values are used to demonstrate this

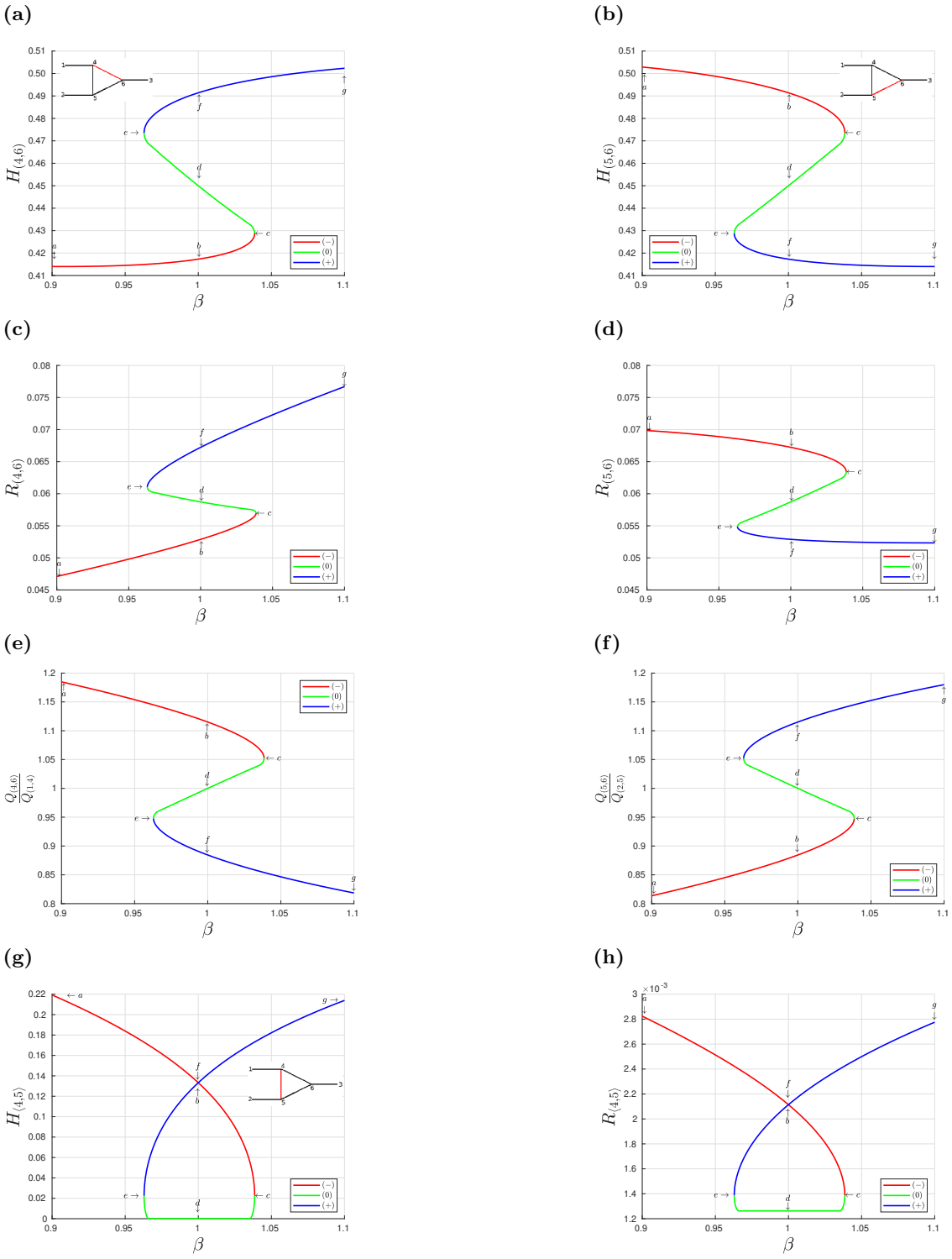

Figure 3.10: Series of plots of variables in the triangle network as the length ratio β changes for the fixed length ratio $\alpha = 0.1$. (a): $H_{(4,6)}$; (b): $H_{(5,6)}$; (c): $R_{(4,6)}$; (d): $R_{(5,6)}$; (e): $Q_{(4,6)}/Q_{(1,4)}$; (f): $Q_{(5,6)}/Q_{(2,5)}$; (g): $H_{\langle 4,5\rangle}$; (h): $R_{\langle 4,5\rangle}$.

principle:

$$L_{\langle 6,7\rangle} = L_{\langle 8,9\rangle} = L_{\langle 12,13\rangle} = 10\mu m, L = 100\mu m, D = 10\mu m, P_2 = 1 - P_1, \tag{3.35}$$

and the inlet pressure, P_1, is the continuation parameter. Using this continuation parameter, we found 27 equilibria in a small neighbourhood around $P_1 = 0.5$ for which the flow configuration for every equilibrium is unique, as predicted. However, the equilibria differ from those observed for the previous two networks. The equilibria of the previous networks belonged to a single continuation curve for which the inlet pressure P_1 was the continuation parameter. This is not the case for the triple triangle network; the equilibria of the network all belong to one of nine disconnected continuation curves. Furthermore, these disconnected curves are characterised by the flow configurations of vessels $\langle 6, 7\rangle$ and $\langle 8, 9\rangle$. Only the curves characterised by the flow configurations:

$$(-, -, \cdot), (-, 0, \cdot), (-, +, \cdot), \tag{3.36}$$

are shown in Figure 3.11 for the sake of brevity. The flow configurations and the value of the normalised flow in the redundant vessels when $P_1 = 0$ for the curves in Figure 3.11 have been listed in Table 3.2. The other disconnected continuation curves are similar to the curves in Figure 3.11 but these results have been left out of the thesis for brevity.

It is also important to specify that the haematocrit distribution within the diamond subnetworks is independent of changes in pressure conditions. Some of the properties of these networks, first discussed in Section 1.9.6, provide an explanation for this observation. As the inlet haematocrit is independent of the changes in the boundary pressures, this implies that $H_{(10,12)} = H_{(1,4)}$ and $H_{(11,13)} = H_{(2,5)}$. Given that the haematocrit distribution for a network with a single inlet and outlet is independent of the pressure boundary conditions, this principle also applies to the diamond subnetworks of the triple triangle network because a change in the pressure boundary conditions does not change the inlet haematocrit. However, if the haematocrit boundary conditions were to change, then the number of disconnected paths would decrease. Figure 3.12 shows how the equilibria of the diamond subnetwork, consisting of the nodes $\{1, 4, 6, 7, 10, 12\}$, change as the inlet haematocrit $H_{(1,4)}$ decreases. Eventually the negative and positive solutions encounter fold bifurcations and beyond the critical values of $H_{(1,4)}$ of the fold bifurcations, only one equilibrium remains viable. Therefore, if the values of $H_{(1,4)}$ and $H_{(2,5)}$ were below these critical values, then

all equilibria would only belong to a single continuation curve because only one equilibrium exists in each diamond subnetwork.

$Q_{\langle 6,7\rangle}$	$Q_{\langle 8,9\rangle}$	$Q_{\langle 12,13\rangle}$	Flow orientation	Network diagrams
-0.0818	-0.0817	-0.1673	$(-,-,-)$	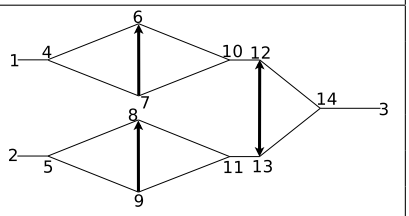
-0.0819	-0.0819	0.0	$(-,-,0)$	
-0.0817	-0.0818	0.1673	$(-,-,+)$	
-0.0818	0.0	-0.1692	$(-,0,-)$	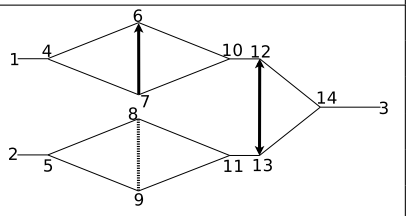
-0.0819	0.0	0.0022	$(-,0,0)$	
-0.0817	0.0	0.1654	$(-,0,+)$	
-0.0818	0.0817	-0.1673	$(-,+,-)$	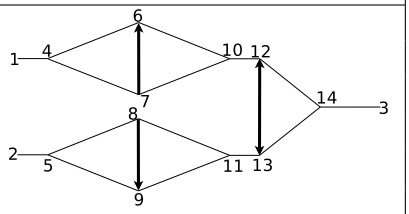
-0.0819	0.0819	0.0	$(-,+,0)$	
-0.0817	0.0818	0.1673	$(-,+,+)$	

Table 3.2: Table of the equilibria for the triple triangle network in Figure 3.11. The flow orientation column is of the form $(s_{\langle 6,7\rangle}, s_{\langle 8,9\rangle}, s_{\langle 12,13\rangle})$. The single arrows on the network diagrams indicate a fixed flow direction, the two headed arrows indicate a varying flow direction and the dashed lines indicate intermediate flow.

As can be seen in Figure 3.12, so long as the inlet haematocrit of one of the diamonds is sufficiently large, the diamond admits three equilibria, distinguished by the flow state in the redundant vessel. Each of the equilibria has an associated haematocrit distribution independent of the pressures at the inlet and outlet. As the haematocrit distributions are separate and do not change with changes in the boundary conditions, the three equilibria are distinct for any changes to the boundary conditions. Therefore, the three equilibria belong to three different paths in parameter space. Therefore, the combination of two diamond networks with this property results in the existence of nine disconnected paths. Given that the two diamond networks admit three equilibria when $H_{(1,4)} = H_{(2,5)} = 0.45$, the triple triangle network admits 9 paths.

3.7 Stability of the equilibria

Gardner et al. (2010) determined that the equilibrium with intermediate flow in the redundant vessel was unstable and the equilibria with negative or positive flow were stable.

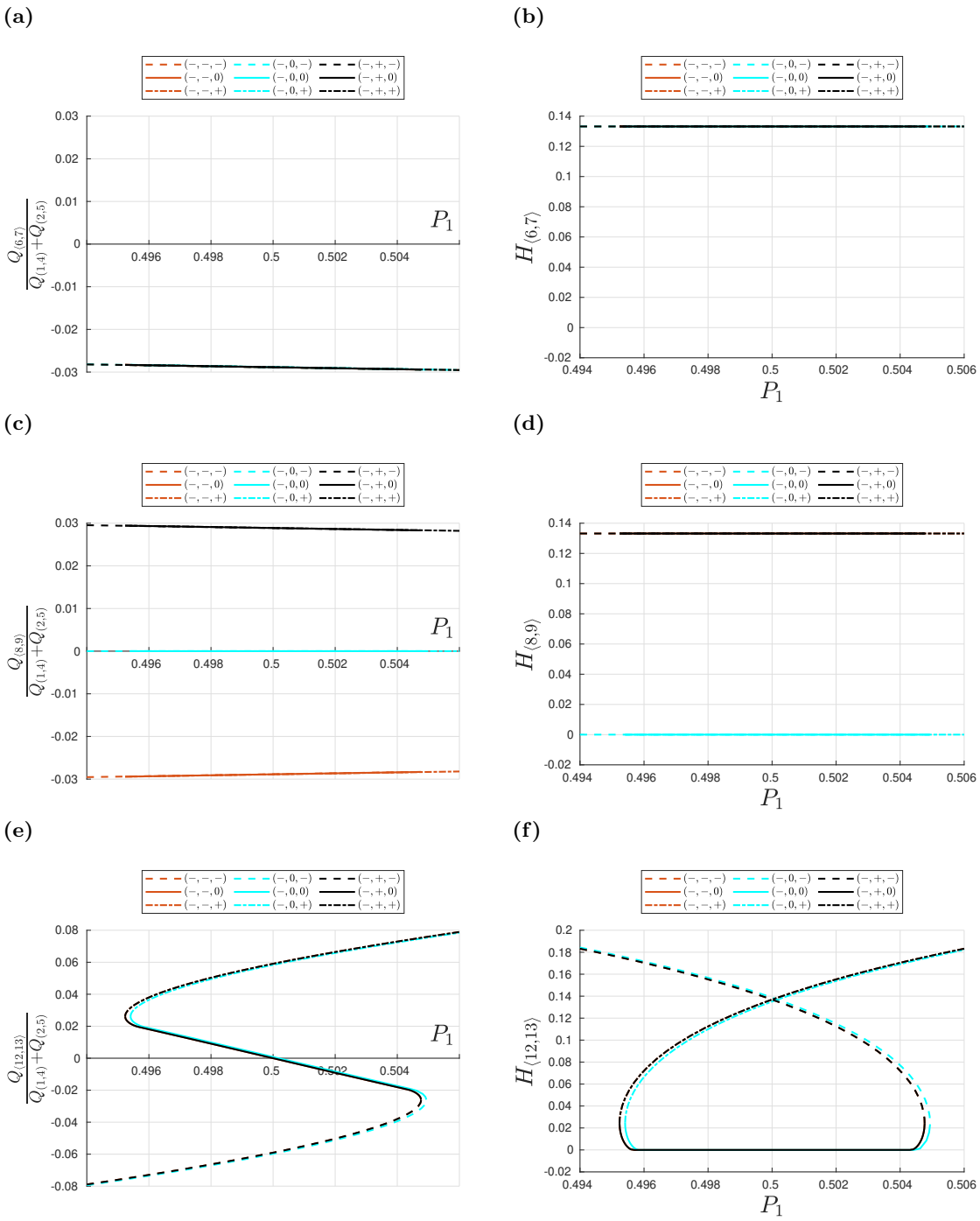

Figure 3.11: Series of plots for volumetric flows and haematocrit variables for the redundant vessels. We plot the equilibria for which the flow in the vessel $\langle 6,7\rangle$ is negative.

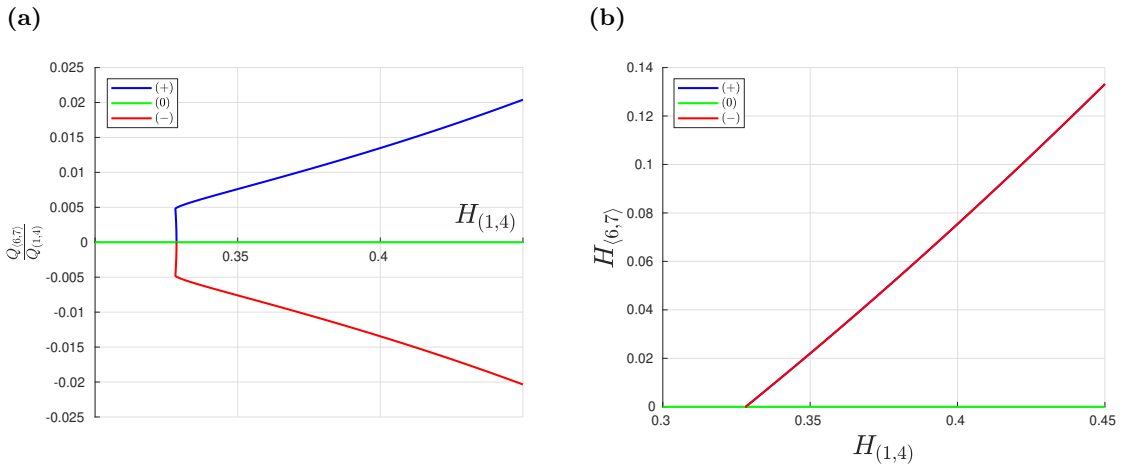

Figure 3.12: Series of plots for volumetric flows and haematocrit variables for the redundant vessel of a diamond subnetwork of the triple triangle network. (a): $Q_{\langle 6,7\rangle}/Q_{(1,4)}$ as a function of the inlet haematocrit $H_{(1,4)}$; (b): $H_{\langle 6,7\rangle}$ as a function of the inlet haematocrit $H_{(1,4)}$.

This section does not attempt to classify the stability of every equilibrium found in the previous sections, but instead, determine if the stability pattern of the square plus triangle network is similar to the stability pattern identified for the triangle network by Gardner et al. (2010). Instead of performing a linear stability analysis of the system of PDEs for the square plus triangle network, we have chosen to solve the equations numerically to assess stability. The system of PDEs for the square plus triangle network can be inferred from the network geometry and the equation construction in Section 1.8, but a summary of the equations for the square plus triangle can be found in Appendix A.2. To solve the time-dependent equations, the PDEs are converted into a system of DDEs of the form:

$$\frac{\mathrm{d}\overline{H}}{\mathrm{d}t} = \overline{u}(t)(H(0,t)H(0,t-\tau(t))), \tag{3.37}$$

$$\frac{\mathrm{d}\overline{\mu}}{\mathrm{d}t} = \overline{u}(t)(\mu(H(0,t),D) - \mu(H(0,t-\tau(t)),D)), \tag{3.38}$$

where $\overline{H}$ is the average haematocrit of the vessel, $\overline{\mu}$ is the average viscosity and $\overline{u}$ is the average propagation speed of the RBCs. Details of this method can be found in Section 2.3. To assess the linear stability of an equilibrium, the haematocrit distribution for the equilibrium is used as the initial condition but with a small perturbation applied to one of the haematocrit values. The numerical solution was then calculated for $t = 30$ and if the numerical solution at $t = 30$ was within 0.001 of the original equilibrium, then that equilibrium was classified as stable.

To understand the relationship between the flow configurations and the stability of the time-dependent equations, we use the following set of parameters to generate a set of equilibria:

$$D = 10\mu m, L = 100\mu m, P_2 = 1 - P_1,$$

$$H_{(1,4)} = H_{(2,5)} = 0.45, L_{\langle 6,7\rangle} = L_{\langle 4,5\rangle} = 50\mu m$$

and P_1 as the continuation parameter. Figure 3.13 shows the set of equilibria for the specified parameters. The stable equilibria are displayed by solid lines and the unstable equilibria are shown by dashed lines. For the results in Figure 3.13, the following flow configurations were stable:

$$(-,-),(-,+),(+,-),(+,+), \tag{3.39}$$

and the equilibria with the flow configurations:

$$(0,-),(0,+),(-,0),(+,0),(0,0), \tag{3.40}$$

were unstable. Therefore, we conclude that the equilibria with intermediate flow in one or both redundant vessels are unstable.

3.8 Discussion

Given the nonlinearity of the network equations, it is difficult to definitively conclude which properties of a network are vital for the formation of multiple equilibria in a single network. Furthermore, vasculature topology and geometry can vary significantly, and so it is difficult to translate the results from numerical studies to other networks. However, we have been successful in our goal of identifying the key properties of network topology that lead to the formation of multiple equilibria. Our results represent a wide range of test cases designed to extract some common properties of the flow behaviour in microvasculature. Each case provided supporting evidence for a variety of conclusions. These conclusions have been summarised in the following six sections

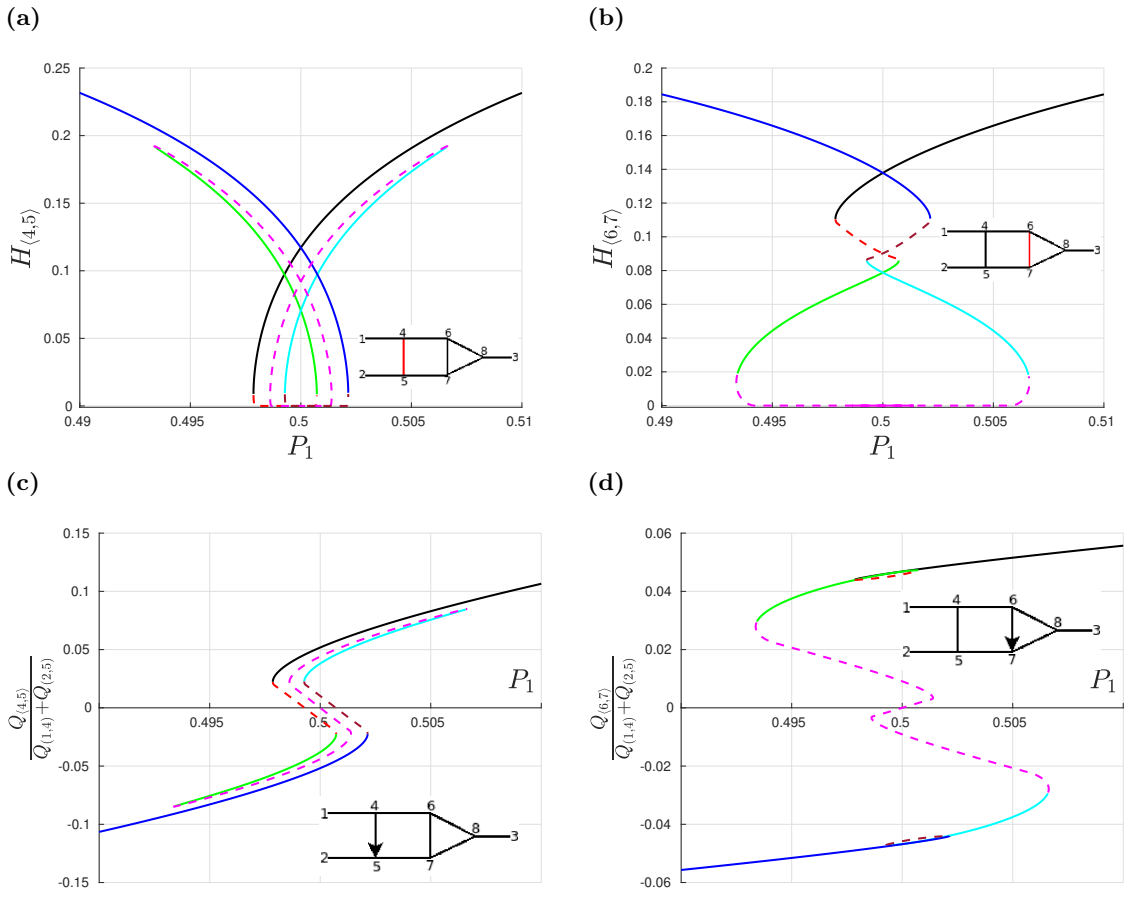

Figure 3.13: Series of plots of the equilibria of the square plus triangle network as the inlet pressure P_1 varies. The solid lines represent the stable equilibria and the dashed lines represent the unstable equilibria.

Pattern of flow state configurations

The main conclusion to draw from these results is the relationship between the equilibria and the flow configurations of the redundant vessels. By classifying the flow in redundant vessels as positive, negative, or intermediate, most equilibria can be classified using a unique combination of these classifiers. Karst et al. (2017) were the first to observe the link between the flow direction and the multiple equilibria, but did not link these multiple flow directions to the network topology. The results of this chapter extend the link between flow direction and the equilibria with the introduction of the intermediate flow states in the redundant vessels. Categorising the equilibria using flow configurations is more advantageous than grouping the equilibria by flow direction because using flow states provides a more granular description of the equilibria. Based on this understanding of the flow configurations of positive, negative, and intermediate flow states in the redundant vessels, predictions for the number of possible equilibria can be based purely upon the network's topology.

Until now, the link between network redundancy and the multiplicity of solutions to the network equations has not been identified. Our results in Section 3.4 show that despite the difficulty of predicting the values of the parameters for which the network would admit multiple equilibria, the existence of multiple equilibria always occurred when the flow in a redundant vessel could travel in both directions. When the definitions of the flow states were applied to these results, the definitions yielded a unique description of the equilibria.

Most of the results in Section 3.4 show that the square plus triangle network admitted two intervals of changing flow direction, one for each redundant vessel. These intervals were disconnected for most of the splitting rules. Therefore, each interval admits only three equilibria, each of which has a different flow state in one of the two redundant vessels. However, for one of the splitting rules that we studied, these intervals of changing flow direction overlap, leading to the formation of an interval for which the square plus triangle network admits five equilibria, as seen in Figures 3.5c and 3.5d. As the network equations are nonlinear and highly coupled, the existence of one region of multiple equilibria in parameter space influences the existence of other regions. However, these equilibria belong to distinct regions in parameter space and this example shows that if the choice of splitting rule and network geometry allows for these intervals to overlap, then the combination of flow configurations create intervals of more than three equilibria. Section 3.5 shows more examples of these overlaps, leading to the creation of an equilibrium for every possible flow configuration. Figures 3.7b, 3.7c and 3.7d show two intervals in the length ratio β for which the flow in the redundant vessel supports the three flow states. As the interval of multiple

viable flow states for vessel $\langle 6, 7\rangle$ is embedded within the interval of multiple flow states for vessel $\langle 4, 5\rangle$, the network supports every configuration of the flow states.

In most of the cases studied, the equilibria always correspond to a unique flow configuration. This not only allows predictions on how many possible equilibria are present in larger networks, it also provides a possible methodology for finding these equilibria. As viable flow configurations of redundant vessels are linked to the existence of multiple equilibria, identifying redundant vessels of larger networks provides a useful starting point for finding the equilibria of a network. As redundant vessels are determined by the network topology, they can be identified without prior knowledge of the equilibria. This could be crucial for using the homotopy function of Equation (3.9). The starting system for this homotopy function only has one equilibrium for a set haematocrit distribution H^*. Therefore, using different starting haematocrit distributions with different corresponding flow directions in the redundant vessels may be a more useful strategy than randomly choosing a starting distribution. Although numerical continuation is never guaranteed to find a solution, in theory, it is possible to track the equilibrium of the starting system to an equilibrium of the target system with the same flow configuration if that flow configuration is viable for the network.

Pattern of fold bifurcations

We have shown that equilibria occur mainly in sets of three, distinguished by a difference in flow state for a single redundant vessel. Most intervals of multiple equilibria in this chapter have been formed by patterns of fold bifurcations which coincide with a change in the flow direction in a redundant vessel. Section 3.5.2 explains how the symmetry of a symmetric triangle network resulted in the existence of three equilibria. This is an intuitive result for the triangle network because it is clear that one of these equilibria is simply the mirror image of the other. Furthermore, Section 3.5.2 also explains the wider phenomenon of equilibria occurring in sets of three, or the prevalence of the common pattern of fold bifurcations. Figure 3.10 shows that the haematocrit distributions of the three equilibria adjust as the geometry of the network changes to account for the breaking of symmetry. As with all examples studied in this chapter, the haematocrit distribution can only account for relatively small changes in the asymmetry of the network. Once the haematocrit distribution can no longer adjust to account for the alteration of the network geometry, the equilibria encounter fold bifurcations, and only one of the equilibria remains viable. Furthermore, the flow direction in the remaining equilibrium is always in the direction that favours the asymmetry of the network. For instance, as the length of the side of the triangle network

increases, the resistance in the side increases. Once the length of the side is sufficiently large, only the (+) equilibrium remains viable because the blood is flowing away from the side of the network with greater resistance.

The pattern of fold bifurcations like those seen in Figure 3.7a are not exclusive to the triangle network. The square plus triangle network also admits these patterns of fold bifurcations. However, the fold bifurcations were not exclusive to a single redundant vessel. In Figures 3.7b and 3.7c two intervals of changing flow direction are created by the same pattern of fold bifurcations. One interval corresponded to a change in the direction of the flow in vessel $\langle 4, 5\rangle$. The other interval was formed by the flow changing direction in vessel $\langle 6, 7\rangle$ for each flow state of vessel $\langle 4, 5\rangle$. This indicates that although the network equations are highly coupled, changes in the flow state of certain redundant vessels can be induced without changing the flow state of other redundant vessels. Therefore, the haematocrit distribution in the network can change locally to account for small differences in network geometry.

Not only can the haematocrit distribution account for the change in the geometry of a network, asymmetry of the boundary conditions can also recover flow configurations that are no longer viable due to a change in the geometry. For example, only the equilibria with the flow configurations:

$$(-,+),(0,+),(+,+), \tag{3.41}$$

are admitted by the square plus triangle network in Figures 3.4 and 3.5 when the boundary conditions of the network were symmetric. When asymmetry was introduced to the pressure boundary conditions, the three equilibria created by a change in the flow direction in vessel $\langle 4, 5\rangle$ are no longer viable, but this coincides with the emergence of three equilibria with a change in the flow direction in vessel $\langle 6, 7\rangle$. Therefore, the change in the flow direction in vessel $\langle 6, 7\rangle$ has been recovered by the asymmetry of the inlet pressures at the cost of removing the change in the flow direction in vessel $\langle 4, 5\rangle$. Based on these results, we can conclude that the underlying process of the emergence of multiple equilibria remains the same in a network, but asymmetries in the geometry or boundary conditions dictate which flow configurations are viable.

Negligible impact of splitting rules

An important result we have obtained is the negligible impact of different splitting rules on the emergence of multiple equilibria. For instance, in Section 3.4, we found that all

five splitting rules admitted multiple equilibria for very similar intervals of inlet pressures. These intervals also contained the same number of equilibria and could be characterised by the same flow configurations. Therefore, regardless of the splitting rule, the classification of the equilibria has remained constant. The only exception to this general trend is that of the simple splitting rule when $P = 2.0$ (see Figure 3.5). The two intervals of changing flow direction overlapped, creating an interval with more than three equilibria. Although this is an important distinction, this example does not fundamentally change the mechanism by which multiple equilibria emerge. We conclude that different splitting rules change the size of the intervals for which multiple equilibria exist but does not have a significant effect on the position of the intervals nor on the flow configurations present in the intervals. It should be noted that the difference between the variables for the three sets of equilibria in Figures 3.4d and 3.5d was greater than in Figures 3.4c and 3.5c. Hence, the difference in the equilibria may eventually diverge for vessels sufficiently distant from the network's inlets.

The existence of intermediate flow provides one possible explanation of why the specific choice of splitting rule has a minimal effect on the number of equilibria. Usually, when an equilibrium has intermediate flow in a redundant vessel, the ratio of flow entering that vessel is less than the critical X_0 parameter. Therefore, the haematocrit within the redundant vessel is 0 and the haematocrit for the other daughter vessel is equal to H_p/r for any splitting rule (H_p is the haematocrit of the parent vessel and r is the flow ratio). Therefore, the equilibrium with intermediate flow is quantitatively and qualitatively similar for all five splitting rules. Equilibria with intermediate flow belong to sets of three, and these three equilibria often form a pattern of fold bifurcations with a change in the flow direction in a redundant vessel. Therefore, the other equilibria in these sets of three are found in similar intervals of parameter space.

It should be noted that our results in this chapter were only generated with networks for which the diameters of the vessels were of a uniform size. Given that all splitting rules have a bias term which depends on the diameters of the daughter vessels, the difference in the functional form of this bias term may result in different patterns of equilibria for networks with nonuniform diameters. The impact of different diameters and diameter ratios is explored in Chapter 4.

Separate paths of equilibria

Our main aim of this chapter was to understand the link between the redundancy of a network and the existence of multiple equilibria. By introducing flow configurations to net-

works, it was possible to uniquely classify most equilibria using the flow in the redundant vessels. Furthermore, flow configurations allow predictions to be made for the maximum number of potential equilibria in a vasculature network. Using this approach, we were able to successfully predict that the maximum number of equilibria admitted by the triple triangle network in Figure 3.11 was twenty-seven. Like the triangle and square plus triangle network, the equilibria admitted a pattern of fold bifurcations for a redundant vessel changing flow direction. However, the equilibria for the triple triangle network had distinct properties.

Unlike the equilibria of the triangle and square plus triangle network, the equilibria of the triple triangle network belong to nine different paths in parameter space instead of one. This result can be extrapolated to conclude that a network containing subnetworks with a single inlet and outlet vessel will admit separate paths of equilibria in parameter space characterised by the combinations of flow configurations of all subnetworks of this type; so long as the value of the haematocrit entering each subnetwork is sufficiently large for the subnetwork to admit multiple equilibria.

The fact that the haematocrit distribution of these subnetworks is independent of the flows in the rest of the network could prove to be useful when resolving the equilibria of much larger networks. Instead of choosing a random haematocrit distribution as the basis of the initial continuation to find an equilibrium of a network, haematocrit distributions based on combinations of haematocrit distributions for smaller network motifs will provide a better initial estimate. By making modifications to the numerical continuation algorithm described in Figure 3.2, the equilibria of larger networks are more easily constructed. For example, if the equilibria of the triple triangle network are resolved using this modification, then the nine combinations of the equilibria for the diamond networks provide a better initial guess for the equilibria of the whole network.

Flow pathways

Results in Section 3.5 show that the region of multiple equilibria is much larger for the square plus triangle network. The shape of these regions may provide some insight into the reason for this phenomenon. The networks admitted larger intervals of multiple equilibria when the length of the redundant vessels were small. Shorter vessels have less resistance than longer vessels provided the haematocrit and diameter remains constant, so shorter redundant vessels incur less of a penalty for blood flow. Therefore, the blood flow pathways through redundant vessels are more viable in either direction because there is less potential

resistance for the blood flow in either direction. This is why, despite the asymmetry of the other vessels in the network, smaller redundant vessels allow for the blood to flow along more potential pathways. Due to the relationship between the number of flow pathways and equilibria, shorter redundant vessels correspond to the existence of more equilibria.

As the number of flow states grows exponentially with the size of the network, it may be computationally infeasible to find all viable flow configurations of a large network. However, if the tumour vasculature does not contain many redundant vessels, then the exponential upper bound may not be a prohibitive barrier to computing all equilibria. (Pries et al., 2010) suggested that a small number of vessels in tumours redirect blood along longer pathways, causing redistribution of blood within the tumour vasculature. These are often referred to as functional shunts. Unlike redundant vessels, these have not been defined by the topology of the network, but share some qualitative characteristics with the redundant vessels. It is not clear how prominent these structures are in the tumour vasculature, and it is possible that shunts are rare (Less et al., 1991). Our results suggest that multiple equilibria are more likely to exist in networks with more redundant vessels, due to the existence of more potential flow pathways, but if redundant vessels are rare, then this would suggest that the presence of multiple equilibria is an unlikely phenomenon.

Instability of intermediate flow

We found that the equilibria with intermediate flow were consistently unstable, while equilibria with positive or negative flow were stable. Intermediate flow in a redundant vessel usually corresponds to zero, or close to zero, haematocrit in that redundant vessel. Therefore, the resistance to blood flow in a redundant vessel for equilibria with intermediate flow is less than the resistance for equilibria with positive or negative flow. We hypothesised that the lower resistance makes the equilibria more susceptible to change because any change in the haematocrit distribution will have a greater impact on an equilibrium with zero haematocrit in a redundant vessel because there is less resistance to the blood flow changing direction. Although this adequately explains the results presented here, it should also be noted that oscillations have been observed for equilibria of networks with one redundant vessel (Ben-Ami et al., 2022; Geddes et al., 2010; Karst et al., 2015). Geddes et al. (2007) observed oscillations for both triangle and diamond networks. Karst et al. (2015) linked the existence of multiple equilibria with different flow directions with stable and unstable limit cycles centred at the non-zero equilibria and found a variety of different dynamic behaviours for a range of different length ratios and inlet haematocrits. Furthermore, their results imply that the equilibria are more likely to be stable for a symmetric

network. Given that the network studied in Section 3.7 was symmetric, it is unsurprising that four of the nine equilibria were stable. Ben-Ami et al. (2022) provide the most clarity on the link between multiple equilibria and stability. They observed that in a phase plane of the inlet haematocrit and diameter ratios for the triangle network, the equilibria with zero flow, or trivial solution, were stable for smaller inlet haematocrit values. Furthermore, a transcritical bifurcation existed for all diameter ratios for which the trivial solution would become unstable, and this transcritical bifurcation would almost exactly coincide with the emergence of multiple equilibria. At least one of these equilibria is always stable and if the network is symmetric, then both non-zero equilibria are stable. With this additional context, we can hypothesise that equilibria with only positive and negative flows are not always stable, but equilibria with intermediate flow are unstable.

We have demonstrated in this chapter that, although it is not possible to predict the existence of multiple equilibria in larger networks based on the equilibria of other networks, network redundancy is key to the formation of multiple equilibria. These conclusions provide useful insights that can be used to find the equilibria of larger networks and explain why multiple equilibria occur. In particular, our results could provide insight into which networks are likely to admit multiple equilibria based on the number of redundant vessels. Finding the equilibria of these networks could then be used to investigate oxygen distribution patterns in cancerous tumours and many other conditions.

Ben-Ami et al. (2022) showed that multiple equilibria are vital to the instabilities and self sustained oscillations of the blood flow for a network with a single redundant vessel. Therefore, one avenue for future work would be to investigate the behaviour of time-dependent flow equations to determine if the multiple equilibria present in larger networks lead to the formation of oscillatory dynamics in the blood flow. Another potential avenue would be to uncover a mechanism for the switching of the solution from one stable state to another. Both avenues could be used to explain the fluctuations observed in oxygen levels in the surrounding tissue. Understanding the link between blood flow in the microcirculation and oxygen fluctuations could be critical to understanding the formation of cycling-hypoxia.

Chapter 4

Influence of scale on the multiplicity of equilibria

4.1 Introduction

In Chapter 3, the link between network redundancy and the multiplicity of solutions was explored. By linking the flow states with the network equilibria, most equilibria were categorised with unique flow configurations that consistently captured the behaviour of the flow in the network. Our results provide insight into previous results by suggesting a possible mechanism for the existence of multiple equilibria found in the literature. For example, (Karst et al., 2017) showed that honeycomb and Voronoi networks admitted multiple equilibria for a range of lengths and diameters, and made the important observation that the equilibria often differed by flow direction, but some equilibria would share the same flow direction. Our results may explain both of these phenomena; according to the network equations, the flow direction can only change in certain vessels known as redundant vessels (Definition 1.2), and vessels for which the flow cannot change direction are referred to as fixed vessels. As described in Section 1.9.5, all vessels that are specified with triangular brackets ($\langle , \rangle$) are redundant vessels and all fixed vessels are denoted by circular brackets. Our results consistently show that multiple equilibria differ by flow state in one or more redundant vessels. The key difference between characterising equilibria using flow state instead of flow direction is that the definition of flow states includes intermediate flow. The flow states for a pair of equilibria can be different despite sharing a common flow direction in a redundant vessel. This not only explains why the multiplicity of equilibria is linked to the change in the flow direction and why this flow direction is only observed in certain

vessels; our results explain why the flow directions for some pairs of equilibria are the same.

As explained in the previous chapter, it is important to show the relationship between flow configurations and equilibria for a wide variety of networks. So far, we have demonstrated the relationship between flow configurations and equilibria for a range of vessel length ratios and scales on a small set of networks. We also showed evidence that the number of equilibria has an upper bound that increases exponentially with the number of redundant vessels. Both of these results provide strong evidence for the relationship between flow configuration and equilibria for all sizes of network. However, so far, we have only demonstrated this phenomenon in networks with small diameters. Furthermore, the diameters of all vessels in the networks in Chapter 3, were of uniform size. As the flow in a vessel is proportional to the fourth power of the diameter (Equation (1.32)), assuming constant viscosity, changes in the diameter potentially have a significant effect on the flow in a network. To further complicate the impact of vessel diameters, viscosity is a nonlinear function of the diameter and haematocrit of a vessel (Equation (1.3)). The parameters of the splitting rule are also often functions of the diameters of the vessels. Therefore, we must show that the equilibria of a network correspond to unique flow configurations for a range of vessel diameters.

So far, all results have been for networks for which all vessels have diameters of 10μm which represents the lower end of the scale on the size of the vessels in the microvasculature. Given most equilibria are regular points[1] of the steady-state network equations, most equilibria exist for at least some small neighbourhood of diameter values. Gardner et al. (2010) have shown that multiple equilibria exist for the triangle network for a wide range of vessel diameters, provided that the inlet haematocrits are sufficiently large. In this chapter, we investigate if the flow configurations of networks are unique as the vessel diameters vary. Due to the difficulty of investigating how the flow configurations change as the diameters vary, the analysis of how the flow configurations change as the diameters and diameter ratios vary was left out of Chapter 3. If we can show that the uniqueness of flow configurations is consistent as diameters and diameter ratios vary in just one network with multiple redundant vessels, then it is reasonable to conclude that the link between flow configurations and multiple equilibria is applicable for a wide variety of networks.

In addition to understanding how the equilibria of networks change as the diameters of

[1] A regular point, x^*, for a system of equations, F, is a point for which the Jacobian, J_F, has full rank at the point x^*. For example, if $F : \mathbb{R}^N \to \mathbb{R}^N$, then $\text{rank}(J_F(x^*)) = N$.

a network vary, it is important to show that flow configurations remain consistent for different diameter ratios because it is unlikely that vasculature networks have uniform vessel diameters. Cecil Murray (Murray, 1926), found that the work against blood flow in microcirculation was minimised when the volumetric flows in all vessels were proportional to the cube of the diameter of the vessel. The implication of Murray's law is that the sum of the cubes of the diameters of vessels entering a vessel junction is equal to the sum of the cubes of the diameters leaving the junction (Sherman, 1981). If this law is applied to vessel networks, then the vessel diameters should never be uniform. Furthermore, tumour vasculature is known to be chaotic (Carmeliet and Jain, 2000). In any case, the vessels in microvasculature should not all have the same diameters. It is not inherently true that vasculature networks with variable diameter ratios would admit the same patterns of flow configurations as those with consistent diameters. Not only does the difference in diameters impact the resistance to blood flow, the splitting rules usually bias flow according to the diameters of the daughter vessels (Bernabeu et al., 2020; Pries et al., 1990; Pries and Secomb, 2005). Therefore, we must determine whether equilibria have unique flow configurations for a range of different diameter ratios to show that this principle is consistent for all networks.

Numerical continuation will be used again in this chapter to investigate the impact of changing diameters and diameter ratios. The homotopy functions for numerical continuation in this chapter are the same as the homotopy functions described in Section 3.2. As continuation is used to investigate the change in the equilibria as the diameters increase, the diameters will eventually be larger than the vessel lengths according to the model. As the haematocrit distribution of a network does not change as long as the vessel lengths are scaled uniformly, this does not present a problem for the study of different diameter ratios.

The remainder of this chapter is broken up by the following sections: Section 4.2 describes the network constructions to be used in this chapter, Section 4.3 shows the impact of uniform scaling of network diameters, Section 4.4 contains the results of varying the diameter ratios of networks, and Section 4.5 contains the discussion of the results and future directions.

4.2 Network construction for the test cases

To investigate the effect of different network configurations on the number of equilibria, we return to the square plus triangle network first described in Section 3.3. The square plus triangle network consists of 8 nodes such that Nodes 1 and 2 are inlet nodes and Node 3 is the only outlet node. The interior nodes are labelled $4, 5, 6, 7, 8$: Nodes $4, 5, 6, 7$

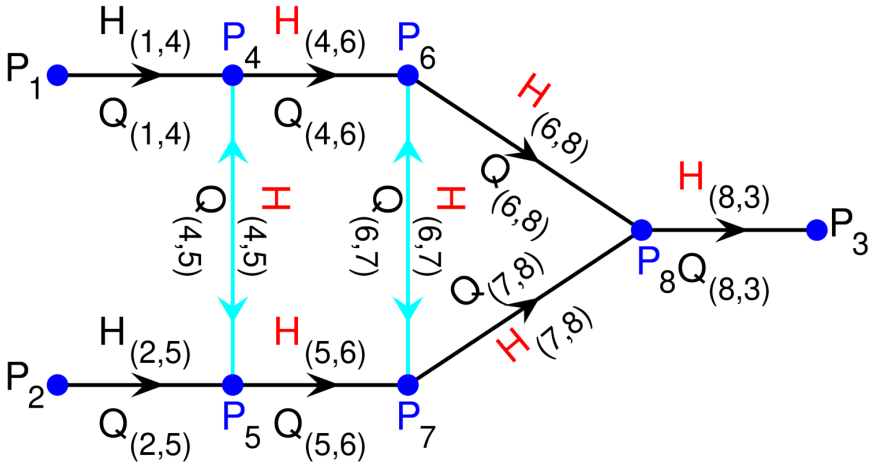

Figure 4.1: Diagram of the square plus triangle network.

form a quadrilateral and Nodes $6, 7, 8$ form a triangle (see Figure 4.1). As the network has two inlets and one outlet, it is possible to simplify the boundary pressures so that $P_1 \in [0, 1]$, $P_2 = 1 - P_1$, and $P_3 = 0$ without altering the haematocrit distribution of any equilibrium (see Section 3.3 for details). The square plus triangle network contains two redundant vessels instead of one, namely, $\langle 4, 5\rangle$ and $\langle 6, 7\rangle$. The order of redundant vessels used in this chapter is $(\langle 4, 5\rangle, \langle 6, 7\rangle)$, for which the possible flow configurations are $(-,-), (-,0), (-,+), (0,-), (0,0), (0,+), (+,-), (+,0)$ and $(+,+)$.

4.3 Large diameters

Few publications contain results that describe how the number of equilibria of networks changes as vessel diameters vary. Gardner et al. (2010) investigated how the number of equilibria of the triangle network changes as the size of vessel diameters vary. They found that multiple equilibria exist for a greater range of inlet haematocrits when the vessel diameters of the triangle network are smaller, but they limited their study to investigating this effect in networks for which the vessel diameters are all the same size. The network equations are based on the ratios of flow in the network, and the flow in a vessel is inversely proportional to the vessel length. Therefore, scaling all vessel lengths uniformly in a network does not affect the equilibria. This result does not hold for vessel diameters. The flows are proportional to the reciprocal of the viscosity, and the viscosity is a nonlinear function of a vessel's haematocrit and diameter. As a result, the flow ratio will change as the diameter changes even if the diameters all change by the same scale. Consider, the bifurcation in Figure 1.3a. Assume that $P_u - P_v = P_v - P_w = 1, D_{(u,v)} = D_{(v,w)} = 10\mu m, L_{(u,v)} =$

$L_{(v,w)} = 100\mu m$, $H_{(u,v)} = 0.45$ and $H_{(v,w)} = 0.4$. Then the ratio of flows is given by:

$$\frac{Q_{(v,w)}}{Q_{(u,v)}} = \frac{\frac{10000\pi}{12800\mu(0.4,10)}}{\frac{10000\pi}{12800\mu(0.45,10)}} = \frac{\mu(0.45,10)}{\mu(0.4,10)} = 1.1731, \tag{4.1}$$

where $\mu(H,D) = \mu_p\mu^{(\text{rel})}(H,D)$, μ_p is the viscosity of the plasma and $\mu^{(\text{rel})}(H,D)$ is given by Equation (1.3). If we change the diameters of the two vessels to $D_{(u,v)} = D_{(v,w)} = 20\mu m$, then the flow ratio is:

$$\frac{Q_{(v,w)}}{Q_{(u,v)}} = \frac{\mu(0.45,20)}{\mu(0.4,20)} = 1.1385. \tag{4.2}$$

Although this is not a large difference given that the diameters of the network can influence the number of equilibria in the triangle network, we anticipate a similar behaviour for the square plus triangle network (Gardner et al., 2010).

In Section 3.4, we investigated the effect of different splitting rules on the equilibria, but only for the square plus triangle network with uniform diameters. As in Chapter 3, it is important to verify our findings for more than one splitting rule to control bias in our results introduced by a specific splitting rule. Section 3.4 directly compared the Gardner[2] (Gardner et al., 2010; Pries et al., 1990), Pries (Pries and Secomb, 2005) and Simple splitting rules. The conclusion to this comparison was that the flow configuration is unique for every equilibrium regardless of the choice of splitting rules. Given the similarities between the equilibria using different splitting rules in Chapter 3, it is not necessary to use all five splitting rules in this chapter, but all bifurcation diagrams are generated using the Gardner and Simple splitting rule. As a reminder, all splitting rules are in the form of Equation (1.13):

$$\psi_{(v,w)}(r_{(v,w)}) = \begin{cases} 0 & \text{if } r_{(v,w)} < X_0 \\ 1 & \text{if } r_{(v,w)} > 1 - X_0 \\ \frac{e^A(r_{(v,w)}-X_0)^P}{e^A(r_{(v,w)}-X_0)^P + (1-r_{(v,w)}-X_0)^P} & \text{if } X_0 \leq r_{(v,w)} \leq 1 - X_0 \end{cases} \tag{1.13}$$

where the indices u, v and w denote the nodes present in Figure 1.3a, $r_{(v,w)} = Q_{(v,w)}/Q_{(u,v)}$, and the coefficients X_0, A and P are defined by the specific splitting rule. The definitions for the key splitting rule coefficients for the Gardner and Simple splitting rules can be found

[2]The Gardner splitting rule was first described by Pries et al. (1990). We call this the Gardner splitting rule to distinguish this rule from the other splitting rule described by Pries and Secomb (2005) and because this splitting rule was used by Gardner et al. (2010) to obtain important results for the triangle network.

in Table 4.1.

Splitting rule	P	A	X_0
Gardner	$1 + 6.98\frac{1-H_{(u,v)}}{D_{(u,v)}}$	$-\frac{6.96}{D_{(u,v)}} \log\left(\frac{D_{(v,w)}}{D_{(v,z)}}\right)$	$\frac{0.4}{D_{(u,v)}}$
Simple	1.4	$-\frac{7}{D_{(u,v)}} \frac{(D_{(v,w)}-D_{(v,z)})}{(D_{(v,w)}+D_{(v,z)})}$	0.05

Table 4.1: Summary of the different functional forms that are used in Equation (1.13) to generate the different haematocrit splitting rules. The indices of the vessels correspond to the bifurcation unit in Figure 1.3a and the functions P, A and X_0 determine the ratio of RBCs $Q_{(v,w)}H_{(v,w)}/Q_{(u,v)}H_{(u,v)}$.

To better understand how the diameters of the vessels affect the equilibria of a network, we will test how the equilibria change when all diameters of the square plus triangle network are scaled by the same constant. The square plus triangle network admits up to nine equilibria when the network is symmetric. Therefore, we will use lengths and boundary conditions that are symmetric for the two sides of the square plus triangle network. For this example, we can choose the following variables:

$$L_{\langle 4,5\rangle} = L_{\langle 6,7\rangle} = 10\mu m, L = 100\mu m, H_{(1,4)} = H_{(2,5)} = 0.45, P_1 = P_2 = 0.5.$$

For vessel diameter values of $D = 10\mu m$, the square plus triangle network admits nine equilibria for both splitting rules. These nine equilibria are uniquely defined by their respective flow configurations, and given that the square plus triangle network only contains two redundant vessels, these equilibria represent the full range of flow configurations. Before describing how these equilibria change as the diameters of the network vary, it is important to remind the reader of the definitions of intermediate flow. Definition 3.1 defines the intermediate flow in networks with a single redundant vessel and Definition 3.2 defines the intermediate flow in networks with multiple redundant vessels. To summarise the main properties of both definitions: for a set of three equilibria, a, b and c, if:

$$Q^{(a)}_{\langle x,y\rangle} < 0, Q^{(b)}_{\langle x,y\rangle} \leq 0, Q^{(c)}_{\langle x,y\rangle} > 0 \text{ or } Q^{(a)}_{\langle x,y\rangle} < 0, Q^{(b)}_{\langle x,y\rangle} \geq 0, Q^{(c)}_{\langle x,y\rangle} > 0,$$

and:

$$|Q^{(a)}_{\langle x,y\rangle}| > |Q^{(b)}_{\langle x,y\rangle}| \text{ and } |Q^{(c)}_{\langle x,y\rangle}| > |Q^{(b)}_{\langle x,y\rangle}|,$$

then the network has intermediate flow in vessel $\langle x, y\rangle$ for equilibrium b. Equilibria for which the flow in a redundant vessel does not meet the requirements for intermediate flow are described as having positive or negative flow if the flow direction in the vessel is positive

or negative, respectively.

Each of these nine equilibria of the square plus triangle network present when $D = 10\mu$m are used as the starting solutions to the homotopy function in Equation (3.12), with D as the continuation parameter. In this section, we use the convention that all equilibria in the bifurcation diagrams are labelled with the same flow configuration for the square plus triangle when $D = 10\mu$m.

Figure 4.2 displays the bifurcation diagrams for normalised flow in redundant vessels for the square plus triangle network. The nine flow configurations, identified by the legend, remain viable for an interval of diameters between $(8\mu m, 27\mu m)$ for both splitting rules. For a diameter value of $\approx 27\mu m$, pairs of equilibria converge at fold bifurcations. Above this range, only three equilibria with the flow configurations $(-,-), (+,+)$ and $(0,0)$ remain viable. Another pair of fold points can be found at $D \approx 30\mu m$ and so the only valid flow configuration for diameters greater than $30\mu m$ is that of $(0,0)$. As with the diameter values of $\approx 27\mu m$, pairs of equilibria meet at fold bifurcations at diameter values between $7\mu m$ and $8\mu m$. For $D \lesssim 7\mu m$, only the equilibrium $(0,0)$ remains viable. Therefore, multiple flow configurations remain viable for a wide interval of D.

However, it should be noted that the equilibria do not have unique flow configurations for all values of D. For example, there are five equilibria with the following flow configurations:

$$(-,-), (-,-), (0,0), (+,+), (+,+), \tag{4.3}$$

when $D \approx 30\mu$m. This contradicts our claim that each equilibrium has a unique flow configuration, but given that this occurs in such a narrow interval of D, we conclude that these exceptions are rare. There are other possible exceptions close to the fold points close to $D \approx 27\mu$m and $D \approx 8\mu$m. Because some of the fold points represent limit points for equilibria with intermediate flow in one of the two redundant vessels, these fold points disrupt the grouping of the equilibria into sets of three required to apply the definition of intermediate flow. Given that these intervals are small, these exceptions can be safely ignored without compromising the general principle.

The results in Figure 4.2 suggest that the choice of splitting rule affects how the equilibria change as the diameters of the vessels vary, but the qualitative behaviour is the same for both splitting rules. More specifically, the equilibria meet in the same pairs of flow

configurations and for approximately the same diameter values. For example, the equilibria with the flow configurations $(-,-)$ and $(+,+)$ meet when $D \approx 30\mu m$ and $D \approx 7\mu m$ for both splitting rules. Other pairs of flow configurations also consistently meet for the two splitting rules. These have been labelled in Figures 4.2b and 4.2d but they are also present in Figures 4.2a and 4.2c. The main difference between the two sets of equilibria is the rate at which the flows converge towards the $(0,0)$ equilibrium, with the flows converging to 0 more quickly for the Gardner splitting rule. Apart from this difference, the two splitting rules exhibit qualitatively similar behaviour in closely aligned intervals of D.

As shown in Figure 4.2, multiple equilibria are not viable for all diameter values when the inlet haematocrit values are 0.45. Therefore, although the theory of flow configurations is consistent with changing diameters, Figure 4.2 would indicate that multiple equilibria are only viable for the smaller scale of vessel diameters in microcirculation. An inlet haematocrit of 0.45 is widely accepted to be a phenomenologically realistic value for the inlet haematocrits. However, Gardner et al. (2010) showed that for most vessel diameters, the triangle network admitted multiple equilibria, provided that the inlet haematocrits were larger than the critical value of the inlet haematocrit for the value of the diameters of the triangle network.

If $D = 10\mu$m and H_{in} is the continuation variable for the square plus triangle network such that $H_{(1,4)} = H_{(2,5)} = H_{in}$, nine equilibria exist for most values of H_{in}. However, as H_{in} decreases, these equilibria meet at fold bifurcations until eventually only one equilibrium remains (see Figure 4.3). This suggests that the behaviour of the square plus triangle network is similar to that of the triangle network for the same choice of the splitting rule. For each value of D a critical value of the inlet haematocrits $H_{in}^{\text{crit}_3}$ exists for which multiple equilibria exist for $H_{in} \geq H_{in}^{\text{crit}_3}$. However, unlike the triangle network, the square plus triangle network may not admit an equilibrium for all possible flow configurations for all values of $H_{in} > H_{in}^{\text{crit}_3}$. For example, $H_{in}^{\text{crit}_3} \approx 0.3$ but for $0.3 \lesssim H_{in} \lesssim 0.33$, the square plus triangle only admits three equilibria.

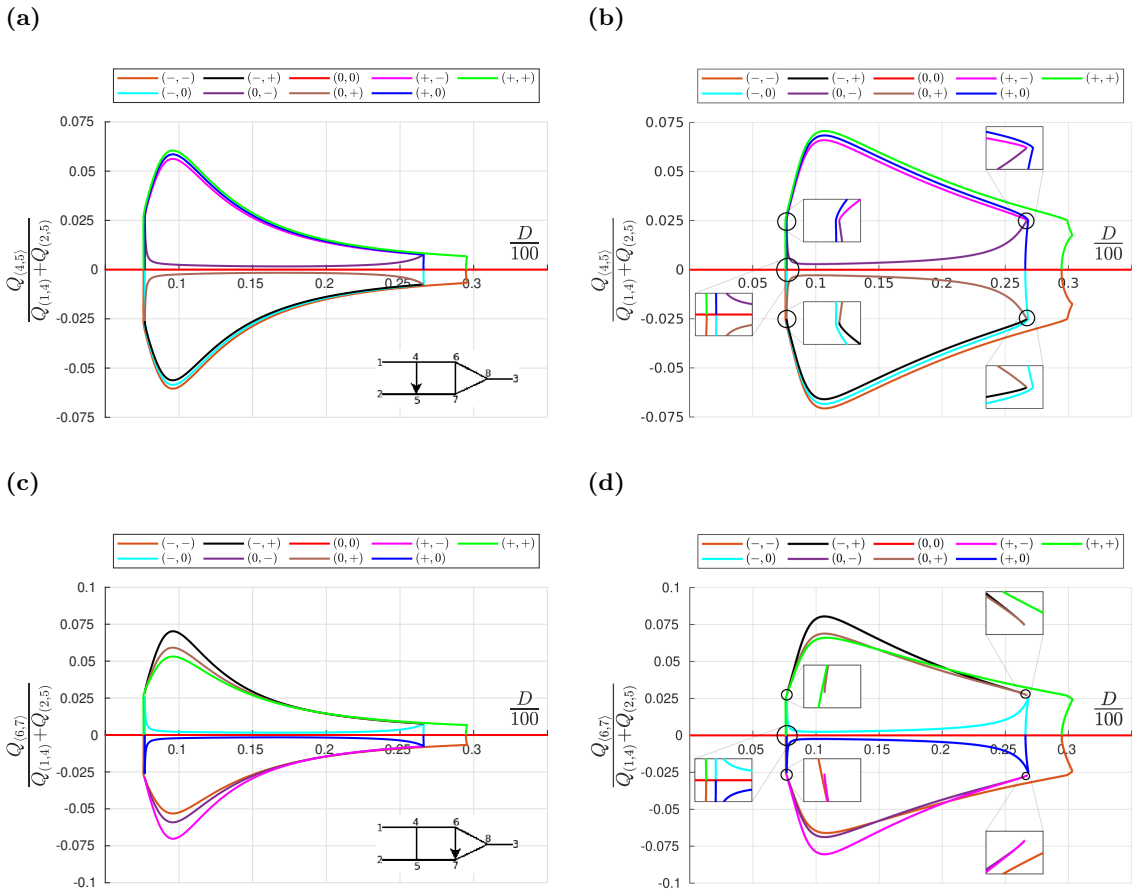

Figure 4.2: Series of plots of the normalised flow in the redundant vessels in the square plus triangle network, $\langle 4,5\rangle$ and $\langle 6,7\rangle$, as the diameters of the network vary using two splitting rules when $H_{in} = 0.45$. (a): $Q_{\langle 4,5\rangle}$ for the Gardner splitting rule; (b): $Q_{\langle 4,5\rangle}$ for the simple splitting rule; (a): $Q_{\langle 6,7\rangle}$ for the Gardner splitting rule; (a): $Q_{\langle 6,7\rangle}$ for the simple splitting rule.

As with the results generated by Gardner et al. (2010), it is possible to generate a region of multiple equilibria in the (D, H_{in}) plane. Unlike the triangle network, this region will contain subregions for which the square plus triangle network admits multiple equilibria but does not admit nine equilibria. Figure 4.4 shows the different regions of multiple equilibria in the (D, H_{in}) plane. According to the diagram, the point $(30, 0.45)$ belongs to the region for which the square plus triangle network admits only one equilibrium, which corresponds to our results in Figure 4.2. The regions of 1 equilibrium and nine equilibrium are separated by a thin regions of three and five equilibria or regions of three and seven equilibria. Therefore, for every value of D, the square plus triangle network will have the corresponding critical values $H_{in}^{\text{crit}_3}, H_{in}^{\text{crit}_9}$ and $H_{in}^{\text{crit}_5}$ or $H_{in}^{\text{crit}_7}$ such that:

$$H_{in}^{\text{crit}_3} < H_{in}^{\text{crit}_5} \leq H_{in}^{\text{crit}_9}, \tag{4.4}$$

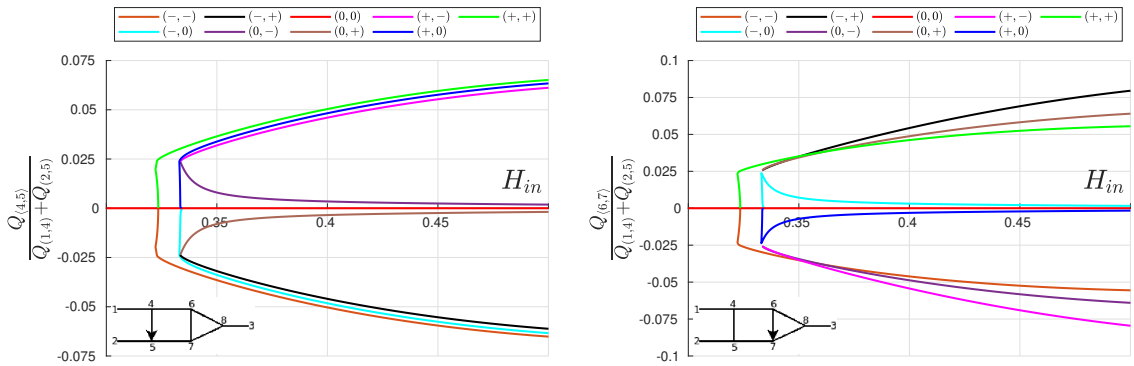

Figure 4.3: Bifurcation diagrams of the normalised flow in the redundant vessels in the square plus triangle network, $\langle 4,5\rangle$ and $\langle 6,7\rangle$, as the inlet haematocrits $H_{in} = H_{(1,4)} = H_{(2,5)}$ vary and $D = 10\mu$m. (a): bifurcation diagram of $Q_{\langle 4,5\rangle}$. (b): bifurcation diagram of $Q_{\langle 6,7\rangle}$.

or:

$$H_{in}^{\text{crit}_3} < H_{in}^{\text{crit}_7} \leq H_{in}^{\text{crit}_9}. \tag{4.5}$$

The square plus triangle network admits at least three equilibria for $H_{in} > H_{in}^{\text{crit}_3}$, five equilibria for $H_{in} > H_{in}^{\text{crit}_5}$, seven equilibria for $H_{in} > H_{in}^{\text{crit}_7}$, and nine equilibria for $H_{in} > H_{in}^{\text{crit}_9}$. For example, the values of $H_{in}^{\text{crit}_5}$ and $H_{in}^{\text{crit}_9}$ are both approximately 0.33 in Figure 4.2 but $H_{in}^{\text{crit}_3} < H_{in}^{\text{crit}_5} < H_{in}^{\text{crit}_9}$. The region of three equilibria is created by two curves that seem to run parallel to each other. Both curves have a maxima at $D \approx 50\mu$m after which the two curves slowly decrease and appear to approach a plateau at $D = 200\mu$m. This means that for diameters in an interval around $D = 50\mu$m, multiple equilibria are not viable for $H_{in} = 0.45$ but for all other values of D, the network admits multiple equilibria when $H_{in} = 0.45$.

An explanation of this phenomenon is readily available from the characteristics of the relative viscosity function. For $H = 0$, $\mu^{(rel)}(0, D) = (D/(D - 1.1))^2$ and so the viscosity is monotonically decreasing as the vessel widens. For non-zero values of H, the relative viscosity function admits a minimum point as shown in Figure 4.5a. By plotting the values of D which minimise the relative viscosity for each value of H, we find that for most haematocrit values, the diameter that minimises the viscosity is 50μm (see Figure 4.5b). As most of the blood flow in the square plus triangle network is along the fixed vessels, the haematocrit values in the fixed vessels are similar to the value of H_{in}. Therefore, for phenomenologically realistic values of H_{in}, the viscosity in the fixed vessels relative to the redundant vessels is

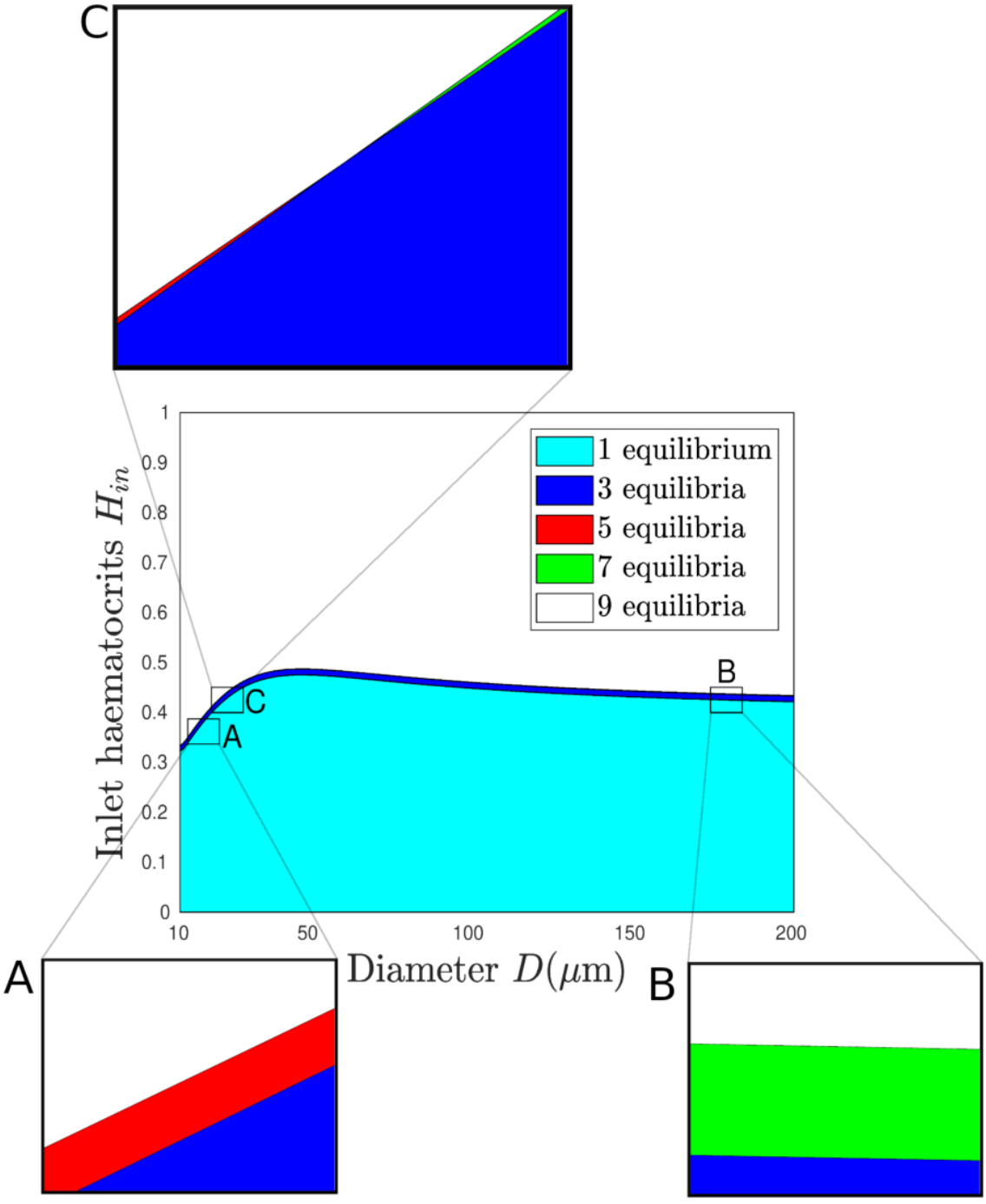

Figure 4.4: Diagram of the regions of multiple equilibria in the (D, H_{in}) plane.

minimal for $D \approx 50\mu$m. As a consequence, the values of H_{in} required for multiple equilibria is greater for $D \approx 50\mu$m.

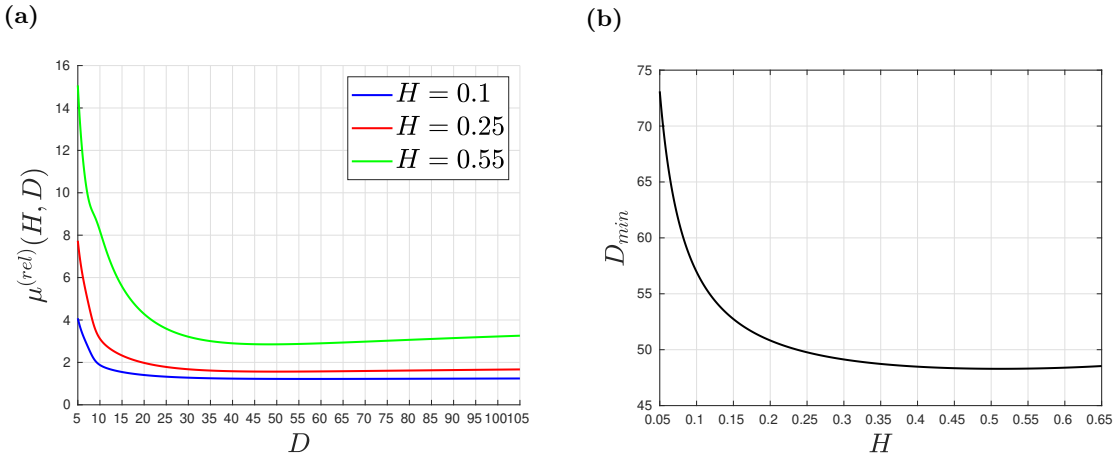

Figure 4.5: (a): Plots of the relative viscosity function for different values of H. (b): Plot of the diameter value that minimise $\mu^{(rel)}(H, D)$.

Figure 4.4 is similar to Figure 7a for the triangle network in (Gardner et al., 2010) and both results show that multiple equilibria are present for a wide range of phenomenologically realistic diameter and inlet haematocrit values. Given that both results indicate that multiple equilibria exist when $H_{in} \approx 0.45$ for most diameter values, we conclude that multiple equilibria exist for most values of D.

An interesting aspect of both results is the plateau for the curves that separate the regions of different numbers of equilibria as D increases. The implication of the plateauing curve is that the region for which multiple equilibria are not present may be very small for most networks, and once the diameters of a network are sufficiently large, the values of H_{in} for which multiple equilibria are viable do not vary significantly. The form of the equations provides an explanation as to why this critical value does not change significantly once the diameters of the network are sufficiently large. As explained previously, it is the form of the relative viscosity function that prevents consistency of the ratio of flows as the diameters are scaled uniformly:

$$\mu^{(\text{rel})}(H, D) = \left[1 + (\mu_{45} - 1)\frac{(1-H)^C - 1}{0.55^C - 1}\left(\frac{D}{D - 1.1}\right)^2\right]\left(\frac{D}{D - 1.1}\right)^2, \tag{4.6}$$

where H is the haematocrit in the vessel; μ_{45}, defined as:

$$\mu_{45} = 6\exp(-0.085D) + 3.2 - 2.44\exp(-0.06D^{0.645}), \tag{4.7}$$

is the relative apparent blood viscosity for a discharge haematocrit $H = 0.45$; and the coefficient C is defined as:

$$C = (0.8 + exp(-0.075D))\left(-1 + \frac{1}{1 + 10^{-11}D^{12}} \right) + \frac{1}{1 + 10^{-11}D^{12}}. \tag{4.8}$$

If we take the limit of C and μ_{45} as $D \to \infty$ then both parameters tend towards a finite limit:

$$\lim_{D\to\infty} C = -0.8, \tag{4.9}$$

$$\lim_{D\to\infty} \mu_{45} = 3.2. \tag{4.10}$$

Then the limit of $\mu^{(rel)}$ is:

$$\lim_{D\to\infty} \mu^{(rel)}(H, D) = 1 + (3.2 - 1)\frac{(1 - H)^{-0.8} - 1}{0.55^{-0.8} - 1} = \mu_{\infty}^{(rel)}(H). \tag{4.11}$$

If we consider the volumetric flow using $\mu_{\infty}^{(rel)}(H)$ instead of $\mu^{(rel)}(H, D)$, then the flow ratio for any two vessels does not change significantly, regardless of the change in the diameter values. Let:

$$Q_{(x,y)}^{(\infty)} = \frac{(P_x - P_y)D_{(x,y)}^4\pi}{128L_{(x,y)}\mu^{(\infty)}(H_{(x,y)})}, \tag{4.12}$$

such that $\mu^{(\infty)}(H) = \mu_p\mu_{\infty}^{(rel)}(H)$. Then we return to the examples given in Equations (4.1-4.2) and consider the same ratios using Equation (4.12) instead of Equation (1.32) for the equation for flow in a vessel. When $D_{(v,w)} = D_{(u,v)} = 10\mu$m, the new flow ratio is:

$$\frac{Q_{(v,w)}^{(\infty)}}{Q_{(u,v)}^{(\infty)}} = \frac{\frac{10000\pi}{12800\mu^{(\infty)}(0.4)}}{\frac{10000\pi}{12800\mu^{(\infty)}(0.45)}} = \frac{\mu^{(\infty)}(0.45)}{\mu^{(\infty)}(0.4)} = 1.1384. \tag{4.13}$$

If the diameters are changed to $D_{(v,w)} = D_{(u,v)} = 20\mu$m, the ratio remains constant:

$$\frac{Q_{(v,w)}^{(\infty)}}{Q_{(u,v)}^{(\infty)}} = \frac{\frac{160000\pi}{12800\mu^{(\infty)}(0.4)}}{\frac{160000\pi}{12800\mu^{(\infty)}(0.45)}} = \frac{\mu^{(\infty)}(0.45)}{\mu^{(\infty)}(0.4)} = 1.1384. \tag{4.14}$$

Therefore, for a fixed haematocrit distribution as the diameters of a network increase, the ratio of flows tend towards a limit. As the network flow equations are equations of the flow ratios, scaling the diameters by the same factor has increasingly little impact on the flow

ratios and, by extension, the existing equilibria.

One potential problem with this explanation is that we have not taken into account the effects of the splitting rule. The coefficients for the splitting rules are usually functions of vessel diameters, so altering the diameters also influences the ratio at a flow bifurcation. However, the splitting rules also depend less on the diameters of the network as the diameters of the network increase. If we consider the limit of the splitting rule coefficients for the Gardner splitting rule described in Table 4.1, the limits are finite:

$$\lim_{D\to\infty} A = 0, \lim_{D\to\infty} X_0 = 0, \lim_{D\to\infty} P = 1. \tag{4.15}$$

These limits are viable regardless of the diameter ratios for the flow bifurcations. Therefore, as the diameter increases, the dependence of the network equations on the diameters decreases. If multiple equilibria exist for a specific diameter that is sufficiently large, the same equilibria will be present for any greater diameter value. Although we have used the Gardner splitting rule to reach this conclusion, this does not change much for the simple splitting rule. $\lim_{D\to\infty} A = 0$ for the simple splitting rule, but $\lim_{D\to\infty} x_0 = 0.05$ and $\lim_{D\to\infty} P = 1.4$. However, the viscosity function would still tend towards $\mu_\infty(H)$ which implies that the flow ratios would also tend toward a limit. Therefore, as long as the splitting rule coefficients tend towards a finit limit as $D \to \infty$, and if multiple equilibria exist for a relatively large diameter values, these equilibria are likely to persist for diameters larger than this critical value.

4.4 Diameter ratios

So far, our results have linked the number of equilibria present with the flow configurations when the diameters of all vessels in the network are equal. As multiple equilibria exist for symmetric networks with equal diameter, multiple equilibria will exist for small perturbations of the diameter ratios because most equilibria are regular points for the steady-state network equations. However, if equilibria only exist for some small region of parameter space and a small perturbation of the diameter ratios could destroy multiple equilibria, then this implies that multi-stability is an unlikely scenario in biologically realistic networks. It will also be important to consider whether specific splitting rules have a greater impact on the equilibria for vessel networks with different diameter ratios because the coefficients of the splitting rules are influenced by the diameters of a network (see Table 4.1).

The square plus triangle network provides a good test case for varying diameter ratios. The functional forms for P, A and X_0 for the Gardner and simple splitting rules change as the diameter ratios vary (see Table 4.1 for details). It is important to choose one splitting rule for which the functional form of P depends on the haematocrit and diameter of the parent vessel. In Section 3.4, our results implied that the principle that the existence of multiple equilibria depends on the viability of multiple flow configurations remaines true regardless of whether P depends on the parent haematocrit. Section 4.3 shows that this remains true for P depending on the parent haematocrit and diameter. The same conclusion can be drawn for the coefficient X_0.

In symmetric networks, the choice of the coefficients, P and X_0, does not influence the qualitative behaviour of the solutions or regions in the parameter space for which multiple equilibria are found. However, it is not possible to conclude that the splitting rules have little impact on the existence of multiple equilibria in general because we have not tested the hypothesis that the choice of splitting rule is not the main contributing factor leading to multiple equilibria in networks with asymmetric diameter ratios. The reason why this is significant is because of the coefficient A. For all splitting rules, if the diameter ratios are equal to 1, $A = 0$ regardless of the specific form. As explained in Section 1.9.4, for a flow bifurcation like the one in Figure 1.3a, the function:

$$\frac{\psi_{(v,w)}(r_{(v,w)})}{r_{(v,w)}} H_{(u,v)} = H_{(v,w)}, \tag{4.16}$$

attains its maximum for some $r_{(v,w)} \in (0.5, 1)$ if $A = 0$. Therefore, for $A \neq 0$, the interval for which the maximum is attained changes. This may have a significant impact on the regions in the parameter space for which multiple equilibria are found. To better understand the impact of asymmetric diameter ratios on the existence of multiple equilibria, we will study how the equilibria of the symmetric square plus triangle network change as we introduce asymmetry to the diameter ratios.

In this section, we will show that, regardless of the splitting rule, most equilibria can be defined with a unique flow configuration, and that multiple equilibria exist in similar intervals in parameter space for both splitting rules.

4.4.1 Effect of changing the diameters of the redundant vessels

In this section we investigate how the equilibria change as the diameter ratios for the redundant vessels vary. We choose the following parameters for the square plus triangle network:

$$L_{\langle 4,5\rangle} = L_{\langle 6,7\rangle} = 10\mu m, L = 100\mu m, D = 20\mu m, H_{(1,4)} = H_{(2,5)} = 0.45, \tag{4.17}$$

$$P_1 = P_2 = 0.5, D_{\langle 4,5\rangle} = D_{\langle 6,7\rangle} = \zeta D \tag{4.18}$$

where L and D denote the length and diameter of all non-specified vessels. The results in Section 4.3 show that nine equilibria exist when $\zeta = 1$ for both the simple and Gardner splitting rules. Therefore, these nine equilibria can be used as starting solutions for numerical continuation using Equation (3.12) as the homotopy function for which $\zeta \in [0, \infty)$ is the continuation parameter. We have used $D = 20\mu$m instead of $D = 10\mu$m because the results in Section 4.3 indicate that the equilibria collapse to a single equilibrium when the vessel diameters are comparable to the diameters of the RBCs. Therefore, if $D = 10\mu m$, it is probable that the number of equilibria collapse to a single equilibrium for $\zeta \approx 0.8$. As we wish to see a variation of ζ before this convergence of equilibria, $D = 20\mu m$ has been chosen.

Figure 4.6 displays the bifurcation diagrams for the normalised flow in the redundant vessels as ζ varies. As with the results from Figure 4.2 the equilibria for the two splitting rules share many of the same qualitative properties. The most obvious similarity is the meeting of the equilibria at fold bifurcations for both splitting rules. The equilibria with flow configurations $(-,+)$ and $(0,+)$ meet at a bifurcation at $\zeta \approx 0.7$, the same is true for the $(+,-)$ and $(0,-)$ equilibria. Understandably, these bifurcations occur for the same value of ζ due to the symmetry of the network. Furthermore, as ζ approaches 0.5, the $(+,+)$ and $(-,-)$ equilibria meet at another fold point. These have been labelled in Figures 4.6b and 4.6d but they are also present in Figures 4.6a and 4.6c. Unlike the results in Figure 4.2, all equilibria present at $\zeta = 1$ persist for larger values of this ratio, and Figure 4.6 seems to indicate that this trend continues for all values of $\zeta > 0.8$, but this cannot be explicitly verified.

As with Figure 4.2, the curves in Figure 4.6 have been labelled with the flow configurations present at $\zeta = 1$. This results in small intervals of multiple equilibria labelled with the same flow configuration. These small neighbourhoods exist close to $\zeta \approx 0.5$ and $\zeta \approx 0.7$. Given that these neighbourhoods are small, we can conclude that the equilibria have unique flow configurations for most values of ζ.

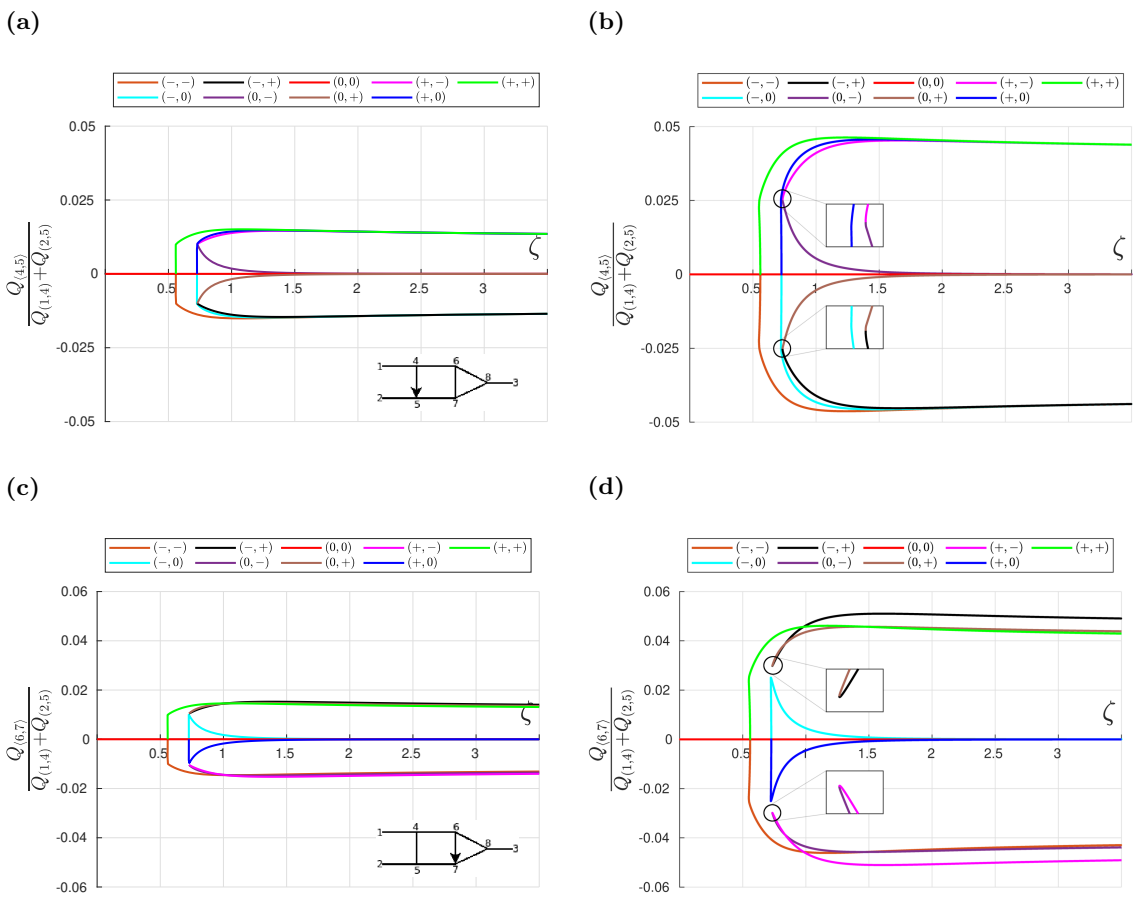

Figure 4.6: Series of plots of the normalised flow in the redundant vessels in the square plus triangle network, $\langle 4,5\rangle$ and $\langle 6,7\rangle$, as the diameter ratio ζ varies using two splitting rules when $H_{in} = 0.45$. (a): $Q_{\langle 4,5\rangle}$ for the Gardner splitting rule; (b): $Q_{\langle 4,5\rangle}$ for the simple splitting rule; (a): $Q_{\langle 6,7\rangle}$ for the Gardner splitting rule; (a): $Q_{\langle 6,7\rangle}$ for the simple splitting rule.

4.4.2 Effect of changing the diameters of the side vessels

We now vary the diameters of one side of the square plus triangle network. In contrast to Section 4.4.1, this test will focus on the effect of changing the diameters of some of the vessels with a fixed flow direction. In this section, we choose the following parameters for the square plus triangle network:

$$L_{(4,5)} = L_{(6,7)} = 10\mu m, L = 100\mu m, D = 20\mu m, H_{(1,4)} = H_{(2,5)} = 0.45, \tag{4.19}$$

$$P_1 = P_2 = 0.5, D_{(1,4)} = D_{(4,6)} = D_{(6,8)} = \xi D \tag{4.20}$$

where D and L denote diameters and lengths that have not been specified. The square plus triangle network admits nine equilibria when $\xi = 1$. These are the same equilibria used as starting solutions for numerical continuation in Section 4.4.1. These equilibria will again be used as starting solutions for numerical continuation, but $\xi \in [0, \infty)$ is used as the continuation parameter. Unlike the results in Sections 4.3 and 4.4.1, varying ξ breaks the symmetry of the network. Therefore, we anticipate that altering the diameter ratios of the side vessels of the square plus triangle network will force the blood flow in the redundant vessels to only flow in one direction.

The results in Figure 4.7 reveal that, just as in the previous simulations of changing diameters, the qualitative properties of the two splitting rules remain the same. The equilibria for the two splitting rules form 3 fold bifurcations at approximately the same values of ξ:

$$\xi \approx 0.7, 1.2, 1.4. \tag{4.21}$$

Furthermore, as with the previous results in Section 4.4.1, the flow configurations of the equilibria that meet at these fold points are consistent for the two splitting rules. The equilibria with the flow configurations $(-,+)$ and $(0,+)$ meet at the fold bifurcation at $\xi \approx 1.4$. The same is true for $(+,-)$ and $(+,0)$ at $\xi \approx 1.2$ and $(-,0)$ and $(-,+)$ at $\xi \approx 0.7$. There are more fold bifurcations around $\xi \approx 0.4$ for both splitting rules, but they are not detailed here for the sake of brevity, but the flow configurations of the equilibria for both splitting rules meeting at these fold bifurcations are consistent with one another (These can be seen in Figures 4.7b and 4.7d but they are also present in Figures 4.7a and 4.7c). Therefore, even with the breaking of the symmetry of the diameters of the network, the pattern of fold bifurcations remains consistent regardless of the chosen splitting rule.

Unlike the results in Sections 4.3 and 4.4.1, we have not labelled the equilibria with the flow configurations present when the diameters of the network are all equal but instead used the definition of intermediate flow (Definition 3.2) to evaluate the flow configurations for every value of ξ. The convention of labelling the equilibria with the same flow configurations present when the diameters of the network are equal was applied to the results in Sections 4.3 and 4.4.1 because these labels were consistent with the definitions of the flow states for most values of the specified continuation parameters. This is not true for the results in Figure 4.7, so the equilibria exchange flow configurations depending on the position of the fold bifurcations. For example, the $(0,+)$ and $(-,+)$ equilibria meet at a fold bifurcation when $\xi \approx 1.4$, after this fold bifurcation, the definition of intermediate flow no longer applies to the $(-,0)$ equilibrium, which means that because $Q_{\langle 6,7\rangle} > 0$, this equilibrium exchanges flow configurations with the $(-,+)$ equilibrium. However, even with this adjustment, the flow configurations for the equilibria are still unique for all values of $\xi \gtrsim 0.4$. For a small interval around $\xi \approx 0.4$, all equilibria apart from the $(0,0)$ equilibrium end at fold bifurcations. Due to the complicated pattern of fold bifurcations, the definition of intermediate flow no longer consistently applies to many of the equilibria, but because this occurs for such a small interval of ξ, these exceptions can be ignored. Therefore, the uniqueness of the flow configurations is generally true for asymmetric diameter ratios.

We also observe that the number of equilibria rapidly decreases as the vessel diameters decrease below $10\mu m$ For instance, in Figure 4.7, only one equilibrium is present when $\xi \approx 0.4$ and as $D = 20\mu m$. For this ratio, the diameters for one side of the network are approximately $8\mu m$ which is similar in size to red blood cells. This is consistent with the bifurcation diagrams in Sections 4.3 and 4.4.1. For $\xi \gtrsim 1.4$ the number of equilibria remains constant at least in the range that we were able to study. This is very similar to the bifurcation diagrams in Section 4.4.1 but contrasts with the results in Section 4.3. Unlike the results in Section 4.4.1, the equilibria tend towards the equilibria $(0,0)$. Another interesting aspect of these equilibria is the fact that the $(0,0)$ equilibrium is the only equilibrium with intermediate flow in either redundant vessel for $\xi \gtrsim 1.4$.

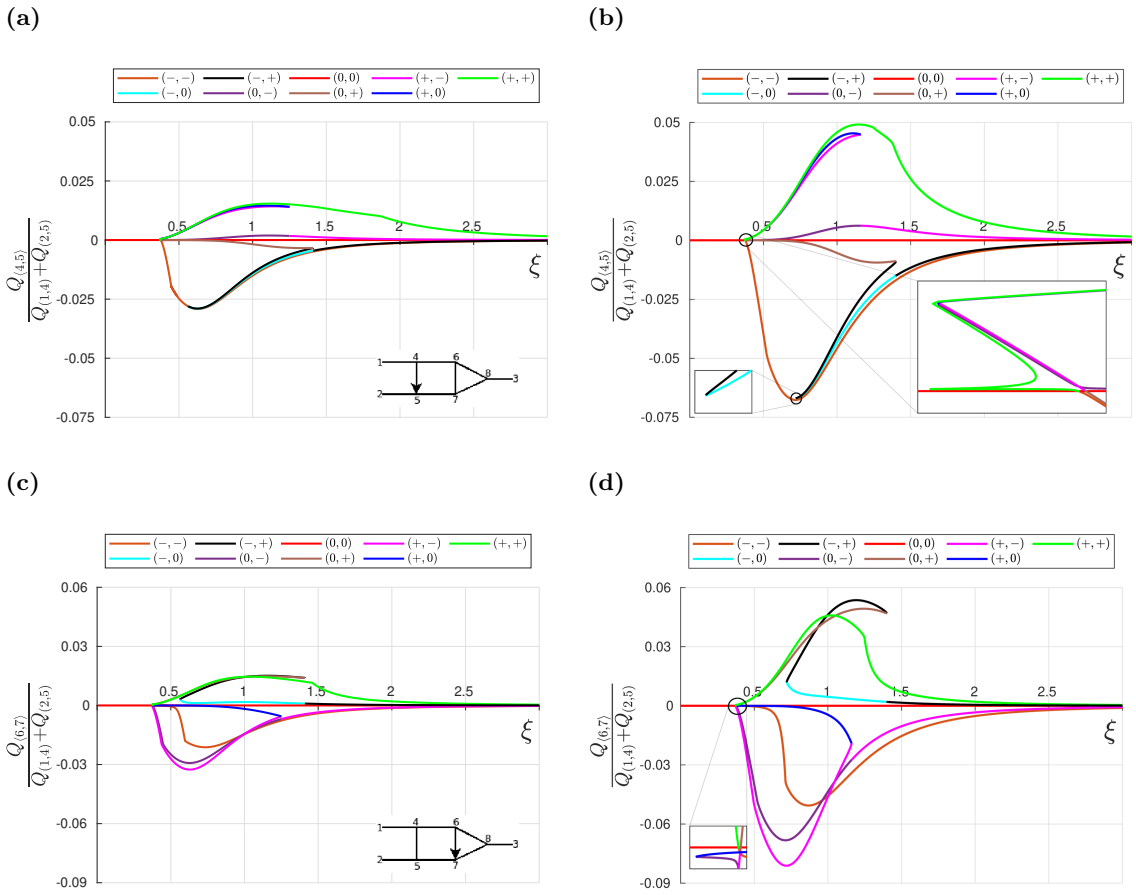

Figure 4.7: Series of plots of the normalised flow in the redundant vessels in the square plus triangle network, $\langle 4,5\rangle$ and $\langle 6,7\rangle$, as the diameter ratio ξ varies using two splitting rules when $H_{in} = 0.45$. (a): $Q_{\langle 4,5\rangle}$ for the Gardner splitting rule; (b): $Q_{\langle 4,5\rangle}$ for the simple splitting rule; (a): $Q_{\langle 6,7\rangle}$ for the Gardner splitting rule; (a): $Q_{\langle 6,7\rangle}$ for the simple splitting rule.

Although we have shown for a variety of different diameter ratios that multiple equilibria exist and have unique flow configurations, we have only tested this for one standardised diameter value ($D = 20\mu$m). However, we can use the same reasoning used in Section 4.3 to justify that this trend will hold for most diameter values. If we return to the example in Equations (4.13-4.14). If we use Equation (4.12) for the volumetric flows but choose a set of diameter values that differ by some ratio such that $D_{(v,w)} = \alpha D_{(u,v)}$. If $D_{(u,v)} = 10\mu$m then the flow ratio for the two vessels is now:

$$\frac{Q^{(\infty)}_{(v,w)}}{Q^{(\infty)}_{(u,v)}} = \frac{\frac{\alpha^4 10000\pi}{12800\mu^{(\infty)}(0.4)}}{\frac{10000\pi}{12800\mu^{(\infty)}(0.45)}} = \frac{\alpha^4\mu^{(\infty)}(0.45)}{\mu^{(\infty)}(0.4)} = 1.1384\alpha^4. \tag{4.22}$$

If $D_{(u,v)} = 20\mu$m then the flow ratio for the two vessels is:

$$\frac{Q^{(\infty)}_{(v,w)}}{Q^{(\infty)}_{(u,v)}} = \frac{\frac{\alpha^4 160000\pi}{12800\mu^{(\infty)}(0.4)}}{\frac{160000\pi}{12800\mu^{(\infty)}(0.45)}} = \frac{\alpha^4\mu^{(\infty)}(0.45)}{\mu^{(\infty)}(0.4)} = 1.1384\alpha^4. \tag{4.23}$$

As the limit of the viscosity function no longer depends on the diameters, the flow ratio is exactly the same regardless of the values of $D_{(u,v)}$ and α. Therefore, as long as the ratio α remains constant, once the vessel diameters are sufficiently large, the flow ratio does not vary significantly. However, we have not taken into account the change in the coefficient A for the splitting rule. Note that in this section, unlike the scenario in Section 4.3 where the vessel diameters are all equal, $A \neq 0$. Although this is important for smaller diameter values, as vessel diameters in a network are above a certain threshold, A has limited influence on the equilibria of the network because the limit of A as the diameters tend to infinity is always 0. The implication of the limits of the viscosity and the coefficients of the splitting rules is that as long as the network admits multiple equilibria for relatively large vessel diameters, these equilibria are likely to persist with similar haematocrit distributions as the diameters are scaled by the same factor.

4.5 Discussion

We concluded in Chapter 3 that the main factor driving the multiplicity of equilibria in a vessel network was the existence of redundant vessels. In this chapter, we have expanded upon this result to networks of different scales by investigating the multiplicity of equilibria in networks with wider vessels and networks with asymmetric vessel diameter ratios. By showing that equilibria have unique flow configurations for a range of different diameter values and diameter ratios, the results in this chapter combined with the results in Chapter 3 show that this is a consistent principle for all network geometries.

Uniqueness of flow state configurations

Although we concluded in Chapter 3 that almost all equilibria have a unique flow configuration, until now we did not test this hypothesis for a variety of vessel diameters and diameter ratios. As most equilibria are regular points of the system of network equations, the existence of multiple equilibria for networks with uniform vessel diameters with unique flow configurations implies that multiple equilibria with the same flow configurations exist for small perturbations of these vessel diameters. However, it is possible that these diameter perturbations are so small that this principle is unlikely to hold in more realistic vessel

networks. Without verifying that the same principle holds for wide variations in the vessel diameters, it was not possible to conclude that our results are applicable for a variety of network geometries.

For most network parameters explored in this chapter, the square plus triangle network admitted equilibria with unique flow configurations. As with Chapter 3, there were a few exceptions to this principle. All exceptions occurred in the vicinity of fold bifurcations and only existed in small intervals in parameter space. Some notable examples of these exceptions can be seen in Figures 4.2, 4.6 and 4.7. As we have shown in this chapter and Chapter, 3, the exceptions to the uniqueness of flow configurations can only be found in small regions in the parameter space, we can conclude that almost all equilibria have unique flow configurations in the redundant vessels.

Critical inlet haematocrits

One of the more surprising results of this chapter was the existence of critical values of the haematocrit for every diameter value in the range $[10, 200]$. Each diameter value of the square plus triangle network had corresponding critical values for the inlet haematocrits for which the network would admit different numbers of equilibria. As a consequence, the plane (D, H_{in}) can be broken up into separate regions of different number of equilibria as shown in Figure 4.4.

The region of only three equilibria in Figure 4.4 is created by two curves that appear to be almost parallel to each other. Both curves have a maximum value for $D \approx 50\mu$m and they both appear to start plateauing as $D \to \infty$. As explained in Section 4.3, an explanation of both of these properties is readily available from the characteristics of the coefficients for the viscosity function. Figure 4.5b showed that for most physically realistic diameter values, the viscosity was minimised for diameters of approximately 50μm. Therefore, a minimised value for the viscosity coincides approximately with the maximum for the two curves creating the region of three equilibria. Furthermore, the value of the diameters for the maximum of the two curves is similar to results generated for the triangle network by Gardner et al. (2010). Gardner et al. (2010) also generated a plot for the region of multiple equilibria in the (H_{in}, D) plane (Figure 7a in (Gardner et al., 2010)). They found that the plane was bisected by a curve for which larger haematocrit values corresponded to multiple equilibria for the triangle network and haematocrit values below the curve corresponded to a unique equilibrium. The maximum of this curve also occured at approximately $D = 50\mu$m. Given the maximum of the curves in Figure 4.4 and Figure 7a in Gardner's publication

occur at diameter values that approximately coincide with values of D that minimise the relative viscosity for most haematocrit values. This may imply that all networks admit a similar peak given the network equations for any network include the same relative viscosity function. If this property of the triangle and square plus triangle network generalises to all networks, this would imply that sections of the tumours vasculature with diameters of approximately 50μm are less likely to admit multiple equilibria.

For sufficiently large vessel diameters, the functions for the viscosity and the splitting coefficients become increasingly insensitive to changes in the diameters of the network as shown by the plateau of the curves separating the regions of multiple equilibria in Figure 4.4. Therefore, if a network motif admits multiple equilibria for sufficiently large vessel diameters, the haematocrit distributions for these equilibria are unlikely to change significantly if the diameters are scaled uniformly by a scaling factor greater than one. Therefore, the multiple equilibria will persist for larger diameters. If the square plus triangle network admits multiple equilibria for some combination of values for the inlet haematocrits and vessel diameters, due to the increasing insensitivity to the diameter values, the haematocrit distributions is unlikely to change significantly as the diameters are increased. As a consequence, the critical values for the inlet haematocrits for which multiple equilibria exist do not change significantly for diameter values above a certain threshold.

Although we have not explicitly solved the network equations for a network with multiple scales for vessel diameters, we have shown that multiple equilibria exist for a range of diameter ratios. Therefore, we hypothesise that multiple flow configurations in a simple network motif with at least one redundant vessel and large diameter vessels would remain viable if the motif was embedded in larger vascular network because of the insensitivity of the network flow equations on the vessel diameters.

Negligible impact of splitting rules

As with the uniqueness of the flow states, we originally concluded that the splitting rule had negligible effect on the equilibria in Chapter 3. However, previously, the dependence on the splitting rules was only evaluated in a square plus triangle network with equal vessel diameters. This chapter completes this analysis to conclude that the qualitative characteristics of the equilibria remain the same regardless of the choice of splitting rule. All bifurcation diagrams for the two splitting rules evaluated in this chapter contained fold bifurcations for approximately the same parameter values, and the equilibria that meet at fold bifurcations consistently have the same flow configurations for the two splitting rules.

In Chapter 3, we argued that the splitting rules were not the main factor contributing to multiple equilibria due to the existence of intermediate flow. Most instances of multiple equilibria occurred when all three flow states were viable in a single redundant vessel. Usually these equilibria belonged to the same paths in the parameter space as the length ratios were altered. Therefore, for both negative and positive flows to be viable, so does intermediate flow. Usually, when an equilibrium has intermediate flow in a redundant vessel, the flow ratio entering that vessel is less than the critical coefficient X_0. Therefore, the haematocrit within the redundant vessel is 0 and the haematocrit for the other daughter vessel is equal to H_p/r for any splitting rule (H_p is the haematocrit of the parent vessel and r is the flow ratio). Therefore, because multiple equilibria usually emerge in sets of three and the network equations are similar for intermediate flow regardless of the splitting rule, the regions in parameter space for which a network admits multiple equilibria for one splitting rule are likely to be similar for all splitting rules. This argument also applies to the splitting rules for which $A \neq 0$.

Flow pathways

A conclusion of Chapter 3 that we expand in this section is the concept of flow pathways. As described in Section 1.9.5, blood flow cannot form a loop. This means that blood flow is limited to a finite number of pathways through the network. These pathways can include either passage through redundant vessels or through fixed vessels. However, as shown using numerous examples, not all flow pathways are viable depending on the network geometry and boundary conditions. Although it is never possible to know exactly for which network parameters multiple flow pathways are viable, we can reasonably argue which network parameters are likely to lead to the formation of multiple equilibria. In Chapter 3 we found that networks with shorter redundant vessels were more likely to admit multiple equilibria. For networks like the square plus triangle network, most flow pathways required traversing redundant vessels. We reasoned that because the resistance in the shorter vessels is less than the resistance in the longer vessels (provided the haematocrit and diameter are the same), it was easier for the blood flow to traverse shorter redundant vessels in either direction. We concluded that if redundant vessels are shorter, then the existence of multiple flow pathways is more likely, and by extension multiple equilibria.

Our results in this chapter support the key findings on the link between potential resistance in redundant vessels and the viability of flow pathways. As the diameter of a vessel increases, the resistance to flow decreases. Figure 4.6 shows how the equilibria of the square

plus triangle network vary as the ratio of the redundant vessel diameters to the fixed vessel diameters vary. For a sufficiently large ratio, there is an equilibrium for every possible flow configuration. As this ratio decreases, these equilibria end at limit points in the form of fold bifurcations. Eventually, once the diameters of the redundant vessels are of a similar size to the diameters of the RBCs, only one possible flow configuration remains viable. This flow configuration coincides with zero volumetric flow in the two redundant vessels. Even in a vessel with 0 haematocrit, as the vessel constricts the resistance increases. Therefore, as the diameters of the redundant vessels decrease, the potential resistance to the flow pathways traversing these vessels increases until eventually these pathways are no longer viable.

The results in Figure 4.6 are intuitive to understand based on the equations for the resistance and the results from Chapter 3. It is less clear how the concept of flow pathways can explain the results in Figure 4.2 for changes to all diameters of vessels. For diameters less than 8μm, the square plus triangle network only admits one equilibrium. This can be intuitively explained by the fact that the diameters of RBCs also have diameters of approximately 8μm. For vessels of similar size to the RBCs, Fåhraeus and Lindqvist (1931) hypothesised that the RBCs travel through blood vessels in a single file and the resistance increases rapidly as the vessel constricts. Therefore, the fact that the only flow pathways that remain viable are the pathways that do not traverse the redundant vessels, could be explained by the RBCs travelling in single file along the sides of the network. The RBCs can not travel down the redundant vessels because this would disrupt the single file movement of the RBCs in either side of the network. Ben-Ami et al. (2022) showed that it is possible to see multiple equilibria in a triangle network with vessel diameters which are similar in size to RBCs. However, this was only observed in a triangle network with one smaller side of the network and for physically unrealistic inlet haematocrit values. It is more difficult to explain why multiple flow pathways are no longer viable for larger diameter values in Figure 4.2. Figure 4.5b shows that the relative viscosity of the blood is at a minimum for $D \approx 50\mu$m for most physically realistic values of the vessel haematocrit. As most of the flow in the square plus triangle network travels down the side vessels, this implies that if the inlet haematocrits are physically realistic values, so are the haematocrit values of the fixed vessels. This implies that for diameter values in some neighbourhood of $D = 50\mu$m, the viscosity of blood in fixed vessels is minimised for these diameter values compared to redundant vessels. This reduces overall potential resistance for the flow pathways that just traverse the fixed vessels. Therefore, the flow pathways that traverse the redundant vessels provide no advantage, and so multiple equilibria do not exist.

A similar case can be seen in Figure 4.7, where as the diameters of the vessels on the side of the network decrease, blood flow is forced to travel exclusively in the fixed vessels. Even if the diameters changing in Figure 4.7 are from one side of the network, as these diameters shrink the RBCs travel in single file down this side of the network when the diameters are of a comparable size to the RBCs. Therefore, any flow in the redundant vessels disrupts this flow. As this diameter ratio increases, we observe that some flow pathways, and by extension multiple equilibria, are no longer viable. As with the example of all vessels dilating, the dilation of these vessels encourages the blood to flow down the pathways with the least potential resistance. Therefore, providing less advantage for blood to traverse the redundant vessels. However, because the vessel diameters for one side of the network do not minimise the viscosity in fixed vessels for one side of the network, multiple flow pathways are still viable.

Given the large parameter space of any vasculature network, it is not possible to formulate simple rules or relations between the parameters that lead to the formation of multiple equilibria. However, by studying the parameters governing the viscosity and resistance of the flow pathways, it is possible to make predictions about the characteristics of networks that admit multiple equilibria. Based on the results in Chapter 3 and this chapter, networks with short and wide redundant vessels, and fixed vessels with diameters in the range $[10, 30]$ micrometers are more likely to admit multiple equilibria. It has been hypothesised that wider redundant vessels, known as functional shunts, have been hypothesised to redirect blood along a longer pathway causing maldistribution of blood within the tumour vasculature (Pries et al., 2010). It is not clear how prominent these structures are in the tumour vasculature, and some results suggest that shunts can be rare (Less et al., 1991), but it is possible that only one shunt is required to sufficiently deviate the blood from the normal blood flow pathways. From our results, functional shunts share some of the same properties as redundant vessels because redundant vessels have the potential to redirect blood flow. As blood flow dictates the haematocrit distribution, this results in uneven RBC distributions, our results support the hypothesis that functional shunts cause hypoxic regions to form and provide a possible mechanism for the maldistribution of RBCs.

Most results in this chapter simply verify that the results in the previous chapter hold for a range of diameter values and diameter ratios. By verifying the uniqueness of flow configurations for most network parameters, our results facilitate predictions to be made for the maximum number of equilibria a network may admit and the geometric characteristics of a network that may lead to multiple equilibria. The aim of the last two chapters was

to identify some key properties of network motifs that could be used to solve the network equations for larger vasculature networks possibly based upon tumour images. Given the relationship between redundant vessels and multiple equlibria, it should be possible to evaluate how likely a vessel network is to admit multiple equlibria by counting the number of possible flow pathways. Therefore, future work could involve investigating the equilibria of small sections of tumour vasculature (subnetworks of approximately $30 - 400$ vessels). The conclusions of the last two chapters could aid in this process by guiding which subnetworks are likely candidates for multiple equilibria. If subnetworks have many short and wide redundant vessels, then these subnetworks are more likely to admit multiple equilibria.

Our aim in this thesis is to propose a new mechanistic explanation for the formation of cycling-hypoxia. This new mechanism is centred around the principle of multi-stability of a network's equilibria. The hypothesis that we wish to test is that networks admit multiple equilibria and the blood flow can switch between these equilibria. As the blood flow dictates the RBC distribution, if the RBC distribution changes then the concentration of oxygen in the surrounding tissue will also change. If the RBC distribution periodically switches between a distribution for which the surrounding tissue is normoxic and one for which the surrounding tissue is hypoxic, then this will result in cycling-hypoxia if this process occurs periodically or almost periodically. To propose this mechanism, we must show examples of networks that admit multiple equilibria and demonstrate that the blood flow can switch between them. So far we have satisfied the first part of this problem by demonstrating the link between network topology and multiple equilibria. In the next chapter, we will demonstrate a couple of possible mechanisms for driving the time-dependent blood flow equations between the equilibria.

Chapter 5

Switching of flow directions in vessel networks

So far this thesis has focused on the topological features of networks that are necessary for the existence of multiple equilibria, without relating these multiple equilibria to the potential existence of cycling-hypoxia. Previous studies have shown that anti-angiogenic drugs can suppress the formation of cycling-hypoxia. Matsumoto et al. (2011) showed that when mice with tumours experiencing cycling-hypoxia were treated with Sunitinib, an anti-angiogenic drug, the tumours no longer experienced cycling-hypoxia. Sunitinib was also shown to reduce the vascular density within the tumours implying that the mechanistic explanation for the presence of cycling-hypoxia must in part depend on the vascular geometry. However, the specific mechanisms by which cycling-hypoxia arises remain elusive. Ben-Ami et al. (2022) showed the formation of self-sustained oscillations of the solution to the time-dependent blood flow equations in a simple triangle network. Although this was a theoretical study of a small vasculature network, they proposed that similar oscillations could drive cycling-hypoxia in tumours. Furthermore, self-sustained oscillations have been observed in a variety of small vascular networks, which could imply that oscillations are a common feature of blood flow in microcirculation (Carr and Lacoin, 2000; Carr et al., 2005; Geddes et al., 2007, 2010; Karst et al., 2015). The important distinction between the oscillations observed by Ben-Ami et al. (2022) and similar work was the link between the formation of these oscillations and multiple equilibria resulting from redundancy in the vasculature.

In this chapter, we propose an alternative mechanism for the emergence of cycling-hypoxia

that exploits the existence of multiple equilibria. We hypothesise that oxygen fluctuations can arise due to the blood flow switching between multiple equilibria. Each equilibrium has a unique RBC distribution within the vascular network. Bernabeu et al. (2020) showed that asymmetric RBC distributions result in an asymmetric distribution of oxygen that could cause the formation of hypoxic regions within tumours. Therefore, if we can show that blood switches between multiple stable equilibria with asymmetric RBC distributions, then it is reasonable to assume this could cause a switching between asymmetric oxygen distributions. This switching may explain cycling-hypoxia so long as the time between switches is longer than the diffusion time scale.

We investigate two different potential causes for these switches: changes in the boundary conditions and stochastic fluctuations. We saw in Chapter 3 that multiple stable equilibria exist for certain choices of the boundary conditions and that altering the boundary conditions causes certain stable equilibria to vanish. The intervals in parameter space for which multiple equilibria exist are often narrow. One common mechanism by which a system may switch between equilibria within a narrow parameter interval is due to a hysteresis resulting from the existence of a bi-stable system. For example, consider an ODE:

$$\dot{x} = f(x, t; \beta), \tag{5.1}$$

that admits a bi-stable interval for the parameter β created by two fold bifurcations at $\beta = \beta_f^{(l)}$ and $\beta = \beta_f^{(u)}$ (Figure 5.1b). For any three values of β, $(\beta_0, \beta_1, \beta_2)$, such that $\beta_f^{(u)} < \beta_0 < \beta_f^{(l)}$, $\beta_1 > \beta_f^{(l)}$, and $\beta_2 < \beta_f^{(u)}$. Let $x_\beta(t)$ denote the solution to the ODE such that $\beta = \beta(t)$ and $x_\beta(0)$ takes the value of the steady-state on the lower branch of the bistable interval in Figure 5.1b. A hysteresis refers to a behaviour exhibited by $x_\beta(t)$ such that the value of $x_\beta(t)$ switches between the stable equilibria and then returns to the original equilibrium. An example of this path is shown in Figure 5.1b. It is also possible to start on the upper stable branch, but the direction of the arrows in Figure 5.1b always consistent. Furthermore, a hysteresis in an interval of bistable equilibria is only possible if the key parameter driving the hysteresis can both increase and decrease in value.

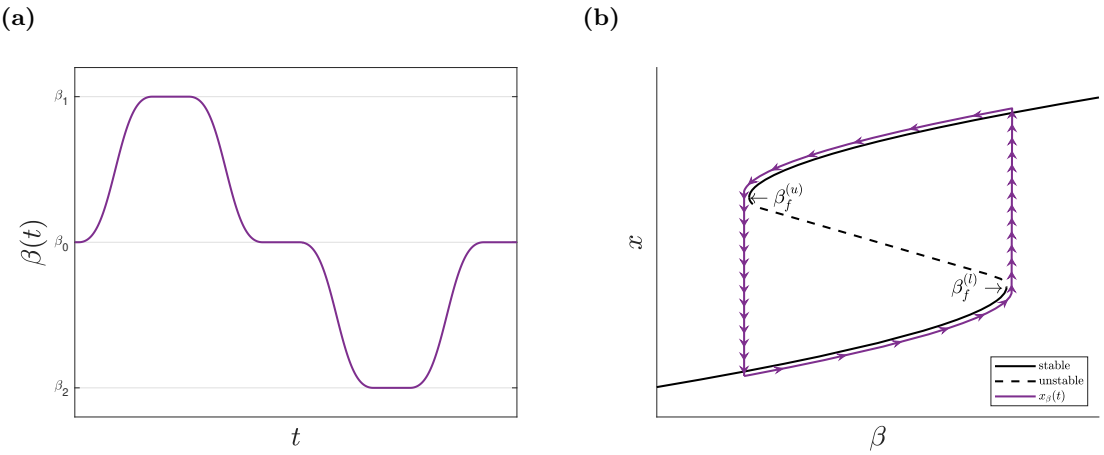

Figure 5.1: (a): example function of $\beta(t)$ driving a hysteresis; (b): resulting hysteresis for the ODE, $\dot{x} = f(x, t; \beta)$.

Hysteresis is a common mechanism in biologically motivated problems (Angeli et al., 2004; Chatterjee et al., 2008; Pomerening et al., 2003; Ozbudak et al., 2004; Sha et al., 2003). In these examples, the hysteresis coincides with a change in the behaviour of the system of equations with related biological consequences and once this change has been induced by a change in the parameters, returning to the original parameter value does not always recover the original behaviour. In the case of blood flow in microcirculation, a hysteresis coincides with a switch between two equilibria with different RBC distributions.

Chapters 3 and 4 contain a variety of examples of complicated patterns of fold bifurcations arising from asymmetry of the network parameters. Therefore, networks could potentially have more than one control parameter driving a hysteresis. However, we will not focus on parameters that change the vessel lengths of the network because these parameters are unlikely to result in a hysteresis because the vessel length parameter can not increase and decease. It is possible that vessel growth could cause the time-dependent solution to switch once. For instance, as shown in Chapter 3, varying the length ratio of vessels can generate complex bifurcation diagrams. Therefore, elongation of vessels driven by growth could potentially drive switches between equilibria when the ratio of two vessels is sufficiently large. However, although changes in length ratios could cause a switch between the equilibria, as there is no mechanism for the vessel to shrink, the solution can not switch back to the original equilibrium. A hysteresis needs both of these events to occur and so changing a vessels length is not a realistic driver of a hysteresis. Furthermore, vessel growth is the results of sprouting of new vessels as opposed to the elongation of preexisting vessels. Although the formation and growth of new vessels may drive the blood flow to change direction in

a network, investigating this potential driver of blood flow switching would require the application of an angiogenesis model. An angiogenesis model would also change the topology of the network, and switching between equilibria driven by changes to the topology of the network could not produce hysteresis because the equations of flow would constantly change with the topology. Therefore, incorporating changes in the vascular topology and length scales is beyond the scope of this investigation.

Vessel diameters are an alternative set of parameters that could form a hysteresis of the solution. It is well known that the tumour microenvironment may compress the vasculature within tumours (Jain et al., 2014; Padera et al., 2004). Intratumour compression has the potential to compress vessels and, in some cases, cause vessels to collapse. Vessel compressions have been linked with the formation of hypoxic regions. As these compressions do not alter the network topology, with the exception of vessel collapse, a changing diameter value is a more realistic driver of hysteresis. However, the model for the time-dependent blood flow assumes that blood vessels are perfect cylinders for simplicity. Although this is a sufficient model for vessels under normal circumstances, compressed blood vessels do not have a circular cross section (Jain et al., 2014). Therefore, the equations for the hydraulic resistance are no longer valid in the compressed vessels. Furthermore, there is some evidence that vessel compression leads to irregular splitting of RBCs downstream of the compressed vessel (Enjalbert et al., 2021). Due to the difficulties associated with capturing the impact of changes in the geometry of the network on blood flow, this chapter focuses on changes to the boundary conditions as potential drivers of hysteresis instead of changing the radius.

The second mechanism that we propose is due to stochastic fluctuations. Unlike changes in the boundary conditions, this mechanism assumes that stochastic fluctuations are an inherent property of blood flow in microcirculation. So far we have used continuum models to describe the proportion of the blood that contains RBCs. In reality, blood contains discrete numbers of RBCs suspended in plasma and so the haematocrit is not a smoothly varying quantity. There is some biological evidence to support the existence of stochastic fluctuations in microcirculation. Fung (1973) observed fluctuations in blood flow in the mesentry of dogs. These stochastic fluctuations manifested themselves as unpredictable changes in the direction of blood flow in vessels. Bedggood and Metha (2012) observed fluctuations of blood flow in human retinas and Pawlik et al. (1981) observed stochastic fluctuations in the cerebral cortex of cats, these fluctuations exhibited properties of white noise and stochastic periodicity. The observation of stochastic periodicity is particularly important for the study of cycling-hypoxia. If a mathematical model of blood flow can predict similar stochastic

periodicity, periodic fluctuations in the flow would coincide with periodic fluctuations of the RBCs. If these period fluctuations of RBCs could be linked to periodicity of the oxygen distribution in the surrounding tissue, this would provide a possible explanation for how cycling-hypoxia arises.

There are a couple of competing theories for the cause of these fluctuations. Fung (1973) suggested that stochasticity is due to fluctuations in the RBC diameter distribution. Due to the discrete nature of RBCs, and since RBCs vary in size, a large RBC that enters a blood vessel temporarily increases the resistance to blood in that vessel. As the size of the RBCs entering the vessels is random, the resulting blood flow is random. Bedggood and Metha (2012) proposed a similar explanation but reasoned that the stochastic fluctuations are caused by larger or smaller RBCs downstream of the blood vessels experiencing stochastic fluctuations. Computational studies have also provided insight into the nature of stochastic fluctuations of blood flow. Balogh and Bagchi (2017, 2018) suggest four possible mechanisms for stochastic fluctuations at flow bifurcations resulting from the properties of blood flow at flow bifurcations in vascular networks. Regardless of the specific mechanism for the formation of these fluctuations, all theories suggest that these fluctuations occur at flow bifurcations. So far, no continuum model that incorporates stochastic fluctuations has been proposed in the literature. Therefore, one goal of this chapter is to understand if the application of stochastic noise to the continuum equations in Section 1.8 induces the blood flow to switch between stable equilibria. If the blood flow switches are driven by stochastic fluctuations, the time taken for the solution to switch from one equilibrium to another and then back is a random variable with an associated probability distribution. By finding this probability distribution, predictions for the time spent in each state can be made. As with a hysteresis of the solutions, each state corresponds to a unique RBC distribution in the network. Therefore, predictions of the time spent in each state translates to predictions for the time between oxygen fluctuations.

This chapter is broken up into the following sections: in Section 5.1 we investigate whether changing the boundary conditions for the time-dependent equations of a bistable system of network equations results in switching between equilibria; in Section 5.2 we present a stochastic model of blood flow and demonstrate the resulting switching between stable states; and in Section 5.3 we interpret our results and present possible directions for future work.

5.1 Deterministic model

Our aim in this chapter is to demonstrate that switching between different equilibria is possible by altering the network boundary conditions. The key result of Chapters 3 and 4 is the relationship between redundant vessels and the existence of multiple equilibria. Redundant vessels, as defined in Definition 1.2, are vessels for which the direction of blood flow is not restricted to a single direction by the network topology. As described in Section 1.9.5, all vessels that are specified with triangular brackets ($\langle, \rangle$) are redundant vessels and all fixed vessels are denoted by circular brackets. To simplify the analysis, all test networks in this chapter are small and contain a single redundant vessel. Therefore, each network has three equilibria distinguished by the flow configuration in the redundant vessel as described in Chapter 3. We will show how solutions to the time-dependent blood flow equations can switch between equilibria with positive, negative, or intermediate flow in the redundant vessel. For a network with a single redundant vessel such that the network admits at least three equilibria. For a set of three equilibria such that the flow direction in the redundant vessel for one of the equilibria is opposite to the direction for the other equilibria, the equilibrium such that the absolute value of the flow in the redundant vessel is less than the absolute value of the flow for the other equilibria has intermediate flow in the redundant vessel (see Definition 3.1 for details). The remaining equilibria have either positive or negative flow depending on whether the flow direction is either positive or negative.

As in Chapters 3 and 4, the equilibria are described using sequences of $0, -$ and $+$ symbols to describe the flow in the redundant vessels. Given that all networks in this chapter have only one redundant vessel, the three possible descriptions of equilibria are: $(-), (0)$ and $(+)$.

Remark 5.1. For geometrically symmetric networks with equal inlet pressures and inlet haematocrits, the flow value in the redundant vessel for the (0) equilibria is 0. In these cases, the (0) equilibrium is known as the trivial equilibrium, and the $(+)$ and $(-)$ equilibria are known as the non-trivial equilibria.

5.1.1 Changes to the pressure boundary conditions

In this section, we investigate whether changes to the inlet pressure can drive time-dependent solutions of a network to switch from one stable equilibrium to another. We start by considering the triangle network shown in Figure 5.2 first introduced in Chapter 3. The steady-state and time-dependent equations can be derived from the network geometry and the equation constructions in Sections 1.7, 1.8 and 2.3 but a summary of the equations can be

found in Section 1.8. The splitting rule that we use throughout this chapter is that of the Gardner splitting rule defined by Equation (1.13) with the coefficients specified in Tables 3.1 and 4.1. As there is only one outlet node, the outlet pressure, P_3, can be set to 0 without loss of generality. Inlet pressures P_1 and P_2, can be rescaled so that $0 \leq P_1, P_2 \leq 1$ without changing the flow characteristics through the network. For instance, if:

$$(P_1, P_2, P_3 = 0, P_4, P_5, P_6), \tag{5.2}$$

are the pressures for a given haematocrit distribution. These values can be replaced by:

$$\left(\frac{P_1}{P_1+P_2}, \frac{P_2}{P_1+P_2}, \frac{P_3=0}{P_1+P_2}, \frac{P_4}{P_1+P_2}, \frac{P_5}{P_1+P_2}, \frac{P_6}{P_1+P_2}\right), \tag{5.3}$$

without changing the haematocrit distribution. For this example, we choose the following parameter values for the triangle network:

$$L = 100\mu\text{m}, D = 10\mu\text{m}, H_{(1,4)}(0,t) = H_{(2,5)}(0,t) = 0.45,$$

$$L_{\langle 4,5\rangle} = 10\mu\text{m}, P_2(t) = 1 - P_1(t),$$

where L and D are the lengths and diameters of the non-specified vessels and the function $P_1(t)$ controls the inlet pressures.

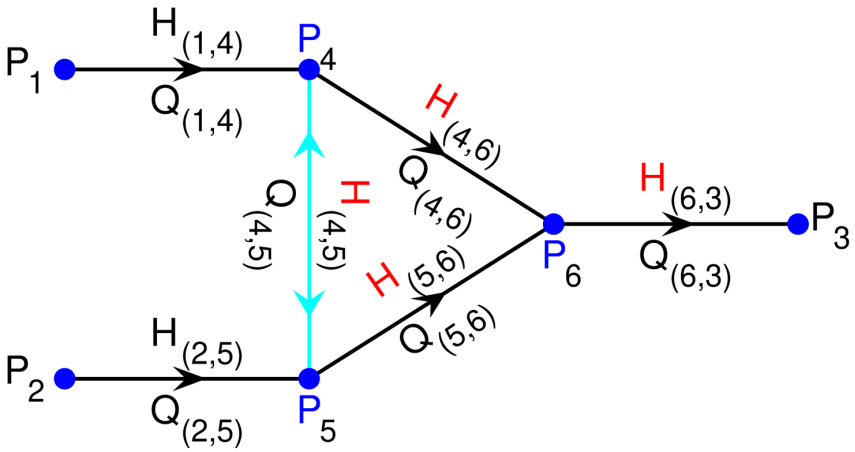

Figure 5.2: Diagram of the triangle network.

We showed in Chapter 3 that the symmetric triangle network admits three equilibria with flow configurations $(-), (0)$ and $(+)$ when the network is symmetric; the inlet haematocrit is sufficiently large; and the pressure and haematocrit boundary conditions are symmetric.

These three equilibria are all present for a small interval of P_1 around $P_1 = 0.5$. Figures 5.3d and 5.3e show the characteristic double fold bifurcation that creates an interval of three equilibria for the triangle network as the inlet pressure P_1 varies.

Figure 5.3 shows the hysteresis of the solution to the time-dependent flow equations and the function $P_1(t)$ that drives the hysteresis. Although the (0) equilibrium is labelled on Figures 5.3b-5.3c, the system does not evolve towards this equilibrium because, according to our results in Chapter 3, any equilibrium with intermediate flow is unstable[1]. In the hysteresis diagrams in Figures 5.3d and 5.3e, the time-dependent solution follows the same path as the equilibrium until the equilibrium hits a fold bifurcation. At this point, the time-dependent solution jumps to the other stable equilibrium. Therefore, provided there is a sufficiently long time period during which $P_1(t)$ takes values for which the network does not admit multiple equilibria, the time-dependent solution will switch to the remaining equilibrium. For example, when $P_1 = 0.4975$, the network only admits the $(-)$ equilibrium. As P_1 takes this value in the interval $[21, 31]$ and this time interval is sufficiently large, the solution switches from the $(+)$ equilibrium to the $(-)$ equilibrium.

5.1.2 Changes to the haematocrit boundary conditions

Next, we study the impact of changing the inlet haematocrits. The principle behind changing the inlet haematocrits is fundamentally the same as that for changing the pressure boundary conditions. Networks admit multiple equilibria that depend on the inlet haematocrits. However, unlike changes in pressure boundary conditions, changes to the inlet haematocrit boundary conditions will not have an immediate impact because it takes time for the haematocrit to propagate through the network. As before, if we consider a triangle network with the following parameter values:

$$L = 100\mu\text{m}, D = 10\mu\text{m}, L_{\langle 4,5\rangle} = 10\mu\text{m}, P_1 = P_2 = 0.5, \tag{5.4}$$

where L and D are the lengths and diameters of the vessels that have not been explicitly specified. If we fix $H_{(2,5)} = 0.45$ and use $H_{(1,4)}$ as a continuation variable, then the equilibria $(-), (0)$ and $(+)$ exist for all values of $H_{(1,4)}$ and are not connected by fold bifurcations (see Figures 5.4a and 5.4b). Due to the symmetry of the network, the same is true for the triangle network if $H_{(2,5)}$ is the continuation variable. We conclude that it is not possible

[1]It is possible for an equilibrium that equilibria with intermediate flow are stable. For instance, the triangle network admits stable equilibria with intermediate flow. However, this occurs when the inlet haematocrit is too small for the network to admit multiple equilibria and the networks lengths are all equal (Ben-Ami et al., 2022).

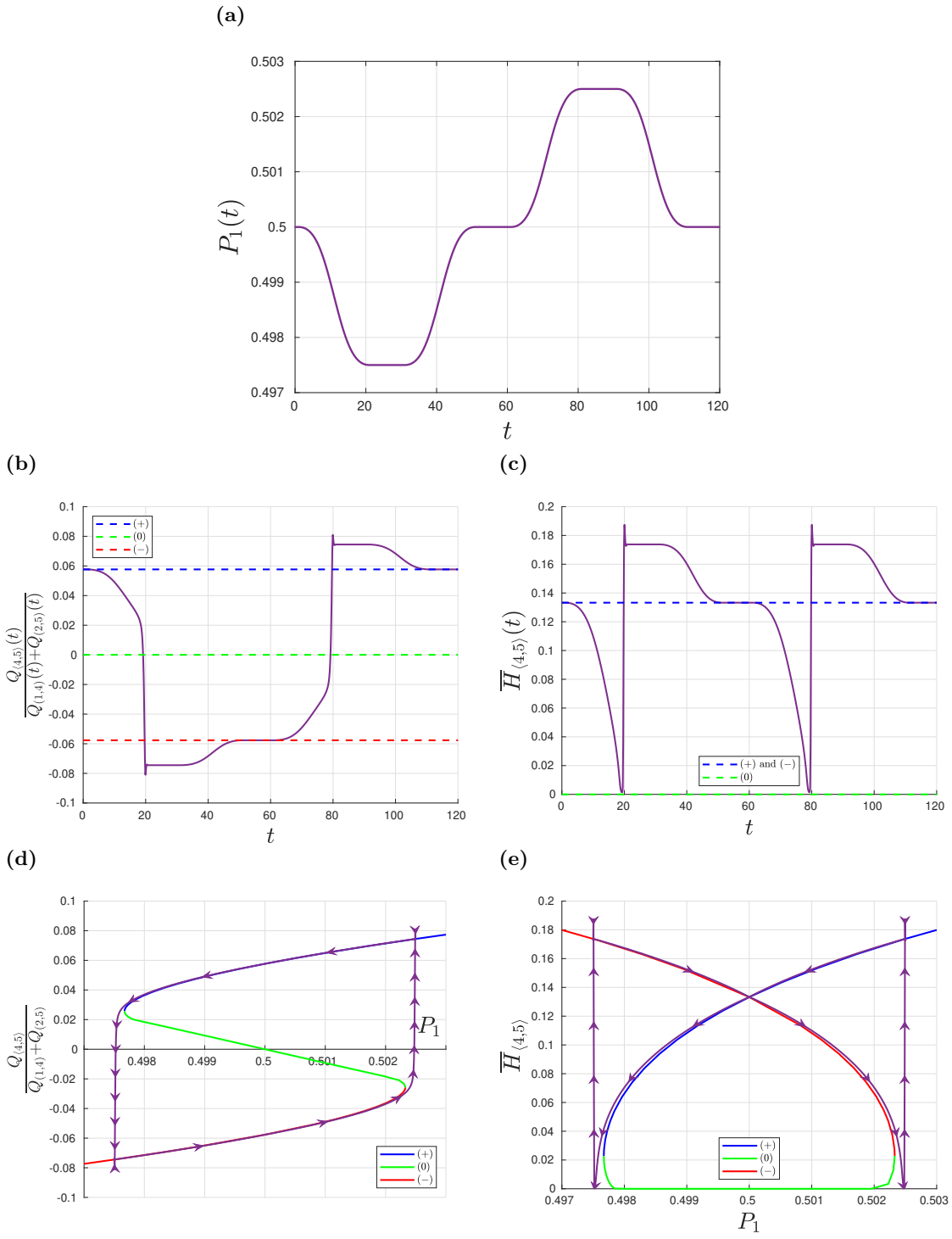

Figure 5.3: Plots of the time-dependent solutions for the triangle network as the pressure boundary conditions vary denoted by the solid purple curves. The $(-), (0)$ and $(+)$ equilibria when $P_1 = 0.5$ are denoted by dashed lines and the $(-), (0)$ and $(+)$ equilibria for varying inlet pressure P_1 are denoted by solid red, green and blue curves. (a): Inlet pressure P_1 as a function of time; (b): normalised flow in the redundant vessel as a function of time; (c): haematocrit in the redundant vessel as a function of time. (d): hysteresis diagram of the normalised flow in the redundant vessel; (e): hysteresis diagram of the haematocrit in the redundant vessel.

to force the solution to switch between equilibria by altering only one inlet haematocrit value. However, if we set $H_{(1,4)} = H_{(2,5)} = H_{(in)}$ and vary $H_{(in)}$, then Figures 5.4c and 5.4d show that if $H_{(in)}$ is less than some critical value, then the network only admits the (0) equilibrium. We conclude that both inlet haematocrits must be varied for the solution to switch between equilibria.

If both inlet haematocrits are changed at the same rate, then no switching occurs (see Appendix D). Therefore, to induce switching, the inlet haematocrits must vary at different rates. Figure 5.6a shows a combination of functions for $H_{(1,4)}(0,t)$ and $H_{(2,5)}(0,t)$ that induce a switch. These functional forms were chosen to first reduce the inlet haematocrits to values for which the network admits a unique equilibrium, then increase them one at a time in order to bias the flow direction in vessel $\langle 4,5\rangle$. As more than one parameter is varied, it is not possible to present the results on a hysteresis diagram. However, Figure 5.6 shows the variables: $Q_{\langle 4,5\rangle}(t), \overline{H}_{\langle 4,5\rangle}(t), \overline{H}_{(4,6)}(t)$ and $\overline{H}_{(5,6)}(t)$ switching between the two equilibria when a combination of functions for the inlet haematocrits in Figure 5.6a is applied.

A successfully induced switch between the non-trivial equilibria of the triangle network in Figure 5.3 is possible because a pressure difference across the redundant vessel can be induced by changing the boundary pressures. We anticipate that similar switches can be induced for any network with two or more inlet vessels using a similar process. It may also be possible to induce switching in networks with a single inlet vessel and multiple outlet vessels, but only if the outlet pressures can be manipulated.

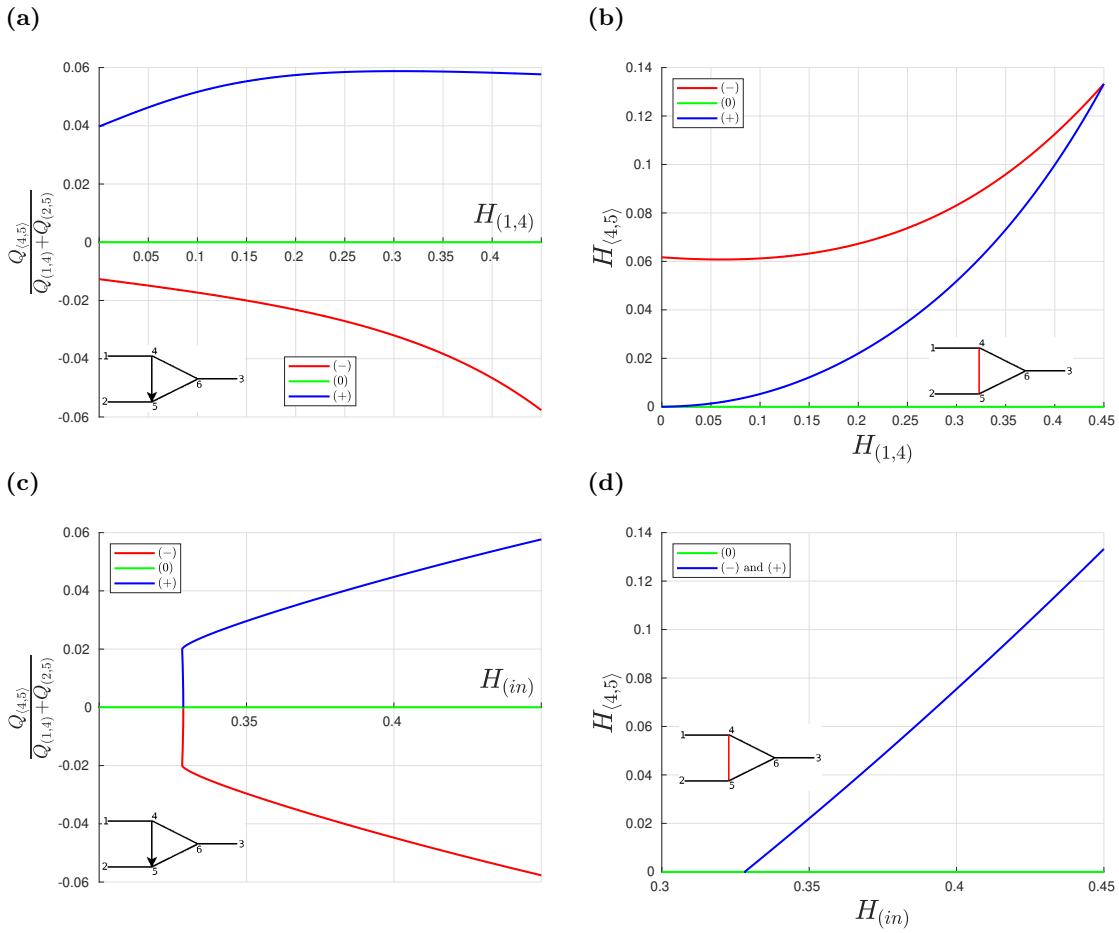

Figure 5.4: Series of plots of the equilibria of the triangle network as the inlet haematocrits vary. (a): Value of the normalised flow in the redundant vessel as inlet haematocrit $H_{(1,4)}$ varies; (b): value of the haematocrit in the redundant vessel as inlet haematocrit $H_{(1,4)}$ varies; (c): value of the normalised flow in the redundant vessel as $H_{(in)} = H_{(1,4)} = H_{(2,5)}$ varies; (d): value of the haematocrit in the redundant vessel as $H_{(in)}$ varies.

We now consider changing the inlet haematocrit to a network with a single inlet and outlet vessel. As shown in Section 1.9.6, the haematocrit distribution for any equilibrium of a network with a single inlet and outlet is independent of the choice of boundary pressures, $(P_{\text{in}}, P_{\text{out}})$, as long as $P_{\text{in}} > P_{\text{out}}$. As the haematocrit distribution does not change with the boundary pressures, the haematocrit distribution effectively acts as a fixed haematocrit distribution. If the haematocrit in each vessel is fixed, then the conservation of flow equations (Equation (1.40)) reduces to a linear set of equations with a single solution. These solutions for the interior nodal pressures scale with the choice of the boundary pressures but as the scaling factor is the same for all pressures, the resulting flow ratios remain constant. This implies that a switch between equilibria cannot be induced for a network with one inlet and one outlet by changing the inlet pressure alone. Therefore, the only control that can be

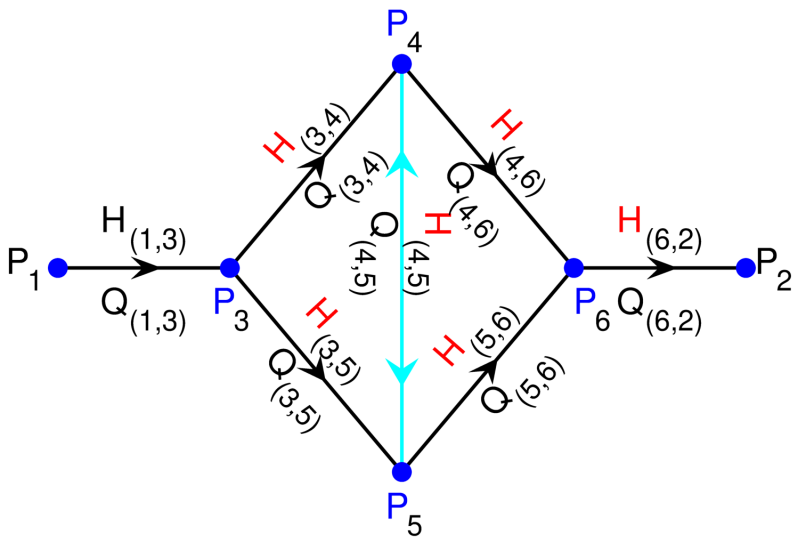

Figure 5.5: Diagram of the diamond network and the associated variables.

used for a network with a single inlet and outlet is the inlet haematocrit[2].

We now consider the diamond network shown in Figure 5.5 with the following parameter values:

$$L = 100\mu\text{m}, D = 10\mu\text{m}, L_{\langle 4,5\rangle} = 10\mu\text{m}, P_1 = 1, P_2 = 0. \tag{5.5}$$

The diamond network is the simplest example of a network with a single inlet and outlet vessel, containing a redundant vessel. The diamond network in Figure 5.5 admits three possible equilibria and has two bifurcations. The first of these flow bifurcations is present at node 3, for which vessel $(1,3)$ is the parent vessel, and vessels $(3,4)$ and $(3,5)$ are daughter vessels. The second bifurcation appears at node 4 or 5 depending on the direction of blood flow in the vessel $\langle 4,5\rangle$. If the bifurcation is present at node 4, vessel $(3,4)$ is the parent vessel and vessel $\langle 4,5\rangle$ and $(4,6)$ are the daughter vessels. If the bifurcation is present at node 5, vessel $(3,5)$ is the parent vessel and vessels $\langle 4,5\rangle$ and $(5,6)$ are the daughter vessels. As with the triangle network, the steady-state and time-dependent equations can be derived from the network geometry and the equation constructions in Sections 1.7, 1.8 and 2.3. A full list of the equations and the variables of the diamond network can be found in Appendix A.3.

For sufficiently large values of $H_{(1,3)}$, the network admits three equilibria, with flow configurations $(-), (0)$ and $(+)$. Figure 5.7 contains the plots of a prescribed function for the

[2]Discounting geometric parameters such as the length and diameters of the vessels

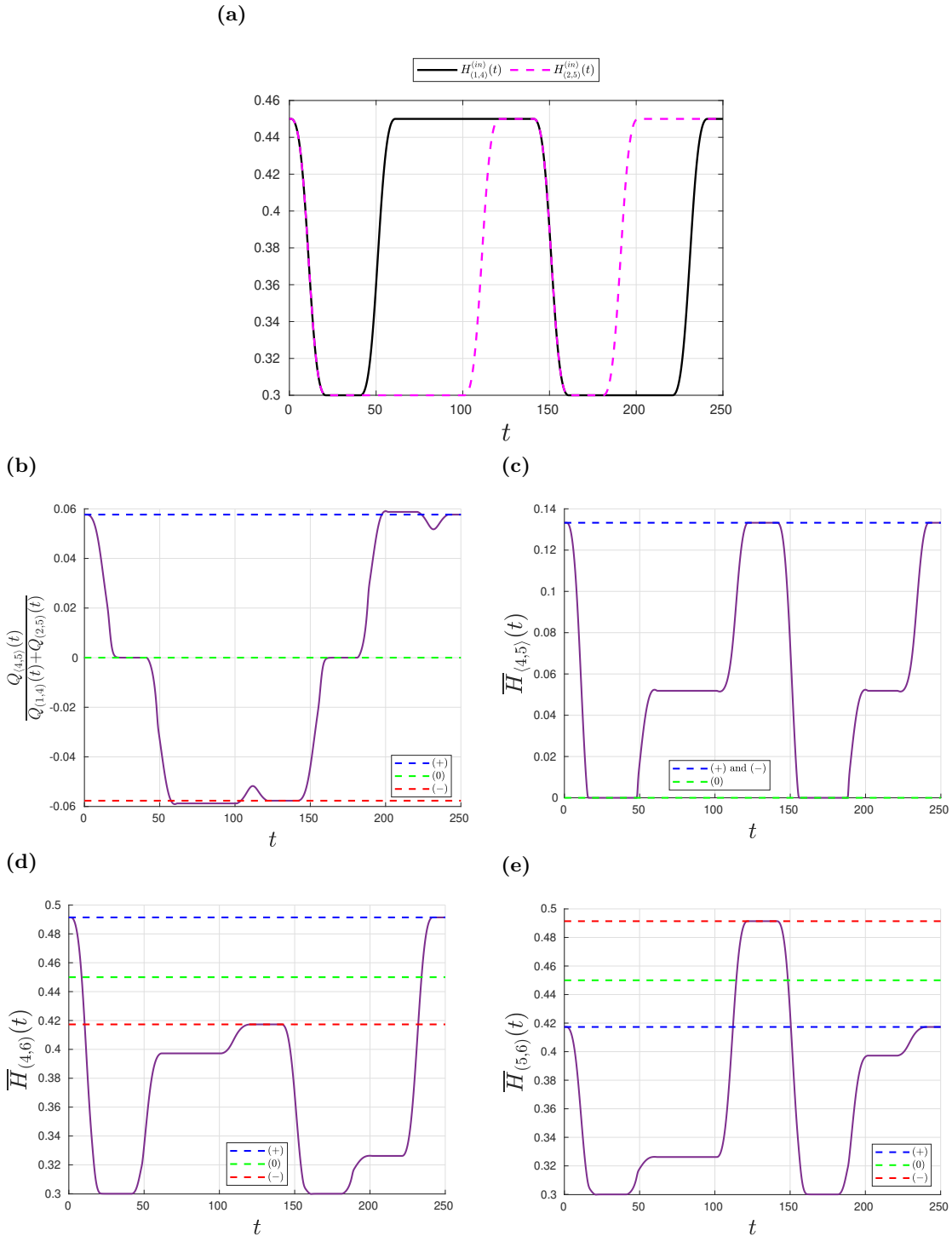

Figure 5.6: The time-dependent solutions for the triangle network as the haematocrit boundary conditions vary and the prescribed inlet haematocrit boundary conditions. The $(-), (0)$ and $(+)$ equilibria when $H_{(1,4)} = H_{(2,5)} = 0.45$ are denoted by dashed red, green and blue lines. (a): Inlet haematocrit for the triangle network as functions of time; (b): normalised flow in the redundant vessel; (c): $\overline{H}_{\langle 4,5\rangle}(t)$; (d): $\overline{H}_{(4,6)}(t)$; (e): $\overline{H}_{(5,6)}(t)$.

inlet haematocrit of the diamond network and the resulting time-dependent solutions. Figures 5.7d and 5.7b show how the time-dependent solution moves from the $(-)$ equilibrium towards the (0) equilibria as $H^{(in)}_{(1,3)}(t)$ decreases, and then towards the $(-)$ equilibria once $H^{(in)}_{(1,3)}(t)$ returns to it's original value. Due to the symmetry of the network, solutions starting at the $(+)$ equilibrium, exhibit a similar behaviour. The reason that it is not possible to induce a switch is because of a history of the solution. If we consider the solution represented by the pink curve in Figure 5.7, once the inlet haematocrit value is reduce to a value such that only the (0) equilibrium exists, the solution will tend towards this equilibrium. As the solution is positive before the inlet haematocrit is less than the haematocrit value at the fold bifurcations, the solution is never the same values as the (0) because this equilibrium is defined by 0 flow in the redundant vessel. Therefore, once the haematocrit has increased to the original value again, the solution tends towards the $(+)$ equilibrium because the flow in the redundant vessel is positive. As no other boundary conditions can be controlled, we deduce that a switch cannot be induced by continuously varying the inlet haematocrit.

5.2 Stochastic model

In the previous section, we saw that altering the boundary conditions can drive time-dependent solutions to switch between equilibria in networks with two or more inlet vessels. Similar behaviour was not observed in networks with a single inlet and a single outlet. Our inability to induce switching between equilibria in the diamond network motivates us now to consider the impact of stochastic fluctuations. Stochastic fluctuations represent the randomness of the proportion of RBCs entering a daughter vessel. Based on experimental observations and computational experiments, stochastic blood flow models should incorporate stochastic fluctuations at flow bifurcations. In this section, this stochastic noise is represented by the addition of haematocrit in one daughter vessel and the subtraction of haematocrit from the other daughter vessel. The application of noise to the haematocrit splitting is the most practical approach to incorporate stochastic fluctuations caused by the complex behaviour of RBCs.

Although stochastic processes are an important component of the dynamics of blood flow at flow bifurcations, the addition of stochastic noise to models of blood flow must preserve the conservation laws for blood flow and RBCs. Furthermore, it is important that the time-averaged proportion of RBCs entering a daughter vessel is equal to the proportion of RBCs predicted by the splitting rules. To incorporate the stochastic effects at flow bifurcations

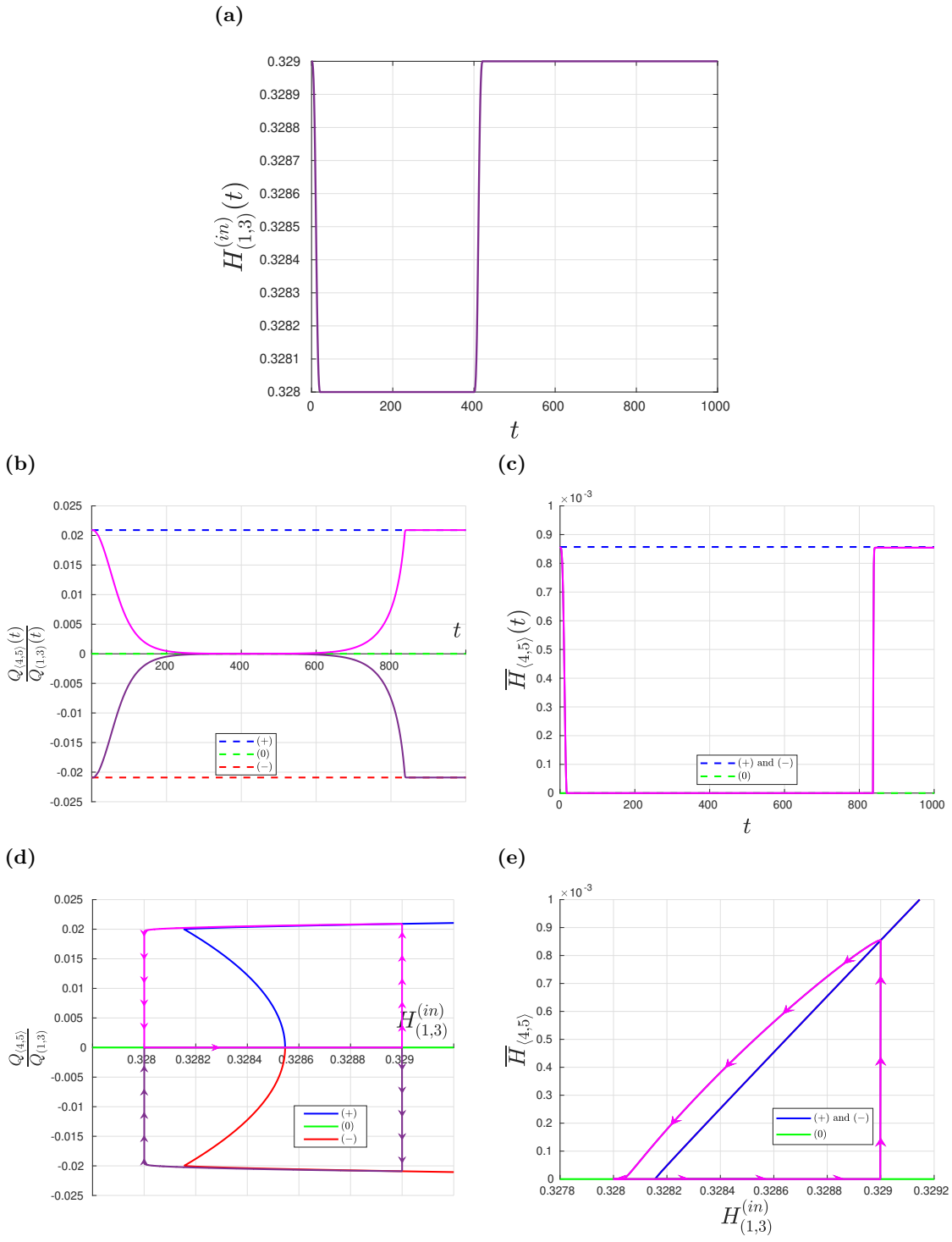

Figure 5.7: Plots of the time-dependent solutions for the diamond network as the haematocrit boundary conditions vary in purple and pink. The $(-), (0)$ and $(+)$ equilibria when $H_{(1,3)} = 0.329$ are denoted by dashed lines and the $(-), (0)$ and $(+)$ equilibria for varying inlet haematocrit $H_{(1,3)}$ are denoted by solid red, green and blue curves. (a): Inlet haematocrit $H_{(1,3)}(t)$ as a function of time; (b): $Q_{\langle 4,5\rangle}(t)/Q_{(1,3)}(t)$ as a function of time; (c): $\overline{H}_{\langle 4,5\rangle}$(t) as a function of time. (d): hysteresis diagram of $Q_{\langle 4,5\rangle}(t)$; (e): hysteresis diagram of $\overline{H}_{\langle 4,5\rangle}(t)$.

and the splitting rules, stochastic noise is applied to the boundary conditions of the time-dependent network Equations described in Section 2.3. For the bifurcation unit depicted in Figure 1.3a, the Equations of haematocrit and viscosity without stochastic fluctuations are as follows:

$$\frac{\mathrm{d}\overline{H}_{(u,v)}}{\mathrm{d}t} = u_{(u,v)}(t)\Delta H_{(u,v)}(t), \tag{5.6}$$

$$\frac{\mathrm{d}\overline{\mu}_{(u,v)}}{\mathrm{d}t} = u_{(u,v)}(t)\Delta \mu_{(u,v)}(t), \tag{5.7}$$

$$\frac{\mathrm{d}\overline{H}_{(v,w)}}{\mathrm{d}t} = u_{(v,w)}(t)\Delta H_{(v,w)}(t), \tag{5.8}$$

$$\frac{\mathrm{d}\overline{\mu}_{(v,w)}}{\mathrm{d}t} = u_{(v,w)}(t)\Delta \mu_{(v,w)}(t), \tag{5.9}$$

$$\frac{\mathrm{d}\overline{H}_{(v,z)}}{\mathrm{d}t} = u_{(v,z)}(t)\Delta H_{(v,z)}(t), \tag{5.10}$$

$$\frac{\mathrm{d}\overline{\mu}_{(v,z)}}{\mathrm{d}t} = u_{(v,z)}(t)\Delta \mu_{(v,z)}(t). \tag{5.11}$$

$\Delta H_{(x,y)}(t)$ and $\Delta \mu_{(x,y)}(t)$ have been introduced to simplify the Equations in Section 2.3:

$$\Delta H_{(x,y)}(t) = H_{(x,y)}(0,t) - H_{(z,y)}(0, t - \tau_{(x,y)}(t)), \tag{5.12}$$

$$\Delta \mu_{(x,y)}(t) = \mu_{(x,y)}(H_{(x,y)}(0,t)) - \mu_{(x,y)}(H_{(x,y)}(0, t - \tau_{(x,y)}(t))), \tag{5.13}$$

where, $(x,y) = (u,v), (v,w)$ or (v,z).The delay term $\tau_{(x,y)}(t)$ is implicitly defined by the following Equation:

$$L_{(x,y)} = \int_{t-\tau_{(x,y)}(t)}^{t} u_{(x,y)}(s)ds. \tag{5.14}$$

The boundary conditions for the delay differential Equations for vessels (v,w) and (v,z) are as follows:

$$H_{(v,w)}(0,t) = \psi_{(v,w)}(r)\frac{1}{r}H_{(u,v)}(0, t - \tau_{(u,v)}(t)), \tag{5.15}$$

$$H_{(v,z)}(0,t) = (1 - \psi_{(v,w)}(r))\frac{1}{1-r}H_{(u,v)}(0, t - \tau_{(u,v)}(t)), \tag{5.16}$$

where $r = Q_{(v,w)}(t)/Q_{(u,v)}(t)$ and $\psi_{(v,w)}$ is a splitting rule. Therefore, the most intuitive approach to introducing stochastic noise to the blood at a flow bifurcation is to apply a stochastic process to the haematocrit inlet boundary conditions of the daughter vessels. Let $\epsilon_{(v,w)}$ and $\epsilon_{(v,z)}$ denote the noise terms applied to each of the daughter vessels, then we

modify Equations (5.15-5.16) into stochastic boundary conditions:

$$H_{(v,w)}(0,t)^{(\mathrm{s})} = \left(\psi_{(v,w)}(r)\frac{1}{r} + kf(r)\epsilon_{(v,w)}\right) H_{(u,v)}(0, t - \tau_{(u,v)}(t)), \tag{5.17}$$

$$H_{(v,z)}(0,t)^{(\mathrm{s})} = \left((1-\psi_{(v,w)}(r))\frac{1}{1-r} + kf(1-r)\epsilon_{(v,z)}\right) H_{(u,v)}(0, t - \tau_{(u,v)}(t)), \tag{5.18}$$

where the function $f(r)$ is chosen to ensure the conservation of RBCs and k is an amplitude parameter. The superscript is used throughout this Chapter to differentiate from the deterministic haematocrit boundary condition, $H_{(x,y)}(0,t)$, from the stochastic boundary condition, $H^{(\mathrm{s})}_{(x,y)}(0,t)$. As stated previously, it is important that the deterministic and stochastic boundary conditions obey the conservation of RBCs:

$$H_{(u,v)}(0, t - \tau_{(u,v)}(t)) = rH_{(v,w)}(0,t) + (1-r)H_{(v,z)}(0,t), \tag{5.19}$$

$$H_{(u,v)}(0, t - \tau_{(u,v)}(t)) = rH^{(\mathrm{s})}_{(v,w)}(0,t) + (1-r)H^{(\mathrm{s})}_{(v,z)}(0,t). \tag{5.20}$$

The relationship between $\epsilon_{(v,w)}$ and $\epsilon_{(v,z)}$ is obtained by subtracting Equation (5.19) from Equation (5.20):

$$0 = rf(r)\epsilon_{(v,w)} + (1-r)f(1-r)\epsilon_{(v,z)}, \tag{5.21}$$

which implies that:

$$rf(r)\epsilon_{(v,w)} = -(1-r)f(1-r)\epsilon_{(v,z)}. \tag{5.22}$$

To ensure that this relationship holds at every time t, $\epsilon_{(v,w)}$ and $\epsilon_{(v,z)}$ must be based on the same stochastic process. Therefore:

$$\epsilon_{(v,w)} = \frac{\mathrm{d}W_t}{\mathrm{d}t}, \tag{5.23}$$

$$\epsilon_{(v,z)} = -\frac{\mathrm{d}W_t}{\mathrm{d}t}, \tag{5.24}$$

where W_t is a Weiner process. The result of this choice of $\epsilon_{(v,w)}$ and $\epsilon_{(v,z)}$ requires that the function f obey the following condition:

$$rf(r) = (1-r)f(1-r). \tag{5.25}$$

There are a number of different possible choices of $f(r)$ that satisfy the condition of Equation (5.25). For example, the following three functions satisfy this condition:

$$f_1(r) = \sqrt{\frac{1}{r} - 1}, \tag{5.26}$$

$$f_2(r) = 2(1 - r), \tag{5.27}$$

$$f_3(r) = \frac{1}{2r}, \tag{5.28}$$

The plots of $rf_1(r), rf_2(r)$ and $rf_3(r)$ are shown in Figure 5.8. It is important to note that the maximum value of $rf(r)$ is the same for all three choices of $f(r)$. The ideal choice of $f(r)$ should have the following four properties:

1. $1 \times f(1) = 0 \times f(0) = 0$,
2. $rf(r)$ is continuous on $[0, 1]$,
3. $rf(r) > 0$ for $k > 0$ and $r \in (0, 1)$,
4. $\int_{r_1}^{1-r_1} |(rf(r))'| \mathrm{d}r$ should be minimised $\forall r_1 \in (0, 0.5)$.

Condition 1 is important because if no blood is flowing into one of the daughter vessels, then all RBCs will enter the other daughter vessel, and so no stochastic fluctuations in the number of RBCs should be possible. Condition 2 ensures that non-physical behaviour is unlikely close to $r = 0$ or $r = 1$. If $r \approx X_0$, then $\psi_{(v,w)}(r) \approx 0$ (see Section 1.7 for details). This means that for some stochastic fluctuations with $\mathrm{d}W_t < 0$, $H^{(\mathrm{s})}_{(v,w)}(0, t) < 0$, but if the amplitude of the stochastic noise also scales with r, the probability of these non-physical values of $H^{(\mathrm{s})}_{(v,w)}(0, t)$ decreases. Condition 3 ensures that the addition of stochastic noise is non-trivial. Condition 4 has been chosen so that the function $rf(r)$ is similar to a step function that takes the value of k for all values of $r \in (0, 1)$ and 0 for $r \in \{0, 1\}$. Ideally, the amplitude of the noise entering a vessel should be independent of the flow, except for $r = 0$ or 1. However, this is incompatible with conditions (1-3). By minimising the average gradient, $rf(r)$ acts more like a constant.

It is clear that $f_3(r)$ satisfies condition 4 better than $f_1(r)$ or $f_2(r)$ but does not satisfy conditions (1-3) simultaneously. $f_1(r)$ and $f_2(r)$ satisfy conditions (1-3) but $f_1(r)$ is a better choice than $f_2(r)$ because:

$$\int_{r_1}^{1-r_1} |(rf_2(r))'| \mathrm{d}r > \int_{r_1}^{1-r_1} |(rf_1(r))'| \mathrm{d}r, \tag{5.29}$$

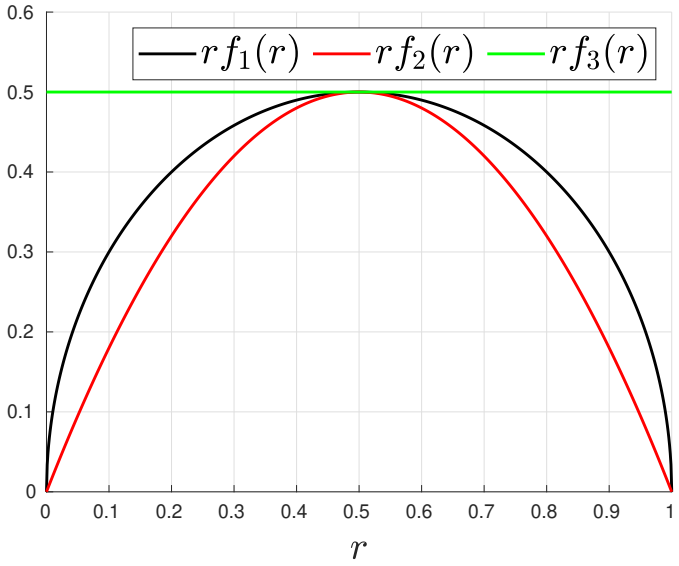

Figure 5.8: Comparison between $rf_1(r), rf_2(r)$ and $rf_3(r)$. $f_1(r), f_2(r)$ and $f_3(r)$ are defined in Equations (5.26-5.28).

for all $r_1 \in (0, 0.5)$.

By defining the new stochastic boundary conditions in Equation (5.17-5.18), the deterministic time-dependent blood flow Equations can be converted into a system of Stochastic Functional Differential Equations (SFDEs) of the form:

$$\mathrm{d}X(t) = g_1(x_t)\mathrm{d}t + g_2(x_t)\mathrm{d}W_t, \tag{5.30}$$

where the functions g_1 and g_2 are bounded and x_t is the set:

$$x_t = \{X(t+\theta) : -\tau \leq \theta \leq 0\} \in C([\tau, 0]; \mathbb{R})\}. \tag{5.31}$$

However, substituting the boundary conditions described by Equations (5.15-5.16) with the boundary conditions described by Equations (5.17-5.18) into Equation (5.32), does not convert the system of DDEs into a system of SFDEs. Let $(x, y) = (v, w)$ or $(x, y) = (v, z)$ at a flow bifurcation, and let $\kappa = kH_{(u,v)}(0, t - \tau_{(u,v)}(t))$. Replacing $H_{(x,y)}(0, t)$ and $H_{(x,y)}(0, t - \tau_{(x,y)}(t))$ with the equivalent stochastic boundary conditions in Equation (5.12) results in the following expression:

$$\Delta H^{(\mathrm{s})}_{(x,y)}(t) = \Delta H_{(x,y)}(t) \pm (\kappa f(r)\mathrm{d}W_t - \kappa f(r_{\tau_{(x,y)}})\mathrm{d}W_{\tau_{(x,y)}}), \tag{5.32}$$

where $W_{\tau_{(x,y)}}$ refers to the Weiner process at times $t - \tau_{(x,y)}(t)$ and $r_{\tau_{(x,y)}} = Q_{(x,y)}(t - \tau_{(x,y)}(t))/Q_{(u,v)}(t-\tau_{(x,y)}(t))$. If Equation (5.12) is replaced by Equation (5.32) in Equations (5.8) and (5.10) results in the following Equations:

$$\mathrm{d}\overline{H}_{(v,w)} = u_{(v,w)}(t)\Delta H_{(v,w)}(t)\mathrm{d}t + u_{(v,w)}(t)(\kappa f(r)\mathrm{d}W_t - \kappa f(r_{\tau_{(v,w)}})\mathrm{d}W_{\tau_{(v,w)}}), \tag{5.33}$$

$$\mathrm{d}\overline{H}_{(v,z)} = u_{(v,z)}(t)\Delta H_{(v,z)}(t)\mathrm{d}t - u_{(v,z)}(t)(\kappa f(1-r)\mathrm{d}W_t - \kappa f(r_{\tau_{(v,z)}})\mathrm{d}W_{\tau_{(v,z)}}). \tag{5.34}$$

However, Equations (5.33-5.34) are not SFDEs because Equations in the form of Equation (5.30) contain only one Weiner process.

Instead, by applying the new boundary conditions to both terms of Equation (5.12, a new expression for $\Delta H^{(\mathrm{s})}_{(x,y)}(t)$ can be derived by applying the stochastic boundary conditions to the vessel inlet at time t:

$$\Delta H^{(\mathrm{s})}_{(x,y)}(t) = \Delta H_{(x,y)}(t) \pm \kappa f(r)\mathrm{d}W_t. \tag{5.35}$$

SFDEs governing the rate of change for $\overline{H}_{(v,w)}$ and $\overline{H}_{(v,z)}$ are derived by replacing Equation (5.12) with Equation (5.35) in Equations (5.8) and (5.16):

$$\mathrm{d}\overline{H}_{(v,w)} = u_{(v,w)}(t)\Delta H_{(v,w)}(t)\mathrm{d}t + u_{(v,w)}(t)\kappa f(r)\mathrm{d}W_t, \tag{5.36}$$

$$\mathrm{d}\overline{H}_{(v,z)} = u_{(v,z)}(t)\Delta H_{(v,z)}(t)\mathrm{d}t - u_{(v,z)}(t)\kappa f(1-r)\mathrm{d}W_t. \tag{5.37}$$

The difference between Equations (5.36-5.37) and Equations (5.33-5.34) is the fact that Equations (5.33-5.34) include the terms $H^{(\mathrm{s})}_{(v,w)}(0, t-\tau_{(v,w)}(t))$ and $H^{(\mathrm{s})}_{(v,z)}(0, t-\tau_{(v,z)}(t))$ while Equations (5.36-5.37) do not. This means that the haematocrits leaving the vessels are determined by $H_{(v,w)}(0, t-\tau_{(v,w)}(t))$ and $H_{(v,z)}(0, t-\tau_{(v,z)}(t))$ instead of $H^{(\mathrm{s})}_{(v,w)}(0, t-\tau_{(v,w)}(t))$ and $H^{(\mathrm{s})}_{(v,z)}(0, t-\tau_{(v,z)}(t))$. Therefore, the SFDEs do not account for the effect of additional haematocrit generated by the Weiner process propagating through the daughter vessels. One potential issue with not accounting for this additional haematocrit exiting the daughter vessels is the fact that the stochastic fluctuations will not propagate through the rest of the network. However, as long as these fluctuations in the inlet haematocrit are taken into account by the Equations governing the average viscosity, the volumetric flows will fluctuate.

As with the system of DDEs, the average haematocrit variables do not influence the overall behaviour of the system because the flow Equations depend on the average viscosity

(see Section 2.3 for details). Therefore, the boundary conditions in Equations (5.9) and (5.11) must be adapted to incorporate the Weiner process. As with the Equations for the haematocrit, the Equations for the average viscosity are converted into SFDEs by replacing $\Delta\mu_{(x,y)}(t)$ in Equation (5.13) with a new expression for the difference in viscosity that includes the Weiner process, $\Delta\mu^{(\mathrm{s})}_{(x,y)}(t)$. Substituting $H^{(\mathrm{s})}_{(v,w)}(0,t)$ into Equation (5.13) yields the following Equation:

$$\Delta\mu^{(\mathrm{s})}_{(x,y)}(t) = \mu_{(x,y)}(H_{(x,y)}(0,t) + \kappa f(r)\mathrm{d}W_t/\mathrm{d}t) - \mu_{(x,y)}(H_{(x,y)}(0, t - \tau_{(x,y)}(t))). \tag{5.38}$$

If Equation (5.13) is replaced with Equation (5.38) in Equations (5.9) and (5.11), the resulting Equations are not SFDEs because the $\mathrm{d}W_t/\mathrm{d}t$ term is within the viscosity function. Therefore, another approximation is required. Consider the following linear approximation of $\mu_{(x,y)}$:

$$\mu_{(x,y)}(H_{(x,y)}(0,t) + \kappa f(r)\mathrm{d}W_t/\mathrm{d}t) \approx \mu_{(x,y)}(H_{(x,y)}(0,t)) + \mu'_{(v,w)}(H_{(v,z)}(0,t))\kappa f(r)\mathrm{d}W_t/\mathrm{d}t. \tag{5.39}$$

The justification of using the first-order Taylor expansion has been omitted from the main text but can be found in Appendix C. Substituting $\mu_{(x,y)}(H_{(x,y)}(0,t) + \kappa f(r)\mathrm{d}W_t/\mathrm{d}t)$ with the approximation in Equation (5.39), results in the following expression for the viscosity difference:

$$\Delta\mu^{(\mathrm{s})}_{(x,y)}(t) = \Delta\mu_{(x,y)}(t) + \mu'_{(v,w)}(H_{(v,w)}(0,t))\kappa f(r)\mathrm{d}W_t/\mathrm{d}t. \tag{5.40}$$

SFDEs for the average viscosity in vessels (v,w) and (v,z) can be derived using a similar method to the derivation of Equations (5.36-5.37). The substitution of Equation (5.13) with Equation (5.40) in Equations (5.9) and (5.11) yields the following SFDEs:

$$\mathrm{d}\overline{\mu}_{(v,w)} = \Delta\mu_{(v,w)}(t)\mathrm{d}t + u_{(v,w)}(t)\mu'_{(v,w)}(H_{(v,w)}(0,t))\kappa f(r)\mathrm{d}W_t, \tag{5.41}$$

$$\mathrm{d}\overline{\mu}_{(v,z)} = \Delta\mu_{(v,z)}(t)\mathrm{d}t - u_{(v,z)}(t)\mu'_{(v,z)}(H_{(v,w)}(0,t))\kappa f(1-r)\mathrm{d}W_t. \tag{5.42}$$

So long as the amplitude parameter, k, is relatively small compared to the haematocrit predicted by the deterministic boundary conditions in Equations (5.15-5.16), the linear approximation of the viscosity function is sufficiently accurate to capture the stochastic effects on the viscosity of the blood.

All other Equations for the average haematocrit and viscosity in the vessels not in the triangle network do not include a Weiner process. Therefore, they are automatically in

the form of Equation (5.30) such that $g_2(x_t) = 0$. Therefore, Equations (5.36-5.37) and (5.41-5.42), and the other deterministic flow Equations, form a system of SFDEs.

An important property of SFDEs is the dependence of the solution on the initial conditions. Unlike stochastic differential Equations, not only does the distribution of the variables at time t depend on the initial conditions, it is possible for the steady-state distribution to differ for two sets of initial conditions (Longtin, 2009). This dependence on the initial conditions presents some challenges in understanding the underlying role of stochastic fluctuations on the dynamics of blood flow. It is important to isolate the effects of varying parameters from different choices of initial conditions. As the objective is to understand whether the blood flow switches between stable equilibria, all initial conditions considered in this chapter are set equal to stable equilibria of the deterministic time-dependent network Equations. It may be possible that two different stable equilibria result in different steady-state distributions for the SFDEs for some network. If this case arises, both initial conditions will be investigated separately.

Several numerical schemes have been suggested to solve stochastic delay differential Equations (Akhtari, 2019; Baker and Buckwar, 2000; Buckwar, 2000; Mao, 2003). The schemes devised by Mao (2003) and Buckwar (2000) both allow the time delay to depend on the solution at time t. However, it is important that the time delay is different in each vessel and the scheme devised by Buckwar (2000) is only applicable to SDDEs for which the time delay is the same for every variable. Therefore, we use the scheme devised by Mao (2003) because it allows delays in each vessel to depend on the history of the solution and differ for each vessel (Mao, 2003). A set of restrictions on the form of the functions g_1 and g_2 in Equation (5.30) are required for the scheme devised by Mao (2003) to be applicable. In our case, not all of these conditions can be proven analytically. We justify our use of this method by proving those conditions that we can and using different time steps to verify the numerical solutions converge to the same distributions. A description of Mao et al.'s scheme and the results of these numerical experiments can be found in Appendix B.

5.2.1 Types of switching

Motivated by the results presented in Figure 5.7, we focus on the diamond network when investigating the impact of stochastic effects on blood flow. For simplicity, stochastic effects are negated for the second flow bifurcation. As one of the daughter vessels is always vessel $\langle 4, 5\rangle$, for the blood flow to switch between the two equilibria, $Q_{\langle 4,5\rangle}(t) = 0$ for some time t. Therefore, the ratios $Q_{\langle 4,5\rangle}(t)/Q_{(3,4)}(t)$ or $Q_{\langle 5,4\rangle}(t)/Q_{(3,5)}(t)$ must eventually be smaller

than X_0 of the splitting rule in Equation (1.37). When the flow ratio is below this threshold, the deterministic boundary condition for vessel $\langle 4, 5\rangle$ is 0. Therefore, if the Weiner process is negative when these ratios are less than X_0, the stochastic boundary condition is not physical.

We also restrict our attention to symmetric diamond networks in this thesis. Karst et al. (2015) found that for certain choices of asymmetric lengths, $L_{(4,6)}$ and $L_{(5,6)}$, the deterministic blood flow equations would admit unstable limit cycles for the $(-)$ or $(+)$ equilibria (Karst et al., 2015). As the purpose of this section is to investigate the switching behaviour between stable equilibria, restricting the diamond network to be symmetric networks ensures that the $(-)$ and $(+)$ equilibria are both stable.

Figure 5.9 shows the time-dependent solution to the stochastic network equations for the diamond network with the following parameters:

$$L = 100\mu m, D = 10\mu m, H_{(1,3)}(0, t) = 0.3966, k = 0.00001, \tag{5.43}$$

for three different random seeds represented by black, green and turquoise curves. All three realisations start at the $(-)$ equilibrium. Figure 5.9a shows that stochastic effects can drive changes in the flow direction in the redundant vessel, and the fluctuation of the flow is between the two stable equilibria associated with the deterministic model. Figures 5.9c and 5.9d reveal that the differences in the values of $H_{(3,4)}$ and $H_{(3,5)}$ for the two stable equilibria are minimal. This explains why relatively little noise is required to change the flow direction. It is possible that switching only occurs between equilibria for which the haematocrit values in the daughter vessels of a bifurcation are sufficiently close. In theory, as long as the amplitude parameter is non-zero, it is possible for a single perturbation or a sequence of perturbations to drive the solution from one equilibrium to the other, but the probability of this event occurring depends on the size of the interval and the size of the amplitude parameter, k. Therefore, to adequately understand under which conditions switching occurs with any regularity, the influence of k and the parameters of the network on these switching events must be determined.

Another interesting property of this switching is the difference in haematocrit values for the two stable equilibria in Figures 5.9e and 5.9f, this difference is much greater than the difference in Figures 5.9c and 5.9d. The haematocrit values in $H_{(4,6)}$ and $H_{(5,6)}$ are not directly affected by the stochastic fluctuations at the first flow bifurcation and k is relatively

small compared to the difference in the values of $H_{(4,6)}$ or $H_{(5,6)}$. Therefore, small stochastic fluctuations upstream have a larger potential impact on the haematocrit downstream in a network. To fully investigate the downstream effects, large networks with multiple redundant vessels should be studied, but this is beyond the scope of this thesis.

One distinctive feature of the solutions in Figure 5.9 is the spontaneous switching between the $(-)$ and $(+)$ equilibria. As the stochastic blood flow equations are not deterministic, it is not possible to predict with absolute certainty when the blood flow will switch between the two stable equilibria. As one of the goals of applying stochastic noise is to propose stochastic fluctuations as a potential cause or contributing factor to cycling-hypoxia, it is important to make predictions on how long the blood flow will remain in each state. Therefore, the spontaneous change in the direction of the flow presents the challenge of predicting how long the blood flow remains in each state. However, it is possible to predict the duration of full switches. A full switch will be defined later in this Section, but intuitively, a full switch occurs when the blood flow in the redundant vessel changes direction twice. Predicting the duration of the switches facilitates making predictions for the time between oxygen fluctuations.

We have devised two definitions of a full switch; a threshold switch and a checkpoint switch. A threshold switch is defined by thresholds that the numerical solution must hit and a checkpoint switch is based upon the propagation of flow in the redundant vessel in a network. Before defining a threshold switch, the concept of σ-negative and σ-positive thresholds must first be defined.

Definition 5.1. (Threshold for network with two stable equilibria)
Let $\mathcal{N}$ be a network with a single redundant vessel, $\langle x, y\rangle$, such that the network admits three equilibria with the following flow configurations $\{(-), (0), (+)\}$ such that the $(-)$ and $(+)$ equilibria are stable. Let $Q^{(+)}_{\langle x,y\rangle}$ and $Q^{(-)}_{\langle x,y\rangle}$ denote the value of the normalised flow in the redundant vessel for the $(+)$ and $(-)$ equilibria respectively. The σ-positive and σ-negative thresholds, $(Q^{(+)}_{\sigma}, Q^{(-)}_{\sigma})$ are defined as:

$$Q^{(+)}_{\sigma} = \sigma Q^{(+)}_{\langle x,y\rangle}, Q^{(-)}_{\sigma} = \sigma Q^{(-)}_{\langle x,y\rangle}, \tag{5.44}$$

where $\sigma \in (0, 1]$.

Now that σ-negative and σ-positive thresholds have been defined, we can now define the $(-) \to (+)$ and $(+) \to (-)$ σ-threshold switches.

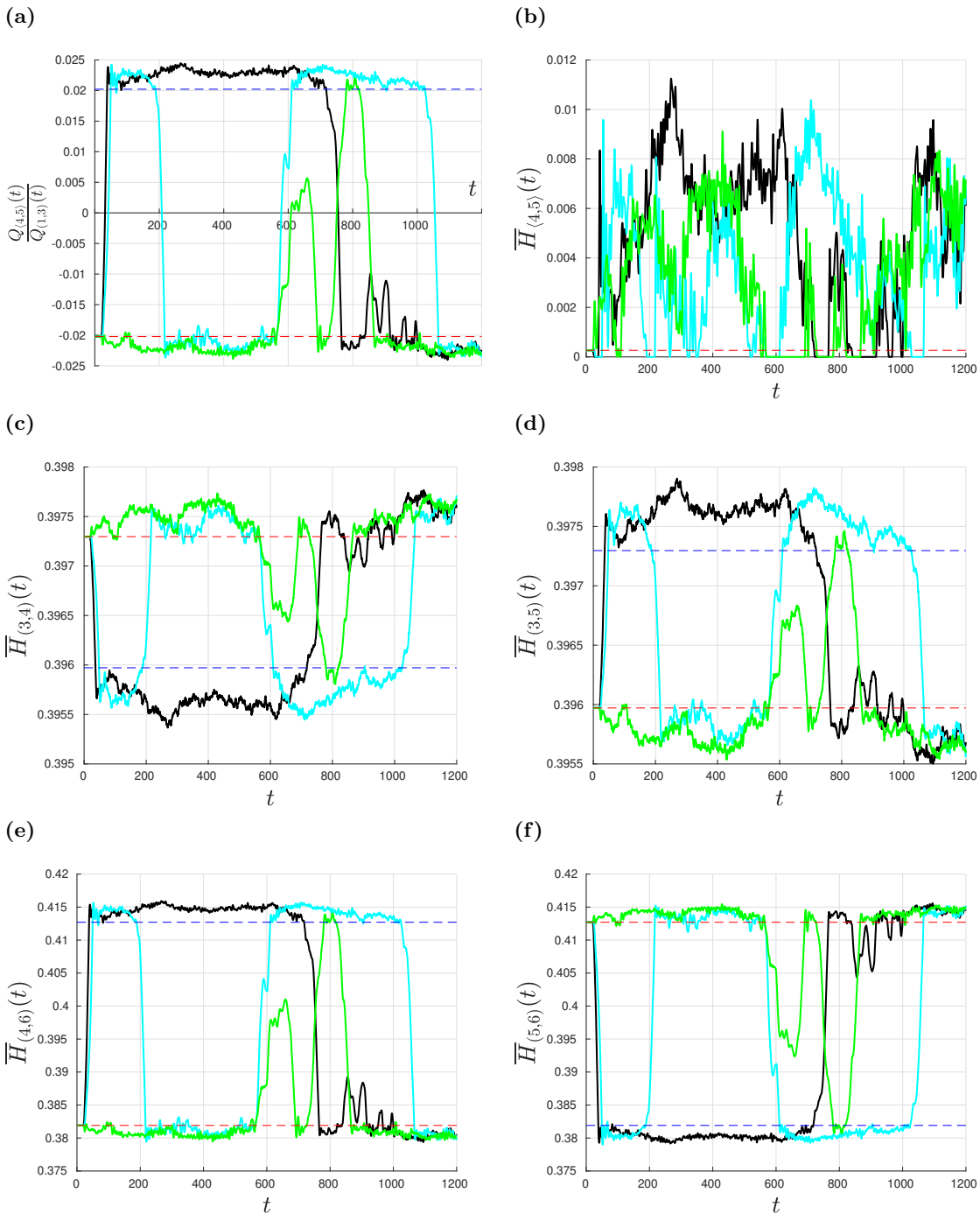

Figure 5.9: Plots of select variables for three different realisations of the time-dependent solutions of the SFDEs of the diamond network. (a): normalised flow in the redundant vessel; (b): $\overline{H}_{\langle 4,5\rangle}(t)$; (c): $\overline{H}_{(3,4)}(t)$; (d): $\overline{H}_{(3,5)}(t)$; $\overline{H}_{(4,6)}(t)$; $\overline{H}_{(5,6)}(t)$.

Definition 5.2. (Threshold switch)
Let $\mathcal{N}$ be a network with a single redundant vessel, $\langle x, y\rangle$, such that the network admits three equilibria with the following flow configurations $\{(-), (0), (+)\}$ for which the $(-)$ and $(+)$ equilibria are stable. A $(-) \to (+)$ σ-threshold switch is a section of the solution to the SFDEs of a network consisting of the following two phases.

Perturbation phase:
Let $Q_{\langle x,y\rangle}(t) = Q_\sigma^{(-)}$ at t_{start} and $Q_{\langle x,y\rangle}(t) = Q_\sigma^{(+)}$ at t_0 such that:

$$Q_\sigma^{(-)} < Q_{\langle x,y\rangle}(t) < Q_\sigma^{(+)}, \forall t \in (t_{\text{start}}, t_0). \tag{5.45}$$

The solution to the SFDEs in the interval $[t_{\text{start}}, t_0]$ is known as the perturbation phase.

Return phase:
Let $Q_{\langle x,y\rangle}(t) = Q_\sigma^{(-)}$ at t_{end} such that: $t_{\text{end}} > t_0$ and $Q_\sigma^{(-)} < Q_{\langle x,y\rangle}(t), \forall t \in [t_0, t_{\text{end}})$. The solution in the interval $[t_0, t_{\text{end}}]$ is known as the return phase.

The $(+) \to (-)$ σ-threshold switch is defined analogously for the solution starting and ending at the positive σ-threshold.

The $(-) \to (+)$ and $(+) \to (-)$ σ-threshold switching times are defined as the time between t_{start} and t_{end} for both directions of the σ-threshold switches.

The $(-) \to (+)$ and $(+) \to (-)$ checkpoint switches can also be defined with phases, but a checkpoint switch contains two relaxation phases, as well as a perturbation and a return phase. After the flow direction in the redundant vessel changes direction, there is a time delay before the blood flow fully propagates through the vessel.

Definition 5.3. (Checkpoint switch)
Let $\mathcal{N}$ be a network with a single redundant vessel, $\langle x, y\rangle$, such that the network admits three equilibria with the following flow configurations $\{(-), (0), (+)\}$ such that the $(-)$ and $(+)$ equilibria are stable. A $(-) \to (+)$ checkpoint switch is a section of the solution to the SFDEs of a network consisting of the following four phases.

Perturbation phase:
Let $Q_{\langle x,y\rangle}(t) = Q_{\langle x,y\rangle}^{(-)}$ at t_{start} and $Q_{\langle x,y\rangle}(t) = Q_{\langle x,y\rangle}^{(+)}$ at t_0 such that:

$$Q_{\langle x,y\rangle}^{(-)} < Q_{\langle x,y\rangle}(t) < Q_{\langle x,y\rangle}^{(+)}, \forall t \in (t_{\text{start}}, t_0). \tag{5.46}$$

The solution to the SFDEs in the interval $[t_{\text{start}}, t_0]$ is known as the perturbation phase.

1st relaxation phase
Let t_1 denote the time such that:

$$L_{\langle x,y\rangle} = \int_{t_0}^{t_1} u_{\langle x,y\rangle}(s)ds, \tag{5.47}$$

and $Q_{\langle x,y\rangle}(t) > Q^{(-)}_{\langle x,y\rangle}, \in (t_0, t_1)$. The 1st relaxation phase is the section of the solution in the interval $[t_0, t_1]$.

Return phase:
Let $Q_{\langle x,y\rangle}(t) = Q^{(-)}_{\langle x,y\rangle}$ at t_2 such that: $t_2 > t_1$ and $Q^{(-)}_{\langle x,y\rangle} < Q_{\langle x,y\rangle}(t), \forall t \in [t_1, t_2)$. The solution in the interval $[t_1, t_2]$ is known as the return phase.

2nd relaxation phase
Let t_{end} denote the time such that:

$$L_{\langle x,y\rangle} = \int_{t_2}^{t_{\text{end}}} u_{\langle y,x\rangle}(s)ds, \tag{5.48}$$

and $Q_{\langle x,y\rangle}(t) < Q^{(+)}_{\langle x,y\rangle}, \in [t_2, t_{\text{end}})$. The 2nd relaxation phase is the section of the solution in the interval $[t_2, t_{\text{end}}]$.

The $(+) \rightarrow (-)$ checkpoint switch is defined analogously for the solution starting and ending at $Q^{(+)}_{\langle x,y\rangle}$.

The $(-) \rightarrow (+)$ and $(+) \rightarrow (-)$ checkpoint switching times are defined as the time between t_{start} and t_{end} for both directions of the checkpoint switches. If the first relaxation phase is interrupted by the solution returning to the original equilibrium before the RBCs can fully propagate through the redundant vessel, then the checkpoint switch has not occurred. If the solution returns to the opposite threshold before the second relaxation phase has completed, then that section of the curve that incorporates the brief reversal of the flow direction is considered part of the return phase.

Remark 5.2. If $|Q^{(+)}_{\langle x,y\rangle}| = |Q^{(-)}_{\langle x,y\rangle}|$, then there is no difference between the $(-) \rightarrow (+)$ and $(+) \rightarrow (-)$ switches or switching times. Therefore, the $(-) \rightarrow (+)$ and $(+) \rightarrow (-)$ switches and switching times will simply be referred to as the σ-threshold and checkpoint switches, and the σ-threshold and checkpoint switching times.

It should be noted here that the perturbation phase of a checkpoint switch is the same as the perturbation phase of the equivalent 1-threshold switch. Furthermore, the combination of the $1st$ relaxation phase and the return phase of the checkpoint switch would also define a 1-threshold switch return phase. Therefore, every checkpoint switch has an embedded 1-threshold switch but the opposite implication does not apply.

Figure 5.10 shows the phases of the two types of switch metric for the same realisation of the SFDEs for the diamond network. Figure 5.10a shows a $(+) \to (-)$ 0.8-threshold switch and Figure 5.10b shows a $(+) \to (-)$ checkpoint switch. The negative and positive 0.8-thresholds are represented by the red and blue dotted dashed lines in Figure 5.10a and the values of $Q^{(-)}_{\langle 4,5\rangle}$ and $Q^{(+)}_{\langle 4,5\rangle}$ are represented by the red and blue dashed lines in Figure 5.10b. The perturbation and return phases are represented by purple and black for both types of switching. The two relaxation phases for the checkpoint switch are represented in pink. $(-) \to (+)$ switches are also presented in Figure 5.10 but only one switch has been explicitly highlighted to represent the phases of a switch.

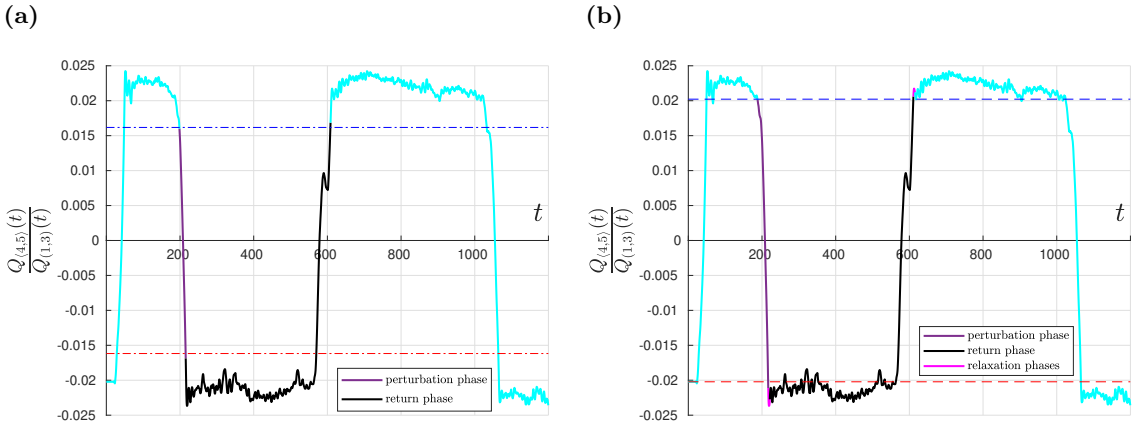

Figure 5.10: Plots of the turquoise solution in Figure 5.9a with the two methods of measuring switching. The dashed red and blue lines denote the $(-)$ and $(+)$ equilibria and the dotted dashed red and blue lines denote the $\times 0.8$ threshold of the two equilibria. (a): Threshold switching; (b) Checkpoint switching.

Before using switching to evaluate the network behaviour, the different behaviour of the switching definitions must first be identified to isolate the effects of our method for evaluating the switching behaviour. Figure 5.10, shows that the two switching methods predict a similar time for the switch for this example, but checkpoint switching predicts a longer time for the switch. Given the similarities of the method, it is possible to conclude that a checkpoint switch is always longer than a threshold switch because checkpoint switching includes two of the same phases as threshold switching. However, this does not indicate

whether the switching time distributions are similar. Threshold switching may predict more switching and potentially more significantly shorter switches. Given the complicated nature of the SFDEs, it is not possible to determine analytical expressions for the distributions of the two switching times, but by performing multiple simulations, it is possible to create an approximation to the distribution curves.

To approximate these distribution curves, the network SFDEs were solved for $10,000$ random seeds. Realisations for the SFDEs were computed until two switches were observed. This was due to the observation that an initial switch was usually observed immediately after the noise terms were applied to the equations[3]. If a switch was not observed before $t_{\text{end}} = 24 \times 60 \times 60$, the simulation was stopped and restarted using a different random seed. The second recorded switching times were used to generate a distribution using MATLAB's inbuilt distribution fitting application. The distribution chosen for the fit was that of a non-parametric fit for only positive values. In Figure 5.11 we compare the two switching time metrics for the amplitude parameter of $k = 0.001$. The distributions and associated histograms for the data used to generate the two curves are presented in Figures 5.11a and 5.11b. The two distributions are plotted on the same axes in Figure 5.11c. Figure 5.11c clearly shows the similarities between the two distribution curves. Due to the fact that it takes time for the solution to travel between the thresholds for either switching metric, we expected that there would always be a minimum switching time, $t_{min} > 0$, representative of the minimum time required for a switch to occur for both switching metrics. As expected, the two curves show a probability density of 0 close to $t = 0$. Both curves also have a single modal peak which appears earlier for threshold switching as expected. After this peak, the probability density of both types of switching appears to decrease exponentially. Unfortunately, there is no known distribution curve that adequately fits the data, and so it is difficult to know which measurements of the distributions are most important to compare to the data. However, the modes of the distribution curves provide a clear distinction between the curves.

Figure 5.12 shows how the distribution of the two switching times changes as the amplitude k of the noise term varies. The shapes of the distributions remain similar as k varies (Results not shown). Modal switching times for both types of switching decrease as k increases. Thus, we expect more rapid switching as the amplitude of the fluctuations increases. Figures 5.12c and 5.12d show the plots for the logarithm of the modal switching times against the logarithm of k. As expected, the modal switching time decreases as

[3]This can be observed in Figure 5.9.

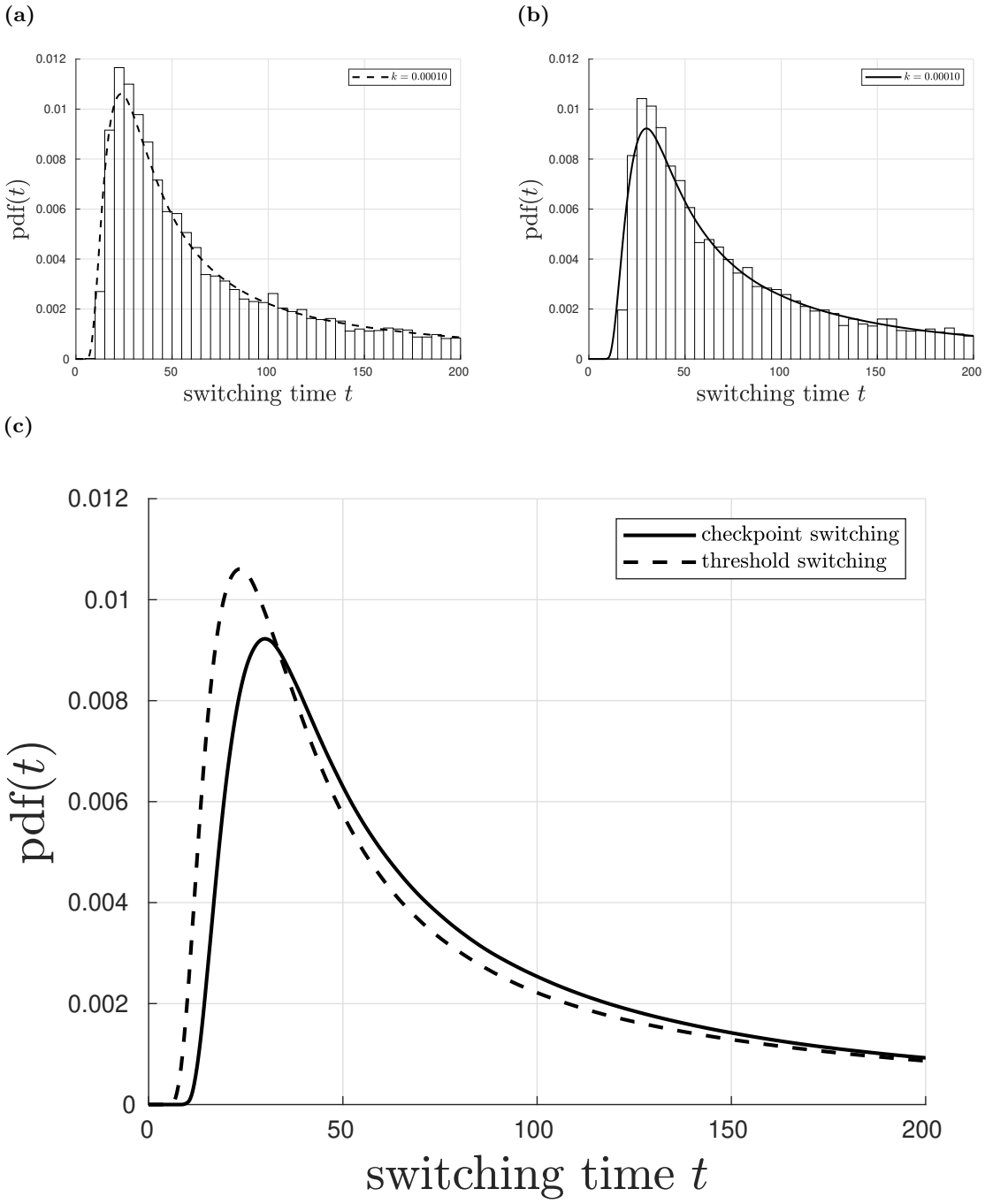

Figure 5.11: Series of plots showing the comparison between threshold and checkpoint switching for the diamond network when $k = 0.00010$. (a): Best fit to the distribution curve of threshold switching with the associated histogram for the data; (b): Best fit to the distribution curve of checkpoint switching with the associated histogram for the data; (c): Comparison of the distribution curves in (a) and (b).

k increases. However, the line of best fit for threshold switching is steeper than the line for checkpoint switching, and the confidence interval for threshold switching is also much smaller. One explanation for this observation is that the duration of relaxation phases in checkpoint switching is highly variable. Regardless of these differences, the distributions of switching times exhibit a similar behaviour for both definitions of switching times. We conclude that either definition can be used. However, we will use checkpoint switching for the remainder of the chapter. This effectively means that the two stable equilibria of the deterministic network equations are defined by positive or negative flow in the redundant vessel for which the RBCs have fully propagated from one side of the network to the other. The state before and after a full checkpoint switch requires that the RBCs have propagated fully through the redundant vessel. As this property is also shared by the equilibria, checkpoint switching is a more natural way to count switching.

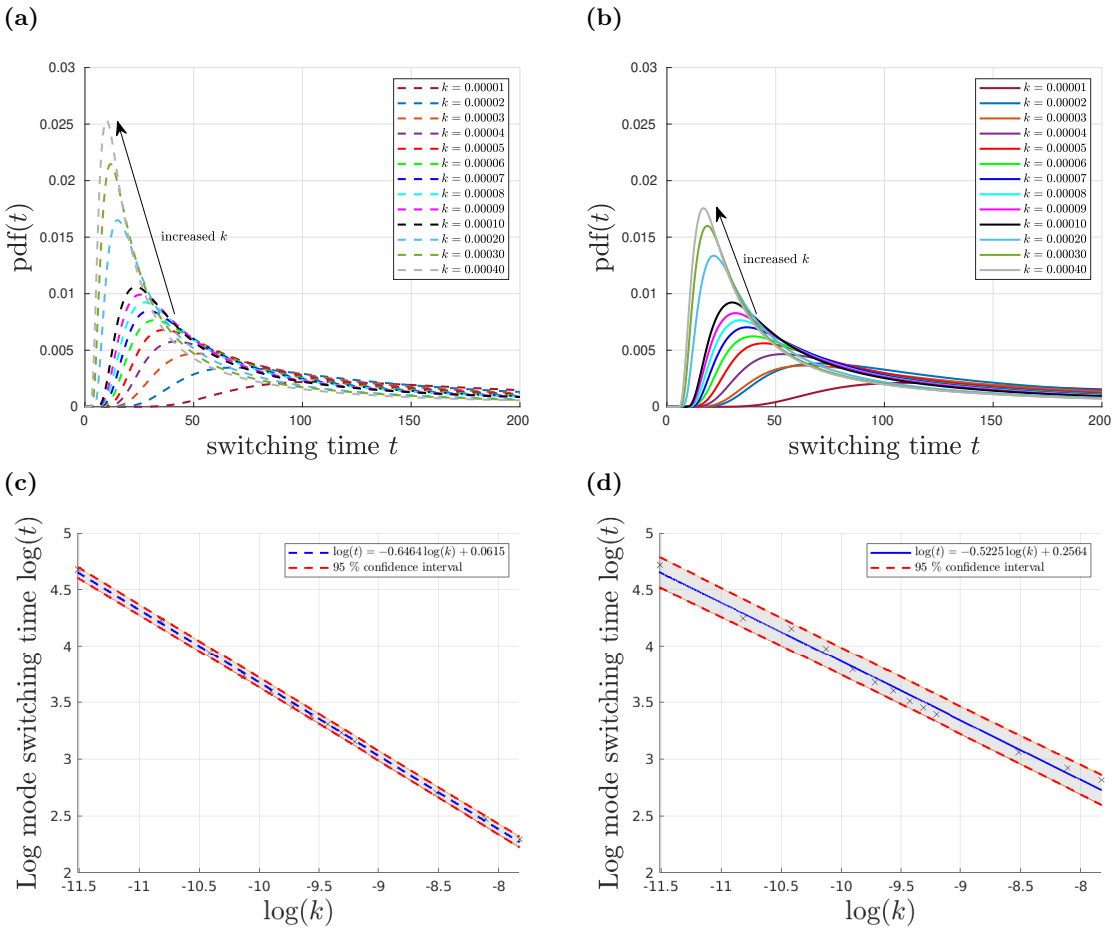

Figure 5.12: Plots showing the evolution of the switching time distribution curves as the noise amplitude parameter k varies. (a): Distribution curves for the threshold switching times for a threshold of 0.8; (b): Distribution curves for the checkpoint switching times; (c): plot of the logarithm of the modal threshold switching times against the logarithm of the noise amplitude parameter k; (d): plot of the logarithm of the modal checkpoint switching times against the logarithm of the noise amplitude parameter k.

5.2.2 Relationship between haematocrit and switching time

The duration of the switching times influences tissue oxygen levels. If the switches are rapid, then the oxygen levels of the tissue may become more evenly distributed. If the switches are slow, then parts of the tissue may experience hypoxia for long time periods. For this reason, it is important to understand how the network parameters influence the distribution of switching times. In this section, we investigate how key parameters, such as the length of the redundant vessel and the size of the inlet haematocrit impact switching times. As blood flow must fully propagate through the redundant vessel for a switch to occur, we anticipate that vessel length will have a significant impact on the distribution of switching times. The inlet haematocrit is likely to be important because multiple equilibria exist only

for sufficiently large values of the inlet haematocrit. Furthermore, as the inlet haematocrit increases, the difference between the values of $H_{(3,4)}$ and $H_{(3,5)}$ for non-trivial equilibria increases. Varying the inlet pressure is not considered because the diamond network has a single inlet and outlet vessel. As discussed in Section 1.9.6, the haematocrit distribution of an equilibrium in networks with a single inlet and outlet vessel is independent of the inlet and outlet pressure, as long as the inlet pressure is larger than the outlet pressure. We anticipate that other network parameters, including vessel diameters, may influence the switching times. We postpone consideration of these effects to future work.

Ideally, we would determine the switching time distributions for a range of values in the $(L_{\langle 4,5\rangle}, H_{(1,3)})$ plane. Given the computational cost of approximating the switching time distribution for one set of parameter values, it is not feasible to evaluate the switching times for a wide range of values of $L_{\langle 4,5\rangle}$ and $H_{(1,3)}$). Even for a course grid of points in the $(L_{\langle 4,5\rangle}, H_{(1,3)})$ plane, calculating a sufficient number of switching times for each point is too computationally expensive. The distribution curves in Figure 5.12 required $10,000$ switching times to generate each distribution curve. We found that generating the same distribution curves in Figure 5.12 using $1,000$ switching times produced modal times that were sufficiently close to the modal times in Figure 5.12. Therefore, as long as there were at least $1,000$ switching times, a sufficient approximation of the modal switching time could be computed. The time given for a simulation to find switching times was also relaxed from $t = 24 \times 60 \times 60$ to $t = 2.5 \times 60 \times 60$. Instead of stopping the simulation as soon as the second switch occurs, the simulation was run for the full time and the switching times were recorded throughout the simulation[4]. This meant that some simulations would predict more than one switch and others would record none. Even with these relaxations of the times constraints for a single realisation of the equations, finding enough switching times for a grid of points in the $(L_{\langle 4,5\rangle}, H_{(1,3)})$ plane is too inefficient.

Instead of investigating the differences in the switching times for each point in a grid of points for the pair of parameters $(L_{\langle 4,5\rangle}, H_{(1,3)})$, we show how the switching time changes as the inlet haematocrit varies for four different values of $L_{\langle 4,5\rangle}$ shown in Figure 5.13a. This approach provides information on the impact of the emergence of multiple equilibria of different lengths and the trend as the inlet haematocrit increases.

Figure 5.13b shows how the switching times distribution changes as the inlet haematocrit

[4]Switching times were only counted after the first switch so that the methodology was consistent with that in Section 5.2.1.

$H_{(1,3)}$ varies when $L_{\langle 4,5\rangle} = 100\mu$m. Due to the computational difficulty of finding switching times, we restrict our attention to the cases for which $H_{(1,3)} \leq 0.5$. With $H_{(1,3)} \leq 0.5$, we find that the modal switching time increases as the inlet haematocrit increases. This trend is more pronounced in the log-log plot of the inlet haematocrit and the modal switching time presented in Figure 5.13c. Due to the tight confidence intervals and the simple relationship between the inlet hematocrit and the modal switching time, we predict that this trend will extend to values of $H_{(1,3)}$ greater than 0.5. The linear relationship between $\log(t_{mode})$ and $\log(H_{(1,3)})$ is valid for other values of $L_{\langle 4,5\rangle}$ displayed in Figure 5.13a (Results not found). Figure 5.13d compares all linear fits between $\log(t_{mode})$ and $\log(H_{(1,3)})$ for all lengths of $L_{\langle 4,5\rangle}$ represented in Figure 5.13a. Except for a small difference for the gradient values, the lines are parallel. The only difference between the fits is the value of $H_{(1,3)}$ at which the lines emerge. These values correspond exactly to the value of $H_{(1,3)}$ at which multiple equilibria emerge, as shown in Figure 5.13a. This suggests that the length of the redundant vessel does not directly influence the distribution of switching times. Figure 5.13d suggests that for each value of $L_{\langle 4,5\rangle}$, there is a corresponding critical value of $H_{(1,3)}$ ($H^*_{(1,3)}$) for which the network admits multiple equilibria. The value of t_{mode} is the same for all values of $H^*_{(1,3)}$ and $\log(t_{mode})$ increases linearly with $\log(H_{(1,3)})$.

Now that the relationship between $(L_{\langle 4,5\rangle}, H_{(1,3)})$ and t_{mode} has been established, the next task is to understand why the modal switching time is the same for all critical values of $H_{(1,3)}$. As can be seen in Figure 5.7e, non-trivial equilibria correspond with the emergence of non-zero values of $H_{\langle 4,5\rangle}$. Therefore, we hypothesise that a linear relationship between the values of $H_{\langle 4,5\rangle}$ for the non-trivial equilibria and $\log(t_{mode})$ for all values of $L_{\langle 4,5\rangle}$. Figure 5.14a shows the linear relationship between $H_{\langle 4,5\rangle}$ and $\log(t_{mode})$ when $L_{\langle 4,5\rangle} = 100\mu$m. As in Figure 5.13c, the confidence interval is close to the line of best fit. The fits for other values of $L_{\langle 4,5\rangle}$ are left out of this thesis for brevity. In Figure 5.14b when we compare all fits, we find that the relationship between $H_{\langle 4,5\rangle}$ and $\log(t_{mode})$ does not depend on the value of $L_{\langle 4,5\rangle}$. As the viscosity of the blood depends on the haematocrit, Figure 5.14b shows that the main factor that determines the modal switching time is the viscosity of the blood.

5.3 Discussion

In this chapter, we have presented a viable hypothesis for the formation of cycling-hypoxia in cancerous tumours. Previous studies of blood flow models suggest that fluctuations in oxygen within the tumour microenvironment can be caused by oscillations in blood flow in

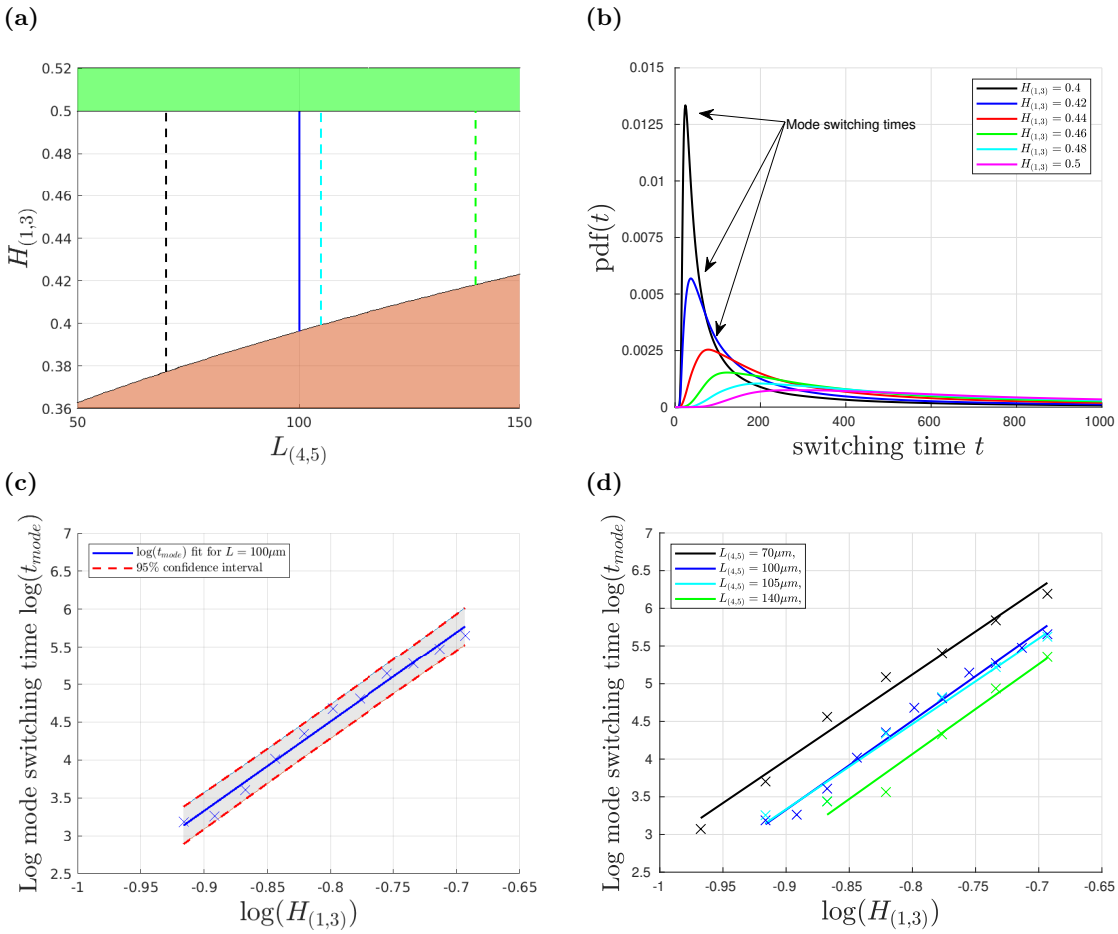

Figure 5.13: (a): Area plot of $H_{(1,3)}$ against $L_{\langle 4,5\rangle}$ for which the orange area indicates the area of the region for which multiple equilibria are not possible and green indicates the area of haematocrit values that we are not modelling; (b): Distributions of switching times for $L_{\langle 4,5\rangle} = 100\mu m$; (c): Plot of the $\log(t_{mode})$ against the $\log(H_{(1,3)})$ when $L_{\langle 4,5\rangle} = 100\mu m$; (d): Plots of $\log(t_{mode})$ against $\log(H_{(1,3)})$ for the lengths indicated in (a).

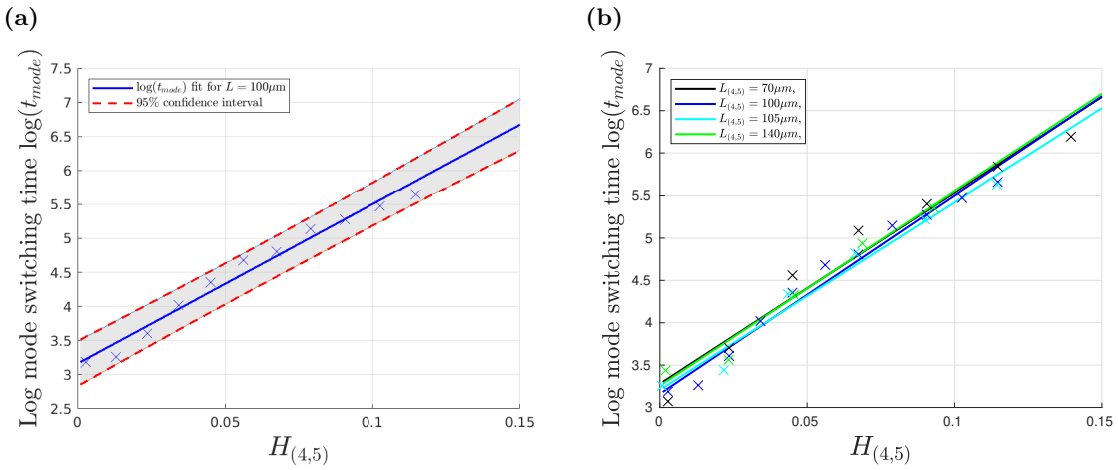

Figure 5.14: (a): Plot of $\log(t_{mode})$ against the value of $H_{\langle 4,5\rangle}$ for the $(-)$ or $(+)$ equilibria when $L_{\langle 4,5\rangle} = 100\mu m$; (b): Plots of $\log(t_{mode})$ against the values of $H_{\langle 4,5\rangle}$ for the $(-)$ or $(+)$ equilibria for the lengths indicated in Figure 5.13a.

the microvasculature. Oscillations in blood flow can form as a result of structural features of a network that lead to the existence of Hopf bifurcations of the deterministic blood flow equations detailed in Sections 1.8 and 2.3 (Ben-Ami et al., 2022; Karst et al., 2015). Ben-Ami et al. (2022) showed that self-sustained oscillations were present in triangle networks with significant vessel diameter asymmetry, and Karst et al. (2015) obtained a similar result for diamond networks with asymmetric vessel lengths. In both cases, self-sustained oscillations only arose when the networks admitted multiple equilibria.

The mechanism by which solutions to the time-dependent blood flow equations switch between stable equilibria tested in this chapter relies on the existence of multiple equilibria which differ in terms of the direction of blood flow in a redundant vessel. We proposed two mechanisms that may explain this phenomenon: one deterministic and one stochastic. Both mechanisms have been shown to be viable in simple networks with a single redundant vessel.

The deterministic mechanism relies on a sufficiently large perturbation of the network boundary conditions to drive a switch in the time-dependent solution of the governing equations between different stable equilibria. A hysteresis occurs when the solution to a system of differential equations switches between stable equilibria of the system as parameters of the equation are altered. Ben-Ami et al. (2022) showed that symmetric triangle networks for which the lengths and diameters of the vessels were all equal admitted two stable equilibria and one unstable equilibrium for sufficiently large inlet haematocrits. This observation is consistent with our results in Chapter 3 which showed that equilibria without intermediate flow in the redundant vessels are stable for symmetric networks.

We have shown that hysteresis behaviour can occur in a symmetric triangle network as the pressure boundary conditions vary. By creating asymmetry of the boundary pressures, the pressure difference across the redundant vessel is forced to reverse. As the flow in a network is in the same direction as the pressure difference, the flow in the redundant vessel changes direction. This mechanism may persist in asymmetric triangles, but as shown by Ben-Ami et al. (2022), asymmetric triangle networks admit one stable equilibria, two unstable equilibria, and one unstable limit cycle. Therefore, a hysteresis would drive the time-dependent solution between a stable equilibrium and a limit cycle. Regardless of the specifics of the network geometry, the key to the mechanism is creating a sufficient asymmetry of the boundary conditions to create a change in the pressure difference across the redundant vessel.

The main limitation of this mechanism is that it relies on an external source to drive changes in flow. Furthermore, these changes occur on the same time scales as changes in the boundary conditions. Therefore, while such switches between multiple equilibria may explain the formation of heterogeneous oxygen distributions and fluctuations in these distributions, this mechanism does not predict the time scales for these fluctuations. For example, consider equation for P_1 in Figure 5.3a, if the time for which P_1 is at its minimum or maximum value persisted for longer time periods, the time for the solution to complete a hysteresis loop is longer.

By contrast, self-sustained oscillations belong to a closed system. The resulting fluctuations in the oxygen distribution are dictated by the frequency of the oscillations rather than by an imposed change in the boundary conditions. However, several mechanisms may explain the changes in the boundary conditions. For instance, changes in the boundary conditions could be driven by self-sustained oscillations in other parts of a network. If there is more than one source of oscillations in the network, more complex switching patterns could arise as a consequence of these oscillations going in and out of phase.

Another limitation of the deterministic mechanism of changing flow directions is that a redundant vessel must be downstream of two or more inlets. Figure 5.7 shows that changes in the flow direction in a redundant vessel did not occur in the diamond network. This is because the deterministic time-dependent flow equations have an inherent history that prevents the flow of the redundant vessel from changing direction.

The addition of a stochastic noise term at a flow bifurcation was shown to induce switching of flow direction within the redundant vessel in the diamond network. To our knowledge, this is the first time that stochastic noise has been incorporated into the continuum equations, but it has been well documented that stochastic effects arise in microcirculation (Bedggood and Metha, 2012; Fung, 1973; Pawlik et al., 1981). Furthermore, the number of red blood cells entering daughter vessels downstream of flow bifurcations has been shown to undergo random fluctuations in computational models that track individual red blood cells (Balogh and Bagchi, 2017, 2018).

One possible explanation for these switching events of the blood flow in the diamond network is the relationship between the haematocrit in the daughter vessels of the flow bifurcation at node 3 and the flow direction in the redundant vessel for the stable equilibria. The haematocrit values for the daughter vessels are unequal for the non-trivial equilibria.

$H_{(3,4)} > H_{(3,5)}$ for the $(-)$ equilibria and $H_{(3,5)} < H_{(3,4)}$ for the $(+)$ equilibria. Each stochastic fluctuation increases the inlet haematocrit of one daughter vessel and decreases the inlet haematocrit of the other. If the blood flow in the redundant vessel is positive and the solution is close to the $(+)$ equilibrium, then $H_{(3,5)}(0,t) < H_{(3,4)}(0,t)$. For sufficiently large stochastic fluctuations or series of stochastic fluctuations, the value of $H_{(3,5)}(0,t)$ increases and $H_{(3,4)}(0,t)$ decreases. As the direction of the flow in the redundant vessel depends on the values of haematocrit in the daughter vessels, the direction of blood flow is forced to change. Once this change has occurred, the solution is now closer to the $(-)$ equilibrium.

Another interesting aspect of the stochastic behaviour in a diamond network is the propagation of stochastic behaviour through the network. As discussed in Section 5.2.1, small stochastic fluctuations upstream in the diamond network can result in much larger downstream differences in haematocrit of certain vessels. This is probably a consequence of the haematocrit values of the daughter vessels of bifurcations being larger than the parent haematocrit (see Section 1.9.4 for details). Therefore, small perturbations in the value of the haematocrit upstream in a network have a more significant impact on the haematocrit downstream in a network after successive flow bifurcations. Although we have only shown this behaviour in the diamond network, this difference in the downstream haematocrit values in a network is likely to be common for a variety of network geometries due to the properties of the flow bifurcations discussed in Section 1.9.6. It is also possible that the propagation effect could result in further switching between equilibria. In Section 5.1.2, we observed that the solution to the time-dependent flow equations switched between two stable equilibria when the haematocrit boundary conditions for the network were altered. Although this clearly shows that changes in flow direction in the redundant vessel of the network can be driven by this mechanism, it depends on an upstream external mechanism that dictates the change in haematocrit boundary conditions. The propagation of stochastic behaviour in a network could be one potential mechanism driving the changes in the haematocrit boundary conditions for network motifs.

We showed in Section 5.2 that time-dependent solutions to the stochastic blood flow equations may lead to changes in flow direction in the redundant vessel and that the solutions may switch between the two non-trivial equilibria. Given the random nature of the solutions, the time it takes to switch between non-trivial equilibria and then back to the original equilibrium is also random. However, as described in Section 5.2, the numerical solution rarely returns exactly to one of the two non-trivial equilibria if at all. Therefore, measuring

the time for the values of the solution to exactly return to the values of one of the two equilibria may be impossible. To describe the switch, we introduce two alternative definitions of a switching time. Although the distributions for the two definitions of switching time were different, the characteristics of the two curves were consistent. The two distributions contain a minimum switching time and a single modal peak for values of $t > 0$. Both distributions also contain a long tail that begins at $t = t_{mode}$. Examples of these distributions can be seen in Figure 5.11. The peaks of the distributions (modal switching times) increased as the amplitude of the fluctuations increased. In particular, higher noise levels increased the likelihood that a faster switch would occur. Furthermore, the modal times were fitted to a power law, allowing predictions to be made about the modal switching times for different values of the amplitude parameter (see Figure 5.12).

The most important result in Section 5.2 is the link between the haematocrit of the redundant vessels and the modal switching times. As shown in Section 5.2, the length of the redundant vessel does not directly affect the switching time. For each value of $L_{\langle 4,5\rangle}$, a critical value of the inlet haematocrit exists for which the deterministic time-dependent flow equations admit multiple stable equilibria. We have shown that the modal switching times at these critical values of the inlet haematocrit are equal or practically indistinguishable. The gradient of the linear relationship between the logarithm of the inlet haematocrit and the logarithm of the modal switching time is independent of the length of the redundant vessel. To better understand why this relationship holds, we studied the correlation between the haematocrit value in the redundant vessel for the two non-trivial stable equilibria and the modal switching time. The coefficients of the linear fits between the logarithm of the modal switching time and the haematocrit in the redundant vessel were sufficiently close to conclude that the linear relationship was the same for all lengths of the redundant vessel (Figure 5.14b). We conclude that the viscosity in the redundant vessel for the equilibria is the dominant factor determining the modal switching time, since the viscosity is a function of the haematocrit in the vessel and the speed of propagation is a function of the viscosity. Therefore, the haematocrit values in the redundant vessel of the non-trivial equilibria are the best predictor of the modal switching time regardless of the other network parameters. If the result generalises to larger, asymmetric networks, then the network equilibria may provide sufficient information to predict the distributions of switching times.

We have identified a novel mechanism stimulating cycling-hypoxia within the tumour microenvironment. Before our proposed switching mechanism can be used to predict blood flow in tumours, several challenges must be overcome. First, the amplitude parameter

should be estimated so that stochastic noise matches physical noise. The amplitude parameter can be viewed as a control parameter that dictates the standard deviation of the additional haematocrit entering a daughter vessel. The addition or subtraction of haematocrit at a flow bifurcation has at least two different physical interpretations. Fung (1973) proposed that stochastic fluctuations arise from the distribution of RBC diameters. If this were the primary mechanism for stochastic fluctuations, the amplitude parameter represents the additional increase in haematocrit as a result of larger or smaller than normal RBCs at a specific time point. However, we anticipate that larger vessels would be subject to smaller fluctuations because they typically contain more RBCs, and therefore the influence of the larger RBCs would be expected to be averaged out by the addition of smaller RBCs. If the fluctuations are caused by additional RBCs entering one of the two daughter vessels due to complex interactions between the RBCs, the noise amplitude parameter would be relatively large for smaller vessels and relatively small for large blood vessels. Given that k must be fixed for every flow bifurcation, further work is needed to determine how the amplitude of the fluctuations depend on the diameters of the parent and daughter vessels.

Another significant challenge is performing the necessary computations to determine the switching times in larger networks. All switching time distributions were approximated because a Fokker-Planck equation does not exist for stochastic equations that are non-Markovian. Therefore, multiple realisations of the equations are required to accurately approximate the switching time distributions. Given the relatively large number of realisations required to approximate the switching time for a simple network like the diamond network, computing the switching times for larger networks is likely to be computationally infeasible. Methods from large deviation theory could be used to approximate the average time for the system to transition between stable states (De La Cruz et al., 2018; Dykman et al., 1994). Large deviation theory can provide sufficient approximation to the mean first passage time between two states of a system of SDEs. Once these times are known for a range of parameters, the systems of SDEs can be coupled to create a large system of SDEs. The mean first passage times for the subsystems of SDEs can then be used to predict the mean first passage time between states of the large system without the requirement to directly compute each mean first passage time between every equilibria. To apply this technique to flow in microcirculation, the small systems of SDEs are applied to network motifs and the large system of SDEs is created by coupling the SDEs of the motifs together. These techniques may only be capable of finding an imprecise prediction for the switching times for larger networks. However, imprecise approximations may be sufficient to explain the formation of cycling-hypoxia.

Once some of these challenges can be overcome, these models could be used to make predictions on how best to treat instances of cycling-hypoxia. Switching behaviour is only possible due to the existence of a redundant vessel. The removal of these vessels may remove instances of cycling-hypoxia. As stated in Section 5, anti-angiogenic drugs have been shown to reduce instances of cycling-hypoxia in mice (Matsumoto et al., 2011). Modelling stochastic blood flow in larger networks, possibly derived from tumour images, could be used to better understand which measurements of a network are linked to these switching events. For example, measurements from TDA for the number of looped structures in vasculature first discussed in Section 1.1 could be a useful predictor of which vascular networks are likely to result in the emergence of switching events. Stolz et al. (2022) used TDA to measure the number of voids and loops in tumours within mice over several days. If these measurements can be linked to switching event sof blood flow, then they can act as a predictor of likeliehood of switching events in tumours. Stolz et al. (2022) measured how the number of loops and voids changed as tumours were treated with bevacizumab, and found that the number of loops decreased and the number of voids increased. Therefore, if the number of loops and voids can be linked to the switching events, these measurements could be used to infer the required dosage of anti-angiogenic drugs to reduce the likliehood of switching from occuring. This will hopefully act as a proxy for the required dosage to prevent cycling-hypoxia.

Chapter 6

Discussion

6.1 Thesis summary

Our research goal was to propose a possible mechanism for the emergence of cycling-hypoxia, or short term fluctuations in hypoxia, within cancerous tumours. Although we have not verified that our proposed mechanism leads to fluctuations in tissue oxygen levels, Bernabeu et al. (2020) established that heterogeneous haematocrit distributions cause regions of chronic-hypoxia to form. Therefore, we conclude that fluctuations in haematocrit distributions have the potential to cause cycling-hypoxia. The research was organised into three main chapters in which we sought to uncover the role of network redundancy on the multiplicity of solutions for the steady-state network equations and demonstrated time-dependent mechanisms which could be responsible for changing flow directions in redundant vessels (Definition 1.2). Anti-angiogenic drugs have been shown to reverse or prevent the formation of cycling-hypoxia (Matsumoto et al., 2011). Anti-angiogenic drugs are usually mono-clonal antibodies that block the receptors of Vascualar Endothelial Growth Factor (VEGF), preventing the formation of new blood vessels. As discussed in Section 1.1, the vasculature in vessels is often heterogeneous and dense. It has been theorised that anti-angiogenic drugs are effective treatments against chronic-hypoxia because they normalise the vasculature allowing blood to flow more easily through the vasculature (Jain, 2005). Given that anti-angiogenic drugs are also effective at treating cycling-hypoxia, we hypothesised that blood flow in microvasculature must also be an important factor driving the formation of cycling-hypoxia. Therefore, mechanistic models of cycling-hypoxia should incorporate blood flow in microcirculation.

The aim of Chapter 3 was to show that the upper bound for the number of equilibria

can be obtained by the number of redundant vessels and that each equilibrium is uniquely distinguished by the flow states (Definitions 3.1 and 3.2) of the blood in the redundant vessels. By showing these key features of the network equilibria for a variety of network geometries, we have expanded on the work on the multiplicity of solutions carried out so far. Gardner et al. (2010) showed that a simple triangle network with three nodes admits up to three equilibria for which the flow direction in the redundant vessel for one of the equilibria was always opposite to the flow direction for the remaining two equilibria. Karst et al. (2017) expanded on this result by showing that the equilibria of more complex networks often had a unique set of flow directions in the network's vessels. Furthermore, they observed that the flow direction only changed for a small set of the networks vessels.

Our work in Chapter 3 is distinguished by the fact that we identified the specific vessels in which the flow changes as redundant vessels and we also identified that the solutions appear in triples. More specifically, the triples would always have a common structure based on the flow direction in a redundant vessel. In Section 3.5.2 we discussed how the equilibria of a symmetric triangle network admitted a very clear structure. As the network was symmetric, the network admitted three equilibria: one with a positive flow direction in the redundant vessel, one with a negative flow direction in the redundant vessel, and the remaining equilibrium had zero flow in the redundant vessel. Due to the symmetry of the network, the two non-zero equilibria were mirror images of each other. When asymmetry to the network geometry is introduced by altering the length of one of the side vessels, the two equilibria that were mirror images of one another are no longer mirror images, but the structure of the equilibria remains for some small interval of the changing vessel length. Therefore, so long as multiple equilibria exist in the triangle network, the blood in the redundant vessel for one equilibrium will always be in the opposite direction to the other two and the flow in one redundant vessel is close to zero relative to the other two equilibria. This pattern was common for all equilibria that differed by the flow direction in a single redundant vessel for the networks we studied. Based on the consistency of this observation, we conclude that it is likely that this pattern of multiple equilibria is common to all vascular networks. Using these principles, we devised a categorisation system for the equilibria of any network that distinguished if the flow in each redundant vessel was negative, positive, or intermediate (Definitions 3.1 and 3.2). We referred to each category as a flow configuration, and we showed that for most network geometries and boundary conditions, each equilibrium admitted by a network was unique. Furthermore, we showed that the key factors that dictate if an equilibrium with a specific flow configuration exists are the network geometry and boundary conditions. We showed that with the exception

of small intervals in the parameter space, the choice of splitting rule was not a key factor dictating which flow configurations were viable.

We tested the uniqueness of the flow configurations in four networks in total and found that the equilibrium had unique flow configurations for most choices of network parameters with very few exceptions. Most of these exceptions occur in small intervals of key parameters. In addition, we showed that multiple regions of parameter space can be found in which the equilibria are distinguished by their flow configuration for asymmetric networks. We found that the existence of multiple redundant vessels can also influence the size of the regions of multiple equilibria. For example, in Section 3.5.1, we directly compared the regions of multiple equilibria in the plane of two length ratios admitted by the triangle network, containing one redundant vessel, to the square plus triangle network, containing two redundant vessels. We found that the region or multiple equilibria in the plane for the square plus triangle network was larger than the region for the triangle network. Therefore, we conclude that a network with more redundant vessels is more likely to admit multiple equilibria, since there is a greater chance that the flow direction in a redundant vessel can flow in either direction if a network has more redundant vessels.

We also found that networks with shorter redundant vessels were more likely to admit multiple equilibria. The shorter the redundant vessel, the lower the potential resistance to blood flow in either direction. Therefore, shorter redundant vessels resulted in a much wider variation in the lengths of fixed vessels (vessels that are not redundant) for which the networks admit multiple equilibria. Shorter redundant vessels share many of the same properties as functional shunts. Functional shunts are vessels with minimal resistance that are hypothesised to cause hypoxia by redirecting blood flow to the tumour vasculature (Pries et al., 2010). Given that shorter redundant vessels are more likely to result in multiple equilibria and have lower resistance than longer vessels, they act analogously to functional shunts.

We also found that the resistance in redundant vessels has a significant impact on the stability of the equilibria. We verified that for a symmetric square plus triangle network, the equilibria with intermediate flow in either redundant vessel were unstable when multiple equilibria exist. As the absolute value of the flow in the redundant vessels is less for the equilibria with intermediate flow, this corresponds to fewer RBCs entering the redundant vessel compared to the number of RBCs entering for the equilibrium with positive or negative flow. Since the resistance in a vessel is a function of the haematocrit within the vessel,

we hypothesise that equilibria with intermediate flow in a redundant vessel are unstable because the smaller resistance values in redundant vessels means that the flow in the redundant vessel is more susceptible to small perturbations to the system. However, multiple equilibria can exist, and an equilibrium with intermediate flow is stable. Ben-Ami et al. (2022) showed that a triangle network with asymmetric vessel diameters can admit a stable equilibrium with intermediate flow. These cases are restricted to small regions in parameter space; and can therefore largely be ignored. Further instability of the equilibria with intermediate flow does not guarantee the stability of the equilibria with no intermediate flow, although our results indicate a relationship between intermediate flow and instability.

Finally, we demonstrated the uniqueness of flow configurations in the triple triangle network containing two diamond subnetworks. Each diamond subnetwork contains one inlet vessel, one outlet vessel, and a redundant vessel. The triple triangle network admitted nine separate solution branches as the inlet pressures varied. These nine equilibria are distinguished by the flow configurations of the redundant vessels associated with each diamond subnetwork. The reason these solution branches exist is because the haematocrit distribution for the equilibria of the diamond subnetworks is independent from the changes to the boundary pressures. Therefore, there will be at least one equilibrium of the network will exist for every combination of equilibria of the diamond subnetworks. As the independence of the haematocrit distribution from the boundary pressure conditions is a common property for all networks with a single inlet and outlet, we conclude that a network will admit at least one equilibrium for every combination of equilibria of subnetworks with a single inlet and outlet.

The results in Chapter 3 were generated in networks in which all vessels had the same diameter. The main aim of Chapter 4 was to verify the key findings in Chapter 3 apply to networks with heterogeneous vessel diameters. In particular, we sought to show that, for most parameter values, each equilibrium has a unique flow configuration. Despite the fact that we showed that this principle held for a range of length ratios and boundary conditions in Chapter 3, the importance of showing that this holds more generally for different diameter ratios should be highlighted because of the nonlinearity of the viscosity and the dependence of the flow on the fourth power of the vessel diameter. As in Chapter 3, we show that each equilibrium has a unique flow configuration for most choices of the vessel diameters. Furthermore, we need to verify that the choice of splitting rule has little impact on which flow configurations remain viable.

All results in Chapter 4 supported our hypothesis that the network flow configurations

were unique for most choices of the parameter values. Therefore, we conclude that our results are applicable to networks with heterogeneous diameters. As discussed in Chapter 1, the diameters of vessels in tumours can take a wide range of values. We showed that multiple equilibria exist for almost the entire range of vessel diameters, and that multiple equilibria also exist for a wide range of diameter ratios. The only exception to this general principle was if the diameters of the blood vessels were similar to the size of the RBCs. In Chapter 4 we performed three different continuations for the square plus triangle network to verify the consistent behaviour of the equilibria as the diameters vary: varying the diameters of all vessels, varying the diameters of the redundant vessels, and varying the diameters of one side of the network. In all three cases, if the diameters of the vessels were similar in size to the RBCs, only one equilibrium remained viable. Furthermore, in all three cases, this equilibrium had zero flow in both redundant vessels.

Gardner et al. (2010) found an interesting relationship between the vessel diameters and inlet haematocrit for the triangle network when the diameters of the network were all the same. For each diameter value, a critical inlet haematocrit value exists such that the network would admit multiple equilibria if and only if the inlet haematocrit exceeded this critical value. In our study of the square plus triangle network we identified a similar critical value for the inlet haematocrit for each diameter value. When we plotted these critical values as a function of the diameters of the vessels, the curve attained a maximum value for a diameter of approximately 50μm and then gradually decreased to a limiting value. This result is similar to results from Gardner et al. (2010), who found that the maximum value for the critical haematocrit values also occurred for vessel diameters of approximately 50μm. This value for the diameter also coincides with the diameter that minimises the viscosity for most haematocrit values. This suggests that a diameter value of approximately 50μm maximises blood flow through the main flow pathways and minimises the flow through any redundant vessels.

As in Chapter 3, the geometry of the network dictates which flow configurations are viable. Although the resistance to flow in a vessel depends upon the haematocrit variable as well as the length and diameter parameters, the link between resistance and equilibria can be drawn by considering the function for the resistance (Equation 1.7). For a fixed haematocrit value, the resistance increases as the diameter decreases or the length increases. Even though the resistance also depends on the haematocrit which is a variable of the system, it is still possible to explain the unviability of certain flow configurations using the changes in the resistance resulting from the changes to the geometry. The resistance in the vessel is at its lowest when the haematocrit is equal to zero. Even if the haemaocrit in a vessel is

zero, the resistance in the vessel continues to increase as the diameter tends towards zero. Therefore, regardless of the haematocrit distribution in the remainder of the network, it is possible for the value of the resistance in a single vessel to exceed the value of the resistance in other network vessels regardless of the haematocrit distribution. For example, the bifurcation diagrams in Section 4.4.1 show that as the vessels of the two redundant vessels of the square plus triangle network constrict, the blood can no longer flow in either direction along the redundant vessels because the resulting resistance in the redundant vessels would be too high. As the blood can no longer flow along the redundant vessels, the flow pathways which traverse the redundant vessels can no longer sustain equilibria. By contrast, if the two redundant vessels are dilated, all nine equilibria corresponding to the nine flow configurations remain viable because the potential resistances in the two redundant vessels continues to decrease. A similar observation can be made for the bifurcation diagrams in Sections 4.3 and 4.4.2. Section 4.3 shows how the equilibria of the square plus triangle network change as all vessels of the network dilate or constrict at the same rate. As the vessels constrict only the equilibrium with no flow in either redundant vessel remains viable. Section 4.4.2 shows how the equilibria of the square plus triangle network change as the vessels of one side of the network dilate or constrict. As with the results in Sections 4.3 and 4.4.1, as the vessels constrict, only one equilibrium remains viable. However, unlike the results in Sections 4.3 and 4.4.1, the results Section 4.4.2 show the effect of only constricting fixed vessels. The square plus triangle network contains of two flow pathways that only consist of fixed vessels for the two sides of the network. As these pathways only contain fixed vessels, the blood must flow down these pathways and so by constricting one of the two main flow pathways, the blood is forced to flow down the other pathway. Therefore, only one equilibrium with zero flow in the two redundant vessels remains viable. A similar scenario can be observed when one of the two main flow pathways dilates. As the vessels dilate, the resistance to the flow in the pathway decreases and some of the flow configurations are no longer viable. We hypothesise the flow configurations are no longer viable because the resistance in the dilating vessel is decreasing encouraging more of the blood flow flow along this flow pathway. As a result fewer of the flow configurations with intermediate flow remained viable because the potential resistances of the fixed vessels were so imbalanced that the intermediate flow could not longer exist in just one redundant vessel. Chapters 3 and 4 clearly show that the viability of flow configurations is dictated by the network's geometry. Due to the relationship between the geometry and the potential resistance to blood flow, we hypothesise that the resistance in vessels along the different potential flow pathways dictate which flow configurations are viable. Therefore, symmetric networks allow for more flow configurations to be viable because the difference in the resistance in flow pathways

differing by the flow direction in redundant vessels is sufficiently small to allow for multiple flow configurations to coexist. Based on these results, we hypothesise that multi-stability would not be expected in regions of the tumour with narrow vessels such as those created in the early stages of angiogenesis but could exist in regions with wider, more mature vessels.

In Chapter 5, we proposed a new mechanism for the formation of cycling-hypoxia based on switching events between multiple stable equilibria. As stated, equilibria with heterogeneous haematocrit distribution can result in chronic-hypoxia (Bernabeu et al., 2020). Therefore, it is plausible that the blood flow switching between multiple equilibria with heterogeneous haematocrit distribution could cause cycling-hypoxia. Chapters 3 and 4 showed that for a network motif to admit multiple equilibria, it must be possible for the blood in at least one redundant vessel to flow in either direction. Given the consistency of this principle for all network motifs that we studied, we conclude that for multiple equilibria to exist in tumour vasculature, it must also be possible for the blood to flow in either direction in at least one redundant vessel. Given the relationship between flow in the redundant vessels and multiple equilibria, if the blood flow changes direction periodically in at least one redundant vessel, then the resulting change in the haematocrit distribution may result in the formation of cycling-hypoxia. In Chapter 5 we demonstrated two potential mechanisms for changing blood flow direction in simple network motifs. As with the results in Chapters 3 and 4, by demonstrating the two mechanisms in smaller network motifs, we can conclude that it is plausible that a similar mechanism may drive blood flow switching in tumour vasculature.

The first mechanism of switching blood flow that we demonstrated in Chapter 5 is that of a hysteresis of the equilibria. A hysteresis of a system occurs when the state of the system depends upon the history of the previous states. Hysteresis of systems are common in other biological models and often control the biological behaviour of a system. A hysteresis loop is often caused by a bi- or multi-stable region created by fold bifurcations. In Chapter 3 we have shown the formation of a region of multi-stability for the square plus triangle network created by changing the pressure boundary conditions. Therefore, it was expected that altering the pressure boundary conditions of the network forces the time-dependent solution to switch between the equilibria so long as a network admits a bi-stable interval. In Section 5.1.1, we showed that by changing the ratio of the inlet pressures for the triangle network, a hysteresis loop is created. The physical interpretation of this switch between the equilibria is that if the ratio between the inlet pressures is sufficiently asymmetric, the blood flow is forced to travel in a certain direction along the redundant vessel. If this ratio is reversed then the pressure gradient along the redundant vessel is reversed, and the blood

flow changes direction. A similar scenario can be observed for changes to the haematocrit boundary conditions. Although the inlet haematocrits do not directly affect the pressure gradient across the redundant vessel, the inlet haematocrits affect the resistance in the two inlet vessels. As the pressures of the interior nodes are implicitly defined by the resistance of the vessels, the pressure gradient across the redundant vessel can be forced to change. In Section 5.1.2, we showed one example of a hysteresis for the triangle network arising from altering the haematocrit boundary conditions. However, this mechanism is limited for two reasons. First, it requires a sufficiently large variation in the boundary conditions to cause the pressure difference across the redundant vessel to change. This may be reasonable for some networks, but this mechanism is unable to induce switching in the diamond network. Secondly, this mechanism relies on an external input to drive switching. As a result, it is difficult to predict the time spent in each state because this mechanism relies on assumptions about the time it takes for the difference between the boundary conditions to be sufficiently large to reverse the direction of flow in the redundant vessel.

The second mechanism for blood flow switching that we proposed in Chapter 5 was a stochastic mechanism. This mechanism relies upon the assumption that the haematocrit entering the daughter vessels at a flow bifurcation is subject to white noise or random fluctuations. This is a justifiable assumption, Fung (1973) observed random partitioning of RBCs at flow bifurcations in dog mesentry and random fluctuations in blood flow is a common observation within the mirocirculation (Bedggood and Metha, 2012; Pawlik et al., 1981). To our knowledge, this is the first time that it has been attempted to incorporate white noise into a model of blood flow in microcirculation.

We tested our model using a simple diamond network with two flow bifurcations. However, stochastic fluctuations were only applied to one of the flow bifurcations for simplicity. With the addition of stochastic noise, the blood flow in the redundant vessel changed direction randomly. This was a significant improvement over the deterministic mechanism for switching based on altering boundary conditions. Unlike the deterministic mechanism, the stochastic mechanism could force the blood flow in the redundant vessel of the diamond network to change direction. Therefore, the stochastic mechanism does not rely on external inputs to force the blood flow in the redundant vessel to change direction and this mechanism can force a switch between the stable equilibria for more networks.

The stochastic switching mechanism also had the added advantage of facilitating predictions for the time between the blood flow changing direction. The time taken for the blood

flow to change direction for the deterministic mechanism is dictated by the time taken for the boundary conditions to sufficiently change to force the blood flow to reverse. As this time was a controlled input, this does not allow for predictions to be made for the time between switches. By contrast, the stochastic switching mechanism did not depend on the controlled inputs and so the time between switches is a feature of the model. However, these times were random due to the random nature of the time-dependent solutions. Despite the random time between changes, it is still possible to make some predictions on when a switch will occur. To understand how long the time-dependent solution spent in the vicinity of the two stable equilibria of the diamond network, we defined the concept of switching times (Definitions 5.2 and 5.3) which can be intuitively understood as the time it takes for the time-dependent solution to start at one equilibrium, and switch to the other equilibrium before returning to the original equilibrium. By solving the time-dependent equations with white noise for a large number of random seeds, it was possible to approximate the distribution of the two definitions of switching times. By approximating the distribution curves for the switching times, it is possible to infer the probability of how long the blood flow in a redundant vessel will flow in a certain direction. By extension, this also acts as a prediction for time that the associate haematocrit distribution is present in the network. As the haematocrit distribution dictates the oxygen distribution in the surrounding tissue, the predictions for the switching times can be used to infer the time between fluctuations for cycling-hypoxia.

We did not directly use the stochastic switching model to infer the time between oxygen fluctuations in cycling-hypoxia because it was important to demonstrate the deterministic and stochastic switching mechanisms in simple networks before demonstrating that the mechanisms are also present in larger networks. It is also not possible to determine how large the amplitude of the stochastic fluctuations should be at the flow bifurcation. However, it is possible to demonstrate how switching times may change as the geometry and boundary conditions are altered. We specifically studied how the modal switching times for the diamond network changed as inlet haematocrit and length or the redundant vessel varied. We found that all lengths of the redundant vessel had an associated critical value for the inlet haematocrit. The diamond network would only admit multiple equilibria if the inlet haematocrit was larger than this critical value. By plotting the log of the modal switching times against the log of the inlet haematocrit, we found that relationship between the log of the modal switching time and the log the inlet haematocrit was always linear and positive. Furthermore, the gradient of this linear relationship was the same regardless of the length of the redundant vessel and the modal switching time was always the same for

each critical haematocrit value. In Chapter 5 we also plot the log of the modal switching time against the value of the haematocrit in the redundant vessel for the stable equilibria. We found that the relationship between these these two variables is also linear and that the coefficients for this linear relationship are the same for all lengths of the redundant vessel.

6.2 Future work and perspectives

Our results reveal several possible avenues for future work. The most obvious avenue is to use our findings to identify multiple equilibria in networks extracted from images of tumour vasculature. Throughout this thesis we have used numerical continuation to find the equilibria of networks. Numerical continuation deforms the equations of a starting system of equations to the equations for flow in a network. The starting system that we have primarily used is that of the network flow equations with a constant haematocrit distribution because this starting system admits one equilibrium that is simple to compute. Once a network has been extracted from a tumour image and the boundary conditions estimated, numerical continuation can be used to determine if multiple equilibria exist. The mechanism that we proposed for the cause of cycling-hypoxia is the blood flow switching between stable equilibria of the network. If the network only admits one equilibrium, then blood flow switching, and by extension cycling-hypoxia, is not possible according to our proposed mechanism. Therefore, if a network extracted from tumour vasculature admits multiple equilibria, then the tumour vasculature has the potential to cause cycling-hypoxia even without explicitly simulating the time-dependent blood flow. When determining whether a network admits multiple equilibria, it is important to capture as many vessels as possible to generate realistic predictions. Imaging techniques now have the resolution to capture most vessels in the tumour microenvironment (Maslov et al., 2008; Upputuri et al., 2015). The results of Chapters 3 and 4 could prove useful in finding more equilibria for larger networks. In the discussion of Chapter 3 we proposed an adjustment to the homotopy function that was initially used to find an equilibrium of the network. So far, we have used a randomly chosen haematocrit distribution for the starting system of the homotopy function. The equilibrium of the starting system is unique; therefore, so is the associated flow configuration. Instead of randomly choosing the haematocrit distribution for the starting system, it is possible to choose a distribution corresponding to each possible flow configuration. We hypothesise that if a network admits an equilibrium with a certain flow configuration, numerical continuation using a starting system with the same flow configuration is more likely to find the corresponding equilibrium for the full system of flow equations. Therefore, by performing numerical continuation for multiple starting systems with the full range

of flow configurations, even if the network does not admit a flow an equilibrium for each flow configuration, this method is a more systematic approach to finding multiple equilibria.

In this thesis, we have categorised vessels as fixed or redundant. Blood can flow in either direction in redundant vessels and only in one direction in a fixed vessel. Another avenue that we have not explored is the effect of having multiple connected redundant vessels. All redundant vessels in the network motifs that we studied were connected only to fixed vessels. It is possible that a network with two connected redundant vessels does not admit every possible combination of flow states for these two redundant vessels. It may be the case that tumour vasculature contains many connected redundant vessels, so it is important to understand how this scenario could affect the number of equilibria. It may be possible to define redundant flow pathways constructed from multiple connected redundant vessels for which similar predictions can be derived for the maximum number of equilibria from the number of redundant pathways.

In Chapter 1 we discussed the difference between tumour and healthy vasculature, and some of the treatments for cycling-hypoxia. We reviewed some of the vasculature metrics that have been used to quantify the differences between healthy vasculature and tumour vasculature, and the metrics used to quantify the normality of the vasculature. Furthermore, the geometry of the vasculature would appear to be a key factor driving cycling-hypoxia because anti-angiogenic drugs have been shown to be effective at preventing instances of cycling-hypoxia (Matsumoto et al., 2011). Given that the mechanism of action of anti-angiogenic drugs affects the tumour vasculature, blood flow clearly plays an important role in the formation of cycling-hypoxia. Research into multiple equilibria of tumour vasculature could be combined with metrics to quantify the vasculature to explain why this form of treatment is so effective. For example, Stolz et al. (2022) used TDA to compared measurements of tumour vasculature such as loops and voids defined by TDA, with other vasculature measurements by assessing the correlation between the measurements. This analysis could be extended by correlating these TDA measurements with the number of equilibria that tumour vasculature admits. If these two quantities correlate, then this would show that a greater number of loops and fewer voids imply a greater number of equilibria exist. Furthermore, the number of loops and voids has already been used to assess the impact of Bevacizumab, an anti-angiogenic drug, on tumour vasculature using TDA (Stolz et al., 2022). By combining this analysis with a study of the number of possible equilibria, the correlation between the number of loops with the dosage of anti-angiogenic drugs and the number of equilibria could be assessed. If these quantities are correlated, estimates for the

dosage required for an equilibrium of a network to be unique, or for the number of equilibria to fall below a certain threshold, could be derived from the number of loops or voids. Even without simulating blood flow in vasculature, this would provide a reasonable prediction of the dose required to prevent switching from occurring because switching blood flow is dependent on the existence of multiple flow pathways.

Our stochastic model of blood flow has the potential to provide insight into the mechanisms driving cycling-hypoxia. However, the model is based on several simplifying assumptions; therefore, without verification, it is not possible to assess the accuracy of the model. This presents a disadvantage compared to other potential driving mechanisms of cycling-hypoxia, such as self-sustained oscillations. Self-sustained oscillations depend only on the physical principle of blood flow at small Reynolds numbers; therefore, because this model has been derived from physical principles that have been experimentally verified, this mechanism relies on fewer assumptions (Ben-Ami et al., 2022; Carr et al., 2005; Geddes et al., 2007; Karst et al., 2015). The best way to verify our model would be with the use of a microfluidic device. Measuring the switching time distributions using a microfluidic device would enable us to test the validity of our model. However, it may be difficult to perform these experiments because of the limitations of these devices. Roman et al. (2016) experimented with square microfluidic channels in with feed haematocrits as high as 0.6. If we assume that the feed haematocrit is equal to the discharge haematocrit of a vessel, a feed haematocrit of this value should imply that observing multiple equilibria within a microfluidic device is, in theory, possible. However, they made the observation that a discrepancy between the feed haematocrit and the discharge haematocrit exists. Fenton et al. (1985) performed similar experiments with a feed haematocrit of 0.4 for a microfluidic device with a parent channel with a width of 20μm. They observed that the tube haematocrit for this experiment was only 0.2. If we use Equation (1.8) to solve for the discharge haematocrit using the a tube haematocrit of 0.2, then the discharge haematocrit should be 0.3 not 0.4. Therefore, a large feed haematocrit is not a guarantee of a large discharge haematocrit. Roman et al. (2016) also observed that for feed haematocrits greater than 0.6 often resulted in channels becoming plugged with RBCs. Furthermore, the microfludic devices studied by Fenton et al. (1985) and Roman et al. (2016) consisted only of a single flow bifurcation. These limitations of microfluidic devices would need to be addressed in order to perform sufficiently accurate measurements to verify the existence of stochastic switching events.

A natural extension of our work would be to couple the blood flow switching model with an oxygen diffusion model. Oxygen diffusion models have already shown that chronic-hypoxia

can result from heterogeneous haematocrit distributions (Bernabeu et al., 2020), therefore, introducing time-dependent blood flow would demonstrate possible instances of cycling-hypoxia. However, the oxygen diffusion model used by Bernabeu et al. (2020) was based on the assumption of constant haematocrit in blood vessels and that the oxygen distribution was in a steady-state. As the haematocrit distribution within each vessel is constantly changing in our stochastic blood flow model, obtaining a similar result to that of Bernabeu et al. (2020) would require a time-dependent oxygen diffusion model or a separation of time scales to use the steady-state diffusion model.

So far we have shown switching behaviour in a small network motif where noise is only applied at the first flow bifurcation. To make our model more widely applicable, we must also show that switching behaviour can occur in larger networks. However, this introduces difficulty in computing the switching times accurately. As discussed in Chapter 5, computing the switching time distributions for a simple network was computationally expensive and is likely to scale poorly when white noise is incorporated at multiple flow bifurcations. Therefore, progressing this research may require techniques from large deviation theory to improve computational time. Large deviation theory can be used to find the mean first passage time for a system of stochastic differential equations to transition between two stable equilibria (Dykman et al., 1994; Lv et al., 2014; Roma et al., 2005). With reduced computation time, it may be possible to simulate switching events for larger networks by estimating the switching times for subnetworks of the larger networks. For example, switching times for a network generated by repeated generations of inverted triangle networks could be estimated from the switching times for each individual inverted triangle subnetwork. It is also possible to find the mean first passage time between the limit cycle of one equilibrium and a stable equilibrium (De La Cruz et al., 2018). Limit cycles can form in asymmetric network motifs and so an important avenue of study will be to estimate the passage time between stable equilibria and limit cycles.

6.3 Conclusion and final remarks

In this thesis, we examined the impact of redundant vessels on blood flow in tumour vasculature. We have extended the theory relating to the existence of multiple equilibria within vascular networks and used this theory to develop a novel model for the formation of cycling-hypoxia within tumours. In the longer term, these results could assist with the development of new cancer treatments designed to reduce cycling-hypoxia. As tumours experiencing cycling-hypoxia often contain more aggressive and resilient phenotypes than

normoxic tumours, reducing cycling-hypoxia has the consequence of indirectly improving patient prognosis. By utilising numerical continuation, we have demonstrated a clear link between the presence of redundant vessels and the existence of multiple equilibria. We proposed a new mechanism for cycling-hypoxia based on the change in the direction of blood flow in redundant vessels. This mechanism is based on stochastic perturbations or RBC partitioning at flow bifurcations. A consequence of this proposed switching mechanism is that it demonstrates how reducing the number of redundant vessels could reduce the likelihood of cycling-hypoxia, even when the detailed pattern of blood flow through a vessel network is unknown.

One of the most significant implications of our research is its potential to improve our understanding of the mechanisms by which anti-angiogenic drugs impact cycling-hypoxia in future work. TDA has already been shown as an effective means to measure the topological structures of vasculature such as the presence of void and loops (Stolz et al., 2022). If these measurements can be linked to the emergence of switching behaviour, it will be possible to use these measurements as a proxy for the likelihood of switching events. These TDA measurements can then be used to study how different dosing strategies effect the emergence of these switching events. Anti-angiogenic drugs lose effectiveness over time due to adaptation of the tumour microenvironment (Bergers and Hanahan, 2008; Haibe et al., 2020). Therefore, it is important to develop an effective dosing strategy to maximise the effectiveness of these treatments before the tumour develops resistance to them. Given that cycling-hypoxia selects for more aggressive and treatment resistant cell phenotypes than chronic-hypoxia (Muz et al., 2015), agents that remodel the vasculature reducing cycling-hypoxia while increasing chronic-hypoxia may still provide a health benefit to patients.

To our knowledge, this thesis constitutes the first instance of incorporating stochastic white noise into mathematical models of blood flow in the microcirculation. Our aim was to produce continuum models that accurately capture the discrete dynamics of blood flow at flow bifurcations. Although our primary goal was to use mathematical modelling to investigate potential mechanisms of cycling-hypoxia, our approach could be adapted to study other aspects of blood flow in the microcirculation.

Appendix A

Network equations

All network equations in this thesis can be derived from the network topology and the construction of the equations described in Sections 1.7 and 1.8. The construction of the steady-state equations defining the equilibria of a network can be found in Section 1.7 and the construction of the time-dependent equations for networks can be found in Section 1.8. This appendix includes a full set of time-dependent equations for each network that we study in this thesis. The steady-state equations for each network can be inferred from the time-dependent equations

A.1 Network equations

To simplify the descriptions of network equations in this appendix, the common parameters, variables and equations used to describe the network equations have been summaries in this section. This section has been broken up into the following subsections: Section A.1.1 describes the functions common to all network equations, Section A.1.2 describes the equations common to the network PDEs, and Section A.1.3 describes the equations common to the network DDEs.

A.1.1 Network functions

Relative viscosity function for the blood in vessel (v, w):

$$\mu^{(\text{rel})}_{(v,w)}(H_{(v,w)}) = \left[1 + (\mu_{45} - 1)\frac{(1 - H_{(v,w)})^C - 1}{0.55^C - 1}\Theta\right]\Theta, \tag{A.1}$$

$$\Theta = \left(\frac{D_{(v,w)}}{D_{(v,w)} - 1.1}\right)^2, \tag{A.2}$$

$$\mu_{45} = 6\exp(-0.085D_{(v,w)}) + 3.2 - 2.44\exp(-0.06D^{0.645}_{(v,w)}), \tag{A.3}$$

$$C = (0.8 + exp(-0.075D_{(v,w)}))(\Lambda - 1) + \Lambda, \tag{A.4}$$

$$\Lambda = \frac{1}{1 + 10^{-11}D^{12}_{(v,w)}}. \tag{A.5}$$

Viscosity of the blood in vessel (v, w):

$$\mu_{(v,w)}(H_{(v,w)}) = \mu_p\mu^{(\text{rel})}_{(v,w)}(H_{(v,w)}). \tag{A.6}$$

Spitting rule for the ratio of RBCs entering daughter vessel (v, w) from parent vessel (u, v) in Figure 1.3a:

$$\psi_{(v,w)}(r_{(v,w)}, H_{(u,v)}(L_{(u,v)}, t)) = \begin{cases} 0 & \text{if } r_{(v,w)} \leq X_0, \\ \frac{e^A(r_{(v,w)} - X_0)^P}{e^A(r_{(v,w)} - X_0)^P + (1 - r_{(v,w)} - X_0)^P} & \text{if } X_0 < r_{(v,w)} < 1 - X_0, \\ 1 & \text{if } r_{(v,w)} \geq 1 - X_0, \end{cases} \tag{A.7}$$

$$r_{(v,w)} = \frac{Q_{(v,w)}(t)}{Q_{(u,v)}(t)}. \tag{A.8}$$

The forms of the parameters X_0, A and P depend on the splitting rule. Volumetric flow in vessel (v, w):

$$Q_{(v,w)}(t) = \frac{(P_v(t) - P_w(t))\pi D^4_{(v,w)}}{128L_{(v,w)}\overline{\mu}_{(v,w)}(t)}. \tag{A.9}$$

Average velocity of the haematocrit in vessel (v, w):

$$\overline{u}_{(v,w)}(t) = \frac{4Q_{(v,w)}(t)}{\pi D^2_{(v,w)}}. \tag{A.10}$$

A.1.2 Equations for network PDEs

Average haematocrit of the blood in vessel (v, w):

$$\overline{H}_{(v,w)}(t) = \frac{1}{L_{(v,w)}} \int_0^{L_{(v,w)}} H_{(v,w)}(x,t)\mathrm{d}x. \tag{A.11}$$

Average viscosity of the blood in vessel (v, w):

$$\overline{\mu}_{(v,w)}(t) = \frac{1}{L_{(v,w)}} \int_0^{L_{(v,w)}} \mu_{(v,w)}(H_{(v,w)}(x,t))\mathrm{d}x. \tag{A.12}$$

Partial differential equation for the haematocrit in vessel (v, w):

$$\frac{\partial H_{(v,w)}}{\partial t} + \overline{u}_{(v,w)}(t)\frac{\partial H_{(v,w)}}{\partial x} = 0. \tag{A.13}$$

A.1.3 Equations for network DDEs

Implicit equation for the time delay, $\tau_{(v,w)}(t)$, in vessel (v, w):

$$L_{(v,w)} = \int_{t-\tau_{(v,w)}(t)}^{t} \overline{u}_{(v,w)}(s)ds. \tag{A.14}$$

Delayed differential equation for the average haematocrit in vessel (v, w):

$$\frac{\mathrm{d}\overline{H}_{(v,w)}}{\mathrm{d}t} = \frac{\overline{u}_{(v,w)}(t)}{L_{(v,w)}}(H_{(v,w)}(0,t) - H_{(v,w)}(0, t-\tau_{(v,w)}(t))). \tag{A.15}$$

Delayed differential equation for the average viscosity in vessel (v, w):

$$\frac{\mathrm{d}\overline{\mu}_{(v,w)}}{\mathrm{d}t} = \frac{\overline{u}_{(v,w)}(t)}{L_{(v,w)}}(\mu_{(v,w)}(H_{(v,w)}(0,t)) - \mu_{(v,w)}(H_{(v,w)}(0, t-\tau_{(v,w)}(t)))). \tag{A.16}$$

A.2 Square plus triangle network

This Appendix includes the boundary conditions and flow conservation equations for the system of PDEs or DDEs associated with the time-dependent equations for the square plus triangle network in Figure 3.3b. The forms of the differential equations can be found in Section A.

Conservation of flow equations

$$0 = Q_{(1,4)}(t) + Q_{(6,4)}(t) + Q_{(5,4)}(t), \tag{A.17}$$

$$0 = Q_{(2,5)}(t) + Q_{(7,5)}(t) + Q_{(4,5)}(t), \tag{A.18}$$

$$0 = Q_{(4,6)}(t) + Q_{(7,6)}(t) + Q_{(8,6)}(t), \tag{A.19}$$

$$0 = Q_{(5,7)}(t) + Q_{(6,7)}(t) + Q_{(8,7)}(t), \tag{A.20}$$

$$0 = Q_{(3,8)}(t) + Q_{(6,8)}(t) + Q_{(7,8)}(t). \tag{A.21}$$

Boundary conditions

$$H_{(4,6)}(0,t) = \begin{cases} \frac{\psi_{(4,6)}(r_{(4,6)}(t), H_{(1,4)}(L_{(1,4)},t))H_{(1,4)}(L_{(1,4)},t)}{r_{(4,6)}(t)} & Q_{(4,5)} > 0, \\ \frac{H_{(1,4)}(L_{(1,4)},t)Q_{(1,4)}(t) + H_{(4,5)}(0,t)Q_{(5,4)}(t)}{Q_{(4,6)}(t)} & Q_{(4,5)} \leq 0, \end{cases} \tag{A.22}$$

$$H_{(5,7)}(0,t) = \begin{cases} \frac{\psi_{(5,7)}(r_{(5,7)}(t), H_{(2,5)}(L_{(2,5)},t))H_{(2,5)}(L_{(2,5)},t)}{r_{(5,7)}(t)} & Q_{(4,5)} \leq 0, \\ \frac{H_{(2,5)}(L_{(2,5)},t)Q_{(2,5)}(t) + H_{(4,5)}(L_{(4,5)},t)Q_{(4,5)}(t)}{Q_{(5,7)}(t)} & Q_{(4,5)} > 0, \end{cases} \tag{A.23}$$

$$H_{(6,8)}(0,t) = \begin{cases} \frac{\psi_{(6,8)}(r_{(6,8)}(t), H_{(4,6)}(L_{(4,6)},t))H_{(4,6)}(L_{(4,6)},t)}{r_{(6,8)}(t)} & Q_{(6,7)} > 0, \\ \frac{H_{(4,6)}(L_{(4,6)},t)Q_{(4,6)}(t) + H_{(6,7)}(0,t)Q_{(7,6)}(t)}{Q_{(6,8)}(t)} & Q_{(6,7)} \leq 0, \end{cases} \tag{A.24}$$

$$H_{(7,8)}(0,t) = \begin{cases} \frac{\psi_{(7,8)}(r_{(7,8)}(t), H_{(5,7)}(L_{(5,7)},t))H_{(5,7)}(L_{(5,7)},t)}{r_{(7,8)}(t)} & Q_{(6,7)} \leq 0, \\ \frac{H_{(5,7)}(L_{(5,7)},t)Q_{(5,7)}(t) + H_{(6,7)}(L_{(6,7)},t)Q_{(6,7)}(t)}{Q_{(7,8)}(t)} & Q_{(6,7)} > 0, \end{cases} \tag{A.25}$$

$$H_{(4,5)}(0,t) = \frac{\psi_{(4,5)}(r_{(4,5)}, H_{(1,4)}(L_{(1,4)},t))H_{(1,4)}(L_{(1,4)},t)}{r_{(4,5)}(t)} \text{ if } Q_{(4,5)} > 0, \tag{A.26}$$

$$H_{(4,5)}(L_{(4,5)},t) = \frac{\psi_{(5,4)}(r_{(5,4)}, H_{(2,5)}(L_{(2,5)},t))H_{(2,5)}(L_{(2,5)},t)}{r_{(5,4)}(t)} \text{ if } Q_{(4,5)} \leq 0, \tag{A.27}$$

$$H_{(6,7)}(0,t) = \frac{\psi_{(6,7)}(r_{(6,7)}, H_{(4,6)}(L_{(4,6)},t))H_{(4,6)}(L_{(4,6)},t)}{r_{(6,7)}(t)} \text{ if } Q_{(6,7)} > 0, \tag{A.28}$$

$$H_{(6,7)}(L_{(6,7)},t) = \frac{\psi_{(7,6)}(r_{(7,6)}, H_{(5,7)}(L_{(5,7)},t))H_{(5,7)}(L_{(5,7)},t)}{r_{(7,6)}(t)} \text{ if } Q_{(6,7)} \leq 0, \tag{A.29}$$

$$H_{(8,3)}(0,t) = \frac{H_{(6,8)}(L_{(6,8)},t)Q_{(6,8)}(t) + H_{(7,8)}(L_{(7,8)},t)Q_{(7,8)}(t))}{Q_{(8,3)}(t)}, \tag{A.30}$$

where:

$$r_{(4,6)}(t) = \frac{Q_{(4,6)}(t)}{Q_{(1,4)}(t)}, r_{(5,4)}(t) = \frac{Q_{(5,4)}(t)}{Q_{(2,5)}(t)}, r_{(5,7)}(t) = \frac{Q_{(5,7)}(t)}{Q_{(2,5)}(t)}, r_{(4,5)}(t) = \frac{Q_{(4,5)}(t)}{Q_{(1,4)}(t)},$$
$$r_{(6,8)}(t) = \frac{Q_{(6,8)}(t)}{Q_{(4,6)}(t)}, r_{(7,6)}(t) = \frac{Q_{(7,6)}(t)}{Q_{(5,7)}(t)}, r_{(7,8)}(t) = \frac{Q_{(7,8)}(t)}{Q_{(5,7)}(t)}, r_{(6,7)}(t) = \frac{Q_{(6,7)}(t)}{Q_{(5,7)}(t)}.$$

A.3 Diamond network

This Appendix includes the boundary conditions and flow conservation equations for the system of PDEs or DDEs associated with the time-dependent equations for the diamond network in Figure 5.5. The forms of the differential equations can be found in Section A.

Conservation of flow equations

$$0 = Q_{(1,3)}(t) + Q_{(4,3)}(t) + Q_{(5,3)}(t), \tag{A.31}$$

$$0 = Q_{(3,4)}(t) + Q_{(5,4)}(t) + Q_{(6,4)}(t), \tag{A.32}$$

$$0 = Q_{(3,5)}(t) + Q_{(4,5)}(t) + Q_{(6,5)}(t), \tag{A.33}$$

$$0 = Q_{(2,6)}(t) + Q_{(4,6)}(t) + Q_{(5,6)}(t). \tag{A.34}$$

Boundary conditions

$$H_{(3,4)}(0,t) = \frac{\psi_{(3,4)}(r_{(3,4)}(t), H_{(1,3)}(L_{(1,3)},t))H_{(1,3)}(L_{(1,3)},t)}{r_{(3,4)}(t)}, \tag{A.35}$$

$$H_{(3,5)}(0,t) = \frac{\psi_{(3,5)}(r_{(3,5)}(t), H_{(1,3)}(L_{(1,3)},t))H_{(1,3)}(L_{(1,3)},t)}{r_{(3,5)}(t)}, \tag{A.36}$$

$$H_{(4,6)}(0,t) = \begin{cases} \frac{\psi_{(4,6)}(r_{(4,6)}(t), H_{(3,4)}(L_{(3,4)},t))H_{(3,4)}(L_{(3,4)},t)}{r_{(4,6)}(t)} & Q_{(4,5)} > 0, \\ \frac{H_{(3,4)}(L_{(3,4)},t)Q_{(3,4)}(t) + H_{(4,5)}(0,t)Q_{(5,4)}(t)}{Q_{(4,6)}(t)} & Q_{(4,5)} \leq 0, \end{cases} \tag{A.37}$$

$$H_{(5,6)}(0,t) = \begin{cases} \frac{\psi_{(5,6)}(r_{(5,6)}(t), H_{(3,5)}(L_{(3,5)},t))H_{(3,5)}(L_{(3,5)},t)}{r_{(5,6)}(t)} & Q_{(4,5)} < 0, \\ \frac{H_{(3,5)}(L_{(3,5)},t)Q_{(3,5)}(t) + H_{(4,5)}(L_{(4,5)},t)Q_{(4,5)}(t)}{Q_{(5,6)}(t)} & Q_{(4,5)} \geq 0, \end{cases} \tag{A.38}$$

$$H_{(4,5)}(0,t) = \frac{\psi_{(4,5)}(r_{(4,5)}, H_{(3,4)}(L_{(3,4)},t))H_{(3,4)}(L_{(3,4)},t)}{r_{(4,5)}(t)} \text{ if } Q_{(4,5)} > 0, \tag{A.39}$$

$$H_{(4,5)}(L_{(4,5)},t) = \frac{\psi_{(5,4)}(r_{(5,4)}, H_{(3,5)}(L_{(3,5)},t))H_{(3,5)}(L_{(3,5)},t)}{r_{(5,4)}(t)} \text{ if } Q_{(4,5)} \leq 0, \tag{A.40}$$

$$H_{(6,2)}(0,t) = \frac{H_{(4,6)}(L_{(4,6)},t)Q_{(4,6)}(t) + H_{(5,6)}(L_{(5,6)},t)Q_{(5,6)}(t))}{Q_{(6,2)}(t)}, \tag{A.41}$$

where:

$$r_{(3,4)}(t) = \frac{Q_{(3,4)}(t)}{Q_{(1,3)}(t)}, r_{(3,5)}(t) = \frac{Q_{(3,5)}(t)}{Q_{(1,3)}(t)}, r_{(4,6)}(t) = \frac{Q_{(4,6)}(t)}{Q_{(3,4)}(t)},$$
$$r_{(5,6)}(t) = \frac{Q_{(5,6)}(t)}{Q_{(3,5)}(t)}, r_{(4,5)}(t) = \frac{Q_{(4,5)}(t)}{Q_{(3,4)}(t)}, r_{(5,4)}(t) = \frac{Q_{(5,4)}(t)}{Q_{(3,5)}(t)}.$$

A.4 Triple triangle network

The steady-state and time-dependent network equations for the triple triangle network in Figure 3.3c can be directly formed from the equations for the triangle and diamond networks in Sections 1.8 and A.3.

Appendix B

Time step analysis for network SDFEs

This chapter contains the justification and description of the numerical scheme for solving systems of SFDEs described in (Mao, 2003) and used solve the SFDEs described in Chapter 5.

B.1 Description of the scheme

The method in question is used to solve systems of SFDEs in the form of:

$$\mathrm{d}x(t) = g_1(x_t)\mathrm{d}t + g_2(x_t)\mathrm{d}W(t), \tag{B.1}$$

such that:

$$f : C([-\tau, 0]; \mathbb{R}^n) \to \mathbb{R}^n, g : C([-\tau, 0]; \mathbb{R}^n) \to \mathbb{R}^{n\times m}, \tag{B.2}$$

and

$$x_t = \{x(t+\theta) : -\tau \leq \theta \leq 0\}, \tag{B.3}$$

such that the initial condition $x_0 \in C([-\tau, 0]; \mathbb{R}^n)$. Let $x(t)$ denote the solution to Equation (B.1) and $y(t)$ the approximate solution for Equation (B.1) generated using the Euler-Maryuama numerical method described in (Mao, 2003). Let the step size $\Delta \in (0, 1)$ be a fraction of τ, such that $\Delta = \tau/N$ for some integer $N > \tau$. The discrete Euler-Maruyama

approximate solution $\overline{y}(k\Delta), k \geq -N$ is defined as follows:

$$\begin{cases} \overline{y}(k\Delta) = \xi(k\Delta) & -N \leq k \leq 0, \\ \overline{y}((k+1)\Delta) = \overline{y}(k\Delta) + f(\overline{y}(k\Delta))\Delta g(\overline{y}(k\Delta))\Delta W_k, k \geq 0, \end{cases} \tag{B.4}$$

where $\Delta W_k = W((k+1)\Delta) - W(k\Delta)$, $\xi \in L^p_{\mathcal{F}_0}([-\tau, 0]; \mathbb{R}^n)$ for some $p > 2$, and $\overline{y}_{k\Delta} = \{\overline{y}_{k\Delta}(\theta) : -\tau \leq \theta \leq 0\}$ is a $C([-\tau, 0]; \mathbb{R}^n)$-valued random variable defined as follows:

$$\overline{y}_{k\Delta}(\theta) = \frac{\Delta - (\theta - i\Delta)}{\Delta}\overline{y}((k+i)\Delta) + \frac{\theta - i\Delta}{\theta}\overline{y}((k+i+1)\Delta), \tag{B.5}$$

for $i\Delta \leq \theta \leq (i+1)\Delta, i \in \{-N, -(N-1), ..., -1\}$. Let:

$$y_t = \sum_{k=0}^{\infty} \overline{y}_{k\Delta} 1_{[k\Delta,(k+1)\Delta]}(t). \tag{B.6}$$

The continuous time Euler-Marauyam approximation is as follows:

$$y(t) = \overline{y}(k\Delta) + \int_{k\Delta}^{t} g_1(\overline{y}_s)ds + \int_{k\Delta}^{t} g_2(\overline{y}_s)dW(s). \tag{B.7}$$

For this scheme to be applicable to a system of SFDEs, the functions g_1 and g_2 must satisfy a certain set of criteria described by Mao (2003). Most of these criteria can be analytically proven for the system of SFDEs for flow in the diamond network described in Section 5.2 with the exception of the local Lipschitz condition. Instead of showing this last condition, a time step analysis can be performed to verify the behaviour of the numerical solutions remains consistent regardless of the choice of time step. Unlike deterministic equations, it is not possible to directly compare two numerical solutions using different time steps because the noise generated depends on the time step. Therefore, to compare between two different times steps, the distributions of some output must be compared instead of directly comparing the numerical solutions.

As Chapter 5 mainly focuses on the switching times of the diamond equations, we have compared the different distributions of switching times for the diamond network using different switching times. For the diamond network in Figure 5.5, the following parameters are used to generate distributions of switching times:

$$L = 100\mu m, D = 10\mu m, H_{(1,3)}(0, t) = 0.45. \tag{B.8}$$

The times steps $\mathrm{d}t_1 = 0.0059$,$\mathrm{d}t_2 = 0.0030$ and $\mathrm{d}t_3 = 0.0012$ have been used to generate a sets of switching times which shall be denoted by T_1, T_2 and T_3 by performing $8,000$ simulations from $t = 0$ to $t = 9,000$ and recording the switching times. The Kolmogorov-Smirnov test was used to determine if the three sets of switching times plausibly sampled from the same distribution. A significance level of $\alpha = 0.05$ has been chosen to reject the null hypothesis that two samples are generated using the same probability distribution. The test revealed a p-value of 0.5989 for the comparison between T_1 and T_2, 0.1552 for the comparison between T_1 and T_3 and 0.4964 between T_2 and T_3. All three test show that null hypothesis must be rejected so the three sets are plausibly sampled from the same distribution. By using the same process described in Section 5.2 to generate approximations to the probability distribution of switching times. Figure B.1b shows the approximate distribution curve for $dt = 0.0059$ against a the histogram of the actual switching times. Figure B.1a shows the comparison between the three approximate distribution curves. As can be visually seen, the difference between the curves is minimal and the largest difference between the curves can be seen between the curves generated using $\mathrm{d}t_1$ and $\mathrm{d}t_3$. This is supported by our results from the Kolmogorov-Smirnov test.

Our times step analysis shows that although we can not rigorously prove the Local Lipschitz condition, our numerical method produces consistent distribution curves regardless of the choice of time step provided the time step is sufficiently small to produce a reasonable approximation to the numerical solutions.

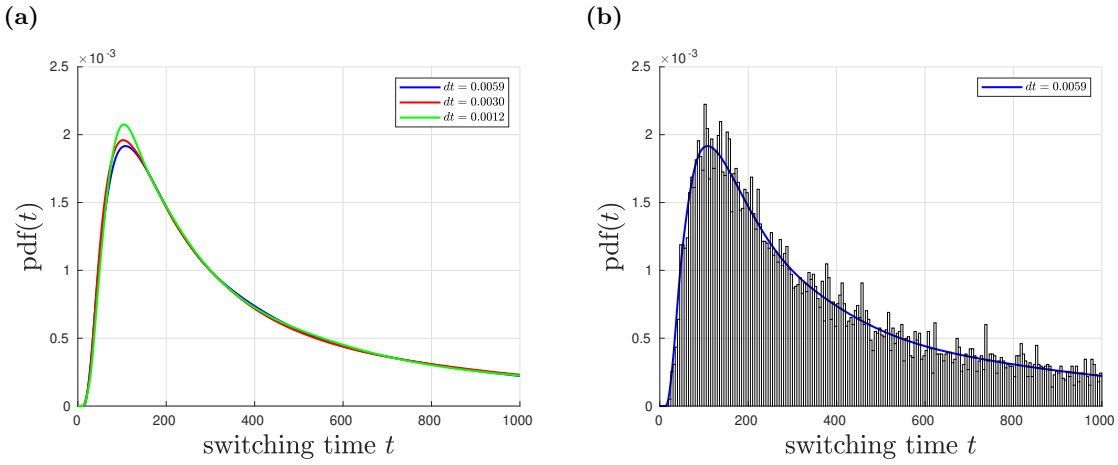

Figure B.1: Series of plots displaying the comparison of the switching time distributions generated using different time steps. (a): Comparison between the distribution curves generated using different time steps; (b): Histogram of the switching times generated using a time step of $dt = 0.0059$.

Appendix C

Stochastic viscosity equation derivation

This Appendix concerns the derivation of the SFDE for the average viscosity (Equations (5.41-5.42)). In Section 5.2, a first-order Taylor expansion is used to model the stochasticity of RBCs at a vessel bifurcation on the viscosity of the blood in the daughter vessels of a flow bifurcation. However, a second-order Taylor expansion is often used for functions of stochastic differential equations. For example, consider the function $w(X_t)$ such that:

$$X_t = \int_{t_0}^{t} a(X_s)\mathrm{d}s + \int_{t_0}^{t} b(X_s)\mathrm{d}W_s, \tag{C.1}$$

If the value of X_t is known at $t = t_0$, using Ito's lemma, $w(X_t)$ can be approximated with the following expansion:

$$w(X_t) = w(X_{t_0}) + L^0 w(X_{t_0})(t - t_0) + L^1 w(X_{t_0})(W_t - W_{t_0}) + R, \tag{C.2}$$

such that:

$$\begin{aligned} R = &\int_{t_0}^{t}\int_{t_0}^{s} L^0 L^0 w(X_z)\mathrm{d}z\mathrm{d}s + \int_{t_0}^{t}\int_{t_0}^{s} L^1 L^0 w(X_z)\mathrm{d}W_z\mathrm{d}s + \\ &\int_{t_0}^{t}\int_{t_0}^{s} L^0 L^1 w(X_z)\mathrm{d}z\mathrm{d}W_s + \int_{t_0}^{t}\int_{t_0}^{s} L^1 L^1 w(X_z)\mathrm{d}W_z\mathrm{d}W_s, \end{aligned} \tag{C.3}$$

and:

$$L^0 = a(x)\frac{\partial}{\partial x} + \frac{1}{2}b(x)^2\frac{\partial^2}{\partial x^2}, \tag{C.4}$$

$$L^1 = b(x)\frac{\partial}{\partial x}. \tag{C.5}$$

Therefore, Equation (C.2) includes a second-order term.

The intention of this appendix is to justify the use of a first-order Taylor expansion in Equation (5.39). The issue with the approximation that we use is that instead of deriving the Taylor series for a stochastic random variable of the form of Equation (C.1), the variable in Equation (5.39) includes a generic noise term. This is problematic because it is not possible to use the Taylor expansion described by Equation (C.2). This appendix has been divided into the following sections: Section C.1 describes the abstract forumation of the problem, Section C.2 describes how this problem applies to the equations in the thesis, Section C.3 describes the modelling approximation used, and Section C.4 provides the numerical verification of the approach described in Section C.3.

C.1 Abstract problem

The fundamental problem that needs to be addressed is how should a system of deterministic DDEs in the following form:

$$\frac{\mathrm{d}x}{\mathrm{d}t} = \overline{u}(t)[v(y(t)) - v(y(t-\tau))], \tag{C.6}$$

$$\frac{\mathrm{d}y}{\mathrm{d}t} = \overline{u}(t)[w(v(y(t))) - w(v(y(t-\tau)))], \tag{C.7}$$

be converted into a system of SDDEs such that the noise term is applied to the differential of x. For this system of DDEs, we wish to apply the noise term, $\epsilon\xi$, to the process defined by $v(y(t))$. Therefore, if we add an additional noise term to this expression, then we obtain the following expression:

$$\frac{\mathrm{d}x}{\mathrm{d}t} = \overline{u}(t)[v(y) + \underbrace{\epsilon\xi}_{\text{noise term}} - v(y(t-\tau))]. \tag{C.8}$$

Multiplying by $\mathrm{d}t$ yields an equation in the form of an SDDE:

$$\mathrm{d}x = \overline{u}(t)[v(y) - v(y(t-\tau))]\mathrm{d}t + \epsilon\overline{u}(t)\underbrace{\mathrm{d}W_t}_{=\xi\mathrm{d}t}. \tag{C.9}$$

The problem with this approach is that if we attempt to perform the same set of steps on Equation (C.7), then we obtain the following equation:

$$\mathrm{d}y = \overline{u}(t)[w(v(y(t)) + \epsilon\xi) - w(v(y(t-\tau)))]\mathrm{d}t. \tag{C.10}$$

However, this is not in the form of an SDDE. One approach to resolving this issue is to take a Taylor expansion of w to ensure that the noise term is not within the function:

$$\mathrm{d}y = \overline{u}(t)\left[\sum_{n=0}^{\infty}\frac{1}{n!}w^{(n)}(v(y(t)))(\epsilon\xi)^n - w(v(y(t-\tau)))\right]\mathrm{d}t. \tag{C.11}$$

However, this approach also has its limitations. Because $\xi\mathrm{d}t = \mathrm{d}W_t$, this implies that $\xi = \mathrm{d}W_t/\mathrm{d}t$, but $O(\mathrm{d}W_t) = O(\sqrt{\mathrm{d}t})$. This implies that the order of the nth term in the Taylor expansion is $O(\mathrm{d}t^{-n/2})$. If $\epsilon \ll 1$, this may not be a significant problem for finding the numerical solution. For a step size of Δt, as long as:

$$\left|\frac{1}{n!}w^{(n)}(v(y(t)))(\Delta t)^{-\frac{n}{2}}\right| < \epsilon^n, \tag{C.12}$$

the sequence will converge. However, for the numerical solution to the SDEs, the numerical solution diverges as the step size decreases. Given this behaviour, a different modelling approach must be used to approximate the stochastic behaviour of y.

C.2 Practical formulation

The practical formulation for which we wish to model is that of the impact of stochastic noise generated by the pattern of bifurcating RBCs at a flow bifurcation in a vascular netowrk. To formulate the practical problem, we replace: w with μ, ϵ with $H_{(u,v)}(1,t)kf(r)$, and $v(y(t))$ with $H_{(v,w)}(0,t)$ or $H_{(v,z)}(0,t)$. As haematocrit entering a vessel at a flow bifurcation depends on the volumetric flows in a network which are functions of the average viscosity in the vessels, this last substitution in valid. Therefore, the abstract problem can be formulated by replacing Equation (C.6) with Equation (5.8) or (5.10), Equation (C.7) with Equation

(5.9) or (5.11), and Equation (C.9) with Equation (5.36) or (5.37). We will assume that $f(r) \in (0, 2)$ for all biologically realistic values of r.

C.3 Modelling Approach

We will use the abstract interpretation of the problem to devise different modelling approaches to simplify the notation. The modelling approach we will take to this problem is to consider a Taylor expansion for a stochastic random variable for which the differential of the variables is defined by a similar expression as that of Equation (C.1). However, we will consider this Taylor expansion for a different time variable $\tilde{t}$. Therefore, instead of finding conditions for the time difference or the constant amplitude ϵ in Equation (C.11), this approach seeks to replace the term $w(v(y(t)) + \epsilon\xi)$ with an approximation that appropriately captures the dynamics for a short time step. Consider the following:

$$w(X_{\tilde{t}}), \tag{C.13}$$

such that $\mathrm{d}X_{\tilde{t}} = \epsilon \mathrm{d}W_{\tilde{t}}$. Then assuming that the value of $X_{\tilde{t}}$ is known at $\tilde{t} = t_0$, using Ito's lemma, we obtain a second-order Taylor expansion for $w(X_{\tilde{t}})$:

$$w(X_{\tilde{t}}) = w(X_{t_0}) + \frac{\epsilon^2}{2} w''(X_{t_0})(\tilde{t} - t_0) + \epsilon w'(X_{t_0})(W_{\tilde{t}} - W_{t_0}) + R. \tag{C.14}$$

where R is defined by Equation (C.3). All the terms of R, with the exception of the last term, are of order $O(\sqrt{\mathrm{d}t}^3)$. If we apply Ito's lemma to the last term, we obtain the following expression:

$$\begin{aligned} \epsilon^2 \int_{t_0}^{\tilde{t}} \int_{t_0}^{s} w''(X_z) \mathrm{d}W_z \mathrm{d}W_s = & \epsilon^2 w''(X_{t_0}) \int_{t_0}^{\tilde{t}} \int_{t_0}^{s} \mathrm{d}W_z \mathrm{d}W_s + \\ & \epsilon^3 \int_{t_0}^{\tilde{t}} \int_{t_0}^{s} \int_{t_0}^{z} w^{(3)}(X_u) \mathrm{d}W_u \mathrm{d}W_z \mathrm{d}W_s + \\ & \frac{\epsilon^4}{2} \int_{t_0}^{\tilde{t}} \int_{t_0}^{s} \int_{t_0}^{z} w^{(4)}(X_u) \mathrm{d}u \mathrm{d}W_z \mathrm{d}W_s. \end{aligned} \tag{C.15}$$

The last of these terms have order $O(\sqrt{\mathrm{d}t}^3)$ or $O(\sqrt{\mathrm{d}t}^4)$, therefore, these terms can be ignored. Using Ito's lemma again, it is possible derive an expression for this first term:

$$\epsilon^2 w''(X_{t_0}) \int_{t_0}^{\tilde{t}} \int_{t_0}^{s} \mathrm{d}W_z \mathrm{d}W_s = \frac{\epsilon^2 w''(X_{t_0})}{2} (W_{\tilde{t}} - W_{t_0})^2 - \frac{(\tilde{t} - t_0)}{2}. \tag{C.16}$$

However, the expectation of this term is equal to 0. As a consequence, we consider $R \approx 0$ and ignore R for the Taylor expansion. Therefore, we will assume that:

$$w(X_{\tilde{t}}) \approx w(X_{t_0}) + \frac{\epsilon^2}{2} w''(X_{t_0})(\tilde{t} - t_0) + \epsilon w'(X_{t_0})(W_{\tilde{t}} - W_{t_0}). \tag{C.17}$$

Given that $\epsilon \ll 1$, it is possible to use a large time step. Therefore, if we let $\tilde{t} - t_0 = 1$ and assume that $W_{\tilde{t}} - W_{t_0} \approx \xi$ then we achieve the following approximation:

$$w(X_{\tilde{t}}) \approx w(X_{t_0}) + \frac{\epsilon^2}{2} w''(X_{t_0}) + \epsilon w'(X_{t_0})\xi. \tag{C.18}$$

To use this approximation in Equation (C.10), set $X_{t_0} = v(y(t))$, and $\xi \mathrm{d}t = \mathrm{d}W_t$:

$$\mathrm{d}y = \overline{u}(t)\left[w(v(y(t))) + \epsilon^2 \frac{w''(v(y(t)))}{2} - w(v(y(t-\tau)))\right]\mathrm{d}t + \epsilon \overline{u}(t) w'(v(y(t)))\mathrm{d}W_t. \tag{C.19}$$

Although this approach uses a different time varaible to derive the approximation, the fact that $\epsilon \ll 1$ means that any error from this method should be relatively small.

To use this approach in the practical problem, we replace $v(y(t))$ with $H_{(v,w)}(0,t)$, ϵ with $H_{(u,v)}(1,t)f(r)k$, and w with μ. It is important to note that this approximation for the stochastic effects on the blood viscosity includes a term with the second derivative of μ. In Section 5.2, this term is negated. This is due to the fact that the second derivative is scaled by k^2. However, to justify the omission of this term, it must be computationally verified the impact of this term is negligible.

C.4 Numerical verification

One method of determining the impact of the term with the second derivative in Equation (C.19) is to compare the distribution of switching times in the diamond network for the set of SDDEs including and excluding this term. If the distribution curves are not significantly different, then we can conclude that the term can be omitted. Let $p_i(t)$ and $p_e(t)$ denote the probability density functions of the switching times including and excluding the term with the second derivative of μ respectively. There are two metrics that we use to compare $p_e(t)$ with $p_i(t)$. The first is the two-sample Kolmogorov-Smirnov test. This test indicates if two sets of data have been sampled from different continuous distributions. The null hypothesis for this test is that the two sets of data are of the same continuous distribution. We will use a 95% confidence interval. Therefore, if the p value for the test is greater than 0.05 then we

conclude that the two sets of data are from the same continuous distribution according to this test.

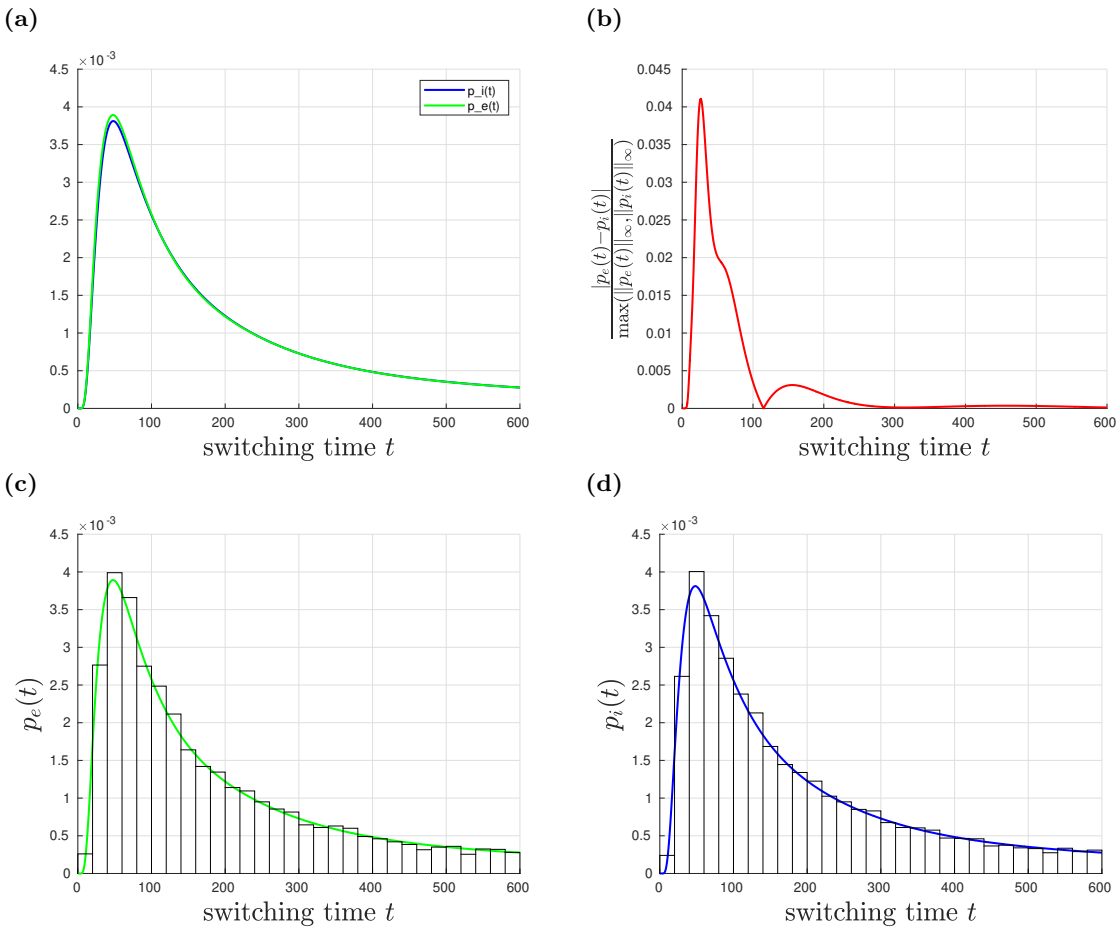

Figure C.1: (a): Comparison of $p_e(t)$ and $p_i(t)$. (b): Relative difference between $p_e(t)$ and $p_i(t)$. (c): $p_e(t)$ and a histogram of the samples used to generate the approximate distribution curve. (d): $p_i(t)$ and a histogram of the samples used to generate the approximate distribution curve.

The second metric we use is the relative difference between the two curves. Let:

$$\mathcal{M}(p_e, p_i, t) = \frac{|p_e(t) - p_i(t)|}{\max(\|p_e(t)\|_\infty, \|p_i(t)\|_\infty)}, \tag{C.20}$$

Then $\|\mathcal{M}(p_e, p_i, t)\|_\infty$ gives a comparable measure between the two curves. As with other results, it is not possible to analytically define the probability density functions, p_e and p_i, for the switching times but they can be approximated. By using the numerical method described in Appendix B, the two distribution curve are approximated by generating $10,000$ iterations of the numerical solution and then using MATLAB's inbuilt kernel distribution, using the normal distribution kernel, to fit the distribution curves to the data. These ap-

proximation can then be used for the metric defined in Equation (C.20). The two-sample Kolmogorov-Smirnov does not use the same approximate distribution function and instead uses the empirical distributions for the two samples. We use MATLAB's inbuilt two sample Kolmogorov-Smirnov to test between two samples.

Figure C.1 displays the comparison for the switching times of the diamond network with the following parameters:

$$L = 100\mu\text{m}, D = 10\mu\text{m}, H_{(1,3)}(0,t) = 0.5, k = 2 \times 10^{-4},$$

where L and D denote the lengths and diameters of the network's vessels. These parameters have been chosen because these are the largest values of k and $H_{(1,3)}(0,t)$ that are used in the thesis. Therefore, the greatest error is likely to occur for these parameter values. Figure C.1a clearly shows that the two curves are not significantly different, and Figure C.1b shows that the metric defined by Equation (C.20) does not exceed 0.05. The p value for the Kolmogorov-Smirnov test is 0.7557. Therefore, we conclude that the addition of the second derivative term does not significantly impact the probability distribution of the switching times.

Although the derivation of the approximation for the blood viscosity described in Section C.3 differs from the derivation from the approximation in Section 5.2, given that the addition of the term with the second derivative does not significantly alter the switching time distribution, either derivation is valid for the purpose of this thesis.

Appendix D

Triangle network with haematocrit controls

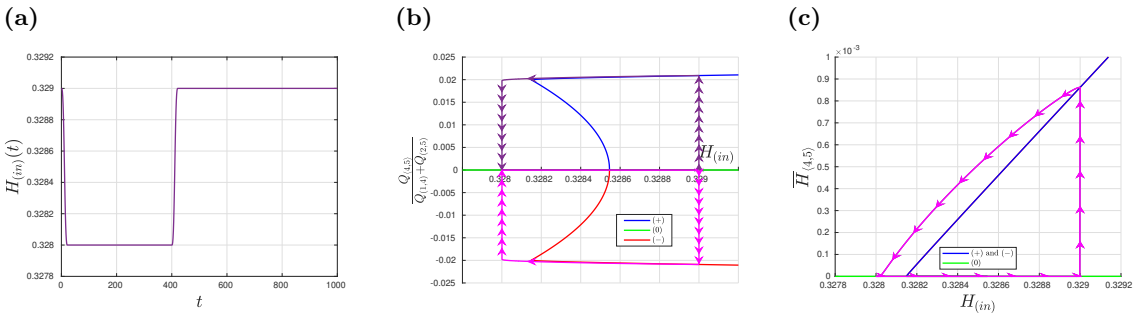

Figure D.1: (a): Plot of $H_{in}(t)$; (b): hysteresis diagram of the normalised flow in the redundant vessel of the triangle network; (c): hysteresis diagram of the average haematocrit in the redundant vessel of the triangle network.

Bibliography

Akhtari B. Numerical solution of stochastic state-dependent delay differential equations: convergence and stability. *Adv Diff Eqns*, 2019(1):1–34, 2019. DOI: 10.1186/s13662-019-2323-x.

Allgower EL and Georg K. *Introduction to numerical continuation methods*, chapter 2, pages 1–2. SIAM, 2003. DOI: 10.1137/1.9780898719154.

Angeli D, Ferrell Jr JE, and Sontag ED. Detection of multistability, bifurcations, and hysteresis in a large class of biological positive-feedback systems. *PNAS*, 101(7):1822–1827, 2004. DOI: 10.1073/pnas.0308265100.

Baker CTH and Buckwar E. Numerical analysis of explicit one-step methods for stochastic delay differential equations. *LMS J Comp Math*, 3:315–335, 2000. DOI: 10.1112/S1461157000000322.

Balogh P and Bagchi P. Direct numerical simulation of cellular-scale blood flow in 3d microvascular networks. *Biophysical journal*, 113(12):2815–2826, 2017. DOI: 10.1016/j.bpj.2017.10.020.

Balogh P and Bagchi P. Analysis of red blood cell partitioning at bifurcations in simulated microvascular networks. *Physics of Fluids*, 30(5):051902, 2018. DOI: 10.1063/1.5024783.

Barber JO, Alberding JP, Restrepo JM, and Secomb TW. Simulated two-dimensional red blood cell motion, deformation, and partitioning in microvessel bifurcations. *Annals of Biomedical Engineering*, 36(10):1690–1698, 2008. DOI: 10.1007/s10439-008-9546-4.

Bedggood P and Metha A. Direct visualization and characterization of erythrocyte flow in human retinal capillaries. *Biomedical Optics Express*, 3(12):3264–3277, 2012. DOI: 10.1364/BOE.3.003264.

Ben-Ami Y, Atkinson GW, Pitt-Francis JM, Maini PK, and Byrne HM. Structural features of microvascular networks trigger blood-flow oscillations. *Bull Math Biol*, 84(85), 2022. DOI: 10.1007/s11538-022-01046-y.

Bergers G and Hanahan D. Modes of resistance to anti-angiogenic therapy. *Nature Reviews Cancer*, 8(8):592–603, 2008. DOI: 10.1038/nrc2442.

Bernabeu MO, Köry J, Grogan JA, Markelc B, Beardo A, d'Avezac M, Enjalbert R, Kaeppler J, Daly N, Hetherington J, et al. Abnormal morphology biases hematocrit distribution in tumor vasculature and contributes to heterogeneity in tissue oxygenation. *PNAS*, 117(45):27811–27819, 2020. DOI: 10.1073/pnas.2007770117.

Browder T, Butterfield CE, Kräling BM, Shi B, Marshall B, O'Reilly MS, and Folkman J. Antiangiogenic scheduling of chemotherapy improves efficacy against experimental drug-resistant cancer. *Cancer Research*, 60(7):1878–1886, 2000.

Buckwar E. Introduction to the numerical analysis of stochastic delay differential equations. *Journal of computational and applied mathematics*, 125(1-2):297–307, 2000. DOI: 10.1016/S0377-0427(00)00475-1.

Carmeliet P and Jain RK. Angiogenesis in cancer and other diseases. *Nature*, 407(6801): 249–257, 2000. DOI: 10.1038/35025220.

Carmeliet P and Jain RK. Molecular mechanisms and clinical applications of angiogenesis. *Nature*, 473(7347):298–307, 2011. DOI: 10.1038/nature10144.

Carr RT and Lacoin M. Nonlinear dynamics of microvascular blood flow. *Annals of Biomedical Engineering*, 28(6):641–652, 2000. DOI: 10.1114/1.1306346.

Carr RT, Geddes JB, and Wu F. Oscillations in a simple microvascular network. *Annals of Biomedical Engineering*, 33(6):764–771, 2005. DOI: 10.1007/s10439-005-2345-2.

Chatterjee A, Kaznessis YN, and Hu WS. Tweaking biological switches through a better understanding of bistability behavior. *Current Opinion in Biotechnology*, 19(5):475–481, 2008. DOI: 10.1016/j.copbio.2008.08.010.

Davis J and Pozrikidis C. Numerical simulation of unsteady blood flow through capillary networks. *Bull Math Biol*, 73(8):1857–1880, 2011. DOI: 10.1007/s11538-010-9595-3.

De La Cruz R, Perez-Carrasco R, Guerrero P, Alarcon T, and Page KM. Minimum action path theory reveals the details of stochastic transitions out of oscillatory states. *Physical Review Letters*, 120(12):128102, 2018. DOI: 10.1103/PhysRevLett.120.128102.

Deane B and Lantos P. The vasculature of experimental brain tumours: Part 1. a sequential light and electron microscope study of angiogenesis. *Journal of the Neurological Sciences*, 49(1):55–66, 1981. DOI: 10.1016/0022-510X(81)90188-X.

Doedel E, Champneys A, Fairgrieve T, Kuznetsov Y, Sandstede B, and Wang X. Auto 97: Continuation and bifurcation software for ordinary differential equations (with homcont). 06 1999.

Doyeux V, Podgorski T, Peponas S, Ismail M, and Coupier G. Spheres in the vicinity of a bifurcation: elucidating the zweifach–fung effect. *Journal of Fluid Mechanics*, 674: 359–388, 2011. DOI: 10.1017/S0022112010006567.

Dykman MI, Mori E, Ross J, and Hunt P. Large fluctuations and optimal paths in chemical kinetics. *The Journal of Chemical Physics*, 100(8):5735–5750, 1994. DOI: 10.1063/1.467139.

Enjalbert R, Hardman D, Krüger T, and Bernabeu MO. Compressed vessels bias red blood cell partitioning at bifurcations in a hematocrit-dependent manner: Implications in tumor blood flow. *PNAS*, 118(25):e2025236118, 2021. DOI: 10.1073/pnas.2025236118.

Faivre S, Demetri G, Sargent W, and Raymond E. Molecular basis for sunitinib efficacy and future clinical development. *Nature Reviews Drug Discovery*, 6(9):734–745, 2007. DOI: 10.1038/nrd2380.

Fenton BM and Zweifach B. Microcirculatory model relating geometrical variation to changes in pressure and flow rate. *Annals of Biomedical Engineering*, 9(4):303–321, 1981. DOI: 10.1007/BF02364653.

Fenton BM, Carr RT, and Cokelet GR. Nonuniform red cell distribution in 20 to 100 μm bifurcations. *Microvascular Research*, 29(1):103–126, 1985. DOI: 10.1016/0026-2862(85)90010-X.

Ferrara N, Hillan KJ, Gerber HP, and Novotny W. Discovery and development of bevacizumab, an anti-vegf antibody for treating cancer. *Nature Reviews Drug Discovery*, 3 (5):391, 2004. DOI: 10.1038/nrd1381.

Fåhraeus R and Lindqvist T. The viscosity of the blood in narrow capillary tubes. *American Journal of Physiology-Legacy Content*, 96(3):562–568, 1931. DOI: 10.1152/ajplegacy.1931.96.3.562.

Fry BC, Lee J, Smith NP, and Secomb TW. Estimation of blood flow rates in large microvascular networks. *Microcirculation*, 19(6):530–538, 2012. DOI: 10.1111/j.1549-8719.2012.00184.x.

Fung YC. Stochastic flow in capillary blood vessels. *Microvascular Research*, 5(1):34–48, 1973. DOI: 10.1016/S0026-2862(73)80005-6.

Gaehtgens P. Heterogeneity of capillary perfusion. *Journal of Vascular Research*, 28(1-3): 197–200, 1991. DOI: 10.1159/000158862.

Ganesan P, He S, and Xu H. Analysis of retinal circulation using an image-based network model of retinal vasculature. *Microvascular Research*, 80(1):99–109, 2010. DOI: 10.1016/j.mvr.2010.02.005.

Gardner D, Li Y, Small B, Geddes JB, and Carr RT. Multiple equilibrium states in a micro-vascular network. *Mathematical Biosciences*, 227(2):117–124, 2010. DOI: 10.1016/j.mbs.2010.07.001.

Geddes JB, Carr RT, Karst NJ, and Wu F. The onset of oscillations in microvascular blood flow. *SIAM Journal on Applied Dynamical Systems*, 6(4):694–727, 2007. DOI: 10.1137/060670699.

Geddes JB, Carr RT, Wu F, Lao Y, and Maher M. Blood flow in microvascular networks: a study in nonlinear biology. *Chaos: An Interdisciplinary Journal of Nonlinear Science*, 20(4):045123, 2010. DOI: 10.1063/1.3530122.

Gilkes DM, Semenza GL, and Wirtz D. Hypoxia and the extracellular matrix: drivers of tumour metastasis. *Nature Reviews Cancer*, 14(6):430, 2014. DOI: 10.1038/nrc3726.

Goldsmith HL, Cokelet GR, and Gaehtgens P. Robin fahraeus: evolution of his concepts in cardiovascular physiology. *American Journal of Physiology-Heart and Circulatory Physiology*, 257(3):H1005–H1015, 1989.

Grogan JA, Connor AJ, Markelc B, Muschel RJ, Maini PK, Byrne HM, and Pitt-Francis JM. Microvessel chaste: an open library for spatial modeling of vascularized tissues. *Biophysical Journal*, 112(9):1767–1772, 2017. DOI: 10.1016/j.bpj.2017.03.036.

Hagenbach E. Ueber die bestimmung der zähigkeit einer flüssigkeit durch den ausfluss aus röhren. *Annalen der Physik*, 185(3):385–426, 1860. DOI: 10.1002/andp.18601850302.

Haibe Y, Kreidieh M, El Hajj H, Khalifeh I, Mukherji D, Temraz S, and Shamseddine A. Resistance mechanisms to anti-angiogenic therapies in cancer. *Frontiers in Oncology*, 10: 221, 2020. DOI: 10.3389/fonc.2020.00221.

Jain RK. Normalizing tumor vasculature with anti-angiogenic therapy: a new paradigm for combination therapy. *Nature Medicine*, 7(9):987, 2001. DOI: 10.1038/nm0901-987.

Jain RK. Normalization of tumor vasculature: an emerging concept in antiangiogenic therapy. *Science*, 307(5706):58–62, 2005. DOI: 10.1126/science.1104819.

Jain RK, Martin JD, and Stylianopoulos T. The role of mechanical forces in tumor growth and therapy. *Annual Review of Biomedical Engineering*, 16:321–346, 2014. DOI: 10.1146/annurev-bioeng-071813-105259.

Karst NJ, Storey BD, and Geddes JB. Oscillations and multiple equilibria in microvascular blood flow. *Bull Math Biol*, 77(7):1377–1400, 2015. DOI: 10.1007/s11538-015-0089-1.

Karst NJ, Geddes JB, and Carr RT. Model microvascular networks can have many equilibria. *Bull Math Biol*, 79(3):662–681, 2017. DOI: 10.1007/s11538-017-0251-z.

Katanov D, Gompper G, and Fedosov DA. Microvascular blood flow resistance: role of red blood cell migration and dispersion. *Microvascular Research*, 99:57–66, 2015. DOI: 10.1016/j.mvr.2015.02.006.

Kiani MF, Pries AR, Hsu LL, Sarelius IH, and Cokelet GR. Fluctuations in microvascular blood flow parameters caused by hemodynamic mechanisms. *American Journal of Physiology-Heart and Circulatory Physiology*, 266(5):H1822–H1828, 1994. DOI: 10.1152/ajpheart.1994.266.5.H1822.

Kuznetsov YA, Kuznetsov IA, and Kuznetsov Y. *Elements of applied bifurcation theory*, volume 112. Springer, 1998. DOI: 10.1007/978-1-4757-3978-7.

Less JR, Skalak TC, Sevick EM, and Jain RK. Microvascular architecture in a mammary carcinoma: branching patterns and vessel dimensions. *Cancer Research*, 51(1):265–273, 1991.

LeVeque RJ. *Finite difference methods for ordinary and partial differential equations: steady-state and time-dependent problems*. SIAM, 2007. DOI: 10.1137/1.9780898717839.

Longtin A. Stochastic delay-differential equations. In *Complex time-delay systems*, pages 177–195. Springer, 2009. DOI: 10.1007/978-3-642-02329-3_6.

Lv C, Li X, Li F, and Li T. Constructing the energy landscape for genetic switching system driven by intrinsic noise. *PLoS One*, 9(2):e88167, 2014. DOI: 10.1371/journal.pone.0088167.

Mao X. Numerical solutions of stochastic functional differential equations. *LMS J Comp Math*, 6:141–161, 2003. DOI: 10.1112/S1461157000000425.

Maslov K, Zhang HF, Hu S, and Wang LV. Optical-resolution photoacoustic microscopy for in vivo imaging of single capillaries. *Optics Letters*, 33(9):929–931, 2008. DOI: 10.1364/OL.33.000929.

Matsumoto S, Batra S, Saito K, Yasui H, Choudhuri R, Gadisetti C, Subramanian S, Devasahayam N, Munasinghe JP, Mitchell JB, et al. Antiangiogenic agent sunitinib transiently increases tumor oxygenation and suppresses cycling hypoxia. *Cancer Research*, 71(20):6350–6359, 2011. DOI: 10.1158/0008-5472.CAN-11-2025.

McCormack PL and Keam SJ. Bevacizumab. *Drugs*, 68(4):487–506, 2008. DOI: 10.2165/00003495-200868040-00009.

Mohtasham N, Babakoohi S, Salehinejad J, Montaser-Kouhsari L, Shakeri MT, Shojaee S, Sistani NS, and Firooz A. Mast cell density and angiogenesis in oral dysplastic epithelium and low-and high-grade oral squamous cell carcinoma. *Acta Odontologica Scandinavica*, 68(5):300–304, 2010. DOI: 10.3109/00016357.2010.494622.

Murray CD. The physiological principle of minimum work: I. the vascular system and the cost of blood volume. *PNAS of the United States of America*, 12(3):207, 1926. DOI: 10.1073/pnas.12.3.207.

Muz B, de la Puente P, Azab F, and Azab AK. The role of hypoxia in cancer progression, angiogenesis, metastasis, and resistance to therapy. *Hypoxia*, 3:83–92, 2015. DOI: 10.2147/HP.S93413.

Ozbudak EM, Thattai M, Lim HN, Shraiman BI, and Van Oudenaarden A. Multistability in the lactose utilization network of escherichia coli. *Nature*, 427(6976):737–740, 2004. DOI: 10.1038/nature02298.

Padera TP, Stoll BR, Tooredman JB, Capen D, Tomaso Ed, and Jain RK. Cancer cells compress intratumour vessels. *Nature*, 427(6976):695–695, 2004. DOI: 10.1038/427695a.

Pawlik G, Rackl A, and Bing RJ. Quantitative capillary topography and blood flow in the cerebral cortex of cats: an in vivo microscopic study. *Brain Research*, 208(1):35–58, 1981. DOI: 10.1016/0006-8993(81)90619-3.

Pogue BW, O'Hara JA, Wilmot CM, Paulsen KD, and Swartz HM. Estimation of oxygen distribution in rif-1 tumors by diffusion model-based interpretation of pimonidazole hypoxia and eppendorf measurements. *Radiation Research*, 155(1):15–25, 2001. DOI: 10.1667/0033-7587(2001)155[0015:EOODIR]2.0.CO;2.

Poiseuille J. Recherches experimentales sur le mouvement des liquides dans les tubes de très petits diamètres. *'Académie Royale des Sciences de l'Institut de France*, 1846.

Pomerening JR, Sontag ED, and Ferrell JE. Building a cell cycle oscillator: hysteresis and bistability in the activation of cdc2. *Nature Cell Biology*, 5(4):346–351, 2003. DOI: 10.1038/ncb954.

Pop S, Richardson G, Waters S, and Jensen OE. Shock formation and non-linear dispersion in a microvascular capillary network. *Mathematical medicine and biology: a journal of the IMA*, 24(4):379–400, 2007. DOI: 10.1093/imammb/dqm007.

Pries A, Ley K, Claassen M, and Gaehtgens P. Red cell distribution at microvascular bifurcations. *Microvascular Research*, 38(1):81–101, 1989. DOI: 10.1016/0026-2862(89)90018-6.

Pries A, Secomb T, Gessner T, Sperandio M, Gross J, and Gaehtgens P. Resistance to blood flow in microvessels in vivo. *Circulation Research*, 75(5):904–915, 1994. DOI: 10.1161/01.RES.75.5.904.

Pries AR and Secomb TW. Microvascular blood viscosity in vivo and the endothelial surface layer. *American Journal of Physiology-Heart and Circulatory Physiology*, 289(6):H2657–H2664, 2005. DOI: 10.1152/ajpheart.00297.2005.

Pries AR and Secomb TW. Blood flow in microvascular networks. In *Microcirculation*, pages 3–36. Elsevier, 2008. DOI: 10.1016/B978-0-12-374530-9.00001-2.

Pries AR, Secomb TW, Gaehtgens P, and Gross J. Blood flow in microvascular networks: Experiments and simulation. *Circulation Research*, 67(4):826–834, 1990. DOI: 10.1161/01.RES.67.4.826.

Pries AR, Neuhaus D, and Gaehtgens P. Blood viscosity in tube flow: dependence on diameter and hematocrit. *American Journal of Physiology-Heart and Circulatory Physiology*, 263(6):H1770–H1778, 1992. DOI: 10.1152/ajpheart.1992.263.6.H1770.

Pries AR, Höpfner M, Le Noble F, Dewhirst MW, and Secomb TW. The shunt problem: control of functional shunting in normal and tumour vasculature. *Nature Reviews Cancer*, 10(8):587–593, 2010. DOI: 10.1038/nrc2895.

Roma DM, O'Flanagan RA, Ruckenstein AE, Sengupta AM, and Mukhopadhyay R. Optimal path to epigenetic switching. *Physical Review E*, 71(1):011902, 2005. DOI: 10.1103/PhysRevE.71.011902.

Roman S, Merlo A, Duru P, Risso F, and Lorthois S. Going beyond 20 μm-sized channels for studying red blood cell phase separation in microfluidic bifurcations. *Biomicrofluidics*, 10(3):034103, 2016. DOI: 10.1063/1.4948955.

Schiavo F, Lindblom EK, and Toma-Dasu I. Towards the virtual tumor for optimizing radiotherapy treatments of hypoxic tumors: a novel model of heterogeneous tissue vasculature and oxygenation. *Journal of Theoretical Biology*, page 111175, 2022. DOI: 10.1016/j.jtbi.2022.111175.

Secomb TW. Blood flow in the microcirculation. *Annual Review of Fluid Mechanics*, 49: 443–461, 2017. DOI: 10.1146/annurev-fluid-010816-060302.

Secomb TW and Pries AR. Blood viscosity in microvessels: Experiment and theory. *Comptes Rendus Physique*, 14(6):470–478, 2013. DOI: 10.1016/j.crhy.2013.04.002.

Secomb TW, Dewhirst MW, and Pries AR. Structural adaptation of normal and tumour vascular networks. *Basic & clinical pharmacology & toxicology*, 110(1):63–69, 2012. DOI: 10.1111/j.1742-7843.2011.00815.x.

Secomb T, Hsu R, Dewhirst M, Klitzman B, and Gross J. Analysis of oxygen transport to tumor tissue by microvascular networks. *International Journal of Radiation Oncology Biology Physics*, 25(3):481–489, 1993. DOI: 10.1016/0360-3016(93)90070-C.

Sha W, Moore J, Chen K, Lassaletta AD, Yi CS, Tyson JJ, and Sible JC. Hysteresis drives cell-cycle transitions in xenopus laevis egg extracts. *PNAS*, 100(3):975–980, 2003. DOI: 10.1073/pnas.023534910.

Shannon AM, Bouchier-Hayes DJ, Condron CM, and Toomey D. Tumour hypoxia, chemotherapeutic resistance and hypoxia-related therapies. *Cancer Treatment Reviews*, 29(4):297–307, 2003. DOI: 10.1016/S0305-7372(03)00003-3.

Sharma B, Sriram G, Saraswathi T, Sivapathasundharam B, et al. Immunohistochemical evaluation of mast cells and angiogenesis in oral squamous cell carcinoma. *Indian Journal of Dental Research*, 21(2):260, 2010. DOI: 10.4103/0970-9290.66655.

Sherman TF. On connecting large vessels to small. the meaning of murray's law. *The Journal of General Physiology*, 78(4):431–453, 1981. DOI: 10.1085/jgp.78.4.431.

Shieh YS, Hung YJ, Hsieh CB, Chen JS, Chou KC, and Liu SY. Tumor-associated macrophage correlated with angiogenesis and progression of mucoepidermoid carcinoma of salivary glands. *Annals of Surgical Oncology*, 16(3):751–760, 2009. DOI: 10.1245/s10434-008-0259-6.

Stolz BJ, Kaeppler J, Markelc B, Braun F, Lipsmeier F, Muschel RJ, Byrne HM, and Harrington HA. Multiscale topology characterizes dynamic tumor vascular networks. *Science Advances*, 8(23):eabm2456, 2022. DOI: 10.1126/sciadv.abm2456.

Sweeney PW, Walker-Samuel S, and Shipley RJ. Insights into cerebral haemodynamics and oxygenation utilising in vivo mural cell imaging and mathematical modelling. *Scientific Reports*, 8(1):1–15, 2018. DOI: 10.1038/s41598-017-19086-z.

Tan E, Yan M, Campo L, Han C, Takano E, Turley H, Candiloro I, Pezzella F, Gatter K, Millar E, et al. The key hypoxia regulated gene caix is upregulated in basal-like breast tumours and is associated with resistance to chemotherapy. *British Journal of Cancer*, 100(2):405, 2009. DOI: 10.1038/sj.bjc.6604844.

Tawfik Y and Owens RG. A mathematical and numerical investigation of the hemodynamical origins of oscillations in microvascular networks. *Bull Math Biol*, 75(4):676–707, 2013. DOI: 10.1007/s11538-013-9825-6.

Upputuri PK, Sivasubramanian K, Mark CSK, and Pramanik M. Recent developments in vascular imaging techniques in tissue engineering and regenerative medicine. *BioMed Research International*, 2015, 2015. DOI: 10.1155/2015/783983.

Vogel AW. Intratumoral vascular changes with increased size of a mammary adenocarcinoma: new method and results. *Journal of the National Cancer Institute*, 34(5):571–578, 1965. DOI: 10.1093/jnci/34.5.571.

Ward C, Langdon SP, Mullen P, Harris AL, Harrison DJ, Supuran CT, and Kunkler IH. New strategies for targeting the hypoxic tumour microenvironment in breast cancer. *Cancer Treatment Reviews*, 39(2):171–179, 2013. DOI: 10.1016/j.ctrv.2012.08.004.

Welter M, Fredrich T, Rinneberg H, and Rieger H. Computational model for tumor oxygenation applied to clinical data on breast tumor hemoglobin concentrations suggests vascular dilatation and compression. *PloS one*, 11(8):e0161267, 2016. DOI: 10.1371/journal.pone.0161267.

Yamaura H and Sato H. Quantitative studies on the developing vascular system of rat hepatoma. *Journal of the national cancer institute*, 53(5):1229–1240, 1974. DOI: 10.1093/jnci/53.5.1229.